

PHASE MECHANICS AND DECOMPRESSION THEORY IN DEPTH

B.R. Wienke
Nuclear Weapons Technology/Simulation And Computing
Applied And Computational Physics Division
Los Alamos National Laboratory
Los Alamos, N.M. 87545

ABSTRACT

Decompression theory and phase mechanics are detailed in a Seven Chapter series, with topics motivated and strategically developed in their relationship to diving. Topics span many disciplines and focus in a number of decompression arenas. Targeted audience is the commercial diver, instructor, hyperbaric technician, underwater researcher, and technical diver looking for greater detail, and especially the doctor, physiologist, physicist, chemist, mathematician, engineer, or biologist by training. Topics include energy and thermodynamics, pressure and density, flow mechanics and gas kinetics, free and dissolved phase transfer, nucleation and cavitation, bubbles and surfactants, mixed gases, statistics, risk and probability, binomial and related distributions, computing and models, and altitude effects. References are included. This monograph extends Basic Decompression Theory And Application, as well as Basic Diving Physics And Application and Technical Diving In Depth.

Specifically, we cover a number of linked topics:

- 1. basic physics and fundamental concepts;*
- 2. basic statistics and risk analysis;*
- 3. nucleation and cavitation, persistence, time scales, and metrics;*
- 4. seeds, bubbles, equations of state, and material properties;*
- 5. energy, thermodynamics, hydrodynamics, and pressure mechanics;*
- 6. gas laws, flow dynamics, and phase transfer;*
- 7. perfusion and diffusion limited processes;*
- 8. critical tensions and phase volumes;*
- 9. altitude similarity and protocols;*
- 10. mixed gases, oxygen dose, deep stops, and decompression;*
- 11. inert gas transport and isobaric counterdiffusion;*
- 12. probabilistic decompression, statistical methods, and maximum likelihood;*
- 13. staging, validation, and model testing;*
- 14. dive tables, meter algorithms, and computational issues.*

Material presentation is phase mechanics first, followed by decompression theory. This facilitates continuity and discussion. New material is woven into previous material, and, as such, is necessary for further and extended development.

Pages – 184, Tables – 34, Figures – 40, References – 167

AUTHOR SKETCH

Bruce Wienke is a Program Manager in the Nuclear Weapons Technology/ Simulation And Computing Office at the Los Alamos National Laboratory (LANL), with interests in computational decompression and models, gas transport, and phase mechanics. He contributes to underwater symposia, educational publications, technical periodicals and decompression workshops, having authored seven monographs (*Technical Diving In Depth, Decompression Theory, Physics, Physiology And Decompression Theory For The Technical And Commercial Diver, High Altitude Diving, Basic Diving Physics And Application, Diving Above Sea Level, Basic Decompression Theory And Application*) and some 200 technical journal articles. Diving environs include the Caribbean, South Pacific, Asia, inland and coastal United States, Hawaii, and polar Arctic and Antarctic for sundry technical, scientific, military, and recreational activities. He functions on the LANL Nuclear Emergency Strategy Team (NEST), in exercises often involving Special Warfare Units, above and below water. He heads Southwest Enterprises, a consulting company for research and applications in overlapping areas of applied science and simulation, functions as an Expert Witness in diving litigation, and SEAL

Wienke is an Instructor Trainer/Technical Instructor with the National Association Of Underwater Instructors (NAUI), serves on the Board Of Directors (Vice Chairman for Technical Diving, Technical and Decompression Review Board Member), is a Master Instructor with the Professional Association Of Diving Instructors (PADI) in various capacities (Instructor Review Committee), is an Institute Director with the YMCA, and is an Instructor Trainer/Technical Instructor with Scuba Diving International/Technical Diving International (SDI/TDI). Wintertime he hobbies skiing, coaching, and teaching as a Racing Coach and Instructor, certified United States Ski Coaches Association (USSCA) and Professional Ski Instructors of America (PSIA), and races in the United States Ski Association (USSA) Masters Series Competition, holding a 8 NASTAR racing handicap. Other interests include tennis, windsurfing, and mountain biking. He quarterbacked the 63 Northern Michigan Wildcats to an NCAA II Championship (Hickory Bowl).

Wienke received a BS in physics and mathematics from Northern Michigan University, MS in nuclear physics from Marquette University, and PhD in particle physics from Northwestern University. He belongs to the American Physical Society (APS), American Nuclear Society (ANS), Society Of Industrial And Applied Mathematics (SIAM), South Pacific Underwater Medical Society (SPUMS), Undersea And Hyperbaric Medical Society (UHMS), and American Academy Of Underwater Sciences (AAUS). He is a Fellow of the American Physical Society, and a Technical Committee Member of the American Nuclear Society.

Wienke, a former dive shop owner in Santa Fe, presently serves as a Consultant for decompression algorithms in the Industry. He has worked with DAN on applications of high performance computing and communications to diving, and is a Regional Data Coordinator for Project Dive Exploration. Scubapro, Suunto, Mares, Dacor, HydroSpace, Plexus, Abysmal Diving, and Atomic Aquatics engage him (or have) as Consultant for meter algorithms. He is the developer of the Reduced Gradient Bubble Model (RGBM), a dual phase approach to staging diver ascents over an extended range of diving applications (altitude, nonstop, decompression, multiday, repetitive, multilevel, mixed gas, and saturation). A number of dive computers (Suunto, Mares, Dacor, Plexus, HydroSpace, and others coming online) incorporate the modified and full iterative RGBM into staging regimens, for technical and recreational diving. Aggressive computers with RGBM for helitrox, trimix, heliox, nitrox, air, and combinations are in the pipeline. ABYSS, a commercial software product, features some of the RGBM dynamical diving algorithms developed by him for Internet users and technical divers. He is also Associate Editor for the International Journal Of Aquatic Research And Education, and is a former Contributing Editor of *Sources*, the NAUI Training Publication. NAUI Technical Training has adopted the RGBM for technical and recreational training, and employs RGBM trimix, heliair, nitrox, and air tables. Wienke is a Contributing Editor of *Advanced Diver* magazine.

TABLE OF CONTENTS

PROLOGUE

UNITS AND EQUIVALENCES

PHYSICS AND FUNDAMENTAL RELATIONSHIPS / Mechanics / Thermodynamics / Hydrodynamics / Electrodynamics

STATISTICS AND DATA CORRELATION / Distributions / Maximum Likelihood Fit / Nonlinear Least Squares Fit

1. NUCLEATION PROCESSES / Quiescent Nucleation / Cavitation / Tribonucleation / Gas Turbulent Nucleation / Chemical Nucleation / Ensemble Theory
2. MATERIAL PROPERTIES / Gases / Solids / Fluids / Compressibility And Cubical Expansion / Time Scales / Bubble Metrics
3. GAS, FLUID, AND PHASE KINETICS / Boltzmann Transport Equation / Moment Flow Equations / Collisional Dynamics / High Pressure Flow / Phase Transfer / Mass Transport / Doppler Effect / Pulmonary And Circulatory Networks
4. CRITICAL TENSIONS AND PHASE VOLUMES / Critical Tensions / Saturation Curve / Critical Phase Volumes / Reduced Haldane Gradients / Ascent Staging / Tables And Meters / Altitude Extrapolation And Ratios / Hypobaric And Hyperbaric Asymptotics
5. MIXED GASES AND DECOMPRESSION / Mixtures And Biological Reactivities / Diving Mixtures And Equivalent Depths / Isobaric Countertransport / Oxygen Rebreathing And Dose
6. COMPARATIVE PROFILES AND OPERATIONAL DIVING / Haldane Profiles / Empirical Practices / RGBM Profiles And Validation / Reverse Profiles / Deep Stops / Helium Strategies / Probabilistic Decompression / Saturation Bends Probability / Table And Profile Risks
7. COMPUTING AND DECOMPRESSION ALGORITHMS / Computing Advances / Monte Carlo Bubble Simulations / Project Dive Exploration / Multilevel Dive Profile Analysis / Computational Algorithms / RGBM Computational Issues

EPILOGUE

RGBM RECREATIONAL AIR AND NITROX TABLES

RGBM TECHNICAL MIXED GAS AND DECOMPRESSION TABLES

REFERENCES

INDEX

PROLOGUE

This exposition links phase mechanics to decompression theory with equations and corresponding dialogue. Theory and application are, at times, more an artform than exact science. Some believe deterministic modeling is only fortuitous. Technological advance, elucidation of competing mechanisms, and resolution of model issues over the past 90 years has not been rapid. Model applications tend to be *ad hoc*, tied to data fits, and difficult to quantify on just first principles. Almost any description of decompression processes in tissue and blood can be disputed, and possibly turned around on itself. The fact that decompression sickness occurs in metabolic and perfused matter makes it difficult to design and analyze experiments outside living matter. Yet, for application to safe diving, we need models to build tables and meters. And, regardless of biological complexity, certain coarse grain physics principles, often neglected in the past, are making a substantial change in diver staging regimens, decompression theory, and coupled data analysis. Happily today, we are looking at both dissolved gases and bubbles in our staging regimens, and not just the dissolved gas approach of Haldane which has been an icon for the past century.

The reader will notice an emphasis on free gas phases (bubbles, nuclei, and whatever else is not dissolved), and comments about free phase models versus (just) dissolved phase models, the present basis for most decompression analysis. Most comments are based on recent experiments coupled to basic physics. While we do not know all the facts yet, many takes the view that phase models correlated with available data, linked to underlying physical principles, and which recover dissolved gas models in appropriate limits, are the types of models which should be extended, refined, and used in table and meter algorithms. Coupled to model algorithms is statistical analyses of decompression risk data, folded into meaningful and useful table and meter format, an area under active study. Models such as the RGBM have already gained widespread popularity, acceptance, and grow in prominence, particularly in the deep, decompression, and mixed gas sectors. This is due to released Tables, meter implementations, computer software, and wholesale positive results and feedback by real divers across all venues. Some have called it a revolution in diving.

The intent here is to present a working view of physical phase mechanics, then followed by application to decompression theory in diving. mostly focusing on theory with application, including equations. The discussion is neither a medical nor physiological synthesis. Such aspects are simplified, and for some certainly oversimplified. Nonetheless, it is directed toward the diver and reader with some rudimentary understanding of decompression. Background in the physical or life sciences is helpful, but certainly not requisite. Basically, the mechanistics of tissue gas exchange, bubbles and nucleation, supersaturation, perfusion and diffusion, and related mechanisms are discussed.

The physics, biology, engineering, physiology, medicine, and chemistry of diving center on pressure, and pressure changes. The average individual is subject to atmospheric pressure swings of 3% at sea level, as much as 20% a mile in elevation, more at higher altitudes, and all usually over time spans of hours to days. Divers and their equipment can experience compressions and decompressions orders of magnitude greater, and within considerably shorter time scales. While effects of pressure change are readily quantified in physics, chemistry, and engineering applications, the physiology, medicine, and biology of pressure changes in living systems are much more complicated. Caution is needed in transposing biological principles from one pressure range to another. Incomplete knowledge and mathematical complexities often prevent extensions of even simple causal relationships in biological science. Causal relationships between observables are, of course, the pervue of physics, and that difficult process in living systems is biophysics. Other source material and further development can be found in the References.

Material detailed builds upon and extends topics presented in *Physics, Physiology, And Decompression Theory For The Technical And Commercial Diver, Basic Diving Physics And Application, Diving Above Sea Level, High Altitude Diving, Basic Decompression Theory And Application, Technical Diving In Depth*, as referenced in the text.

Good reading and good diving.

UNITS AND EQUIVALENCES

Standard (SI) and English units are employed. By convention, by usage, or for ease, some nonstandard units are employed. Pressure and depth are both measured in feet of sea water (*fsw*) and meters of sea water (*msw*), with $1 \text{ atm} = 33 \text{ fsw} = 10 \text{ msw}$ to good approximation. Specific densities, η (dimensionless), in pressure relationships are normalized to sea water density.

Table 1. Equivalence And Unit Conversion Table.

Time	
$1 \text{ megahertz} = 10^6 \text{ hertz} = 10^6 \text{ sec}^{-1}$	
Length	
$1 \text{ m} = 3.28 \text{ ft} = 1.09 \text{ yd} = 39.37 \text{ in}$	
$1 \mu\text{m} = 10^4 \text{ angstrom} = 10^3 \text{ nm} = 10^{-6} \text{ m}$	
$1 \text{ km} = .62 \text{ mile}$	
$1 \text{ fathom} = 6 \text{ ft}$	
$1 \text{ nautical mile} = 6,080 \text{ ft} = 1.15 \text{ mile} = 1.85 \text{ km}$	
$1 \text{ light year} = 9.46 \times 10^{12} \text{ km} = 5.88 \times 10^{12} \text{ mile}$	
Speed	
$1 \text{ km/hr} = 27.77 \text{ cm/sec}$	
$1 \text{ mile/hr} = 5280 \text{ ft/sec}$	
$1 \text{ knot} = 1.15 \text{ mi/hr} = 51.48 \text{ cm/sec}$	
Volume	
$1 \text{ cm}^3 = .06 \text{ in}^3$	
$1 \text{ m}^3 = 35.32 \text{ ft}^3 = 1.31 \text{ yd}^3$	
$1 \text{ l} = 10^3 \text{ cm}^3 = .04 \text{ ft}^3 = 1.05 \text{ qt}$	
Mass and Density	
$1 \text{ g} = .04 \text{ oz}$	
$1 \text{ kg} = 32.27 \text{ oz} = 2.20 \text{ lb}$	
$1 \text{ g/cm}^3 = .57 \text{ oz/in}^3$	
$1 \text{ kg/m}^3 = .06 \text{ lb/ft}^3$	
Force and Pressure	
$1 \text{ newton} = 10^5 \text{ dyne} = .22 \text{ lb}$	
$1 \text{ g/cm}^2 = .23 \text{ oz/in}^2$	
$1 \text{ kg/m}^2 = .20 \text{ lb/ft}^2$	
$1 \text{ atm} = 33 \text{ fsw} = 10 \text{ msw} = 1.03 \text{ kg/cm}^2 = 14.69 \text{ lbs/in}^2$	
Energy and Power	
$1 \text{ cal} = 4.19 \text{ joule} = 3.96 \times 10^{-3} \text{ btu} = 3.09 \text{ ft lb}$	
$1 \text{ joule} = 10^7 \text{ ergs} = .74 \text{ ft lb}$	
$1 \text{ keV} = 10^3 \text{ eV} = 1.60 \times 10^{-16} \text{ joule}$	
$1 \text{ amu} = 931.1 \text{ MeV}$	
$1 \text{ watt} = 3.41 \text{ btu/hr} = 1.34 \times 10^{-3} \text{ hp}$	
Electricity and Magnetism	
$1 \text{ coul} = 2.99 \times 10^9 \text{ esu}$	
$1 \text{ amp} = 1 \text{ coul/sec} = 1 \text{ volt/ohm}$	
$1 \text{ volt} = 1 \text{ newton coul m} = 1 \text{ joule/coul}$	
$1 \text{ gauss} = 10^{-4} \text{ weber/m}^2 = 10^{-4} \text{ newton/amp m}$	
$1 \text{ f} = 1 \text{ coul/volt}$	

Standard mathematical and physical conventions are followed. Bold face quantities are vectors, while roman face quantities are scalars. Fundamental constants are tabulated below in Table 2. Full discussion of constants and impacts can be found in the References, particularly the physics and chemistry entries.

Table 2. Fundamental Constants.

$$\begin{aligned}
g_0 &= 9.80 \text{ m/sec}^2 && (\text{Sea Level Acceleration Of Gravity}) \\
G_0 &= 6.67 \times 10^{-11} \text{ newton m}^2/\text{kg}^2 && (\text{Gravitational Constant}) \\
M_0 &= 5.98 \times 10^{24} \text{ kg} && (\text{Earth Mass}) \\
\Gamma_0 &= 1.98 \text{ cal/min cm}^2 && (\text{Solar Constant}) \\
c &= 2.998 \times 10^8 \text{ m/sec} && (\text{Speed Of Light}) \\
h &= 6.625 \times 10^{-34} \text{ joule sec} && (\text{Planck Constant}) \\
R &= 8.317 \text{ joule/gmole K}^\circ && (\text{Universal Gas Constant}) \\
k &= 1.38 \times 10^{-23} \text{ joule/gmole K}^\circ && (\text{Boltzmann Constant}) \\
N_0 &= 6.025 \times 10^{23} \text{ atoms/gmole} && (\text{Avogadro Number}) \\
m_0 &= 9.108 \times 10^{-31} \text{ kg} && (\text{Electron Mass}) \\
e_0 &= 1.609 \times 10^{-19} \text{ coulomb} && (\text{Electron Charge}) \\
r_0 &= .528 \text{ angstrom} && (\text{First Bohr Orbit}) \\
\epsilon_0 &= (4\pi)^{-1} \times 1.11 \times 10^{-10} \text{ f/m} && (\text{Vacuum Permittivity}) \\
\mu_0 &= 4\pi \times 10^{-7} \text{ h/m} && (\text{Vacuum Permeability}) \\
\kappa_0 &= (4\pi\epsilon_0)^{-1} = 8.91 \times 10^9 \text{ m/f} && (\text{Coulomb Constant}) \\
\alpha_0 &= \mu_0/4\pi = 1 \times 10^{-7} \text{ h/m} && (\text{Ampere Constant}) \\
\sigma_0 &= 5.67 \times 10^{-8} \text{ watt/m}^2 \text{ K}^{\circ 4} && (\text{Stefan - Boltzmann Constant})
\end{aligned}$$

Metrology is the science of measurement, and broadly construed, encompasses the bulk of experimental science. In the more restricted sense, metrology refers to the maintenance and dissemination of a consistent set of units, support for enforcement of equity in trade by weights and measure laws, and process control for manufacturing.

A measurement is a series of manipulations of physical objects or systems according to experimental protocols producing a number. The objects or systems involved are test objects, measuring devices, or computational operations. The objects and devices exist in and are influenced by some environment. The number relates to the some unique feature of the object, such as the magnitude, or the intensity, or the weight, or time duration. The number is acquired to form the basis of decisions effecting some human feature or goal depending on the test object.

In order to attain the goal of useful decision, metrology requires that the number obtained is functionally identical whenever and wherever the measurement process is performed. Such a universally reproducible measurement is called a *proper measurement* and leads to describing *proper quantities*. The equivalences in Table 1 relate *proper quantities* and the fundamental constants in Table 2 permit closure of physical laws. Unit conversion follows from Table 2, via the chain rule, where the identities in Table 1 define equivalence ratios that work like simple arithmetic fractions as far as unit conversions are concerned. Units cancel just like numbers.

PHYSICS AND FUNDAMENTAL RELATIONSHIPS

Mechanics

Matter has definite mass and volume, can change form and phase, and consists of tiny atoms and molecules. A gram molecular weight (*gmole*) of substance, that is, an amount of substance in grams equal to its atomic weight, A , possesses Avogadro's number, N_0 , of atoms or molecules, some 6.025×10^{23} constituents. Molecules of a gas are in constant motion. Liquid molecules are free to move and slide over each other, while loosely bound. Molecules in a solid are relatively fixed, but can oscillate about their lattice points.

Matter cannot be created nor destroyed, but it can be transformed by chemical and nuclear reactions. In the most general sense, matter and energy are equivalent. For instance, the nuclear and chemical binding energies of molecules and atoms result from very small mass reductions in constituent particles (mass defect) when in bound states. The postulate of conservation of mass-energy is fundamental, and cannot be derived from any other principle. Stated simply, mass-energy can neither be created nor destroyed. All of observable science is based on this premise.

The concepts of mass and corresponding occupied volume are fundamental perceptions. The mass, m , in unit volume, V , is the mass density,

$$\rho = \frac{m}{V},$$

and gases are usually the least dense, followed by fluids, and then solids. Weight density is the weight per unit volume. Specific density, η , is the ratio of material density to density of water. States of matter usually have much different densities. Matter interactions are generically termed mechanics.

Mechanics is concerned with the effects of forces to produce or retard motion (kinetic energy), change position, induce material deformation, or cause chemical and nuclear reactions (potential energy). Forces may be gravitational, nuclear, or electromagnetic in origin. Mechanical properties describe the change in shape of matter when external forces are applied. Examples include the simple bending of a beam, the propagation of sound waves, the permanent deformation of metals into useful shapes, and the flow of liquids and gases around obstacles. For matter in the gaseous state, the usual force is the hydrostatic pressure, and deformation is a change in volume. For matter in the solid state, both tensile and shearing forces come into play to produce deformations.

Time rate of change of distance is velocity, v , or, using vector notation,

$$\mathbf{v} = \frac{d\mathbf{s}}{dt}$$

with $d\mathbf{s}$ the infinitesimal change in position over change in time, dt . Time rate of change of velocity is acceleration, \mathbf{a} ,

$$d\mathbf{a} = \frac{d\mathbf{v}}{dt}$$

Force is a push or a pull. Newton's first law states that a body in motion tends to stay in motion unless acted upon by an unbalanced force. Forces, \mathbf{F} , acting upon bodies of mass, m , produce accelerations, \mathbf{a} , linked by Newton's second law,

$$\mathbf{F} = m\mathbf{a}.$$

In vectors terms, velocity, \mathbf{v} , and acceleration, \mathbf{a} , are rates of change in position, \mathbf{r} , and velocity, \mathbf{v} , as shown. With t the time, the most general form of the force law is,

$$\mathbf{F} = \frac{d\mathbf{p}}{dt},$$

with \mathbf{p} the momentum, defined in terms of mass, m , and velocity, \mathbf{v} ,

$$\mathbf{p} = m\mathbf{v},$$

allowing for changes in mass to generate force. Such situation obviously presents itself in the relativistic case, where mass depends on velocity. Another case where force depends on rate of mass loss occurs with fuel burnup in rocket propulsion systems. Newton's third law states that for every action, there is an equal and opposite reaction. Stated another way, for every applied force, there is an equal and opposite reaction force, a stipulation requiring the conservation of momentum in all reactions.

The rectilinear equations above generalize for the curvilinear case. Angular momentum, \mathbf{L} , about some fixed point a distance, \mathbf{r} , away, is defined as,

$$\mathbf{L} = \mathbf{r} \times \mathbf{p}$$

and the corresponding torque, \mathbf{N} , is then,

$$\mathbf{N} = \frac{d\mathbf{L}}{dt}$$

Obviously, in terms of the force, \mathbf{F} ,

$$\mathbf{N} = \mathbf{r} \times \mathbf{F}$$

A force applied to an element of surface area, at angle, θ , to the surface element normal, generates a pressure, P , given by,

$$P = \cos \theta \frac{dF}{dA},$$

with dF and dA scalar elements of force and area. Pressure at a point is equal in all directions, and thus is not a specifically directed (vector) quantity.

Energy in simplest terms is the ability to do work. Or equivalently, the ability to do work requires an interchange of energy between a system and its surroundings. Energy takes two main forms, kinetic and potential. Kinetic energy is the energy associated with motion. Potential energy is the energy associated with position in a force field. Binding energy is the energy associated with changes in both kinetic and potential energies in bound composite systems, undergoing chemical, nuclear, or molecular interactions. Electromagnetic and acoustical energies are kinetic and potential energies associated with light and pressure waves. Heat energy can be kinetic energy associated with random molecular translations, vibrations, and rotations, or potential energy of frictional surface distortions and stress fatigue, nuclear and chemical reactions, and phase transformations. In all processes known to man, mass-energy is conserved, which is to say that mass can be converted to energy, and vice versa.

In the most general (relativistic) sense, mass and energy are equivalent, as mentioned, which follows as a consequence of the constancy of the speed of light in any inertial frame. An inertial frame is a frame of reference moving with constant velocity (no acceleration). Einstein postulated that the laws of physics are identical for two observers moving with constant velocity with respect to each other (first law of relativity), and that the speed of light, c , is constant independent of relative motion between reference frames (second law of relativity). This requires that the mass, m , of a body moving with speed, v , increases over its resting value, m_0 , according to the relativistic equation,

$$m = \frac{m_0}{(1 - v^2/c^2)^{1/2}}$$

for c the speed of light. The corresponding total energy, E , becomes,

$$E = mc^2$$

and the momentum, \mathbf{p} , satisfies,

$$\mathbf{p} = m\mathbf{v}$$

as before, but employing the relativistic mass. In the low energy limit, that is, the classical realm,

$$\lim_{v/c \rightarrow 0} \frac{m_0 c^2}{(1 - v^2/c^2)^{1/2}} \approx m_0 c^2 + \frac{1}{2} m_0 v^2$$

so we write the total energy as the sum of rest mass energy, E_0 , plus kinetic energy, K ,

$$E = m_0 c^2 + \frac{1}{2} m_0 v^2 = E_0 + K$$

with

$$\begin{aligned} E_0 &= m_0 c^2 \\ K &= \frac{1}{2} m_0 v^2 \end{aligned}$$

in the usual (nonrelativistic) sense.

Force, \mathbf{F} , acting along a pathlength, $d\mathbf{s}$, does work, dW ,

$$dW = \mathbf{F} \cdot d\mathbf{s},$$

or, in terms of pressure, P , effecting a volume change, dV ,

$$dW = PdV,$$

imparting, or taking, energy to, or from, a system. If there are zero net forces on a system, total energy, $H = K + U$, remains constant, with K kinetic energy and U potential energy. Various forms of the system energy can change, but the total, H , cannot change. If net forces do work on a system and if, when the processes are reversed, the system returns to its initial value of energy, H , the forces are said to be conservative, and the energy of the system is independent of how the work was done. One nonconservative force is friction, since the amount of energy lost to friction by a moving body depends on the distance over which the body slides, and not just on initial and final states. Conservative forces are said to derive from potentials, U , so that we write,

$$\mathbf{F} = -\nabla U,$$

in which case, the total energy, $H = K + U$, is a constant of motion. In a conservative force field, the change in energy associated with initial and final states depends only on initial and final state energies, and is independent of the path chosen between points. Then two (energy) states, i and f , for a conservative transition, are linked according to,

$$H_i = K_i + U_i = H_f = K_f + U_f$$

Potential, U , will depend on position in force fields (gravitation, electromagnetism, strong and weak interactions, and combinations). In the gravitational field of the Earth, we reference the geopotential with respect to position, h ,

$$U = mgh$$

with m the mass, g the local acceleration of gravity, and h measured from any convenient Earth reference point in the vertical direction (center, surface, satellite orbit).

Power, J , is the rate of doing work,

$$J = \frac{dW}{dt},$$

for corresponding small changes in energy and time, dW and dt .

The interactions of matter and energy are sometimes broken down into light, heat, and sound. Macroscopically, this is a classical division, suitably splitting mechanics into major observable categories, but with understanding that each is a detailed science by itself.

Thermodynamics

In thermodynamics, heat denotes the quantity of energy exchanged by thermal interaction of any system with its environment. For example, if a flame is applied to a cool metal plate, the energy content of the plate increases, as evidenced by its temperature increase, and we say that heat has passed from the flame to the plate. If energy losses to the surrounding air can be ignored, the heat transferred from the flame is equal to the energy gain of the plate. In more complex processes, involving mechanical as well as thermal interactions, the heat transferred is more difficult to identify. Thermodynamics focuses on the controlled and slow evolution of heat, energy, and entropy, and the distinctions between them in mechanical systems. While heat is a tenuous concept, linked to observables such as internal energy change and external work, we often deal with systems at different temperatures, exchanging heat in the absence of mechanical interactions, or external forces. Specific heat, c , measures change in heat capacity, dQ , for corresponding change in temperature, dT , per unit mass, m , of substance. At constant pressure, the specific heat is denoted, c_P ,

$$c_P = \frac{1}{m} \left[\frac{dQ}{dT} \right]_P$$

while at constant volume, the specific heat, c_V , is similarly written,

$$c_V = \frac{1}{m} \left[\frac{dQ}{dT} \right]_V$$

Generally, it is c_P that concerns us as divers and underwater. The molal specific heat is the heat capacity per unit mole (n replaces m). Heat, then, is the energy exchanged between parts of mechanical systems at different temperatures. Three fundamental and well known mechanisms include convection, conduction, and radiation. In practical situations, near standard temperatures and pressures, heat exchange usually involves the first two, conduction and convection. Radiative transfer underscores fairly high temperatures.

Heat conduction is the exchange of heat from one body at a given temperature to another body at a lower temperature with which it is in contact. Transfer of molecular kinetic energy occurs directly by molecular impacts or collisions. Heat conduction is governed by Fourier's law,

$$\phi = -K\nabla T,$$

with, ϕ , heat flux, K , conductivity, and, T , temperature.

Heat convection is a special case of conduction that occurs when a fluid or gas flows past the outer boundary of a system. Then the determination of K involves solving the fluid equations of a viscous, heat conducting fluid or gas, coupled to the heat flow equations in the system. Radiative transfer is a different mechanism completely from conduction and convection. The mechanism is electromagnetic wave emission from a heated surface, with the spectrum of wavelengths a complex function of surface temperature. For a point (idealized) source at temperature, T , the radial (isotropic) heat flux, ϕ , is given by the Stefan-Boltzmann relationship,

$$\phi = \sigma T^4,$$

for T the temperature, and σ the radiation constant ($5.67 \times 10^{-8} \text{ watt/m}^2 \text{ K}^4$). The most complex heat transfer phenomena are those in which extended physical systems interact by combinations of the above, in addition to phase transformations such as boiling, condensation, or solidification.

Radiation is absorbed in passing through matter, and the fraction absorbed is characteristic of the material. The ratio of absorbed to incident radiation at a certain wavelength is called the

absorptivity, α , and depends on the wavelength. A body with absorptivity equal to one is called a *black* body. Perfect black bodies do not exist in nature, but there are many approximate black bodies, especially in the infrared, or long wavelength, region. Of the incident radiation that is not absorbed, part is reflected and part is transmitted. The ratio of reflected to incident radiation is called the reflectivity, ρ , and the ratio of transmitted to incident radiation is called the transmissivity, τ . Obviously, the three quantities are related by,

$$\alpha + \rho + \tau = 1.$$

For a black body, $\rho = \tau = 0$, and $\alpha = 1$. A molecule which absorbs radiation at a particular wavelength is also able to emit radiation at the same wavelength. The emissivity, ϵ , is defined to be the ratio of emitted radiation to the maximum possible at a given temperature, and by Kirchoff's law,

$$\epsilon = \alpha.$$

Temperature is a measure of hotness or coldness. But more particularly, temperature is a measure of the average kinetic energy of the molecular ensemble comprising the object, also called the internal energy. For an ideal gas, the mean molal kinetic energy, $\bar{\epsilon}$, satisfies the Boltzmann relationship,

$$\bar{\epsilon} = \frac{3}{2} kT \quad ,$$

with k Boltzmann's constant ($1.38 \times 10^{-23} \text{ j/gmole } K^\circ$), and T the absolute temperature. The first temperature measuring devices, employing displaced air volumes to define hotness or coldness according to the pronouncements of the instrument maker, were called thermometers in the 1600s. The liquid sealed in glass thermometers, based on thermal expansion and contraction, appeared in the latter half of the 1600s.

Use of temperature as a measurement of hotness or coldness is based on two requirements, that is, a universal agreement on calibration and scale, and technology sufficient to produce reliable instruments giving identical readings under the same conditions. Wide adoption of the Fahrenheit scale, F° , was promoted by the trusty mercury (in glass) thermometers constructed in Danzig, by Fahrenheit, in the early 1700s. The scale was based on two fixed points, namely, the melting point of ice and the temperature of a healthy human body (later replaced by the boiling point of water). Celsius, at Uppsala, around the mid 1700s, introduced the Celsius (Centigrade) scale, C° , on which the degree was 1/100 of the interval between the freezing and boiling points of water. Later, in the 1800s, Kelvin introduced the absolute scale, K° , based on the second law of thermodynamics and entropy, ultimately linked by statistical mechanics to an absolute zero, that is, a temperature at which random molecular motion ceases. By 1887, the international community adopted the constant volume hydrogen gas thermometer as defining measurements on the Kelvin scale.

Kelvin (K°), Centigrade (C°), Rankine (R°), and Fahrenheit (F°) temperatures are linearly scaled, and are easily related,

$$F^\circ = \frac{9}{5} C^\circ + 32 \quad ,$$

$$K^\circ = C^\circ + 273 \quad ,$$

$$R^\circ = F^\circ + 460 \quad .$$

Kelvin and Rankine temperatures are employed in the gas laws.

The first law of thermodynamics is really a statement of conservation of energy in any system. Denoting the internal energy of the system, U , the net heat flow into the system, Q , and the work, W , done on the system, the first law requires that infinitesimal changes dQ , dU , and dW satisfy,

$$dU = dQ - dW \quad .$$

The internal energy of an ideal gas is only dependent on temperature, and that is a good approximation in most other real gases near standard temperature and pressure. (32 F° , and 1 atm). Denoting the number of molecules of the gas, N , and the number of moles, n , with R the gas constant and k Boltzmann's constant, we have

$$dU = N\bar{\epsilon}dT = \frac{3}{2} NkdT = \frac{3}{2} nRdT \quad ,$$

as a measure of the internal energy change, dU , for temperature change, dT . Heat flow, dQ , into or out of the system occurs through conduction, convection, or radiation. Mechanical work, dW , performed on, or by, the system is associated with volume change, dV , under pressure, P ,

$$dW = PdV \quad ,$$

so that,

$$dU = dQ - PdV \quad ,$$

in a closed system. We do not live in a reversible world, that is to say, processes usually proceed in only one direction. Collectively, the directionality ascribed to physical processes is termed *entropy*.

From experience, we know that some processes satisfying the first law (conservation of energy) never occur. For instance, a piece of rock resting on the floor will never cool itself down and jump up to the ceiling, thereby converting heat energy into potential energy. The second law defines a state *directional* variable, S , called the entropy, so that for any process, the heat transferred, dQ , is given by,

$$dQ = TdS$$

$$dS \geq 0 \quad .$$

The requirement that the entropy change, dS , associated with the process must be greater than or equal to zero imparts directionality to the process, or the process is forbidden. Put another way by Kelvin, there exist no thermodynamic processes, nor transformations, that extract heat from a reservoir and convert it entirely into work. Dissipative mechanisms, such as friction and viscosity, prevent a reduction in system entropy for any process. Processes for which the entropy change is zero,

$$dS = 0 \quad ,$$

are termed reversible, or *isentropic*, represent an idealization of physical reality. Processes in which no heat is exchanged by the system are called *adiabatic*, that is,

$$dQ = 0 \quad .$$

Combining the first and second laws, and considering mechanical work, PdV , plus all other energy exchanges, dZ ,

$$dW = PdV + dZ \quad ,$$

we see that,

$$dU = TdS - PdV - dZ$$

A useful quantity in engineering applications is the enthalpy change, dH , given by,

$$dH = PdV + VdP + dU$$

because enthalpy is often conserved ($dH = 0$) in thermodynamic transitions. Two other functions, the Gibbs free energy change, dG , and the Helmholtz free energy change, dH , are related by

$$dG = dH - SdT - TdS = VdP - SdT - dZ$$

$$dF = dU - SdT - TdS = -PdV - SdT - dZ$$

and are measures of the work done in reversible thermodynamic processes. Change in Gibbs free energy is the work done exclusive of PdV work in isothermal-isobaric processes, that is, dZ . Change in Helmholtz free energy is the total work done in isothermal processes, or $PdV + dZ$. In phase transitions, the change in Gibbs free energy is zero.

Simple energy considerations applied to the steady flow of a fluid (gas or liquid) in system able to exchange heat and do external work, such as a steam engine, refrigerator, turbine, compressor, and scuba regulator, provide a simple means to relate temperature, internal energy, kinetic and potential energy, and pressure changes to external work and heat. The simple, yet powerful, relationships detailed above can be applied to air and fluid flows in diving systems, such as regulators, compressors, tanks, hoses, and gauges to yield rough estimates of pressures, temperatures, heat, and work. Actual flow patterns can be extremely complicated, requiring numerical solution on high speed computers, especially high pressure flows.

Every substance obeys an equation of state, some fundamental relationship between pressure, temperature, and volume. That of ideal gases is a simple example. Real substances can exist in the gas phase only at sufficiently high temperatures. At low temperature and high pressures, transitions occur to the liquid and solid phases.

The Clausius-Clapeyron equation relates pressure, temperature, volume, and heat of transformation along the solid-liquid, solid-vapor, and liquid-vapor equilibration lines, according to,

$$\frac{dP}{dT} = \frac{l}{T\Delta v},$$

with l the appropriate heat of transformation, and Δv the difference in the specific phase volumes at temperature, T . The equation describes the reversible processes of condensation-vaporization, freezing-melting, and accretion-sublimation, that is, processes proceeding in either direction with the same latent heats of transformation. At the triple point, the latent heats of transformation are additive, specifically, the heat of sublimation equals the sum of the heats of vaporization and melting. For water, the heat of melting is 80 cal/g at 0 C° , while the heat of vaporization is 540 cal/g at 100 C° and standard pressure (1 atm).

Liquids tend to evaporate, or vaporize, by releasing molecules into the space above their free surfaces. If this is a confined space, the partial pressure exerted by released molecules increases until the rate at which molecules return to the liquid equals the rate at which they leave the liquid surface. At this equilibrium point, the vapor pressure is known as the saturation pressure.

Molecular evaporation increases with increasing temperature, hence the saturation pressure increases with temperature. At any one temperature, the pressure on the liquid surface may be higher than this value, but it cannot be lower. Any slight reduction below saturation pressure induces the very rapid rate of evaporation called boiling.

Saturation vapor pressures for liquids vary widely. At 70 F° , vapor pressures of mercury and gasoline differ by a factor of 10^5 approximately.

Hydrodynamics

Conservation of mass for fluid flow is written,

$$\frac{\partial \rho}{\partial t} + \nabla \cdot (\rho \mathbf{v}) = 0$$

for ρ local fluid density, and \mathbf{v} local fluid velocity. Momentum conservation is more complicated, taking the form,

$$\rho \left[\frac{\partial \mathbf{v}}{\partial t} + (\mathbf{v} \cdot \nabla) \mathbf{v} \right] = -\nabla P + \mathbf{F}$$

with pressure, P , and total force, \mathbf{F} . Finally, the energy conservation statement is,

$$\frac{\partial}{\partial t} \left[\frac{1}{2} \rho v^2 + \epsilon \right] + \nabla \cdot \left[\frac{1}{2} \rho v^2 + \epsilon \right] \mathbf{v} = W$$

with internal energy, ϵ , and external energy source, W . A relationship connecting pressure, P , internal energy, ϵ , and density, ρ , the equation of state (EOS) described earlier closes the above flow relationships, permitting exact numerical solution for arbitrary boundary conditions and flow regimes.

The above set are posed in the fixed (Eulerian) reference frame, through which the fluid moves. Another frame, moving with the fluid (Lagrangian), is often more suitable for numerical application, particularly when vortices, subscale disturbances, and turbulence are present. Flow dynamics in regulators (high speed, nozzle deflection, eddying) fall into the latter category, and numerical simulations often rely on Lagrangian analysis in the moving fluid stream. Transformation to the Lagrangian frame in the above set is most simply accomplished using the advective derivative, D/Dt , related to the Eulerian time derivative, $\partial/\partial t$, via,

$$\frac{D}{Dt} = \frac{\partial}{\partial t} + \mathbf{v} \cdot \nabla$$

as the temporal operator in the moving (Lagrangian) frame.

Electrodynamics

Electrodynamics is specifically a study of charges in motion, the associated electric and magnetic fields produced, and their interaction with, and in, matter. The fundamental entity is electrical charge, and only electrical charge, since corresponding magnetic poles have not been found to date. Electrodynamics describes moving charges and time varying fields, while electrostatics and magnetostatics are concerned with stationary charges and constant fields in time, obviously a subcase. Electrical charge is a property of matter, first observed in ancient Greece in materials we now call dielectrics. Centuries ago, it was noted that amber, upon being rubbed, attracts bits of straw and lighter objects. The Greek word for amber is electron. That electrified bodies attract and repel was noted by Cabeo in the early 1700s, while du Fay and Franklin denoted these two types of electricities, positive and negative, a convention still holding today, and established the notion that charge can be neither created nor destroyed (conservation of charge in physical processes).

Two charges, q and Q , attract (or repel) each other with force, \mathbf{F} , given by the Coulomb law,

$$\mathbf{F} = -\kappa_0 \frac{qQ}{r^3} \mathbf{r}$$

for r the distance, κ_0 the Coulomb constant ($8.91 \times 10^9 \text{ m/f}$), and \mathbf{r} the separation vector. A charge, q , moving with velocity, \mathbf{v} , through electric and magnetic fields, \mathbf{E} and \mathbf{B} , experiences a Lorentz force, \mathbf{F} , from both fields,

$$\mathbf{F} = q(\mathbf{E} + \mathbf{v} \times \mathbf{B}).$$

Maxwell's equations are four partial differential equations relating electric field, \mathbf{E} , magnetic field, \mathbf{B} , current density, \mathbf{J} , and charge density, ρ . Defining the displacement, \mathbf{D} , and magnetic intensity, \mathbf{H} ,

$$\begin{aligned} \mathbf{H} &= \frac{\mathbf{B}}{\mu} , \\ \mathbf{D} &= \epsilon \mathbf{E} , \end{aligned}$$

with ϵ and μ the material permittivity and permeability, we can write Maxwell's equations,

$$\nabla \cdot \mathbf{D} = \rho ,$$

$$\begin{aligned}\nabla \times \mathbf{E} &= -\frac{\partial \mathbf{B}}{\partial t} \ , \\ \nabla \cdot \mathbf{B} &= 0 \ , \\ \nabla \times \mathbf{H} &= \mathbf{J} + \frac{\partial \mathbf{D}}{\partial t} \ .\end{aligned}$$

The relationship between \mathbf{H} and \mathbf{B} is analogous to the relationship between \mathbf{D} and \mathbf{E} , that is, \mathbf{H} and \mathbf{D} depend only on the source of the fields, while \mathbf{B} and \mathbf{E} also depend on the local material properties. Thus, \mathbf{B} and \mathbf{E} are fundamental, but \mathbf{H} and \mathbf{D} can be easier to employ in applications.

In a conductor, with conductivity, σ , permeability, μ , and permittivity, ϵ , current density, \mathbf{J} , is linearly coupled to the electric field, \mathbf{E} , by Ohm's law,

$$\mathbf{J} = \sigma \mathbf{E} \ ,$$

serving as a corollary to Maxwell's equations. The current driving potential, V , in the conductor also satisfies the electromotive generalization of Ohm's law,

$$V = iR \ ,$$

with R the electrical resistance, and i the current. Similarly, an electrostatic potential, V , is generated when a conductor cuts through magnetic field lines, that is, the magnitude of the electromotive force is given by,

$$V = \frac{\partial \phi}{\partial t} \ ,$$

with,

$$\phi = \int \mathbf{B} \cdot d\mathbf{A} \ ,$$

and $d\mathbf{A}$ the area swept out by the conductor in cutting magnetic field lines.

Conservation of charge demands that the charge density, ρ , and current density, \mathbf{J} , are related by a continuity equation,

$$\frac{\partial \rho}{\partial t} + \nabla \cdot \mathbf{J} = 0 \ ,$$

which is just a simple statement that any increase, or decrease, in charge in a small volume must correspond to a flow of charge into, or out of, the same volume element. Electrostatics is defined by the condition,

$$\frac{\partial \rho}{\partial t} = 0 \ ,$$

while magnetostatics similarly requires,

$$\nabla \cdot \mathbf{J} = 0 \ ,$$

Magnetic materials have traditionally been considered as elements, alloys, or compounds permitting ordered arrangements, or correlations, among electron magnetic moments or spins. Net magnetic polarization can be ferromagnetic, in which all spins are aligned parallel, antiferromagnetic, in which neighboring spins are aligned antiparallel, or ferrimagnetic, in which spins of two dissimilar atoms are aligned antiparallel. Metals such as iron, cobalt, and nickel are ferromagnetic, while manganese and chromium are antiferromagnetic. The temperature necessary to induce a phase transition from an unordered magnetic state to a magnetically ordered state is the Curie temperature, whether ferromagnetic or antiferromagnetic in the final state. The permanent properties of such materials are useful in magnetic devices, such as computers and transformers.

An essential difference between electric and magnetic interactions appears in the direction of the force. The electrical force acts in the direction of motion, while the magnetic force acts normal to the direction of motion. Hence the magnetic force can only change direction of the moving charge, but cannot do work on it. Interestingly, both the Coulomb and Ampere laws exhibit an inverse square dependence on the separation of source and field point.

STATISTICS AND DATA CORRELATION

Distributions

Random variables often can be categorized by sets of statistical distributions which completely detail the properties of the variables. Distributions also permit the linkage of probability to variable occurrence, and thus connect to risk analysis.

Binomial Distribution

Decompression sickness is a hit, or no hit, situation. Statistics are binary, as in coin tossing. Probabilities of occurrence are determined from the binomial distribution, which measures the numbers of possibilities of occurrence and nonoccurrence in any number of events, given the incidence rate. Specifically, the probability, P , in a random sample of size, N , for n occurrences of decompression sickness and m nonoccurrences, takes the form,

$$P(n) = \frac{N!}{n! m!} p^n q^m ,$$

with,

$$n + m = N ,$$

p the underlying incidence rate (average number of cases of decompression sickness), and q ,

$$q = 1 - p ,$$

the underlying nonincidence. The discrete probability distributions, P , are the individual terms of the binomial expansion of $(p + q)^N$,

$$(p + q)^N = \sum_{n=0}^N P(n) = 1 .$$

In risk analysis, p and q are also the failure and success rates, gleaned, for instance, from random or strategic sampling of arbitrary lot sizes. Obviously, the larger the sample size, the better are the estimates of p or q . Once p or q is determined, the binomial statistics and probabilities are also fixed. The statistical mean, M , and variance, s , are given by,

$$M = \sum_{n=1}^N nP(n) = pN ,$$

$$s = \sum_{n=1}^N (n - M)^2 P(n) = pqN ,$$

the usual measures of a statistical distribution. The square root of the variance is the standard deviation. The cumulative probability for more than n cases of decompression sickness, $P_{>}(n)$, is written,

$$P_{>}(n) = \sum_{j=n+1}^N P(j) = 1 - \sum_{j=0}^n P(j) ,$$

and the probability of less than n cases, $P_{<}(n)$, is similarly,

$$P_{<}(n) = \sum_{j=0}^{n-1} P(j) = 1 - \sum_{j=n}^N P(j) .$$

The probability of nonoccurrence in any set of N trials is simply,

$$P(0) = q^N \quad ,$$

while the probability of total occurrence in the same number, N , of trials is given by,

$$P(N) = p^N \quad .$$

The binomial distribution is a special case of the multinomial distribution describing processes in which several results having fixed probabilities, p_l, q_l , for $l = 1, L$, are possible. Separate probabilities are given by the individual terms in the general multinomial expansion,

$$(p_1 + q_1 + \dots + p_L + q_L)^N = \sum_{n_1, \dots, n_{L-1}=0}^N P(n_1, \dots, n_{L-1}) = 1 \quad ,$$

as in the binomial case. The normal distribution is a special case of the binomial distribution when N is very large and variables are not necessarily confined to integer values. The Poisson distribution is another special case of the binomial distribution when the number of events, N , is also large, but the incidence, p , is small.

Normal Distribution

The normal distribution is an analytic approximation to the binomial distribution when N is very large, and n , the observed value (success or failure rate), is not confined to integer values, but ranges continuously,

$$-\infty \leq n \leq \infty \quad .$$

Normal distributions thus apply to continuous observables, while binomial and Poisson distributions apply to discontinuous observables. Statistical theories of errors are ordinarily based on normal distributions.

For the same mean, $M = pN$, and variance, $s = pqN$, the normal distribution, P , written as a continuously varying function of n ,

$$P(n) = \frac{1}{(2\pi s)^{1/2}} \exp[-(n - M)^2/2s] \quad ,$$

is a good approximation to the binomial distribution in the range,

$$\frac{1}{N+1} < p < \frac{N}{N+1} \quad ,$$

and within three standard deviations of the mean,

$$pN - 3(pqN)^{1/2} \leq n \leq pN + 3(pqN)^{1/2} \quad .$$

The distribution is normalized to one over the real infinite interval,

$$\int_{-\infty}^{\infty} P dn = 1 \quad .$$

The probability that a normally distributed variable, n , is less than or equal to b is,

$$P_{<}(b) = \int_{-\infty}^b P dn \quad ,$$

while the corresponding probability that n is greater than or equal to b is,

$$P_{>}(b) = \int_b^{\infty} P dn .$$

The normal distribution is extremely important in statistical theories of random variables. By the central limit theorem, the distribution of sample means of identically distributed random variables is approximately normal, regardless of the actual distribution of the individual variables.

Poisson Distribution

The Poisson distribution is a special case of the binomial distribution when N becomes large, and p is small, and certainly describes all discrete random processes whose probability of occurrence is small and constant. The Poisson distribution applies substantially to all observations made concerning the incidence of decompression sickness in diving, that is, $p \ll 1$ as the desired norm. The reduction of the binomial distribution to the Poisson distribution follows from limiting forms of terms in the binomial expansion, that is, $P(n)$.

In the limit as N becomes large, and p is much smaller than one, we have,

$$\frac{N!}{(N-n)!} = N^n ,$$

$$q^n = (1-p)^{N-n} = \exp(-pN) ,$$

and therefore the binomial probability reduces to,

$$P(n) = \frac{N^n p^n}{n!} \exp(-pN) = \frac{M^n}{n!} \exp(-M) ,$$

which is the discrete Poisson distribution. The mean, M , is given as before,

$$M = pN$$

and the variance, s , has the same value,

$$s = pN ,$$

because q is approximately one. The cumulative probabilities, $P_{>}(n)$ and $P_{<}(n)$, are the same as those defined in the binomial case, a summation over discrete variable, n . It is appropriate to employ the Poisson approximation when $p \leq .10$, and $N \geq 10$ in trials. Certainly, from a numerical point of view, the Poisson distribution is easier to use than than binomial distribution. Computation of factorials is a lesser task, and bookkeeping is minimal for the Poisson case.

In addition to the incidence of decompression sickness, the Poisson distribution describes the statistical fluctuations in such random processes as the number of cavalry soldiers kicked and killed by horses, the disintegration of atomic nuclei, the emission of light quanta by excited atoms, and the appearance of cosmic ray bursts. It also applies to most rare diseases.

Maximum Likelihood Fit

We can never measure any physical variable exactly, that is, without error. Progressively more elaborate experimental or theoretical efforts only reduce the possible error in the determination. In extracting parameter estimates from data sets, it is necessary to also try to minimize the error (or data scatter) in the extraction process. A number of techniques are available to the analyst, including the well known maximum likelihood approach.

The measure of any random occurrence, p , can be a complicated function of many parameters, $x = (x_k, k = 1, K)$, with the only constraint,

$$0 \leq p(x) \leq 1 \quad ,$$

for appropriate values of the set, x . The measure of nonoccurrence, q , is then by conservation of probability,

$$q(x) = 1 - p(x) \quad ,$$

over the same range,

$$0 \leq q(x) \leq 1 \quad .$$

Multivalued functions, $p(x)$, are often constructed, with specific form dictated by theory or observation over many trials or tests. In decompression applications, the parameters, x , may well be the bubble-nucleation rate, number of venous gas emboli, degree of supersaturation, amount of pressure reduction, volume of separated gas, ascent rate, or combinations thereof. Parameters may also be integrated in time in any sequence of events, as a global measure, though such measures are more difficult to analyze over arbitrary trial numbers.

The likelihood of any binomial outcome, Φ , of N trials is the product of individual measures of the form,

$$\Phi(n) = p^n q^m = p^n (1 - p)^m \quad ,$$

given n cases of decompression sickness and m cases without decompression sickness, and,

$$n + m = N \quad .$$

The natural logarithm of the likelihood, Ψ , is easier to use in applications, and takes the form,

$$\Psi = \ln \Phi = n \ln p + m \ln (1 - p) \quad ,$$

and is maximized when,

$$\frac{\partial \Psi}{\partial p} = 0 \quad .$$

In terms of the above, we then must have,

$$\frac{n}{p} - \frac{m}{1 - p} = 0 \quad ,$$

trivially requiring,

$$p = \frac{n}{n + m} = \frac{n}{N} \quad ,$$

$$1 - p = q = \frac{m}{n + m} = \frac{m}{N} \quad .$$

Thus, the likelihood function is maximized when p is the actual incidence rate, and q is the actual nonincidence rate. The multivalued probability functions, $p(x)$, generalize in the maximization process according to,

$$\frac{\partial \Psi}{\partial p} = \sum_{k=1}^K \frac{\partial \Psi}{\partial x_k} \frac{\partial x_k}{\partial p} = 0 \quad ,$$

satisfied when,

$$\frac{\partial \Psi}{\partial x_k} = 0 \quad \text{for } k = 1, K \quad .$$

In application, such constraints are most easily solved on computers, with analytical or numerical methods.

In dealing with a large number of decompression procedures, spanning significant range in depth, time, and environmental factors, an integrated approach to maximum likelihood and risk is necessary. Integral measures, $p(x, t)$ and $q(x, t)$, can be defined over assumed decompression risk, $\zeta(x, t)$,

$$p(x, t) = 1 - \exp \left[- \int_0^t \zeta(x, t') dt' \right] ,$$

$$q(x, t) = \exp \left[- \int_0^t \zeta(x, t') dt' \right] ,$$

with t' any convenient time scale, and ζ any assumed risk, such as bubble number, saturation, venous emboli count, etc. Employing $p(x, t)$ and $q(x, t)$ in the likelihood function, and then maximizing according to the data, permits maximum likelihood estimation of $\zeta(x, t)$. Such an approach can be employed in decompression table fabrication, yielding good statistical estimates on incidence rates as a function of exposure factors.

A simple application of maximum likelihood can be seen as follows. Suppose a table modeler wants to fit a set of decompression risk data to some 1,000 trial dives, using the temporal function, ζ ,

$$\zeta = \exp (-\chi t)$$

with χ a parameter obtained in likelihood fit. At long times, $t \rightarrow \infty$,

$$p = 1 - \exp \left[- \int_0^\infty \exp (-\chi t' dt') \right] = 1 - \exp (-1/\chi)$$

$$q = 1 - p$$

Suppose there are x cases of decompression sickness (DCS), and y cases of nonincidence,

$$x + y = 1000$$

so the logarithmic likelihood function takes the form,

$$\Psi = x \ln [1 - \exp (-1/\chi)] + y \ln [\exp (-1/\chi)]$$

The maximization condition requires,

$$\frac{\partial \Psi}{\partial \chi} = \left[\frac{-x \exp (-1/\chi)}{\chi^2 (1 - \exp (-1/\chi))} \right] + \left[\frac{y \exp (-1/\chi)}{\chi^2 \exp (-1/\chi)} \right] = 0$$

so that,

$$\exp (-1/\chi) = (y/1000)$$

and,

$$\chi = - \frac{1}{\ln (y/1000)}$$

The above exercise is rather simple, and amenable to analytic quadratures. In most diving applications, however, the risk function is multivalued in fit space, and the data sets are very large in time. Time cutoffs, t , usually span 18 - 24 hours after the dive has ended. And large scale computer analysis is requisite for maximum likelihood folding with risk analysis.

Nonlinear Least Squares Fit

The nonlinear least squares method is similar to the maximum likelihood method, attempting to fit an arbitrary function to a set of data points by minimizing the variance between fitted and actual data points.

For Haldane computational algorithms, the process of constructing closed sets of time limits, tissue halftimes, and limiting tensions becomes an important activity. We detail a method for this closure, applying the approach to some exposure relationships. The approach maximizes the tissue perfusion equation, subject to a depth-time law (theoretical, fitted, inferred, or otherwise) at the exposure time limit, coupling exposure limits, halftimes, depths, and maximum tensions in the process.

Dissolved gas models limit tissue supersaturation, assuming that gas exchange is controlled by perfusion or diffusion in blood-tissue media. A perfusion equation quantifies bulk gas transfer,

$$\frac{\partial(p - p_a)}{\partial t} = -\lambda(p - p_a),$$

with the exchange of inert gas driven by the local gradient, that is, the difference between arterial blood, p_a , and local tissue tension, p . Obviously the exchange process is very complicated, and models are only approximate. The solutions are well known, simple classes of exponential functions, bounded by arterial and initial tissue tensions, p_a and p_i ,

$$(p - p_a) = (p_i - p_a) \exp(-\lambda t),$$

with λ the decay rate, defined in terms of the halftime, τ ,

$$\lambda = \frac{0.693}{\tau}$$

with instantaneous tissue tension, p , in that compartment. Compartments with 2, 5, 10, 20, 40, 80, 120, 240, 360, 480, and 720 minute halftimes, τ , are employed in applications, and halftimes are assumed to be independent of pressure.

Next, algorithms limit degrees of dissolved gas buildup, p , hypothetical absolute compartment supersaturation, by critical values, M , such that,

$$p \leq M,$$

across all compartments at all times during exposure, and upon surfacing. Equivalently, critical ratios, R , and critical gradients, G are also employed, with,

$$R = \frac{M}{P},$$

$$G = M - P,$$

for ambient pressure, P . Critical parameters evolved from self consistent application of assumed tissue response functions to sets of exposure data, that is, trial and error bootstrapping of model equations to observed exposure time limits. Newer compilations ultimately extend older ones to extended data ranges.

In a bulk diffusion framework, nonstop air limits, t_n , roughly satisfy a global transfer law ,

$$dt_n^{1/2} = 465 \text{ fsw min}^{1/2},$$

at depth, d (Hempleman *square root* law), generalized by writing,

$$dt^a = b,$$

for a and b some constants. Ranges subtended today in tables and meters include:

$$0.25 \leq a \leq 0.65,$$

$$250 \text{ fsw min}^a \leq b \leq 500 \text{ fsw min}^a,$$

Certainly the functional form can be generalized and refined,

$$d(t + c)^a = b$$

with a , b , and c constants fitted in least squares methodology. and applied to virtually any gas mixture. This has been done for the RGBM Tables released by NAUI Technical Training.

A separated phase model for nonstop air diving suggests,

$$\delta d (t_n + 1/\lambda) = 8750 \text{ fsw min},$$

for number factor, δ , collectively representing bubble seeds excited by compression-decompression, that is, from surface pressure, P_0 , to ambient pressure, P , and back to P_0 ,

$$\delta = \frac{P}{P_0} - 1.$$

The phase law generalizes obviously to,

$$\delta d (t + 1/\lambda)^a = \frac{d^2}{P_0 + d} (t + 1/\lambda)^a = b,$$

with,

$$P = P_0 + \eta d.$$

The depth-time law and tissue equation present a minimax problem, here, maximization of the tissue equation at depth subject to the constraint of the depth-time law. The standard approach sets the depth derivative of the tissue equation (tension) to zero at the exposure time limit, under the primary constraint of the depth-time equation. First writing ambient gas partial pressure, p_a , as

$$p_a = p_0 + f d,$$

for surface partial pressure, p_0 , mole fraction, f , and then differentiating tension, p , with respect to depth, d , we find in general,

$$\frac{\partial p}{\partial d} = f - f \exp(-\lambda t) + (p_0 + f d - p_i)\lambda \exp(-\lambda t) \frac{\partial t}{\partial d} = 0,$$

as the maximization condition. The time derivative with respect to depth, $\partial t/\partial d$, is evaluated from the assumed exposure law (theoretical, fitted, inferred), and then inserted above. The resulting expression couples halftime, τ , to exposure limit, t_n , and the value of the tissue tension at those values is the (maximized) critical tension, M_0 .

Early table and meter algorithms rested on (Haldane) dissolved gas treatments to schedule diving, with square root-like nonstop limits folded into a multitissue perfusion framework. So, as example, consider the bulk relationship, so that,

$$\frac{\partial t}{\partial d} = -\frac{t}{ad}.$$

Setting $p_i = p_0$, substituting the derivative, and maximizing at the nonstop limit, t_n , there results,

$$1 - \exp(-\lambda t_n) - \frac{\lambda t_n}{a} \exp(-\lambda t_n) = 0.$$

At nonstop time, $t = t_n$, the tissue tension is maximized, that is, $p = M_0$, so that,

$$M_0 = p_a + (p_i - p_a) \frac{a}{a + \lambda t_n}.$$

The maximization condition links λ and t_n together, while M_0 falls out of the tissue equation. The quantity λt_n is pivotal to the solution. Table 1 gives thumbnail solutions to,

$$\exp(x) = 1 + \frac{x}{a},$$

for a , as function of dimensionless parameter, $x = \lambda t_n$,

Table 1. Maximization Parameters.

a	$1/a$	x
.157	6.37	3.00
.323	3.09	2.00
.435	2.29	1.50
.455	2.20	1.40
.488	2.05	1.30
.500	2.00	1.25
.517	1.93	1.20
.549	1.82	1.10
.581	1.72	1.00
.771	1.29	0.50
.951	1.05	0.10
1.00	1.00	0.00

In the separated phase model, we have differentiating,

$$\frac{\partial t}{\partial d} = -\frac{2(t + 1/\lambda)}{ad},$$

so that,

$$1 - \exp(-\lambda t_n) - \frac{2(\lambda t_n + 1)}{a} \exp(-\lambda t_n) = 0,$$

as the maximization constraint. Or, equivalently, one needs,

$$\exp(y) = 1 + \frac{2(y + 1)}{a},$$

with $y = \lambda t_n$. Then, the critical tension, M_0 , is given by,

$$M_0 = p_a + (p_i - p_a) \frac{a}{a + 2(\lambda t_n + 1)}$$

The procedures for constructing a consistent set can be summarized as follows;

1. First, from experiment, wet or dry tests, Doppler, or otherwise, a set of nonstop time limits, t_n , at depth, d , is obtained;

2. Next, the set is fitted to the two parameter power law given above, and the constants a and b determined;
3. Then, with a and b determined, the controlling halftime, τ , is obtained from t_n at d ;
4. Finally, from τ , t_n , d , and a , the critical tension, M_0 , is extracted, closing the whole set;
5. Compute and recalibrate parameters against a set of test profiles, data, or exposure information.

The set a , b , τ , d , t_n , x , y , and M_0 then close self consistently when derived according to the above set of equations and constraints.

Results for some air limits are summarized in Table 2, using nonlinear least squares (NLLS) in fitting t_n to the depth-time relationship, with usual L_2 error norm, the square root of the sum of the squares of the differences in the fit. The labels RGBM, DCIEM, ZHL, Spencer, and USN refer to nonstop time limits for models discussed in the following text.

Table 2. Fits, Limits, Halftimes, And Critical Tensions.

	RGBM	DCIEM	ZHL	Spencer	USN
Fit Parameters					
a	.94	.48	.46	.39	.41
$b(fsw\ min^a)$	6119	362	385	290	355
x	1.40	1.34	1.39	1.65	1.58
y	2.00	1.08	1.65	1.16	1.57
$L_2(fsw)$	12.8	57.7	62.3	85.5	56.5
Nonstop Limits $t_n(min)$					
$d(fsw)$					
30	200	150	290	225	
40	110	90	125	135	200
50	70	70	75	75	100
60	50	50	54	50	60
70	35	35	38	40	50
80	26	25	26	30	40
90	20	20	20	25	30
100	16	15	20	20	25
110	13	12	17	15	20
120	11	10	15	10	15
130	9	8	11	5	10
Halftimes $\tau(min)$ /Critical Tensions $M_0(fsw)$					
$d(fsw)$					
30	69/46	98/44	122/45	134/45	178/45
40	38/53	53/49	68/51	60/52	88/52
50	24/60	33/55	42/57	37/58	52/57
60	17/67	22/61	28/63	23/64	33/64
70	12/74	17/67	20/69	16/71	23/69
80	9/79	12/73	15/73	11/77	16/76
90	7/87	10/87	12/82	8/84	12/83
100	6/94	8/85	9/88	7/90	10/89
110	5/101	6/91	8/84	6/96	8/95
120	4/108	5/96	6/100	4/103	6/101
130	3/114	4/102	5/106	3/109	5/107

The structure and range above is interesting. Surfacing critical tensions, M_0 , and tissue halftimes, τ , are bounded,

$$44 \text{ fsw} \leq M_0 \leq 114 \text{ fsw}$$

$$3 \text{ min} \leq \tau \leq 178 \text{ min}$$

with the DCIEM, ZHL, Spencer, and USN (all Haldane models) exhibiting roughly similar parameter clustering, but with the RGBM (phase model) rather different from the rest. And all said with nonstop time limits, t_n , pretty much the same across all models. In diving practice, this is just another manifestation of differences between dissolved gas (Haldane) and phase (RGBM) models. As will be seen, deeper stops and overall shorter decompression times are the result.

PHASE MECHANICS AND DECOMPRESSION THEORY IN DEPTH
CHAPTER 1: NUCLEATION PROCESSES

Quiescent Nucleation

Henry's law tells us that a gas will tend to separate from solution (pass from the dissolved state to the free state) if the tension of the gas in the dissolved state exceeds its partial pressure in the adjacent free state. And the opposite holds true if the gradient is reversed. Phase separation can be delayed if some remnant of a free phase does not already exist in the liquid, providing a pathway for the dissolved gas to *dump* over into the free state, rendering the dissolved gas *metastable* during the delay. The challenge in tracking phase separation is the presence and quantification of free phase precursors, or seeds, that facilitate gas transfer in a process called *nucleation*.

Metastable states are unstable thermodynamic states lying close to stable configurations, that is, separated by relatively small energy differences. A substance in a metastable state will eventually transition into a stable state. For instance, a supercooled vapor will eventually condense into a liquid, a supercooled liquid will eventually become solid, and a superheated liquid will eventually evaporate into a gas. Bubble formation can be a process in which a gas, or vapor, phase is initially formed from a metastable liquid environment, one that is usually supersaturated with dissolved gas.

Metastable phase transitions deposit an unstable phase onto a stable phase, with aggregates in the stable phase serving as *nuclei* for the transition. Liquid drops in a supercooled vapor, if sufficiently large, become centers of condensation of the vapor, for example. Nuclei will form in both phases because of statistical fluctuations, but the nuclei in the metastable phase will disappear in time, while those in the stable phase will remain. Such nuclei form statistically as a result of thermal fluctuations in the interior of the media, with a certain (small) number reaching *critical* radius for growth. If large enough, nuclei in the stable phase seed the continuing process of phase transitions from the metastable state. For each metastable state, there is a minimum size which nuclei in the stable phase must possess to afford more stability than the metastable state. This size is called the critical radius, r_c . Nuclei smaller than the critical radius will not support phase transitions from the metastable state, and will also disappear in time. In assigning a critical radius to nuclei, spherical aggregate symmetry is assumed, and is requisite to minimize surface energy.

Homogeneous nucleation processes occur in single component systems, while heterogeneous nucleation processes involve more than one component. To describe nucleation, a heterogeneous model, ascribed to Plesset, containing the homogeneous case as a subset, has been useful in applications. A solid hydrophobic sphere, of radius r_0 , is surrounded by a concentric layer of vapor, out to a radius r . The instantaneous (Boltzmann) probability, dw , for the state depends on the difference in free energy, ζ , associated with the vapor phase,

$$dw = \exp(-\zeta/kT) dG \quad ,$$

at temperature, T , for (Gibbs) free energy change, ζ ,

$$\zeta = \frac{4}{3}\pi r^2 \gamma_{lv} + \frac{4}{3}\pi r_0^2 (\gamma_{vs} - \gamma_{ls}) \quad ,$$

and γ_{lv} , γ_{vs} , and γ_{ls} surface tensions associated with the liquid-vapor, vapor-solid, and liquid-solid interfaces. The homogeneous case corresponds to $r_0 = 0$, that is, no solid and only liquid-vapor nucleation.

Tensions, pulling parallel to their respective surfaces, at equilibrium have zero net component,

$$\gamma_{lv} \cos\theta = \gamma_{vs} - \gamma_{ls} \quad ,$$

with liquid-vapor contact angle, θ , measured through the liquid. Wetted (hydrophilic) solids exhibit acute contact angle, occurring when,

$$\gamma_{vs} - \gamma_{ls} > 0 \quad ,$$

so that the meniscus of the liquid phase is concave. In this case, the solid has greater adhesion for the liquid than the liquid has cohesion for itself, the free energy required to maintain the vapor phase is large (because the solid surface tension term is positive), and the probability of nucleation is decreased by the solid impurity. For a nonwetting (hydrophobic) solid, the situation is reversed, that is, the contact angle is obtuse,

$$\gamma_{vs} - \gamma_{ls} < 0 \quad ,$$

the meniscus is convex, the solid has less adhesion for the liquid than the liquid has cohesion for itself, the free energy is reduced because the solid surface tension term is negative, and the probability of formation is increased. In the limiting case, $\cos \theta = -1$, the free energy is given by,

$$\zeta = \frac{4}{3} \pi \gamma_{lv} (r^2 - r_0^2) \quad ,$$

which becomes small for cavity radius, r , near impurity radius, r_0 .

While theories of heterogeneous and homogeneous nucleation work well for a number of liquids, the application of the heterogeneous model to water with impurities is not able to reduce the tensile strength to observable values. The homogeneous theory of nucleation predicts a tensile strength of water near 1,400 *atm*, the heterogeneous theory, with a variety of solid impurities, drops the tensile strength down to 1,000 *atm*, and the measured value for water is approximately 270 *atm*.

In any solution, gas nuclei can be deactivated (crushed) by the application of large hydrostatic pressures. The process of *crushing* is also termed *denucleation*. When denucleated solutions are decompressed in supersaturated states, much higher degrees of supersaturation are requisite to induce bubble formation. In diving, denucleation has been suggested as a mechanism for acclimatization. If denucleation is size selective, that is, greater hydrostatic pressures crush smaller and smaller nuclei, and if number distributions of nuclei increase with decreasing radius (suggested by some experiments), then a conservative deep dive, followed by sufficient surface interval, should in principle afford a margin of safety, by effectively crushing many nuclei and reducing the numbers of nuclei potentially excited into growth under compression-decompression.

The mechanisms of nucleation in the body are obscure. Though nucleation most probably is the precursor to bubble growth, formation and persistence time scales, sites, and size distributions of nuclei remain open questions. Given the complexity and number of substances maintained in tissues and blood, heterogeneous nucleation would appear a probable mechanism.

Tribonucleation

Cavitation

Simply, *cavitation* is the process of vapor phase formation of a liquid when pressure is reduced. A liquid cavitates when vapor bubbles are formed and observed to grow as consequence of pressure reduction. When the phase transition results from pressure change in hydrodynamic flow, a two phase stream consisting of vapor and liquid results, called a cavitating flow. The addition of heat, or heat transfer in a fluid, may also produce cavitation nuclei in the process called boiling. From the physico-chemical perspective, cavitation by pressure reduction and cavitation by heat addition represent the same phenomena, vapor formation and bubble growth in the presence of seed nuclei. Depending on the rate and magnitude of pressure reduction, a bubble may grow slowly or rapidly. A

bubble that grows very rapidly (explosively) contains the vapor phase of the liquid mostly, because the diffusion time is too short for any significant increase in entrained gas volume. The process is called vaporous cavitation, and depends on evaporation of liquid into the bubble. A bubble may also grow more slowly by diffusion of gas into the nucleus, and contain mostly a gas component. In this case, the liquid degasses in what is called gaseous cavitation, the mode observed in the application of ultrasound signals to the liquid. For vaporous cavitation to occur, pressure drops below vapor pressure are requisite. For gaseous cavitation to occur, pressure drops may be less than, or greater than, vapor pressure, depending on nuclei size and degree of liquid saturation. In supersaturated ocean surfaces, for instance, vaporous cavitation occurs very nearly vapor pressure, while gaseous cavitation occurs above vapor pressure.

In gaseous cavitation processes, the inception of growth in nuclei depends little on the duration of the pressure reduction, but the maximum size of the bubble produced does depend upon the time of pressure reduction. In most applications, the maximum size depends only slightly on the initial size of the seed nucleus. Under vaporous cavitation, the maximum size of the bubble produced is essentially independent of the dissolved gas content of the liquid. This obviously suggests different cavitation mechanisms for pressure (reduction) related bubble trauma in diving. Slowly developing bubble problems, such as limb bends many hours after exposure, might be linked to gaseous cavitation mechanisms, while rapid bubble problems, like central nervous system hits and embolism immediately after surfacing, might link to vaporous cavitation.

In a flowing fluid (or body moving through a stationary liquid), the cavitation number, κ , is an indication of the degree of cavitation, or the tendency to cavitate. Describing the similarity in the liquid-gas system, the cavitation number relates gas pressure, p , to absolute pressure, P , through,

$$\kappa = 2 \frac{P - p}{\rho u^2}$$

with ρ and u the fluid density and velocity. Cavitation and cavitating flows have long been of interest in shipbuilding and hydraulic machinery, underwater signal processing, propellor design, underwater detection, material damage, chemical processing, high pressure and temperature flows in nuclear reactors, volatility of rocket fuels, and bubble chambers for detection of high energy particles, to list a few. Cavitation processes in flowing blood and nearby tissue are also of considerable interest to decompression modelers and table designers.

Today we know that the inception of cavitation in liquids involves the growth of submicroscopic nuclei containing vapor, gas, or both, which are present within the liquid, in crevices, on suspended matter or impurities, or on bounding layers. The need for cavitating nuclei at vapor pressures is well established in the laboratory. There is some difficulty, however, in accounting for their presence and persistence. For a given difference between ambient and gas-vapor pressure, only one radius is stable. Changes in ambient, gas, or vapor pressures will cause the nuclei to either grow, or contract. But even if stable hydrostatically, bubbles and nuclei, because of constricting surface tension, will eventually collapse as gas and vapor diffuse out of the assembly. For instance, an air bubble of radius 10^{-3} cm will dissolve in saturated water in about 6 sec, and even faster if the water is undersaturated or the bubble is smaller. In saturated solutions, bubbles will grow by diffusion, and then tend to be quickly lost at free surfaces as buoyant forces raise them up. A 10^{-2} cm air bubble rises at the rate of 1.5 cm/sec in water. If nuclei are to persist in water, or for that matter, any liquid media, some mechanism must prevent their dissolution or buoyant exit.

A number of possibilities have been suggested to account for the presence of persistent, or stabilized, nuclei in undersaturated liquids, liquids that have been boiled, or denucleated. Crevices in the liquid, or surrounding boundary, may exert mechanical pressure on gas nuclei, holding them in place. Microscopic dust, or other impurities, on which gas and vapor are deposited, are stabilized already. Surface activated molecules, (such as hydrogen and hydroxyl ions in water), or surface activated skins formed from impurities may surround the nuclei and act as rigid spheres, offsetting constrictive

surface tension, preventing diffusion of gas out of the nuclei and collapse. In all cases, the end result is a family, or group of families, of persistent nuclei. Time scales for stabilization and persistence of nuclei would obviously equate to the strength and persistence of stabilizing mechanism. Experimentally, trying to differentiate stabilization modes is very difficult, because (eventual) growth patterns of nuclei are the same in all cases. The ultimate crumbling of surrounding shells, release of crevice mechanical pressure, removal of dust and impurity nucleation centers, and deactivation of surface chemicals leads to the onset of cavitation and bubble growth.

Gas Turbulent Nucleation

Chemical Nucleation

Ensemble Theory

PHASE MECHANICS AND DECOMPRESSION THEORY IN DEPTH
CHAPTER 2: MATERIAL PROPERTIES

Gases

Air is a mixture of inert and metabolic gases, composed of hydrogen and oxygen mainly, with variable amounts of carbon dioxide, water vapor, ozone, sulfur dioxide, and nitrogen dioxide, and fixed trace amounts of xenon, helium, krypton, argon, methane, nitrous oxide, hydrogen, and neon. By volume, air is 78.1% nitrogen, 20.9% oxygen, and 1% everything else. Over nominal pressure and temperature ranges encountered in the Earth's atmosphere, air can be treated as an *ideal*, or dilute, gas.

Ideal gas molecules occupy no space, do not interact, scatter elastically from each other, and cannot be distorted upon collision, in short, act as vanishingly small, perfectly elastic, hard spheres in constant random motion from collisions. Real gases, in the limit of very large confining volumes, all behave like ideal gases, as well as over select ranges of pressure, temperature, and density. Simple monatomic (one atom molecules) and diatomic (two atom molecules) gases and mixtures, such as air, at room temperatures and atmospheric pressures are considered ideal, and satisfy an equation of state (EOS) linking pressure P , volume, V , and and temperature, T , of the form,

$$PV = nRT$$

with n the number of moles of gas, and R the universal gas constant (8.317 *joule/mole* – K°). Temperature is measured in absolute, or Kelvin (K°), units. In conservative processes, n is constant and changes in the state variables, P , V , and T , are linked to each other by the P – V – T relationship. If each variable is alternatively held fixed, we get three, well known, ideal gas law corollaries,

$$PV = \gamma_T \quad (\text{Boyle's law}) \quad ,$$

$$\frac{P}{T} = \gamma_V \quad (\text{Amonton's law}) \quad ,$$

$$\frac{V}{T} = \gamma_P \quad (\text{Charles' law}) \quad ,$$

with $\gamma_T = nRT$, $\gamma_V = nR/V$, and $\gamma_P = nR/P$ all constant. The relationships connect any number of arbitrary changes of state for constant temperature, volume, or pressure, respectively. In a mixture of ideal gases, the total pressure is the sum of component gas partial pressures, intuitively obvious, but also known as Dalton's law. Denoting gas partial pressures, p , the total pressure, P , is given by,

$$P = \sum_{j=1}^J p_j \quad ,$$

with p_j the partial pressure of the j^{th} gas species in a J component mixture.

Temperatures, which really measure average kinetic energy of gas molecules in the ensemble, are measured in Centigrade (C°), Fahrenheit (F°), Kelvin (K°), and Rankine (R°) degree units, related by,

$$F^\circ = \frac{9}{5}C^\circ + 32 \quad ,$$

$$K^\circ = C^\circ + 273 \quad ,$$

$$R^\circ = F^\circ + 460 \quad .$$

All gas molecules occupy space, exert short ranged forces on each other, scatter inelastically at times, and possibly distort with collision, in short, act as nonideal gas molecules. Then equations-of-state need include such effects, particularly in appropriate pressure, temperature, and density regimes. The most general form of the equation of state can be cast in *virial* form, in terms of the molal specific volume, v ,

$$v = \frac{V}{n}$$

for n the number of moles,

$$Pv = RT \left[1 + \frac{a}{v} + \frac{b}{v^2} + \frac{c}{v^3} + \dots \right] ,$$

with a, b, c functions mostly of temperature, possibly specific volume. For ideal gases, $a = b = c = 0$, but in general these virial constants are nonzero. Certainly as the specific volume, v , or real volume, V , gets large, the virial expansion collapses to the ideal case. The virial expansion and coefficients can be fitted to sets of experimental data for gases. Such fits to even very complicated gas behavior all have one feature in common. The quantity, pv/T , always approaches the universal gas constant, R , as temperature, T , approaches absolute zero (-273 C° or -460 F°).

Clausius suggested that the volume, V , available to a single gas molecule be reduced by the actual volume occupied by all other molecules in the assembly, as shown in Figure 1. Accordingly, a correction factor, b , enters the ideal gas law through the simple relationship,

$$P(v - b) = RT$$

yielding the Clausius equation of state. Van der Waals, in 1873, suggested a second correction term, accounting for forces between molecules, a , be added to the ideal equation of state,

$$(P + a/v^2)(v - b) = RT$$

giving the van der Waals relationship. Both a and b are functions of temperature, T , and not simple constants. As $a, b \rightarrow 0$, the van der Waals and Clausius equations go over to the ideal gas limit.

The van der Waals equation can be put in virial form by first rewriting,

$$Pv = RT \left[1 - \frac{b}{v} \right]^{-1} - \frac{a}{v}$$

and then using the binomial expansion,

$$\left[1 - \frac{b}{v} \right]^{-1} \approx 1 + \frac{b}{v} + \frac{b^2}{v^2} +$$

so that,

$$Pv = RT + \frac{RTb - a}{v} + \frac{RTb^2}{v^2} +$$

The Beattie-Bridgman equation is a modified virial equation which fits the experimental data over a wide range of pressure, volume, and temperature,

$$Pv = \frac{RT(1 - \delta/vT^3)}{v}(v + \beta) - \frac{a}{v}$$

for α, β , and δ slowly varying (temperature) constants. The van der Waals gas law permits two degrees of freedom (a, b), while the Beattie-Bridgman equation is more flexible, admitting three degrees of freedom (α, β, δ), in fitting experimental data.

Solids

Fluids

Compressibility And Cubical Expansion

Under pressure and temperature changes, all matter undergoes expansion or compression. The coefficient of volume change, κ , under pressure change, at constant temperature, T , is called the *isothermal* compressibility,

$$\kappa = -\frac{1}{V} \left[\frac{\partial V}{\partial P} \right]_T ,$$

and the coefficient of cubical expansion, β , measures the volume change under temperature change, at constant pressure,

$$\beta = \frac{1}{V} \left[\frac{\partial V}{\partial T} \right]_P ,$$

and these quantities can certainly be measured experimentally for any material. The corresponding thermal coefficient, ζ , measures change of pressure, P , with temperature, T , at constant volume, V , and is simply related to κ and β through,

$$\zeta = \left[\frac{\partial P}{\partial T} \right]_V = - \left[\frac{\partial V}{\partial T} \right]_P \left[\frac{\partial V}{\partial P} \right]_T^{-1} = \frac{\beta}{\kappa} .$$

For solids and liquids, β , κ , and ζ are very small, virtually constant over small ranges of temperature and pressure. For gases, the situation is different. Ideal gases, from the equation of state, simply have,

$$\kappa = \frac{1}{P} ,$$

$$\beta = \frac{1}{T} ,$$

so that compressibility and expansion coefficients depend inversely on pressure, P , and temperature, T . The thermal coefficient is similarly given by,

$$\zeta = \frac{P}{T} = \frac{nR}{v} .$$

Time Scales

We know from Doppler measurements in the body and laboratory experiments with bubbles that micronuclei and bubbles have finite lifetimes, ranging from minutes to hours. Seeds and bubbles are transients in all environments, but with virtually intractable time evolution in the body.

Bubble Metrics

During rapid compression from initial ambient pressure, P_i , to increased pressure, P , seeds and micronuclei are subjected to crushing compression which decreases radial size. This produces increased tolerance to supersaturation in blood and tissues since smaller nuclei form macroscopic (unstable) bubbles less readily than larger ones. The greater the crushing pressure, $\Delta P = P - P_i$, the greater the supersaturation required to excite a given number of bubbles in the body. A given

distribution of nuclei in the body has, for each ΔP , a critical radius, r_i . Nuclei with radii less than r_i will not grow into bubbles, while nuclei with radii greater than r_i will be excited into growth. Said another way, all nuclei larger than r_i for any compression-decompression schedule, ΔP , will evolve into macroscopic bubbles while the rest will not. But just how excited micronuclei grow requires a model for the behavior of effective surface tension under compression-decompression, as described earlier. The model can be based on an equation-of-state (EOS), or tied to data fits of *observed* bubble behavior in appropriate media. And the model does not necessarily depend upon the actual number distribution of seeds as a function of size (radius), though an exponential distribution is usually employed or inferred.

Certainly we do not know the exact physical properties of gas seeds and bubbles in the body, but we can make some general comments based on known equation of state relationships. Phenomenological relationships fitted from laboratory experiments are also of interest.

Material Response

Under changes in ambient pressure (and temperature), bubbles will grow or contract, both due to dissolved gas diffusion and Boyle's law. An *ideal* change under Boyle's law is symbolically written. Denoting initial and final pressures and volumes with subscripts, i and f , we have,

$$P_i V_i = P_f V_f$$

with bubble volume,

$$V = \frac{4}{3}\pi r^3$$

for r the bubble radius. The above supposes totally flexible (almost ideal gas) bubble films or skins on the inside, certainly not unrealistic for thin skin bubbles. Similarly, if the response to small incremental pressure changes of the bubble skins is a smooth and slowly varying function, the above is also true in low order. Obviously, the relationship reduces to,

$$P_i r_i^3 = P_f r_f^3$$

for a ideal radial response to pressure change.

But for real structured, molecular membranes, capable of offsetting constrictive surface tension, the response to Boyle's law is modified, and can be cast in terms of Boyle modifiers, ξ ,

$$\xi_i P_i V_i = \xi_f P_f V_f$$

with ξ virial functions depending on P , V , and T . For thin and elastic bubble skins, $\xi = 1$. For all else, $\xi \neq 1$. For gels studied in the laboratory, as an instance, surfactant stabilized micronuclei do not behave like ideal gas seeds with thin elastic films. Instead under compression-decompression, their behavior is always less than ideal. That is to say, volume changes under compression or decompression are always less than computed by Boyle's law, similar to the response of a wetsuit, sponge, tissue bed, or lung membrane. The growth or contraction of seeds according to an EOS is more complex than Boyle's law. The virial expansions has for all P , T , V and mole fractions, n , for R the universal gas constant,

$$PV = nRT \sum_{i=0}^N \alpha_i \left[\frac{nT}{V} \right]^i$$

or, treating the virial expansion as a Boyle modifier, ξ ,

$$\xi PV = nRT$$

across data points and regions. Symbolically, the radius, r , can be cast,

$$r = \sum_{i=0}^N \beta_i \left[\frac{nRT}{P} \right]^{i/3}$$

or, again introducing Boyle modifiers, ζ ,

$$\zeta r = \left[\frac{nRT}{P} \right]^{1/3}$$

for α and β standard virial constants. Obviously, the virial modifiers, ξ and ζ are the inverses of the virial sum expansions as power series. For small deviations from thin film bubble structures, both are close to one.

Permeability Response

Observationally, though, the parameterization can take a different tack. In gel experiments, the EOS is replaced by two regions, the permeable (simple gas diffusion across the bubble interface) and impermeable (rather restricted gas diffusion across the bubble interface). In the permeable region, seeds act like thin film bubbles for gas transfer. In the impermeable region, seeds might be likened to beebes. An EOS of course can recover this response in both limits.

Accordingly, just in gels, the corresponding change in critical radius, r , following compression, $(P - P_i)$, in the *permeable* region, satisfies a relationship,

$$(P - P_i) = 2(\gamma_c - \gamma) \left[\frac{1}{r} - \frac{1}{r_i} \right]$$

with γ_c maximum compressional strength of the surfactant skin, γ the surface tension, and r_i the critical radius at P_i . When P exceeds the structure breakpoint, P_c , an equation for the *impermeable* region must be used. For crushing pressure differential, $(P - P_i)_c = P - P_c$, the gel model requires,

$$(P - P_i)_c = 2(\gamma_c - \gamma) \left[\frac{1}{r} - \frac{1}{r_c} \right] + P_c + 2P_i + P_i \left[\frac{r_c}{r} \right]^3$$

where,

$$r_c = \left[\frac{P_c - P_i}{2(\gamma_c - \gamma)} + \frac{1}{r_i} \right]^{-1}$$

is the radius of the critical nucleus at the onset of impermeability, obtained by replacing P and r with P_c and r_c above.

The allowed tissue supersaturation, $\Delta\Pi$, is given by,

$$\Delta\Pi = 2 \frac{\gamma}{\gamma_c r} (\gamma_c - \gamma)$$

with, in the permeable region,

$$r = \left[\frac{(P - P_i)}{2(\gamma_c - \gamma)} + \frac{1}{r_i} \right]^{-1}$$

and, in the impermeable region,

$$r^3 - 2(\gamma_c - \gamma)r^2 - \frac{P_i}{\zeta} r^3 = 0$$

for,

$$\zeta = (P - P_i)_c - P_c + 2P_i + \frac{2(\gamma_c - \gamma)}{r_c}$$

Thus, allowed supersaturation is a function of three parameters, γ , γ_c , and r_i . They can be fitted to exposures and lab data. But Boyle expansion or contraction needs be applied ad hoc to the excited seeds. Additionally, nuclei generate over times scales, ω , such that,

$$r = r_0 + [1 - \exp(-\omega t)](r_i - r_0)$$

with r_0 . the critical radius at initial time ($t = 0$). The fourth parameter, ω^{-1} , is on the order of many days (Chapter 4).

Discontinuities in types of materials and/or densities at surfaces and interfaces give rise to interfacial forces, called *surface tension*. Discontinuities in density produce cohesive gradients tending to diminish density at the surface region. At the interfaces between immiscible materials, cohesive forces produce surface tension, but adhesional forces between dissimilar materials tend to offset (decrease) the interfacial tension. Surface and interfacial tension are readily observed in fluids, but less readily in solids. In solids, very little stretching of the surface region can occur if the solids are rigid. Upon heating rigid solids to higher temperature, surface tension becomes a discernible effect.

Any two phases in equilibrium are separated by a surface of contact, the existence of which also produces surface tension. The thin contact region is a transition layer, sometimes called the *film* layer. Phases can be solid, liquid, or vapor, with surface tension in each case different. The actual position, or displacement, of the phase boundary may alter the area of the phases on either side, leading to pressure differences in the phases. The difference between phase pressures is known as the surface, or film, pressure. The phase equilibration condition requires the temperatures and chemical potentials (Gibbs free energy) of phases be equal, but certainly not the pressures.

A simple description of measurable surface tension, γ , is linked to the magnitude of cohesive forces in materials a and b , denoted, χ_a and χ_b , wanting to pull the surfaces together, and the adhesional forces, α_a and α_b , wanting to draw the surfaces apart. The net surface tension, γ , is the sum of cohesive forces minus adhesive forces, that is,

$$\gamma = \chi_a + \chi_b - \alpha_a - \alpha_b \quad .$$

Thermodynamically, surface tension contributes a differential work term, $d\omega$, to system balance equations given in terms of surface contact area, dA ,

$$d\omega = \gamma dA \quad ,$$

Surface tension pressure, τ , is surface tension force per unit area, that is, in terms of work function, ω ,

$$\tau = - \left[\frac{\partial \omega}{\partial V} \right]_{S,T} \quad ,$$

at constant entropy, S , and temperature, T . Interfacial tension in liquids is measured by the pressure difference across surfaces, again denoted a and b ,

$$\tau = \gamma \left[\frac{1}{r_a} + \frac{1}{r_b} \right] \quad ,$$

given radii of curvature, r_a and r_b . For thin films, such as bubbles, $r_a \approx r_b = r$, and we see,

$$\tau_{bub} = \frac{2\gamma}{r} \quad ,$$

deduced by Young and Laplace almost two centuries past. For water, $\gamma = 50 \text{ dyne cm}$, while for watery tissue, $\gamma = 18 \text{ dyne cm}$.

The surface of all solids and liquids adsorb foreign molecules from their surroundings. These adsorbed molecules change most of the chemical and physical properties of the underlying substrate. Adhesion, catalysis, corrosion, fracture, lubrication, and wear are affected by the topmost molecular layers on a surface. Understanding these changes involves close study of films themselves, as described. The forces of attraction that cause adsorption are relatively weak and are the long range interactions existing between all atoms and molecules.

Water, gasoline, glycerin, and salad oil are clearly liquids. Pancake syrup, paster, eggwhite, silly putty, paint, glue, and soap are also liquids, that is, they flow on the application of stress, but

border on classification otherwise. In mechanical response, the latter class differs from each other as much as they differ from solids. And the response is variable in time. Syrup becomes sticky as it dries. Dishwashing soap often dries into light flakes. Silly putty flows on tilt, but shatters on sudden impact. Airplane glue is springy and rubbery.

Substances in the latter category are called structured fluids, owing their distinctive and unusual properties to large polyatomic composites, many times the size of a water molecule. Fluids containing polyatomic structures manifest a wide variety of mechanical response and self organization. Body tissues and fluids host an uncountable variety of organic and inorganic matter, with many biochemical substances falling into structured fluid category. Among the structured fluids, a class of self assemblies, called surfactants, are very interesting, possessing properties which can stabilize microbubbles in various stages of evolution by offsetting surface tension.

A surfactant is a structured fluid which is *ambiphilic*, incorporating parts that assume preferential orientations at water-oil (immiscible) interfaces. A surfactant molecule usually consists of a bulky ion at one end, and a counter ion at the other. Isolated molecules cannot usually exist in one media type, or the other, but instead orient themselves into *micelles*, configurations in which like parts clump together, that is head in one substance and tail in the other. Micelles typically possess diameters near $10^{-3} \mu m$, and render the interfaces unlike anything measured in the components. Lipid-aqueous tissue interfaces potentially present favorable environments for surfactants.

Under certain conditions, a surfactant can reduce interfacial surface tension, allowing the interface to grow and wrap around itself. The result is a microbundle full of alternating surfaces and interfaces, spherical in structure to minimize thermodynamic energy constraints. Many substances may be bound up in the microbundle. If small gas nuclei, but typically much larger than a micelle, are in contact with the interfaces, or surfactants directly, a spherical gas micronucleus-microemulsion can develop, varying in size and surfactant content. The assembly is stable when the effective surface tension is zero, when surfactant skin pressure just balances mechanical (Laplace) surface tension. If the effective surface tension of the microbubble, γ , is not zero, the collection will grow or contract until stable, or disassemble. In the case of gas microemulsions, the surfactant is thought to coat the inside boundary layer mostly, with free gas in the interior. The actual picture is probably more complex, but such a picture can be drawn for computational simplicity. Surfactant stabilized micronuclei may theoretically destabilize under compression-decompression processes in diving, perhaps spawning bubble growth fueled by high gas tension in surrounding media. Microbubbles may remain at the interfaces, but probably migrate. Sources of initial gas nuclei, surfactant composition, and tissue sites await description.

PHASE MECHANICS AND DECOMPRESSION THEORY IN DEPTH
CHAPTER 3: GAS, FLUID, AND PHASE KINETICS

Boltzmann Transport Equation

Bilinear Transport Equation

All transfer equations in physics have their roots in the bilinear Boltzmann form. We begin with the bilinear form and then obtain other representations from it. The Boltzmann (bilinear) transport equation is a microscopic balance of molecular fundamental interactions. It takes the general form,

$$\frac{\partial f}{\partial t} + \mathbf{v} \cdot \nabla f + \mathbf{a} \cdot \nabla_{\mathbf{v}} = \int d^3q \sigma q (f' g' - f g)$$

for f and g initial distribution functions for particles with velocity v_f and v_g , σ the cross section for particle collisions, q the relative speed between colliding particles in the distributions, and f' and g' the final distribution functions for same. That is,

$$\begin{aligned} \mathbf{q} &= \mathbf{v}_f - \mathbf{v}_g = \mathbf{v}'_f - \mathbf{v}'_g \\ f &= f(\mathbf{v}_f, x, t) \quad , \quad g = g(\mathbf{v}_g, x, t) \\ f' &= f(\mathbf{v}'_f, x, t) \quad , \quad g' = g(\mathbf{v}'_g, x, t) \end{aligned}$$

The external source, denoted Q , is a positive source of distribution particles, and \mathbf{a} is the particle acceleration from external forces, \mathbf{F} . The units of the distribution functions, f , g , f' , and g' , are the standard number density set in time, that is, particles/volume velocity, with volume, speed, and time in any convenient metric.

The statement tracks changes between inscattered and outscattered particle distributions, f , g , and f' , g' , with incoming and outgoing velocities, \mathbf{v}_f , \mathbf{v}_g and \mathbf{v}'_f , \mathbf{v}'_g respectively. The left hand side of the above equation is streaming operator, L , while the first term on the right hand side is the interaction source, S , and the external source, Q , represents everthing else outside of interactions.

Linear Transport Equation

The linear Boltzmann equation is a special case of the bilinear form.

Diffusion Equation

The diffusion form of the Boltzmann equation is easily recovered from the foregoing.

Rate Equation

The rate equation is obtained as follows from the above.

Moment Flow Equations

Collisional Dynamics

The properties of matter in bulk are predicted from kinetic, or dynamic, theory through application of the laws of mechanics to the individual molecules of the system, and from these laws, deriving expressions for the pressure of a gas, internal energy, and specific heat. Statistical mechanics, more broadly, ignores detailed considerations of molecules as individuals, and applies considerations of probability to the very large ensemble of molecules comprising matter. Both were developed on

the assumption that the laws of mechanics, deduced from the behavior of matter in bulk, could be applied to molecules, atoms, and electrons. In gases, particles are in continuous collisional mode.

If we imagine that at a certain instance in time all the molecules of a gas, except one, are frozen in position, while the remaining single molecule continues to move among the others with ensemble average speed, \bar{v} , and that all molecules are perfectly elastic spheres, we can define a collision cross section, σ , as the area swept out by their total radial separation, $2r$, with r the molecular radius,

$$\sigma = 4\pi r^2 \quad .$$

For gases, molecular radii are on the order of *angstroms* (10^{-10} m). In a time interval, dt , if there are N molecules in volume, V , the number, dN , with centers in the cylinder swept out by the molecule moving with velocity, \bar{v} , is,

$$dN = \sigma \frac{N}{V} \bar{v} dt \quad ,$$

also representing the number of collisions in that time interval. The collisional frequency, f , is the number of collisions per unit time interval,

$$f = \frac{dN}{dt} = \sigma \frac{N}{V} \bar{v} \quad .$$

Collisional frequencies are on the order of 10^{10} sec $^{-1}$. The average distance between collisions, Λ , or the mean free path, equals distance covered, $\bar{v}dt$, divided by number of collisions, dN , that is,

$$\Lambda = \frac{V}{\sigma N} \quad .$$

Typical values for Λ are near 10^{-7} cm for gases. Every collision removes a molecule from N , and the corresponding change, dN , in distance, dx , depends on N , and collision probability, χ ,

$$dN = -\chi N dx \quad ,$$

with, in the simplest case of solid spheres,

$$\chi = \frac{1}{\Lambda} \quad .$$

The standard survival equation follows upon integration of the above, with $N = N_0$ at $x = 0$,

$$N = N_0 \exp(-x/\Lambda) \quad .$$

The viscosity, X , thermal conductivity, K , and diffusivity, D , in the kinetic picture depend on particle transport of momentum, energy, and mass by collisions. Considerations of the momentum, energy, and mass transfer across any imagined surface by molecular collisions yields,

$$X = \frac{1}{3} \frac{N}{V} m \bar{v} \Lambda \quad ,$$

$$K = \frac{1}{2} \frac{N}{V} \bar{v} k \Lambda \quad ,$$

$$D = \frac{1}{3} \bar{v} \Lambda \quad ,$$

with m the molecular mass, and k Boltzmann's constant. Obviously the density, ρ , is given by,

$$\rho = \frac{N}{V} m \quad ,$$

so that,

$$D = \frac{X}{\rho} ,$$

$$H = \frac{3}{2} \frac{X}{\rho} k .$$

Table 1 lists transport coefficients for a number of gases, that is, mean free path, molecular radius, viscosity, thermal conductivity, and diffusivity, at room temperature.

Table 1. Kinetic Transport Coefficients.

gas	Λ (μm)	r (nm)	X ($dyne\ sec/m^2$)	K ($joule/cm\ sec\ K^\circ$)	D (cm^2/sec)
<i>He</i>	0.186	0.109	1.94	0.144	0.124
<i>Ne</i>	0.132	0.132	3.12	0.046	0.358
<i>N₂</i>	0.063	0.188	1.73	0.023	0.072
<i>O₂</i>	0.068	0.179	20.01	0.024	0.073
<i>NH₃</i>	0.045	0.222	0.970	0.021	0.014
<i>CO₂</i>	0.042	.232	1.45	0.030	0.009

High Pressure Flows

Under compression-decompression, breathing gases very nearly approximate ideal gas behavior under nominal temperature and flow regimes. Much of the foregoing applies directly to the gases in high pressure cylinders and the flow through regulators and rebreathers. Consider tanks first.

Tanks

High pressure cylinders are mostly made from steel and aluminum, although prototypes of stainless steel and fiber wound composites have appeared. Carbon steel, used in early tanks, has been replaced with chrome molybdenum steel. Aluminum is alloyed with other metals, such as magnesium and titanium. Steel tanks were introduced in the late 1940s, and aluminum tanks became popular in the 1970s, though the first were imported from France in 1950. Cylinders carry compressed gases for underwater breathing, and are rated according to maximum working pressure, and the corresponding volume occupied by the breathing gas at 1 *atm*. Table 2 summarizes tank characteristics for a number of rated steel and aluminum cylinders. Steel tanks are generally heavier and exhibit negative buoyancy when filled with air. Aluminum tanks are lighter and tend to exhibit positive buoyancy before all tank air is depleted. To recover the buoyancy characteristics of steel tanks, aluminum tanks of the same size must have thicker walls, thus increasing their weight, but not their displacement.

Table 2. Cylinder Specifications.

material	volume (ft^3)	pressure (lbs/in^2)	length (in)	diameter (in)	weight (lbs)	buoyancy (lbs)
steel	15	3300	13.80	4.00	7.5	-1.30
aluminum	14	2015	16.60	4.40	5.4	3.22
aluminum	50	3000	19.00	6.90	21.5	2.25
steel	50	1980	22.50	6.80	20.8	2.43
steel	72	2475	25.00	6.80	29.5	3.48
aluminum	72	3000	26.00	6.90	28.5	3.60
aluminum	80	3000	26.40	7.25	33.3	4.00
aluminum	80	3000	27.00	7.25	34.5	4.12
steel	95	3300	25.00	7.00	39.1	-6.11

Pressures in a tank cylinder increase as temperature increases, decrease as temperature decreases. Denoting the initial pressure and temperature, P_0 and T_0 , and the final pressure and temperature, P and T , we have, assuming an ideal gas,

$$\frac{P_0}{T_0} = \frac{P}{T} \quad ,$$

or,

$$P = \frac{T}{T_0} P_0 \quad ,$$

Put another way, the change in pressure, ΔP , satisfies,

$$\Delta P = P - P_0 = P_0 \left[\frac{T}{T_0} - 1 \right] \quad .$$

The pressure change depends linearly on the temperature ratio, T/T_0 , increasing or decreasing as T increases or decreases.

Regulators

Regulators, rebreathers, and compressors move gases from one reservoir to another at different pressure, and often, temperature. Regulators and rebreathers simply reduce gases at high pressure to low pressure, and compressors elevate gases at low pressure to high pressure. In both cases, gas flows involve high pressures and turbulent flows, for which steady state dynamics are a low order approximation, particularly as time scales decrease. The essence of regulator, rebreather, and compressor flow dynamics can be extracted from a simple high pressure flow model, namely, a fixed reservoir with connecting flow, treating the air as an ideal gas. In zero order, for adiabatic flow, and in the absence of shaft work and elevation changes, the flow temperature change, dT , and velocity change, dv , are related,

$$\frac{dv}{dT} = \frac{1}{v} \frac{\gamma R}{(1 - \gamma)} \quad ,$$

with universal gas constant, R , and $\gamma = 5/3$. With this approximation for laminar flow, the volume flow rate, J , in a hose of length, dl , with cross sectional radius, r , is given by,

$$J = \frac{\pi r^4}{8\eta} \frac{dP}{dl}$$

for dP the pressure drop in dl , and η the viscosity of the fluid (gas).

Rebreathers

Crucial to the operation of rebreathers is a constant and continuous mass flow of breathing gas, subject to oxygen metabolic requirements and depth. Mass balance simply requires that the flow into the breathing bag equals the amount used by the body plus that exhaled into the breathing bag or exhalation bag. Denoting the breathing gas flow rate, F , the metabolic oxygen (consumption) rate, m , the source oxygen fraction, f_{O_2} , and inspired (breathing bag) oxygen fraction, i_{O_2} , mass balance is written,

$$f_{O_2} F = i_{O_2} F + (1 - i_{O_2}) m$$

The source flow rate, F , and oxygen fraction, f_{O_2} , depend on nozzle and mixture. The metabolic rate, m , depends on workload, and the inspired fraction, i_{O_2} , is uniquely determined with the other three specified. Or, for requisite inspired fraction, i_{O_2} , and metabolic rate, m , the source rate, F , and oxygen source fraction, f_{O_2} , can be fixed within limits. Workload rates, m , range, 0.5 - 20.5 l/min , while source flows, F , depend on depth, cylinder and nozzle, with typical values, 5 - 16 l/min . As seen, the source oxygen fraction, f_{O_2} , is uniquely determined by the maximum depth, d_{max} , and maximum oxygen pressure (typically 1.6 - 1.4 atm). Always, inspired oxygen partial pressures are

kept between hyperoxic and hypoxic limits, roughly, 0.16 - 1.6 *atm*. At depth, d , the source flow rate, F , decreases according to,

$$F = \frac{F_0}{1 + d/33}$$

for F_0 the surface rate, unless the flow is depth compensated.

Steady Flow

The most general statement about mass flow continuity takes the form,

$$\frac{\partial \rho}{\partial t} + \nabla \cdot (\rho \mathbf{v}) = 0$$

for mass density, ρ , and velocity, \mathbf{v} . Certainly, within this conservation statement, a variety of turbulent and nonturbulent flow regimes are possible. Most often flows are turbulent (as seen above). For incompressible flow without circulation, the velocity field (vector), \mathbf{v} , satisfies two additional constraint equations,

$$\nabla \cdot \mathbf{v} = 0$$

$$\nabla \times \mathbf{v} = 0$$

the so called steady state condition. The above (with some mathematical finesse), lead to streamline results for pressure, p , density, ρ , elevation, z , and velocity, v ,

$$p + \frac{1}{2}\rho v^2 + \rho g z = \gamma$$

with g the acceleration of gravity, and γ a flow constant.

Yet, to a lower order (nonturbulent) in flow regimes, a steady state approximation to fluid flow dynamics can be stated very simply in terms of energy balances. Denoting initial and final states of a flowing fluid (gas or liquid), i and f , in a system capable of doing external work, W , and exchanging heat, Q , application of the first law yields for the differential increase of total energy, U , of the system,

$$U = Q - (W + p_f V_f - p_i V_i)$$

for p pressures and V volumes. Assuming that the total energy, U , of the flowing system consists of internal energy of the fluid, mu , kinetic energy, $1/2mv^2$, and potential energy, mgz , the balance takes the simple form,

$$Q - (W + p_f V_f - p_i V_i) = m(u_f - u_i) + \frac{1}{2}m(v_f^2 - v_i^2) + mg(z_f - z_i)$$

where z is the position, v is the flow speed, and u is the specific internal energy of the fluid. The representation above is also known as Bernoulli's generalized law. Its importance is well established in that it is the governing relationship for flight, that is, a pressure reduction on the top side of a wing or airfoil, relative to the pressure on the bottom side, results in hydrodynamical lift (then flight). It is also the basic governing relationship for blood flow in the arterial and venous circulation of the body.

Another example is flow through a nozzle, discussed earlier. If the work, W , and heat exchanged, Q , are zero (certainly an idealization), as in air exhausting from the valve of a scuba tank, the initial and final (exiting) flow velocities depend only on initial and final enthalpies, h , with

$$h = mu + pV$$

so that,

$$mv_f^2 = mv_i^2 + 2(h_i - h_f)$$

at the same elevation, z . More generally, the work, W , and heat exchanged, Q , are not zero, and so we see,

$$mv_f^2 = mv_i^2 + 2(h_i - h_f) + 2(Q - W)$$

which takes into account cooling or heating of a tank exhausting or filling a breathing mixture. Both cases assume laminar flow. In perspective, we also recall for incompressible and adiabatic fluid flow with no shaft work,

$$p_i + \frac{1}{2}\rho v_i^2 + \rho g z_i = p_f + \frac{1}{2}\rho v_f^2 + \rho g z_f = \gamma$$

for γ the *streamline* constant in phase space, and,

$$\rho = \rho_i = \rho_f$$

because the fluid is incompressible. Historically, such is Bernoulli's law, and follows easily from the above mass-energy conservation laws.

Phase Transfer

Obviously, the diver is concerned with both dissolved and separated inert gas phases. Both must be considered in coupled fashion. And the dynamics of transfer and exchange differ under pressure. To eliminate free phases, increased pressure is needed. To eliminate dissolved phases, decreased pressure is needed.

Dissolved Phases

All gases dissolve in all liquids, but actual solubilities range over many orders of magnitude. Considering inert gases at room temperature, for illustration, the solubility of xenon in n -octane, a hydrocarbon liquid, is 470 times that of helium in water. Gas solubilities can vary much more for complex solutes and solvents. The solubility of the anesthetic gas halothane in olive oil is more than 10^6 times the solubility of common gases in liquid mercury. Inert gases such as helium and nitrogen are readily soluble in tissue and blood, and their solubility can fuel bubble growth with reduction in ambient pressure, a concern for decompressing divers.

Denoting the ambient partial pressure of a gas, p , and its solubility, S , in a liquid, the relative concentration of the dissolved gas component, c , is given by Henry's law,

$$c = Sp.$$

The corresponding *tension*, or dissolved gas partial pressure, is also p at equilibrium. By convention, partial pressures usually refer to the free gas phase, while tensions refer to the dissolved gas phase, though some folks use them interchangeably. When there exist differences, or *gradients*, between gas partial pressures and/or tensions across regions of varying concentration or solubility, gases will diffuse until partial pressures are equal, in short, move from regions of higher partial pressures to regions of lower partial pressures, regardless of the phases (free or dissolved) of the components. This movement is the crux of the decompression problem in divers and aviators, and modeling this movement is central to the formulation of decompression tables and dive computer algorithms.

Gas is driven across the tissue-blood interface by the gradient, but the rate at which bulk tissue transfers gas also depends on the blood flow rate and the degree of vascularity. Then both blood perfusion rate and gas diffusion rate contribute to the overall transfer process.

1. Perfusion Controlled Transport

Exchange of dissolved tissue and blood gas, controlled by blood flow rates across regions of varying concentration or solubility, is driven by the local tissue-blood gradient, that is, the difference between the arterial blood tension, p_a , and the instantaneous tissue tension, p ,

assuming that blood flow rates are considerably slower than gas diffusion rates across the regions. Such behavior is modeled in time, t , by simple classes of exponential response functions, bounded by p_a and the initial value of p , denoted p_i . These multitissue functions satisfy a differential *perfusion* rate equation,

$$\frac{\partial p}{\partial t} = -\lambda (p - p_a) \quad ,$$

and take the form, tracking both dissolved gas buildup and elimination symmetrically,

$$p - p_a = (p_i - p_a) \exp(-\lambda t) \quad ,$$

$$\lambda = \frac{0.6931}{\tau} \quad ,$$

with perfusion constant, λ , defined by the tissue half-time, τ . Compartments with 2, 5, 10, 20, 40, 80, 120, 180, 240, 360, 480, and 720 minute half-times, τ , are employed, and half-times are independent of pressure.

In a series of dives or multiple stages, p_i and p_a represent extremes for each stage, or more precisely, the initial tension and the arterial tension at the beginning of the next stage. Stages are treated sequentially, with finishing tensions at one step representing initial tensions for the next step, and so on. Exposures are controlled through critical tensions, M , such that, throughout the dive (Chapter 4),

$$p \leq M \quad .$$

2. Diffusion Controlled Transport

Exchange of dissolved tissue and blood gas, controlled by diffusion across regions of varying concentration or solubility, is also driven by the local tissue-blood gradient, but solutions to the diffusion equation control transport. In simple planar geometry, the diffusion equation can be cast,

$$D \frac{\partial^2 p}{\partial x^2} = \frac{\partial p}{\partial t} \quad ,$$

with D the diffusion coefficient. As in the perfusion case, solutions depend on initial values, and also on boundary conditions. Tissue is separated into intravascular and extravascular regions for application of boundary conditions, with the tissue tension, p , equal to the arterial tension, p_a , at the tissue-blood interface. Solving and applying initial and boundary conditions, and then averaging the solutions over the spatial region, of thickness, l , there obtains,

$$p - p_a = (p_i - p_a) \frac{8}{\pi^2} \sum_{n=1}^{\infty} \frac{1}{(2n-1)^2} \exp(-\alpha_{2n-1}^2 D t) \quad ,$$

with,

$$\alpha_{2n-1} = \frac{(2n-1)\pi}{l} \quad .$$

A decay constant, κ , fitted to exposure data, is related to the diffusion coefficient, D ,

$$\kappa = \frac{\pi^2 D}{l^2} = 0.007928 \text{ min}^{-1} \quad ,$$

in the exponential expansion, and plays a similar role to λ in the perfusion controlled case. The diffusion expansion looks like a weighted sum of multitissue perfusion functions with decay constants, $(2n-1)^2 \kappa$. A diffusion equivalent half-time, ω , is simply defined,

$$\omega = \frac{0.693}{\kappa} = 87.4 \text{ min} \quad ,$$

so that halftimes, ω_{2n-1} , in the weighted expansion, are given by,

$$\omega_{2n-1} = \frac{\omega}{(2n-1)^2} .$$

As before, p_i and p_a represent extremes for each stage. Critical gradients, G , control diving through the constraint (Chapter 4),

$$p - p_a \leq G ,$$

Free Phases

To satisfy thermodynamic laws, bubbles in blood and tissue assume spherical shapes in the absence of external or mechanical (distortion) pressures. Bubbles entrain free gases because of a thin film, exerting surface tension pressure on the gas, of magnitude, $2\gamma/r$, with γ the Laplacian surface tension and r the bubble radius. Hydrostatic pressure balance requires that the pressure inside the bubble, Φ ,

$$\Phi = \sum_{j=1}^J P_j ,$$

with P_j bubble partial pressures of component (free) gases, exceed ambient pressure, P , by the surface tension pressure, $2\gamma/r$,

$$\Phi = P + \frac{2\gamma}{r} ,$$

as seen in Figure 1. At small radii, surface tension pressure is greatest, and at large radii, surface tension pressure is least.

Gases will also diffuse into or out of a bubble according to differences in gas partial pressures inside and outside the bubble, whether in free or dissolved phases outside the bubble. In the former case, the gradient is termed free-free, while in the latter case, the gradient is termed free-dissolved. Unless the surface tension, γ , is identically zero, there is always a gradient tending to force gas out of the bubble, thus making the bubble collapse on itself because of surface tension pressure. If surrounding external pressures on bubbles change in time, however, bubbles may grow or contract. The flow regime is depicted in Figure 2.

Bubbles grow or contract according to the strength of the free-free or free-dissolved gradient, and it is the latter case which concerns divers under decompression. The radial rate at which bubbles grow or contract is roughly given by,

$$\frac{\partial r}{\partial t} = \frac{DS}{r}(\Pi - \Phi) ,$$

with D and S tissue diffusivity and solubility, and total tissue tension, Π , the sum of component dissolved gas tensions,

$$\Pi = \sum_{j=1}^J p_j ,$$

as before. A critical radius, r_c , separating growing from contracting bubbles is given by,

$$r_c = \frac{2\gamma}{\Pi - P} ,$$

and bubbles with radius $r > r_c$ will grow, while bubbles with radius $r < r_c$ will contract. Limiting bubble growth and impact upon nerves and circulation are issues when decompressing divers and aviators. The interplay between tissue tension and bubble growth is further complicated with ascent, since ambient pressure changes in time (depending on ascent rate). Figure 4 shows the effects of bubble growth in fast and slow tissue compartments for varying ascent rate.

Mass Transport

Doppler Effect

A change in the observed frequency of sound, light, and other waves, caused by relative source-observer motion, is known as the Doppler effect. One example is a change in train whistle pitch upon approach and retreat. The observed frequency, f' , is higher than the source frequency, f , as source and observer approach each other, and lower as source and observer retreat from each other.

For sound waves that propagate with characteristic velocity, u , in a medium (air, water, tissue), the Doppler shift depends on both source velocity, v_s , and observer velocity, v_o . The number of sound waves per second arriving at the observer can be estimated by simply counting the waves emitted per second by the source, and the change per second in the number of waves in flight from source to observer,

$$f' = f \frac{u - v_o}{u - v_s} ,$$

with source and observer velocities measured along the direction from source to observer (longitudinal component). If the observer is at rest, obviously,

$$\Delta f = f' - f = f \frac{v_s}{u - v_s} ,$$

as the usual case. If the observer is moving, and the source is at rest,

$$\Delta f = f' - f = -f \frac{v_o}{u} .$$

A general definition of the sound speed, u , derives from the pressure derivative with respect to the density,

$$u^2 = \frac{dP}{d\rho} ,$$

which, in the adiabatic limit of no heat flow, reduces to,

$$u^2 = \frac{Y}{\rho} ,$$

$$Y = -V \frac{dP}{dV} ,$$

with Y the *bulk modulus* of the material. For ideal gases, $Y = 5/3 P$, but in solids and liquids, the bulk modulus must be determined.

A gas bubble will scatter sound waves in tissue by virtue of differences in bubble and tissue density, ρ , and bulk modulus, Y . First attempts to detect gas in tissues using ultrasound were designed to measure attenuation in fundamental frequency by scatter or reflection of the sound signal passed across the tissue region under investigation. Such techniques have the advantage that they can localize the gas region. However, both transmission and reflection techniques suffer from the heterogeneous nature of tissue, both in density and bulk modulus. Such an approach, called the pulse echo technique, has given way today to Doppler methods of detecting moving bubbles.

Doppler devices used to monitor bubbles in the circulation, or trap speeders with radar detectors, are simple. High frequency waves, emitted by a sending crystal of a Doppler probe, easily travel through body tissue, with a portion reflected back towards a receiving crystal. Tissue moving toward or away from the sending unit will reflect part of the source signal with a frequency shift determined

by the velocity of the reflecting medium. Integrated Doppler systems discard the unshifted portion of the reflected signal, and only analyze the shifted portion. Shifted signals fall within the human audibility range. In the veins, bubbles reflect more of the signal than flowing blood, with chirps and pops superimposed on continuous flowing blood background sounds. Detected bubbles are graded from 0 to 4, roughly no bubbles to 1,000 or more per minute.

Doppler probes are inserted into leg and arm veins, pulmonary arteries (heart to lung), and even the heart ventricles. Bubbles detected in veins or ventricles are traveling from tissues to the lungs. They may, or may not, be associated with free phases at joints, or in the spinal column, causing DCS at these sites. Doppler prediction of DCS falls in the 10% to 15% success range, even for high grade bubbles (3-4 Doppler grade). While less than totally predictive, the preponderance of high Doppler grade bubbles for a dive profile renders the profile suspect at least. Following a typical nonstop dive to the limits, Doppler bubble levels tend to peak in an hour, or two. Studies by the Divers Alert Network (DAN) at Duke University reported that some 18% of recreational dives produced some level of Doppler bubbling, on tables or decompression meters.

Acoustical signals in the *megahertz* frequency range are typically employed in Doppler analysis. The size and velocity of reflecting bubbles in the flowing media are crucial factors in the reflected return signals. Where flow rates are the highest, the smallest bubbles can be detected with Doppler technology. Roughly, entrained bubbles in the 20 - 40 μm diameter range are detectable in flows ranging 50 -60 *cm/sec*, as depicted in Figure 2, according to bubble flow experiments employing 5 *megahertz* acoustical signals.

Pulmonary And Circulatory Networks

The pulmonary and circulatory organs are connected gas transfer networks, as Figure 3 suggests. Lung blood absorbs oxygen from inspired air in the alveoli (lung air sacs), and releases carbon dioxide into the alveoli. The surface area for exchange is enormous, on the order of a few hundred square meters. Nearly constant values of alveolar partial pressures of oxygen and carbon dioxide are maintained by the respiratory centers, with ventilated alveolar volume near 4 l in adults. The partial pressure of inspired oxygen is usually higher than the partial pressure of tissue and blood oxygen, and the partial pressure of inspired carbon dioxide less, balancing metabolic requirements of the body.

Gas moves in direction of decreased concentration in any otherwise homogeneous medium with uniform solubility. If there exist regions of varying solubility, this is not necessarily true. For instance, in the body there are two tissue types, one predominantly aqueous (watery) and the other (lipid), varying in solubility by a factor of five for nitrogen. That is, nitrogen is five times more soluble in lipid tissue than aqueous tissue. If aqueous and lipid tissue are in nitrogen equilibrium, then a gaseous phases exists in equilibrium with both. Both solutions are said to have a nitrogen tension equal to the partial pressure of the nitrogen in the gaseous phase, with the concentration of the dissolved gas in each species equal to the product of the solubility times the tension according to Henry's law. If two nitrogen solutions, one lipid and the other aqueous, are placed in contact, nitrogen will diffuse towards the solution with decreased nitrogen tension. The driving force for the transfer of any gas is the pressure gradient, whatever the phases involved, liquid-to-liquid, gas-to-liquid, or gas-to-gas. Tensions and partial pressures have the same dimensions. The volume of gas that diffuses under any gradient is a function of the interface area, solubility of the media, and distance traversed. The rate at which a gas diffuses is inversely proportional to the square root of its atomic weight. Following equalization, dissolved volumes of gases depend upon their individual solubilities in the media.

Lipid and aqueous tissues in the body exhibit inert gas solubilities differing by factors of roughly five, in addition to different uptake and elimination rates. Near standard temperature and pressure (32 F°, and 1 atm), roughly 65% of dissolved nitrogen gas will reside in aqueous tissues, and the remaining 35% in lipid tissues at equilibration, with the total weight of dissolved nitrogen about .0035 lb for a 150 lb human.

The circulatory system, consisting of the heart, arteries, veins, and lymphatics, convects blood throughout the body. Arterial blood leaves the left heart via the aorta (2.5 cm), with successive branching of arteries until it reaches arterioles (30 μm), and then systemic capillaries (8 μm) in peripheral tissues. These capillaries join to form venules (20 μm), which in turn connect with the vena cava (3 cm), which enters the right heart. During return, venous blood velocities increase from 0.5 cm/sec to nearly 20 cm/sec. Blood leaves the righthear through the pulmonary arteries on its way to the lungs. Upon oxygenation in the lungs, blood returns to the left heart through the pulmonary veins, beginning renewed arterial circulation. Flow patterns in lowest (still representative) order follow streamlines, for initial and final states, i and f ,

$$mv_f^2 + 2h_f + 2mgz_f = mv_i^2 + 2h_i + 2mgz_i = \gamma$$

with blood mass, m , velocity, v , enthalpy, h , position, z , and constant, γ , as the entrained blood routinely circulates. Obviously, as systemic vessels change size, branch, and recollect, blood cursing through them experiences speed changes according to mass flow conservation, that is, denoting mass flow rate, dm/dt ,

$$\frac{dm}{dt} = \rho_i A_i v_i = \rho_f A_f v_f$$

with A the cross sectional area of the blood vessel and more simply where, $\rho_i = \rho_f$, for incompressible fluids, like blood.

Blood has distinct components to accomplish many functions. Plasma is the liquid part, carrying nutrients, dissolved gases (excepting oxygen), and some chemicals, and makes up some 55% of blood by weight. Red blood cells (erythrocytes) carry the other 45% by weight, and through the protein, hemoglobin, transport oxygen to the tissues. Enzymes in red blood cells also participate in a chemical reaction transforming carbon dioxide to a bicarbonate in blood plasma. The average adult carries about 5 l of blood, 30-35% in the arterial circulation (pulmonary veins, left heart, and systemic circulation), and 60-65% in the venous flow (veins and righthear). About 9.5 ml of nitrogen are transported in each liter of blood. Arterial and venous tensions of metabolic gases, such as oxygen and carbon dioxide differ, while blood and tissue tensions of water vapor and nitrogen are the same. Oxygen tissue tensions are below both arterial and venous tensions, while carbon dioxide tissue tensions exceed both. Arterial tensions equilibrate with alveolar (inspired air) partial pressures in less than a minute. Such an arrangement of tensions in the tissues and circulatory system provides the necessary pressure head between alveolar capillaries of the lungs and systemic capillaries pervading extracellular space.

Tissues and venous blood are typically unsaturated with respect to inspired air and arterial tensions, somewhere in the vicinity of 8-13% of ambient pressure. That is, summing up partial pressures of inspired gases in air, total venous and tissue tensions fall short in that percentage range. Carbon dioxide produced by metabolic processes is 25 times more soluble than oxygen consumed, and hence exerts a lower partial pressure by Henry's law. That tissue debt is called the *inherent unsaturation*, or *oxygen window*, in diving applications

Inert gas transfer and coupled bubble growth are subtly influenced by metabolic oxygen consumption. Consumption of oxygen and production of carbon dioxide drops the tissue oxygen tension below its level in the lungs (alveoli), while carbon dioxide tension rises only slightly because carbon dioxide is 25 times more soluble than oxygen. Figure 4 compares the partial pressures (*fsw*) of oxygen, nitrogen, water vapor, and carbon dioxide in dry air, alveolar air, arterial blood, venous blood, and tissue (cells).

Arterial and venous blood, and tissue, are clearly unsaturated with respect to dry air at 1 atm. Water vapor content is constant, and carbon dioxide variations are slight, though sufficient to establish an outgradient between tissue and blood. Oxygen tensions in tissue and blood are considerably below lung oxygen partial pressure, establishing the necessary ingradient for oxygenation and metabolism. Experiments also suggest that the degree of unsaturation increases linearly with pressure for constant composition breathing mixture, and decreases linearly with mole fraction of inert gas in the inspired mix. A rough measure of the inherent unsaturation, Δ_u , is given as a function of ambient pressure, P , and mole fraction, f_{N_2} , of nitrogen in the air mixture, in *fsw*

$$\Delta_u = (1 - f_{N_2})P - 2.04 f_{N_2} - 5.47 \ .$$

Since the tissues are unsaturated with respect to ambient pressure at equilibrium, one might exploit this *window* in bringing divers to the surface. By scheduling the ascent strategically, so that nitrogen (or any other inert breathing gas) supersaturation just takes up this unsaturation, the total tissue tension can be kept equal to ambient pressure. This approach to staging is called the zero supersaturation ascent.

PHASE MECHANICS AND DECOMPRESSION THEORY IN DEPTH
CHAPTER 4: CRITICAL TENSIONS AND PHASE VOLUMES

Critical Tensions

Bubbles can form in tissue and blood when ambient pressure drops below tissue tensions, according to the rules of established phase mechanics. Trying to track free and dissolved gas buildup and elimination in tissue and blood, especially their interplay, is extremely complex, beyond the capabilities of even supercomputers. But safe computational prescriptions are necessary in the formulation of dive tables and digital meter algorithms. The simplest way to stage decompression, following extended exposures to high pressure with commensurate dissolved gas buildup, is to limit tissue tensions. Historically, Haldane first employed that approach, and it persists today.

To maximize the rate of uptake or elimination of dissolved gases, the *gradient*, simply the difference between p_i and p_a , is maximized by pulling the diver as close to the surface as possible. Exposures are limited by requiring that the perfusion-dominated tissue tensions, p , never exceed criticality, M , for instance, written for each tissue compartment in the US Navy approach employing 5, 10, 20, 40, 80, and 120 minute tissue halftimes, τ ,

$$M = M_0 + \Delta M d \quad ,$$

with,

$$M_0 = 152.7\tau^{-1/4} \quad ,$$

$$\Delta M = 3.25\tau^{-1/4} \quad ,$$

as a function of depth, d , for ΔM the change per unit depth. Figure 1 plots the US Navy critical tensions.

Surfacing values, M_0 , are principal concerns in nonstop diving, while values at depth, $\Delta M d$, concern decompression diving. In both cases, the staging regimen tries to pull the diver as close to the surface as possible, in as short a time as possible. By contrast, free phase (bubble) elimination gradients, as seen, *increase* with depth, directly opposite to dissolved gas elimination gradients which *decrease* with depth. In actuality, decompression is a payoff between dissolved gas buildup and free phase growth, tempered by body ability to eliminate both. But dissolved gas models cannot handle both, so there are problems when extrapolating outside tested ranges.

In absolute pressure units, the corresponding critical gradient, G , is given by,

$$G = \frac{M}{0.79} - P = 1.27 M - P \quad ,$$

with P ambient pressure, and M critical nitrogen pressure. In bubble theories, supersaturation is limited by the critical gradient, G . In decompressed gel experiments, Strauss suggested that $G \approx 20$ *fsw* at ambient pressures less than a few atmospheres. Other studies suggest, $14 \leq G \leq 30$ *fsw*, as a range of critical gradients (G -values).

In diffusion-dominated approaches, the tissue tension is often limited by a single, depth-dependent criterion, such as,

$$M = \frac{709 P}{P + 404} \quad ,$$

a continuous parameterization lying between fixed gradient and multitissue schemes. The corresponding critical gradient, G , is shown in Figure 2.

Blood rich, well perfused, aqueous tissues are usually thought to be *fast* (small τ), while blood poorer, scarcely-perfused, lipid tissues are thought to be *slow* (large τ), though the spectrum of

halftimes is not correlated with actual perfusion rates in critical tissues. As reflected in relationship above, critical parameters are obviously larger for faster tissues. The range of variation with compartment and depth is not insignificant. Fast compartments control short deep exposures, while slow compartments control long shallow, decompression, and saturation exposures.

As is well known, bounce exposures are often limited by a depth-time law of the form,

$$d t_n^{1/2} \leq C \quad ,$$

with t_n the nonstop time limit, and $400 \leq C \leq 500 \text{ fsw min}^{1/2}$. For $C = 465 \text{ fsw min}^{1/2}$, Figure 3 depicts the depth-time relationship. One can obtain the corresponding tissue constant, λ , controlling the exposure at depth d , for nonstop time t_n , by differentiating the tissue equation with respect to depth, d , and setting the result to zero. With $p_a = 0.79 (d + 33)$ at sea level, there results,

$$1 - \exp(-\lambda t_n) (1 + 2\lambda t_n) = 0 \quad .$$

Corresponding critical tensions, M , are then easily obtained from the tissue equation using d , λ , and t_n . In the above case, the transcendental equation is satisfied when,

$$\lambda t_n = 1.25 \quad ,$$

thus providing a means to estimate controlling tissue half-time at depth for corresponding nonstop time limits.

Time remaining before a stop or surfacing, time at a stop, or surface interval before flying can all be obtained by inverting the tissue equation. Taking the perfusion equation, and denoting the limiting critical tension at some desired stage (lower ambient pressure), M , the initial tension, p_i , and the instantaneous tension at that particular time, p , at stage, p_a , the limiting time, t , follows from,

$$t = \frac{1}{\lambda} \ln \left[\frac{p_i - p_a}{p - p_a} \right]$$

as the inversion of the tissue equation in time.

The nonstop time limit, t_n , follows by replacing the instantaneous tension, p , with the (limiting) critical tension, M , that is,

$$t_n = \frac{1}{\lambda} \ln \left[\frac{p_i - p_a}{M - p_a} \right]$$

while time remaining, t_r , at level, p_a , before ascension to new level with limiting critical tension, M , is given by,

$$t_r = \frac{1}{\lambda} \ln \left[\frac{p - p_a}{M - p_a} \right] \quad ,$$

with p the instantaneous tension now the initial tension. These hold for each compartment, λ . Across all compartments, the smallest t_n limits time at the present level when ascent is permitted, while the largest t_r prescribes wait time at the present level when ascent is not permitted. Table 1 lists compartment time limits using the critical tensions, M_0 , from Figure 1 (USN) for the six compartments, $\tau = 5, 10, 20, 40, 80,$ and 120 min , that is, $M_0 = 104, 88, 72, 58, 52, 51 \text{ fsw}$. Note the blank entries in the Table correspond to depths less than the critical tension, so tissue loading to that critical tension is not possible.

Table 1. Compartment Time Limits At Depth.

τ (min)	5	10	20	40	80	120
M_0 (fsw)	104	88	72	58	52	51
d (fsw)						
40					198	269
50				95	123	173
60			100	65	91	129
70			51	50	73	103
80		56	37	41	61	87
90		30	30	34	52	75
100	31	22	25	30	46	66
110	16	18	22	26	41	59
120	12	15	19	24	37	53
130	10	13	17	21	34	48
140	9	12	16	20	31	44
150	8	11	14	18	29	41
160	7	10	13	17	27	38
170	6	9	12	16	25	35
180	6	8	11	15	23	33
190	5	8	11	14	22	31
200	5	7	10	13	21	30

Generally, the t_n are monotonically decreasing functions of depth, while t_r are monotonically increasing functions of depth, for fixed M .

Saturation Curve

In elegant experiments, using both animals and humans, subjects were first saturated at various pressures, Q , then decompressed to lower absolute pressures, P , and closely checked for bends development. Various values of Q and P can be determined in a controlled *titration*, that is, by holding one variable fixed and changing the other very slightly over times spans of a day, or more. In analyzing this saturation data, it is possible to draw a linear relationship, in the hyperbaric regime, separating bends from no bends for ranges of P and Q . For instance, Figure 4 portrays the linear relationship for air, the saturation curve. The line takes the form, in *fsw*,

$$Q = \zeta P + \xi ,$$

with an approximate spread over different studies, depending on statistics,

$$1.20 \leq \zeta \leq 1.40$$

$$7.5 \text{ fsw} \leq \xi \leq 15.3 \text{ fsw} ,$$

and a range of ambient pressures, P ,

$$33 \text{ fsw} \leq P \leq 300 \text{ fsw} .$$

In the hypobaric regime, $P < 33 \text{ fsw}$, recent studies suggest that the air saturation curve passes through the origin as ambient pressure drops, behavior predicted within phase models and discussed at length following.

Hennessy and Hempleman, Yount and Hoffman, and Wienke established a linear titration curve for the data assuming that the same critical volume of released gas provokes mild attacks of decompression sickness. Such analyses also offer explanations for changes in signs and symptoms which follow changes in the nature of the exposure to pressure. Findings press dissolved gas approaches. While the above titration expression is compatible with broad trends, it is clear that dissolved gas limiters, such as tensions, are often not the best critical flags. Indicators such as the volume fraction of separated gas are not only more natural, but seem to correlate more strongly with experiment. Computational algorithms, coupling phase equilibration or observed numbers of bubbles to critical volumes, offer more rational physical alternatives to the matrix of critical tensions. The critical volume hypothesis is an important development in decompression modeling, and certainly extends to breathing mixtures other than air.

Critical Phase Volumes

Another way to limit diving through critical parameters occurs through phase volume limits, often integral constraints across the full pressure schedule. A couple of approaches are plausible, and require tuning and correlations with actual diving exposure data. Consider the Wienke, Yount, and Hennessy approaches, that is, starting with the most recent analyses.

Reduced Gradient Bubble Model

A complete approach to imposing phase volume limits, incorporating both gas diffusion across tissue-bubble interfaces and Boyle expansion-contraction is used in the full blown reduced gradient bubble model of Wienke. The phase volume constraint equation is rewritten in terms of a phase function, ϕ , varying in time,

$$\int_0^\tau \frac{\partial \phi}{\partial t} dt \leq \Phi$$

with, simplifying notation,

$$\dot{\phi} = \frac{\partial \phi}{\partial t}$$

for Φ the separated phase, and τ some (long) cutoff time. Specifically, for Π total gas tension,

$$\dot{\phi} = \left[\frac{\partial V}{\partial t} \right]_{diffusion} + \left[\frac{\partial V}{\partial t} \right]_{Boyle} + \left[\frac{\partial V}{\partial t} \right]_{excitation}$$

for,

$$\begin{aligned} \left[\frac{\partial V}{\partial t} \right]_{diffusion} &= 4\pi DS \int_r^\infty nr \left(\Pi - P - \frac{2\gamma}{r} \right) dr \\ \left[\frac{\partial V}{\partial t} \right]_{Boyle} &= \int_r^\infty n \left(\frac{T}{P} \frac{\partial PV}{\partial t} \frac{1}{T} \right) dr \\ \left[\frac{\partial V}{\partial t} \right]_{excitation} &= \frac{\partial}{\partial t} \left(4\pi \int_0^\infty nr^2 dr \right) \end{aligned}$$

with all quantities as denoted previously, and the bubble number integrand normalized,

$$\int_0^\infty ndr = 1$$

The temporal phase function, $\dot{\phi}$, depends on number of bubbles, n , stimulated into growth by compression-decompression, the supersaturation gradient, G , seed expansion-contraction by radial

diffusion, $\partial r/\partial t$, Boyle expansion-contraction, PV , under pressure changes, and temperature, T , in general. The excitation radius, r , depends on the material properties, and is given for air (μm),

$$r = 0.003929 + 0.001467 \left[\frac{T}{P} \right]^{1/3} + 0.021183 \left[\frac{T}{P} \right]^{2/3}$$

with P given in fsw , and T measured in absolute K° , and with ranges for virial coefficients, aqueous to lipid materials, varying by factors of 0.75 to 4.86 times the values listed above. Values of the excitation radii, r , above range from 0.01 to 0.05 μm for sea level down to 500 fsw . This is compared to excitation radii in other models (VPM and TBDM) which vary in the 1 μm range. Values for pure helium and nitrogen are recounted later. And the air expression above represents a good RGBM fit to exposure data across lipid and aqueous representations.

The phase integral for multiexposures is written, for any number of J dives, or dive segments,

$$\sum_{j=1}^J \left[\dot{\phi} t_{d_j} + \int_0^{t_j} \dot{\phi} dt \right] \leq \Phi$$

with the index j denoting each dive segment, up to a total of J , and t_j the surface interval after the j^{th} segment. For the inequality to hold, that is, for the sum of all growth rate terms to total less than Φ , obviously each term must be less the Φ . Assuming that $t_J \rightarrow \infty$, gives,

$$\sum_{j=1}^{J-1} \left[\dot{\phi} [t_{d_j} + \lambda^{-1} - \lambda^{-1} \exp(-\lambda t_j)] \right] + \dot{\phi} (t_{d_J} + \lambda^{-1}) \leq \Phi.$$

Defining $\dot{\phi}_j$,

$$\dot{\phi}_j (t_{d_j} + \lambda^{-1}) = \dot{\phi} (t_{d_j} + \lambda^{-1}) - \dot{\phi} \lambda^{-1} \exp(-\lambda t_{j-1})$$

for $j = 2$ to J , and,

$$\dot{\phi}_1 = \dot{\phi}$$

for $j = 1$, it follows that

$$\sum_{j=1}^J \dot{\phi}_j (t_{d_j} + \lambda^{-1}) \leq \Phi$$

with the important property,

$$\dot{\phi}_j \leq \dot{\phi}.$$

This implies we employ reduced phase functions extracted from bounce phase functions by writing,

$$\dot{\phi}_j = \xi_j \dot{\phi}$$

with ξ_j a *multidiving* fraction requisitely satisfying,

$$0 \leq \xi_j \leq 1$$

so that, as needed,

$$\dot{\phi}_j \leq \dot{\phi}.$$

The fractions, ξ , applied to $\dot{\phi}$ always reduce them. As time and repetitive frequency increase, the body's ability to eliminate load bubbles and nuclei decreases, so that we restrict the permissible bubble load in time by writing,

$$\dot{\phi}(t_{j-1}^{cum}) = N\beta r_i \left[1 - \frac{r(t_{j-1}^{cum})}{r_i} \right] = \dot{\phi} \exp(-\lambda_r t_{j-1}^{cum})$$

$$t_{j-1}^{cum} = \sum_{i=1}^{j-1} t_i$$

with t_{j-1}^{cum} cumulative dive time. A reduction factor, η_j^{rg} , accounting for creation of new micronuclei is taken to be the ratio of present load over initial load, written,

$$\eta_j^{rg} = \frac{\dot{\phi}(t_{j-1}^{cum})}{\dot{\phi}} = \exp(-\lambda_r t_{j-1}^{cum})$$

For reverse profile diving, the phase function is restricted by the ratio (minimum value) of the bubble load on the present segment to the bubble load at the deepest point over segments. The phase function reduction, η_j^{ex} , is then written,

$$\eta_j^{ex} = \frac{(\dot{\phi})_{max}}{(\dot{\phi})_j} = \frac{(rP)_{max}}{(rP)_j}$$

with rP the product of the appropriate excitation radius and pressure. Because bubble elimination periods are shortened over repetitive dives, compared to intervals for bounce dives, the phase function reduction, η_j^{rp} , is proportional to the difference between maximum and actual surface bubble growth rate, that is,

$$\eta_j^{rp} = 1 - \left[1 - \frac{\dot{\phi}^{min}}{\dot{\phi}} \right] \exp(-\lambda_m t_{j-1})$$

with t_{j-1} consecutive total dive time, λ_m^{-1} on the order of an hour, and $\dot{\phi}^{min}$ the smallest $\dot{\phi}$.

Finally, for multidiving, the phase function reduction factor, ξ , is defined by the product of the three η ,

$$\xi_j = \eta_j^{ex} \eta_j^{rp} \eta_j^{rg} = \frac{(\dot{\phi})_{max}}{(\dot{\phi})_j} \left[1 - \left(1 - \frac{\dot{\phi}^{min}}{\dot{\phi}} \right) \exp(-\lambda_m t_{j-1}) \right] \exp(-\lambda_r t_{j-1}^{cum})$$

with t_{j-1} consecutive dive time, and t_{j-1}^{cum} cumulative dive time, as noted. Since bubble numbers increase with depth, reduction in permissible phase function is commensurate. Multiday diving is mostly impacted by λ_r , while repetitive diving mostly by λ_m .

Varying Permeability Model

The rate at which gas builds up in tissue depends upon both excess bubble number, Λ , and supersaturation gradient, G . The critical volume hypothesis requires that the integral of the product of the two must always remain less than some limit point, αV , with α a proportionality constant. Accordingly this suggests for Yount, and his associated varying permeability model,

$$\int_0^\infty \Lambda G dt \leq \alpha V \quad ,$$

for bubble number excess, Λ , an approximately linear function of excitation seed radius (difference) on compression-decompression, ΔP ,

$$\Lambda = N\beta(r_i - r)$$

with N , β seed constants, r_i , r seed sizes (Chapter 1, Table 1), and V the limiting gas volume. Assuming that tissue gas gradients are constant during compression-decompression, t_d , while decaying exponentially to zero afterwards, and taking limiting condition of the equal sign, yields for a bounce dive,

$$\Lambda G(t_d + \lambda^{-1}) = \alpha V \quad .$$

For compression-decompression, the excitation radius, r , follows from micronuclei growth experiments in gels, but not necessarily in tissue, and assuming equal supersaturation for sets of excitation radii,

$$\frac{2(\gamma_c - \gamma)}{r} - P = \frac{2(\gamma_c - \gamma)}{r_i} - P_i$$

where r and r_i are excitation radii at P and P_i , (Chapter 1, Table 1), are purely phenomenological, and based on laboratory observations and experiments in gels (only).

No accounting of gas transfer across bubbles films, nor Boyle expansion and contraction, enters the Yount (VPM) approach. But Boyle effects might be tracked using appropriate equations-of-state for the seed surfactants (many molecular layers of internal seed coatings). Assigning equations-of-state (EOS) to the lipid and aqueous substances forming the seed surfactants, we have more generally,

$$2(\gamma_c - \gamma) = 135.3 \left[\frac{P}{T} \right]^{1/4} + 73.6 \left[\frac{P}{T} \right]^{1/2} - 15.9 \left[\frac{P}{T} \right]^{3/4}$$

with P measured in *fsw*, and T measured in absolute K° , as standard. Accordingly, this virial expansion of the surface tension EOS suggests,

$$\frac{2(\gamma_c - \gamma)}{r} - P = \frac{2(\gamma_c - \gamma)_i}{r_i} - P_i$$

At sea level, Yount fits to gel data suggest that $r_i = 0.80 \mu m$ for air. Of course, if Boyle expansion and bubble gas diffusion were treated in the VPM, the fits to the data would probably start at much smaller excitation radii, r , as in the RGBM, and such would be correspondingly reflected in r_i . Above, $r \leq r_i$, as, $P \geq P_i$, that is, smaller seeds grow on decompression.

With all exposures, the integral must be evaluated iteratively over component decompression stages, maximizing each G while satisfying the constraint equation. In the latter case, t_d is the sum of individual stage times plus interstage ascent times, assuming the same interstage ascent speed, v . Employing the above iteratively, and one more constant, δ , defined by,

$$\delta = \frac{\gamma_c \alpha V}{\gamma \beta r_i N} = 7500 \text{ fsw min} \quad ,$$

we have,

$$\left[1 - \frac{r}{r_i} \right] G(t_d + \lambda^{-1}) = \delta \frac{\gamma}{\gamma_c} = 522.3 \text{ fsw min} \quad ,$$

from the Spencer bounce and Tektite saturation data.

Separated Phase Model

Before dual phase models, such as the two above, came online, Hennessy and Hempleman looked at the critical phase volume concept in a different manner, assuming a certain volume of separated gas, V , remained in equilibrium with all dissolved gases.

And it goes like this. Suppose a unit volume of tissue, V , is equilibrated with an inert gas at partial pressure, p , and ambient pressure, P . After rapid decompression to ambient pressure, Q , assuming that V is formed and filled by free phases, and that no gas is lost through blood nor tissues, and assuming that the partial pressure of the dissolved gas in the bends tissue, q , remains at the threshold for DCS, a simple mass balance requires,

$$Sp = Sq + Vq$$

with S the solubility of the inert gases. Hydrostatic equilibrium in the gas cavity, V , also requires,

$$q + \Pi = Q + \frac{2\gamma}{r} + \delta$$

for Π the sum of all gases (free) in the pocket (approximately constant), γ the surface tension, and δ the tissue deformation pressure in the pocket of radius r .

The above can be conveniently written

$$q = Q + \kappa$$

with κ a constant for a given tissue and released gas volume distribution. Eliminating q ,

$$p = \left[1 + \frac{V}{S}\right] (Q + \kappa)$$

If the mixture is breathed at constant oxygen partial pressure, p_{O_2} ,

$$p = P - p_{O_2}$$

while if oxygen is a constant proportion, f , of the mixture,

$$p = fP$$

In both cases,

$$P = AQ + B$$

with, specifically for the constant oxygen case,

$$A = 1 + \frac{V}{S}$$

$$B = A\kappa + p_{O_2}$$

and for the constant oxygen proportion case,

$$A = \left[1 + \frac{V}{S}\right] f^{-1}$$

$$B = A\kappa$$

The critical pressure ratio, R , is the usual,

$$R = \frac{P}{Q}$$

For the US Navy Tables (240 minute compartment), $A = 1.375$, $B = 5.2 \text{ fsw}$, and for Swiss Tables (240 minute compartment), $A = 1.401$, $B = 4.7 \text{ fsw}$, while for the lipid and aqueous estimates (olive oil and water) of Hennessy and Hempleman, $A = 1.361$, $B = 3.4 \text{ fsw}$ and $A = 1.604$, $B = 4.0 \text{ fsw}$, respectively.

The above recovers a standard (M -value straightline) representation in the hyperbaric pressure regime, but not the asymptotically correct zero pressure intercept of the hypobaric regime (as we know it today). The approach is dissolved gas based, with no accounting of the microscopic features of bubble dynamics, and with those dynamics essentially buried in the constants, A and B .

The phase volume constants, Φ , αV , and V , in the above serve as limit points for staging diver ascents, replacing the critical tension M -values as limiting parameters. Imbedded in the first two are bubble dynamics which dramatically alter the staging regimens of all (just) dissolved gas schedules, as mostly imbedded in the third. The Hennessy model however was pivotal to modern decompression theory, helping to underscore the importance of bubble dynamics in staging divers.

Reduced Haldane Gradients

Within the Haldane framework of critical tensions, M , it is possible to fold phase volume constraints over M for multiding exposures, thereby incorporating some bubble mechanics into time dependent definitions of critical tensions, M , or critical gradients, G . One set of Haldane gradients, G , appears in Table 2 below, and the gradient representation, G , of the usual form, is the starting point,

$$G = G_0 + \Delta G d$$

at depth, d . The set is routinely extracted from the Spencer nonstop limits (NDLs), and the approach is useful in decompression meters with existing Haldane algorithms and software, needing to properly limit diving with phase mechanics, but not able to process full blown phase models and associated physics.

Table 2. Spencer Critical Gradients.

halftime τ (min)	threshold depth δ (fsw)	surface gradient G_0 (fsw)	gradient change ΔG
2	190	151.0	0.518
5	135	95.0	0.515
10	95	67.0	0.511
20	65	49.0	0.506
40	40	36.0	0.468
80	30	27.0	0.417
120	28	24.0	0.379
240	16	23.0	0.329
480	12	22.0	0.312

For repetitive diving, the gradients, G , above are replaced with a reduced set, \bar{G} , with the property,

$$\bar{G} \leq G \quad .$$

tending to reduce bottom time for repetitive activities and exposures. Because of this constraint, the approach is a reduced (Haldane) gradient model, It is important to note that this model is Haldane pseudo-bubble in nature, also termed a (modified) reduced gradient bubble model in publications. Others, in similar tacts, term the reduction process as a *gradient factor* method, though no formal methodology has been reported. Wienke, linking the reduction process to the full phase reduced gradient bubble model through maximum likelihood profile fits, suggested the following formally in 1990, against the background of the VPM,

$$\dot{\phi} = \Lambda G$$

but abandoning preformed nuclei and generation time scales of weeks. The excitation radius deduced from gel experiments (above) was a starting point for the retrofits to Haldane gradients, but had to be abandoned at an early stage for actual meter and table applications, and to fit the data.

The terms, ΛG and $\Lambda \bar{G}$, differ by effective bubble elimination during the previous surface interval. To maintain the phase volume constraint during multiding, the elimination rate must be downscaled by a set of bubble growth, generation, and excitation factors, cumulatively designated, ξ , such that,

$$\bar{G} = \xi G \quad .$$

A conservative set of bounce gradients, G , can be employed for multiday and repetitive diving, provided they are reduced by ξ . These same ξ are the *gradient factors* available in commercial

diveware operationally, though explicit forms and applications do not necessarily map onto the set described below, formally.

Three bubble factors, η , reduce the driving gradients to maintain the phase volume constraint. The first bubble factor, η^{rg} , reduces G to account for creation of new stabilized micronuclei over time scales, ω^{-1} , of hours,

$$\eta^{rg} = \exp(-\omega t_{cum}) \quad ,$$

$$2 \leq \omega^{-1} \leq 4 \text{ hrs} \quad ,$$

for t_{cum} the cumulative (multiday) dive time. The second bubble factor, η^{ex} , accounts for additional micronuclei excitation on reverse profile dives,

$$\eta^{ex} = \frac{(\Lambda)_{prev}}{(\Lambda)_{pres}}$$

for excitation radius, r , at depth, d , and the subscripts referencing the *previous* and *present* dives. Obviously, η^{ex} remains one until a deeper point than on the previous dive is reached. The third factor, η^{rp} , accounts for bubble growth over repetitive exposures on time scales, χ^{-1} , of hours,

$$\eta^{rp} = 1 - \left[1 - \frac{G^{bub}}{G_0 \exp(-\omega t_{cum})} \right] \exp(-\chi t_{sur}) \quad ,$$

$$10 \leq \chi^{-1} \leq 120 \text{ minutes} \quad ,$$

$$0.05 \leq \frac{G^{bub}}{G_0} \leq 0.90 \quad ,$$

according to the tissue compartment, with t_{sur} the repetitive surface interval.

In terms of individual bubble factors, η , the multidinging fraction, ξ , is defined at the start of each segment, and deepest point of dive,

$$\xi = a\eta^{rg} + b\eta^{rp} + c\eta^{ex}$$

for a , b , and c constants,

$$a + b + c = 1$$

with surface and cumulative surface intervals appropriate to the preceding dive segment. With η bounded by zero and one, ξ are similarly bounded by zero and one. Corresponding critical tensions, M , can be computed from the above,

$$M = \xi G + P \quad ,$$

with G listed in Table 2 above. Both G and ξ are lower bounded by the shallow saturation data,

$$G \geq G^{bd} = 0.303 P + 11 \quad ,$$

for P ambient pressure, and similarly,

$$\xi \geq \xi^{bd} = \frac{0.12 + 0.18 \exp(-480\lambda_{bd})}{0.12 + 0.18 \exp(-\tau\lambda_{bd})} \quad ,$$

$$\lambda_{bd} = 0.0559 \text{ min}^{-1} \quad .$$

A set of repetitive, multiday, and excitation factors, η^{rp} , η^{rg} , and η^{ex} , are drawn in Figures 5, 6, and 7, using conservative parameter values, $\chi^{-1} = 80 \text{ min}$ and $\omega^{-1} = 7 \text{ days}$. Clearly, the repetitive factors, η^{rp} , relax to one after about 2 hours, while the multiday factors, η^{rg} , continue to decrease with increasing repetitive activity, though at very slow rate. Increases in χ^{-1} (bubble elimination

half-time) and ω^{-1} (nuclei generation half-time) will tend to decrease η^{rp} and increase η^{rg} . Figure 5 plots η^{rp} as a function of surface interval in minutes for the 2, 10, 40, 120, and 720 minute tissue compartments, while Figure 6 depicts η^{rg} as a function of cumulative exposure in days for $\omega^{-1} = 7, 14, \text{ and } 21 \text{ days}$. The repetitive fractions, η^{rp} , restrict back to back repetitive activity considerably for short surface intervals. The multiday fractions get small as multiday activities increase continuously beyond 2 weeks. Excitation factors, η^{ex} , are collected in Figure 7 for exposures in the range 40-200 *fsw*. Deeper-than-previous excursions incur the greatest reductions in permissible gradients (smallest η^{ex}) as the depth of the exposure exceeds previous maximum depth. Figure 7 depicts η^{ex} for various combinations of depths, using 40, 80, 120, 160, and 200 *fsw* as the depth of the first dive.

Considering interpolating behavior, a checklist of the properties of η correlating with diving practices can be drawn:

1. η equal one for bounce diving, remaining less than one for repetitive diving within characteristic time scales of hours;
2. η decrease with increasing exposure time;
3. η increase with increasing surface interval time;
4. η scale the faster tissue compartments the most;
5. η decrease with depths of dive segments;
6. η scale short surface interval repetitive and deeper than previous dives the most;
7. η relate to the generation time scales for microbubble formation, the permissible bubble excess, and a time constant characteristic of bubble inflation rate.

In repetitive applications, the set η impose restrictions to model parameters directly:

1. reduce permissible bubble numbers, and hence, repetitive bottom time;
2. reduce permissible gradients, and hence multiexposure time;
3. penalize deeper than previous dives;
4. impact the fastest tissues the most, and hence, deeper diving.

Ascent Staging

Clearly, from all of the foregoing, the dominant modes for staging diver ascents depend upon the preponderance of separated or dissolved phases in the tissues and blood, their coupling, and their relative time scales for elimination. This is (and will always be) the central consideration in staging hyperbaric or hypobaric excursions to lower ambient pressure environments. The dynamics of elimination are directly opposite, as depicted in Figure 8. To eliminate dissolved gases (the central tenet of Haldane decompression theory), the diver is brought as close as possible to the surface. To eliminate free phases (the coupled tenet of bubble decompression theory), the diver is maintained at depth to both crush bubbles and squeeze gas out by diffusion across the bubble film surface. Since both phases must be eliminated, the problem is a playoff in staging. In mathematical terms, staging is a minimax problem, and one that requires full blown dual phase models, exposure data, and some consensus of what is an acceptable level of DCS incidence.

Another transfer pathway that needs highlighting is seen in Figure 9. Many competing transfer pathways exist between tissues and blood (dissolved and free gas phases in both). The central problem of the table and meter designer is to stage ascents so that both free and dissolved phases

are removed from tissues by the capillary system in optimal fashion. This is equally as difficult since we know little about the composition and susceptibility of tissue sites, blood perfusion rates, and geometries for modeling gas transfer. And even if we did, the complexity of the model and the computing power of our largest and fastest supercomputers would mitigate solutions. As seen graphically in Figure 10, the complexity of ascent rates, tissue tensions, and ambient pressures on bubble growth, especially with tensions and ambient pressures varying widely on ascent, is not a simply tracked quantity in diving exposures even when we know all the variables.

Attempts to track free phases within patently dissolved phase models may not optimize, but still can be mocked up for consistency with phase dynamics. One approach is to slow ascent rates and/or introduce safety stops strategically. As far as net gas exchange is concerned, most combinations of stops and rates can be equivalenced to almost any other set at given pressure, so there is always some leeway. Growth minimization and free phase elimination favor slow ascents. Figure 10 plots surfacing radius of an initially small bubble ($r = 0.36 \mu m$), held in both fast and slow tissue compartments, as a function of ascent rate. The results are typical for classes of bounce and repetitive diving, and underscore growth minimization with slow ascent rate due to increased ambient pressure on the average.

Based on suggestions at an American Academy Of Underwater Sciences ascent workshop, recorded by Lang and Egstrom, discretionary safety stops for 2-4 *min* in the 10-20 *fsw* zone are recommended. Calculations reported by Wienke and Lewis and summarized in Tables 1 and 2, underscore the bases of the suggestions for a number of reasons. Relative changes in three computed trigger points, tissue tension, separated phase volume, and bubble radius, are listed for six compartments following a nominal bounce dive to 120 *fsw* for 12 *min*, with and without a safety stop at 15 *fsw* for 3 *min*. Stop procedures markedly restrict bubble and phase volume growth, while permitting insignificant levels of dissolved gas buildup in the slow tissues. The reduction in growth parameters far outstrips any dissolved gas buildup in slow compartments, and faster compartments naturally eliminate dissolved gases during the stop, important for deeper diving.

Table 3. Relative Changes In Critical Parameters After Safety Stop

τ (<i>min</i>) halftimes	tissue tension relative change	critical volume relative change	bubble radius relative change
5	-21%	-34%	-68%
10	-11%	-24%	-39%
20	-6%	-11%	-24%
40	-2%	-8%	-18%
80	1%	3%	-2%
120	2%	4%	1%

Safety stop time can be added to bottom time for additional conservatism, but the effect of neglecting stop time is also small, as seen in Table 4. A stop at 15 *fsw* for 2 *min* is roughly equivalent to more than halving the standard ascent rate at depths in excess of 120 *fsw*. Procedures such as this, as well as reduced nonstop time limits, appear beneficial in multiday, multilevel, and repetitive diving. A safety stop near 15 *fsw* is easier than 10 *fsw* in adverse water conditions, such as surge and surface disturbances. Slower ascent rates afford additional advantages, but safety stops in the 2-4 *min* range are easier and more efficient.

Table 4. Comparative Surfacing Tissue Tensions

τ (<i>min</i>) halftimes	surfacing tension (<i>fsw</i>) 120 <i>fsw</i> /15 <i>min</i>	surfacing tension (<i>fsw</i>) 120 <i>fsw</i> /12 <i>min</i> 15 <i>fsw</i> /3 <i>min</i>	surfacing tension (<i>fsw</i>) 120 <i>fsw</i> /15 <i>min</i> 15 <i>fsw</i> /3 <i>min</i>
5	101.5	77.0	79.7
10	87.5	73.0	78.1
20	66.9	59.0	64.0
40	49.9	45.7	49.2
80	39.0	36.9	38.9
120	34.9	33.5	34.8

At altitude the same procedures can be employed, with depths, ascent rates, and stops conservatively scaled by the altitude correction factors (ratio of sea level pressure to ambient pressure at altitude) when using tables for which critical tensions need extrapolation at reduced ambient pressure. Tables with critical tensions fitted to altitude data have their own rules, as do meters.

Generally, bubble growth and excitation are compounded at altitude because of reduced pressure. Recent modeling work and experiments underscore this fact, indicating why critical tension models often fall short in hypobaric applications. Bubbles grow faster as they get bigger, and as pressure drops. With decreased pressure, bubbles will also expand by Boyle's law. Bigger bubbles are not as constricted by Laplacian film tension, while reduced pressure supports a faster rate of tissue gas diffusion into the bubble itself. Lanphier and Lehner performed extensive aerial decompression studies with goats, concluding that aerial decompression sickness strongly resembles underwater decompression sickness following saturation exposure. For ranging profiles followed by decompression to reduced ambient pressure, a high incidence of chokes was noted. Chokes is thought to result from microemboli interfering with pulmonary function. It is easy to speculate that rapid decompression to reduced pressure contributes to the buildup and growth of pulmonary emboli for the same reasons. Lanphier also concluded that slow tissue ($\tau \geq 80$ *min*) compartments do not correlate with chokes, suggesting that pulmonary microemboli are linked to fast compartments. Clearly, such an assertion also points out differences between types of decompression sickness, inferred critical tissue halftimes, and bubble formation time scales. Chokes and limb bends result from different critical insults, at different places, and over possibly different time scales.

The point to be made here in all cases is simple. Increased offgassing pressures reduce bubble growth rates dramatically in shallow zones, while impacting dissolved gas buildup in the slowest compartments minimally. Fast compartments also offload gas during safety stops, important for repetitive diving. Stops and slow ascent rates are always advisable, but particularly following multiexposures.

Tables And Meters

Operational diving requires arbitrary numbers of dives to various depths over periods of hours, and often days. Once a standard set of decompression tables has been constructed, with bounce diving the simple case of nonstop decompression, a repetitive dive procedure is a necessity. After any air dive, variable amounts of dissolved and free residual nitrogen remain in body tissues for periods of 24 *hr*, and more. Similarly, elevated tissue tensions can promote, or sustain, bubble growth over the same time scales. This residual gas buildup (dissolved and free) will shorten the exposure time for subsequent repetitive dives. The longer and deeper the first dive, the greater the amount of residual tissue nitrogen affecting decompression on subsequent dives. Nonstop depth-time allowances for repetitive dives are reduced in such circumstance. Within bubble models, residual free gas phases are also included in procedures, imposing additional constraints on repetitive diving.

The many possibilities are easily tracked in continuous time mode by computers, as mentioned, but tables face a more difficult task.

Considering only dissolved gases, one standard table approach, developed by Workman, groups combinations of depth and exposure times according to the surfacing tension in the slowest compartment. Then it is possible to account for desaturation during any arbitrary surface interval. The remaining excess nitrogen at the start of the next dive can always be converted into equivalent time spent at the deepest point of the dive. So called penalty time is then added to actual dive time to updated appropriate tissue tensions. Surfacing tensions in excess of 33 *fsw* (absolute) in the slowest compartment are assigned letter designations (groups), A to O, for each 2 *fsw* over 33 *fsw*. Any, and all, exposures can be treated in this manner. To credit outgassing, a Surface Interval Table, accounting for 2 *fsw* incremental drops in tensions in the slowest compartment, is also constructed. Such procedures are bases for the US Navy Air Decompression and Repetitive Surface Interval Tables, with the 120 *min* compartment (the slowest) controlling repetitive activity. Standard US Navy Tables provide safe procedures for dives up to 190 *fsw* for 60 *min*. Dives between 200 and 300 *fsw* were tested and reported in the exceptional exposure US Navy tables, including a 240 *min* compartment. The Swiss tables, compiled by Buhlmann, incorporate the same basic procedures, but with a notable exception. While the US Navy tables were constructed for sea level usage, requiring some safe extrapolation procedure to altitude, the Swiss tables are formulated and tested over a range of reduced ambient pressure. The controlling repetitive tissue in the Buhlmann compilation is the 635 *min* compartment. Similar approaches focusing on deep and saturation diving have resulted in decompression tables for helium-oxygen (heliox), helium-oxygen-nitrogen (trimix), and recent mixtures with some hydrogen (hydrox). Clearly, the USN and Swiss Repetitive Tables can be easily converted to other (longer or shorter) controlling tissues by arithmetic scaling of the 120 *min* or 635 *min* compartment to the desired controlling tissue halftime (simple ratio). To scale the USN Tables to 720 *min*, for instance, the repetitive intervals need only be multiplied by $720/120 = 6$.

While it is true that the table procedures just described are quite easily encoded in digital meters, and indeed such devices exist, digital meters are capable of much more than table recitations. Pulsing depth and pressure at short intervals, digital meters can monitor diving almost continuously, providing rapid estimates of any model parameter. When employing the exact same algorithms as tables, meters provide additional means to control and safety beyond table lookup. When model equations can be inverted in time, meters can easily compute time remaining before decompression, time at a stop, surface interval before flying, and optimal ascent procedure. Profiles can be stored for later analysis, and the resulting data bank used to tune and improve models and procedures. Considering utility and functionality, meter usage should increase in diving, supported by technological advance in computing power, algorithmic sophistication, and general acceptance, though it will probably be some time though before tables are supplanted.

A set of (modified) USN Tables is given in Table 5. The set has reduced nonstop time limits, consistent with present safety margins associated with lower Doppler scores (Spencer reduction), and has been computer validated for multilevel diving. It is based on the US Navy Tables. A set of modern phase (RGBM) tables for recreational diving can be seen in the Appendix. This set is a no-group, no-calculation, no-fuss set of tables for air and nitrox. Surface intervals of 1 *hr*, safety stops in the 15 *fsw* zone, and depth reductions on successive dives are requisite. Tables span sea level to 10,000 *ft* elevation. A set of mixed gas, technical RGBM Tables is also appended. These are discussed in the mixed gas section (Chapter 5).

On the heels of growing interest in underwater science and exploration following World War II, monitoring devices have been constructed to control diver exposure and decompression procedures. Devices, with records of varying success, include mechanical and electrical analogs, and within the past 15 years, microprocessor based digital computers. With inexpensive microprocessor technology, recent years have witnessed explosive growth in compact digital meters usage. All use the simple dissolved tissue gas model proposed by Haldane some 80 years ago, but given the sophistication

of these devices, many feel that broader models can be incorporated into meter function today, increasing their range and flexibility. Although the biophysics of bubble formation, free and dissolved phase buildup and elimination is formidable, and not fully understood yet, contemporary models treating both dissolved and free phases, correlated with existing data, and consistent with diving protocols might extend the utility of diving computers. An approach treating bubble nucleation, excitation, and growth in tissue and blood is needed. In the industry, such new models are termed bubble mechanical, because they focus on bubbles and their interactions with dissolved gas.

Decompression computers are sophisticated items these days. Basically a decompression meter is a microprocessor computer consisting of a power source, pressure transducer, analog to digital signal converter, internal clock, microprocessor chip with RAM (random access memory) and ROM (read only memory), and pixel display screen. Pressure readings from the transducer are converted to digital format by the converter, and sent to memory with the elapsed clock time for model calculations, usually every 1 - 3 *sec*. Results are displayed on the screen, including time remaining, time at a stop, tissue gas buildup, time to flying, and other model flag points, usually Haldanean (perfusion) tissue control variables. Some 3 - 9 volts is sufficient power to drive the computer for a couple of years, assuming about 100 dives per year. The ROM contains the model program (step application of model equations), all constants, and queries the transducer and clock. The RAM maintains storage registers for all dive calculations ultimately sent to the display screen. Dive computers can be worn on the wrist, incorporated in consoles, or even integrated into *heads – up* displays in masks. A typical dive computer is schematized in Figure 2.

Statistics point to an enviable track record of decompression meter usage in nominal diving activities, as well as an expanding user community. When coupled to slow ascent rates and safety stops, computer usage has witnessed a very low incidence rate of decompression sickness, below 0.01% according to some reports. Computers for nitrox and trimix are presently online today, with heliox and trimix units a rather simple modification of any nitrox unit, using existing decompression algorithms.

But there is certainly more to the story as far as table and meter implementations. To encompass such far reaching (and often diverse) changes in a unified framework requires more than the simple Haldane models we used for the past century with many *ad hoc* caveats. To model gas dynamics modelers and table designers need address both free and dissolved gas phases, their interplay, and their impact on diving protocols. Biophysical models of inert gas transport and bubble formation all try to prevent decompression sickness. Developed over years of diving application, they differ on a number of basic issues, still mostly unresolved today:

1. the rate limiting process for inert gas exchange, blood flow rate (perfusion) or gas transfer rate across tissue (diffusion);
2. composition and location of critical tissues (bends sites);
3. the mechanistics of phase inception and separation (bubble formation and growth);
4. the critical trigger point best delimiting the onset of symptoms (dissolved gas buildup in tissues, volume of separated gas, number of bubbles per unit tissue volume, bubble growth rate to name a few);
5. the nature of the critical insult causing bends (nerve deformation, arterial blockage or occlusion, blood chemistry or density changes).

Such issues confront every modeler and table designer, perplexing and ambiguous in their correlations with experiment and nagging in their persistence. And here comments are confined just to Type I (limb) and II (central nervous system) bends, to say nothing of other types and factors. These concerns translate into a number of what decompression modelers call dilemmas that limit

or qualify their best efforts to describe decompression phenomena. Ultimately, such concerns work their way into table and meter algorithms, with the same caveats. Phase models treat these issues in a natural way. But first, let's go back to the beginning.

Tables and schedules for diving at sea level can be traced to a model proposed in 1908 by the eminent English physiologist, John Scott Haldane. He observed that goats, saturated to depths of 165 feet of sea water (*fsw*), did not develop decompression sickness (DCS) if subsequent decompression was limited to half the ambient pressure. Extrapolating to humans, researchers reckoned that tissues tolerate elevated dissolved gas pressures (tensions), greater than ambient by factors of two, before the onset of symptoms. Haldane then constructed schedules which limited the critical supersaturation ratio to two in hypothetical tissue compartments. Tissue compartments were characterized by their half-time, τ . Half-time is also termed *half-life* when linked to exponential processes, such as radioactive decay. Five compartments (5, 10, 20, 40, 75 *min*) were employed in decompression calculations and staged procedures for fifty years.

Some years following, in performing deep diving and expanding existing table ranges in the 1930s, US Navy investigators assigned separate limiting tensions (*M-values*) to each tissue compartment. Later in the 1950s and early 1960s, other US Navy investigators, in addressing repetitive exposures for the first time, advocated the use of six tissues (5, 10, 20, 40, 80, 120 *min*) in constructing decompression schedules, with each tissue compartment again possessing its own limiting tension. Temporal uptake and elimination of inert gas was based on mechanics addressing only the macroscopic aspects of gas exchange between blood and tissue. Exact bubble production mechanisms, interplay of free and dissolved gas phases, and related transport phenomena were not quantified, since they were neither known nor understood. Today, we know more about dissolved and free phase dynamics, bubbles, and transport mechanisms, but still rely heavily on the Haldane model. Inertia and simplicity tend to sustain its popularity and use, and it has been a workhorse.

The establishment and evolution of gas phases, and possible bubble trouble, involves a number of distinct, yet overlapping, steps:

1. nucleation and stabilization (free phase inception);
2. supersaturation (dissolved gas buildup);
3. excitation and growth (free-dissolved phase interaction);
4. coalescence (bubble aggregation);
5. deformation and occlusion (tissue damage and ischemia).

Over the years, much attention has focused on supersaturation. Recent studies have shed much light on nucleation, excitation and bubble growth, even though *in vitro*. Bubble aggregation, tissue damage, ischemia, and the whole question of decompression sickness trigger points are difficult to quantify in any model, and remain obscure. Complete elucidation of the interplay is presently asking too much. Yet, the development and implementation of better computational models is necessary to address problems raised in workshops, reports and publications as a means to safer diving.

For purposes of continuity, a chronological ordering of models is taken below. Obviously, models get better in time, and as the list progresses. Time span across these models is roughly a century, and only the main ones appear.

1. Bulk Diffusion Model

Diffusion limited gas exchange is modeled in time by a sum of exponential response functions, bounded by arterial and initial tissue tensions. However, instead of many tissue compartments, a single bulk tissue is assumed for calculations, characterized by a gas diffusion constant, *D*. Tissue is separated into intravascular (blood) and extravascular (cells) regions. Blood containing dissolved inert and metabolic gases passes through the intravascular zone, providing initial

and boundary conditions for subsequent gas diffusion into the extravascular zone. Diffusion is driven by the difference between arterial and tissue tensions, according to the strength of a single diffusion coefficient, D , appropriate to the media. Diffusion solutions, averaged over the tissue domain, resemble a weighted sum over effective tissue compartments with time constants, $\lambda_{2n-1} = \alpha_{2n-1}^2 D$, determined by diffusivity and boundary conditions, with $\alpha_{2n-1} = (2n-1)\pi/l$ for tissue thickness, l .

Applications fit the time constant, $\kappa = \pi^2 D/l^2$, to exposure data, with a typical value employed by the Royal Navy given by, $\kappa = 0.007928 \text{ min}^{-1}$, approximating the US Navy 120 *min* compartment used to control saturation, decompression, and repetitive diving. Corresponding critical tensions in the bulk model,

$$M = \frac{709P}{P + 404},$$

fall somewhere between fixed gradient and multitissue values. At the surface, $M = 53 \text{ fsw}$, while at 200 *fsw*, $M = 259 \text{ fsw}$. A critical gradient,

$$G = \frac{P(493 - P)}{(P + 404)},$$

also derives from the above. Originally, a critical gradient, G , near 30 *fsw* was used to limit exposures. Such value is too conservative for deep and bounce exposures, and not conservative enough for shallow exposures. Hempleman introduced the above relationship, providing the means to parameterize bounce and saturation diving.

Bulk diffusion models (BDM) are attractive because they permit the whole dive profile to be modeled with one equation, and because they predict a $t^{1/2}$ behavior of gas uptake and elimination. Nonstop time limits, t_n , are related to depth, d , by the bulk diffusion relationship, seen in Figure 3,

$$dt_n^{1/2} = C,$$

with approximate range, $400 \leq C \leq 500 \text{ fsw min}^{1/2}$, linking nonstop time and depth simply through the value of C . For the US Navy nonstop limits, $C \approx 500 \text{ fsw min}^{1/2}$, while for the Spencer reduced limits, $C \approx 465 \text{ fsw min}^{1/2}$. In the Wienke-Yount model, $C \approx 400 \text{ fsw min}^{1/2}$.

2. Multitissue Model

Multitissue models (MTM), variations of the original Haldane model, assume that dissolved gas exchange, controlled by blood flow across regions of varying concentration, is driven by the local gradient, that is, the difference between the arterial blood tension and the instantaneous tissue tension. Tissue response is modeled by exponential functions, bounded by arterial and initial tensions, and perfusion constants, λ , linked to the tissue halftimes, τ , for instance, 1, 2, 5, 10, 20, 40, 80, 120, 180, 240, 360, 480, and 720 *min* compartments assumed to be independent of pressure.

In a series of dives or multiple stages, initial and arterial tensions represent extremes for each stage, or more precisely, the initial tension and the arterial tension at the beginning of the next stage. Stages are treated sequentially, with finishing tensions at one step representing initial tensions for the next step, and so on. To maximize the rate of uptake or elimination of dissolved gases the gradient, simply the difference between arterial and tissue tensions is maximized by pulling the diver as close to the surface as possible. Exposures are limited by requiring that the tissue tensions never exceed

$$M = M_0 + \Delta M d,$$

as a function of depth, d , for ΔM the change per unit depth. A set of M_0 and ΔM are listed in Table 6.

Table 6. Classical US Navy Surfacing Ratios And Critical Tensions.

halftime τ (<i>min</i>)	critical ratio R_0	critical tension M_0 (<i>fsw</i>)	tension change ΔM
5	3.15	104	2.27
10	2.67	88	2.01
20	2.18	72	1.67
40	1.76	58	1.34
80	1.58	52	1.26
120	1.55	51	1.19

At altitude, some critical tensions have been correlated with actual testing, in which case, an effective depth, d , is referenced to the absolute pressure, P (in *fsw*),

$$d = P - 33$$

with surface pressure, P_h , at elevation, h ,

$$P_h = 33 \exp(-0.0381h)$$

for h in multiples of 1,000 *ft*. However, in those cases where critical tensions have not been tested, nor extended, to altitude, an exponentially decreasing extrapolation scheme, called similarity, has been employed. Extrapolations of critical tensions, below $P = 33$ *fsw*, then fall off more rapidly than in the linear case. A similarity extrapolation holds the ratio, $R = M/P$, constant at altitude. Estimating minimum surface tension pressure of bubbles near 10 *fsw*, as a limit point, the similarity extrapolation might be limited to 10,000 *ft* in elevation, and neither for decompression nor heavy repetitive diving.

Models of dissolved gas transport and coupled bubble formation are not complete, and all need correlation with experiment and wet testing. Extensions of basic (perfusion and diffusion) models can redress some of the difficulties and deficiencies, both in theory and application. Concerns about microbubbles in the blood impacting gas elimination, geometry of the tissue region with respect to gas exchange, penetration depths for gas diffusion, nerve deformation trigger points for pain, gas uptake and elimination asymmetry, effective gas exchange with flowing blood, and perfusion versus diffusion limited gas exchange, to name a few, motivate a number of extensions of dissolved gas models.

The multitissue model addresses dissolved gas transport with saturation gradients driving the elimination. In the presence of free phases, free-dissolved and free-blood elimination gradients can compete with dissolved-blood gradients. One suggestion is that the gradient be split into two weighted parts, the free-blood and dissolved-blood gradients, with the weighting fraction proportional to the amount of separated gas per unit tissue volume. Use of a split gradient is consistent with multiphase flow partitioning, and implies that only a portion of tissue gas has separated, with the remainder dissolved. Such a split representation can replace any of the gradient terms in tissue response functions.

If gas nuclei are entrained in the circulatory system, blood perfusion rates are effectively lowered, an impairment with impact on all gas exchange processes. This suggests a possible lengthening of tissue halftimes for elimination over those for uptake, for instance, a 10 *min*

compartment for uptake becomes a 12 *min* compartment on elimination. Such lengthening procedure and the split elimination gradient obviously render gas uptake and elimination processes asymmetric. Instead of both exponential uptake and elimination, exponential uptake and linear elimination response functions can be used. Such modifications can again be employed in any perfusion model easily, and tuned to the data.

3. Thermodynamic Model

The thermodynamic model (TM) suggested by Hills, and extended by others, is more comprehensive than earlier models, addressing a number of issues simultaneously, such as tissue gas exchange, phase separation, and phase volume trigger points. This model is based on phase equilibration of dissolved and separated gas phases, with temporal uptake and elimination of inert gas controlled by perfusion and diffusion. From a boundary (vascular) thin zone, gases diffuse into the cellular region. Radial, one dimensional, cylindrical geometry is assumed as a starting point, though the extension to higher dimensionality is straightforward. As with all dissolved gas transfer, diffusion is controlled by the difference between the instantaneous tissue tension and the venous tension, and perfusion is controlled by the difference between the arterial and venous tension. A mass balance for gas flow at the vascular cellular interface, enforces the perfusion limit when appropriate, linking the diffusion and perfusion equations directly. Blood and tissue tensions are joined in a complex feedback loop. The trigger point in the thermodynamic model is the separated phase volume, related to a set of mechanical pain thresholds for fluid injected into connective tissue.

The full thermodynamic model is complex, though Hills has performed massive computations correlating with the data, underscoring basic model validity. One of its more significant features can be seen in Figure 11. Considerations of free phase dynamics (phase volume trigger point) require deeper decompression staging formats, compared to considerations of critical tensions, and are characteristic of phase models. Full blown bubble models require the same, simply to minimize bubble excitation and growth.

4. Varying Permeability Model

The varying permeability model (VPM) treats both dissolved and free phase transfer mechanisms, postulating the existence of gas seeds (micronuclei) with permeable skins of surface active molecules, small enough to remain in solution and strong enough to resist collapse. The model is based upon laboratory studies of bubble growth and nucleation.

Inert gas exchange is driven by the local gradient, the difference between the arterial blood tension and the instantaneous tissue tension. Compartments with 1, 2, 5, 10, 20, 40, 80, 120, 240, 480, and 720 halftimes, τ , are again employed. While, classical (Haldane) models limit exposures by requiring that the tissue tensions never exceed the critical tensions, fitted to the US Navy nonstop limits, for example, the varying permeability model, however, limits the supersaturation gradient, through the phase volume constraint. An exponential distribution of bubble seeds, falling off with increasing bubble size is assumed to be excited into growth by compression-decompression. A critical radius, r_c , separates growing from contracting micronuclei for given ambient pressure, P_c . At sea level, $P_c = 33 \text{ fsw}$, $r_c = 0.8 \text{ }\mu\text{m}$. Deeper decompressions excite smaller, more stable, nuclei.

Within the phase volume constraint, a set of nonstop limits, t_n , at depth, d , satisfy a modified law, $dt_n^{1/2} = 400 \text{ fsw min}^{1/2}$, with gradient, G , extracted for each compartment, τ , using the nonstop limits and excitation radius, at generalized depth, $d = P - 33 \text{ fsw}$. Tables 2 and 7 summarize t_n , G_0 , ΔG , and δ , the depth at which the compartment begins to control exposures.

Table 7. Critical Phase Volume Time Limits.

depth d (fsw)	nonstop limit t_n (min)	depth d (fsw)	nonstop limit t_n (min)
30	250.	130	9.0
40	130.	140	8.0
50	73.	150	7.0
60	52.	160	6.5
70	39.	170	5.8
80	27.	180	5.3
90	22.	190	4.6
100	18.	200	4.1
110	15.	210	3.7
120	12.	220	3.1

Gas filled crevices can also facilitate nucleation by cavitation. The mechanism is responsible for bubble formation occurring on solid surfaces and container walls. In gel experiments, though, solid particles and ragged surfaces were seldom seen, suggesting other nucleation mechanisms. The existence of stable gas nuclei is paradoxical. Gas bubbles larger than $1 \mu m$ should float to the surface of a standing liquid or gel, while smaller ones should dissolve in a few *sec*. In a liquid supersaturated with gas, only bubbles at the critical radius, r_c , would be in equilibrium (and very unstable equilibrium at best). Bubbles larger than the critical radius should grow larger, and bubbles smaller than the critical radius should collapse. Yet, the Yount gel experiments suggest the existence of stable gas phases, so no matter what the mechanism, effective surface tension must be zero. Although the actual size distribution of gas nuclei in humans is unknown, these experiments in gels have been correlated with a decaying exponential (radial) distribution function. For a stabilized distribution accommodated by the body at fixed pressure, P_c , the excess number of nuclei excited by compression-decompression must be removed from the body. The rate at which gas inflates in tissue depends upon both the excess bubble number, and the supersaturation gradient, G . The critical volume hypothesis requires that the integral of the product of the two must always remain less than some volume limit point, αV , with α a proportionality constant.

5. Reduced Gradient Bubble Model

The RGBM departs from the VPM in a number of ways, abandoning gel parameterizations. Colloidal suspensions, such as gel, are far different than aqueous and lipid materials coating bubbles and seeds in the body. Additionally, typical gel-type micronuclei, with persistence time scales of tens of hours to days, have never been found in the body in any circumstance. Present wisdom suggests that seeds are produced by tribonucleation (tissue friction). The full blown RGBM treats coupled perfusion-diffusion transport as a two step flow process, with blood flow (perfusion) serving as a boundary condition for tissue gas penetration by diffusion. Depending on time scales and rate coefficients, one or another (or both) processes dominate the exchange. However, for most meter implementations, perfusion is assumed to dominate, simplifying matters and permitting online calculations. Additionally, tissues and blood are naturally undersaturated with respect to ambient pressure at equilibration through the mechanism of biological inherent unsaturation (oxygen window), and the model includes this debt in calculations.

The RGBM assumes that a size distribution of seeds (potential bubbles) is always present, and that a certain number is excited into growth by compression-decompression. An iterative

process for ascent staging is employed to control the inflation rate of these growing bubbles so that their collective volume never exceeds a phase volume limit point. Gas mixtures of helium, nitrogen, and oxygen contain bubble distributions of different sizes, but possess the same phase volume limit point.

The RGBM postulates bubble seeds with lipid or aqueous skin structure. Bubble skins are assumed permeable under all crushing pressure, unlike the VPM. The size of seeds excited into growth is inversely proportional to the supersaturation gradient. At increasing pressure, bubble seeds permit gas diffusion at a slower rate. The model assumes bubble skins are stabilized by surfactants over calculable time scales, producing seeds that are variably persistent in the body. Bubble skins are probably molecularly activated, complex, biosubstances found throughout the body. Whatever the formation process, the model assumes the size distribution is exponentially decreasing in size, that is, more smaller seeds than larger seeds in exponential proportions. The RGBM also employs an equation-of-state for the skin surfactants, linked to lipid and aqueous biophysical structures. Gas diffusion across the bubble film interface, and Boyle expansion and contraction under ambient pressure change are also tracked in the RGBM.

In tracking seed excitation and number, gas transport into and out of bubbles, and Boyle-like expansion and contraction under pressure changes, the RGBM incorporates a spectrum of tissue compartments, ranging from 1 *min* to 480 *min*, depending on gas mixture (helium, nitrogen, oxygen). Phase separation and bubble growth in all compartments is a central focus in calculations, over appropriate time scales, and the model uses nonstop time limits tuned to recent Doppler measurements, conservatively reducing them along the lines originally suggested by Spencer (and others), but within the phase volume constraint.

The Haldane folded RGBM reduces the phase volume limit in multiding by considering free phase elimination and buildup during surface intervals, depending on altitude, time, and depth of previous profiles. Repetitive, multiday, and reverse profile exposures are tracked and impacted by critical phase volume reductions over appropriate time scales. The model generates bubble seed distributions on time scales of minutes to hours, adding new bubbles to existing bubbles in calculations. Phase volume limit points are also reduced by the added effects of new bubbles. In the Haldane folded algorithm, deep stops can be injected into staging procedures with a simple time-depth scaling law correlated with calculations from the full iterative RGBM model.

The modified (folded) RGBM extends the classical Haldane model to repetitive diving, by conservatively reducing the gradients, G . A conservative set of bounce gradients, G , can always be used for multiday and repetitive diving, provided they are multiplicatively reduced by a set of bubble factors, all less than one (Chapter 4). Three bubble factors reduce the driving gradients to maintain the phases volume constraint. The first bubble factor reduces G to account for creation of new stabilized micronuclei over time scales of days. The second factor accounts for additional micronuclei excitation on reverse profile dives. The third bubble factor accounts for bubble growth over repetitive exposures on time scales of hours. Their behavior is depicted in Figures 5, 6, and 7.

The RGBM (both versions) is a diveware implementation, accessible on the Internet at various sites. Additionally, the RGBM has been encoded into a number of commercial decompression meter products. Specific comparisons between RGBM and Haldane predictions for staging are summarized (Chapter 6), with resultants generic for phase versus dissolved gas models. NAUI uses RGBM Tables for trimix, helitrox, nitrox, and altitude dive training.

6. Tissue Bubble Diffusion Model

The tissue bubble diffusion model (TBDM), according to Gernhardt and Vann, considers the diffusive growth of an extravascular bubble under arbitrary hyperbaric and hypobaric loadings.

The approach incorporates inert gas diffusion across the tissue-bubble interface, tissue elasticity, gas solubility and diffusivity, bubble surface tension, and perfusion limited transport to the tissues. Tracking bubble growth over a range of exposures, the model can be extended to oxygen breathing and inert gas switching. As a starting point, the TBDM assumes that, through some process, stable gas nuclei form in the tissues during decompression, and subsequently tracks bubble growth with dynamical equations. Diffusion limited exchange is invoked at the tissue-bubble interface, and perfusion limited exchange is assumed between tissue and blood, very similar to the thermodynamic model, but with free phase mechanics. Across the extravascular region, gas exchange is driven by the pressure difference between dissolved gas in tissue and free gas in the bubble, treating the free gas as ideal. Initial nuclei in the TBDM have assumed radii near $3 \mu m$ at sea level, to be compared with $0.65 \mu m$ in the RGBM.

As in any free phase model, bubble volume changes become more significant at lower ambient pressure, suggesting a mechanism for enhancement of hypobaric bends, where constricting surface tension pressures are smaller than those encountered in hyperbaric cases. As seen in Figure 12, the model has been coupled to statistical likelihood, correlating bubble size with decompression risk, a topic discussed in a few chapters. For instance, a theoretical bubble dose of $5 ml$ correlates with a 20% risk of decompression sickness, while a $35 ml$ dose correlates with a 90% risk, with the bubble dose representing an unnormalized measure of the separated phase volume. Coupling bubble volume to risk represents yet another extension of the phase volume hypothesis, a viable trigger point mechanism for bends incidence.

Bubbles, which are unstable, are thought to grow from micron size, gas nuclei which resist collapse due to elastic skins of surface activated molecules (surfactants), or possibly reduction in surface tension at tissue interfaces or crevices. If families of these micronuclei persist, they vary in size and surfactant content. Large pressures (laboratory experiments) are necessary to crush them. Micronuclei are small enough to pass through the pulmonary filters, yet dense enough not to float to the surfaces of their environments, with which they are in both hydrostatic (pressure) and diffusion (gas flow) equilibrium. When nuclei are stabilized, and not activated to growth or contraction by external pressure changes, the skin (surfactant) tension offsets both the Laplacian (film) tension and any mechanical help from surrounding tissue. Then all pressures and gas tensions are equal. However, on decompression, the seed pockets are surrounded by dissolved gases at high tension and can subsequently grow (bubbles) as surrounding gas diffuses into them. The rate at which bubbles grow, or contract, depends directly on the difference between tissue tension and local ambient pressure, effectively the bubble pressure gradient, denoted G . At some point in time, a critical volume of bubbles, or separated gas, is established and bends symptoms become statistically more probable. On compression, the micronuclei are crunched down to smaller sizes across families, apparently stabilizing at new reduced size. Bubbles are also crunched by increasing pressure because of Boyle's law, and then additionally shrink if gas diffuses out of them. As bubbles get smaller and smaller, they probably restabilize as micronuclei.

Under compression-decompression, gas nuclei may grow as bubbles, depending on their effective bubble radius. Below a certain critical radius, r , listed in Table 8 below as a function of pressure according to a bubble model (varying permeability), as fitted to gel experiments, bubbles tend to collapse on themselves, while at larger equilibrium radius, they grow as gas diffuses into them. Stabilized nuclei evolve into unstable bubbles when their effective surface tension is greater than zero, or a sufficient diffusion gradient exists to drive gas into, or out of, the nucleus. At sea level, the model excitation radius is near $0.8 \mu m$, smaller than living cells, having dimensions starting at a few μm .

Table 8. Varying Permeability Model Excitation Radii.

pressure P (fsw)	excitation radius r (μm)	pressure P (fsw)	excitation radius r (μm)
13	0.89	153	0.49
33	0.80	183	0.45
53	0.72	283	0.35
73	0.66	383	0.29
93	0.61	483	0.24
113	0.57	583	0.21

However, the EOS excitation radii of the reduced gradient bubble model, Table 1 (Chapter 7), are much smaller than those of the varying permeability model above, certainly no surprise because lipid and aqueous tissues are not colloidal gel suspensions.

Micronuclei can be broadly classified as *homogeneous* or *heterogeneous*, depending upon their composition and that of the surrounding media. If the composition of both micronuclei and parent media are essentially the same, the nucleation process is termed homogeneous. If the composition of micronuclei and parent media differ, the nucleation process is termed heterogeneous. Spontaneous bubble formation in pure supersaturated liquids under explosive decompression is mainly homogeneous, while bubble formation on dust particles in supersaturated fluids is mostly heterogeneous. Homogeneous nucleation and bubble formation usually require large decompressions (many tens of atmospheres), while heterogeneous nucleation and bubble formation processes transpire with very small decompressions (tenths of atmospheres). Homogeneous nucleation in body tissue under nominal and controlled conditions of decompression appears much less likely than heterogeneous nucleation, considering pressure change and host of organic and inorganic body substances.

Nucleation theory is consistent with a number of diving observations. Divers might increase tolerance against bubble formation, and therefore bends, by following four simple practices:

1. make the first dive a deep, short (crush) dive, thereby constricting micronuclei down to smaller, safer size;
2. make succeeding dives progressively more shallow, thus diving within crush limits of the first dive and minimizing excitation of smaller micronuclei;
3. make frequent dives (every other day), thus depleting the number of micronuclei available to form troublesome bubbles;
4. for extended range and decompression diving, switch to pure oxygen in the shallow zone (20 fsw) to both shrink bubbles with inert gases and eliminate inert dissolved gases.

An underlying point can be made here. If nucleation sites are extinguished, reduced in number, or ill-disposed to excitation, bubble formation and risk are commensurately reduced. Regeneration times for classes of micronuclei are estimated to be near days, underscoring physiological adaptation to recurring pressure environments. The mechanics of nucleation, stabilization, and bubble growth are fairly complex, with stabilization mechanisms not quantified. Source and generation mechanisms before stabilization are not well understood. Some candidates include cosmic radiation and charged particles, dissolved gases in fluids we drink, lymph draining tissues into veins, collisional coalescence, blood turbulence and vorticity, exercise, the stomach, and the thin air-blood endothelium in the lungs. Once formed, micronuclei must stabilize very rapidly with surfactant material. Passing through the pulmonary filters of the lungs, only sub-micron sizes might survive. If nuclei are persistent, it is not clear that they populate all tissue sites, nor possess the same size distributions. Most argue that gel findings are not relevant because biological fluids are formed, and contained, in a sealed environment (the body). The Strauss and Yount studies suggest the existence of gas micronuclei in gels. Partially

stable nuclei seem to pervade all manner of fluids. But gel nuclei would seem to share little with nuclei formed in the body, since the materials stabilizing body nuclei are not colloidal gel.

Abandoning preformed nuclei, other methods of instantaneous bubble formation are certainly possible. Cavitation, produced by the rapid tearing, or moving apart, of tissue interfaces, is a candidate, as well as surface friction (tribonucleation). Crevices in tissues may form or trap gas phases, with later potential for release. Vorticity in blood flow patterns might cause small microbubbles. Stable, or unstable, the copious presence of microbubbles in the venous circulation would impact dissolved gas elimination adversely, also possibly impairing the lungs or the arterial network. The presence of bubbles in the arterial circulation might result in embolism. Bubble clogging of the pulmonary circulation is thought to relate to the chokes, a serious form of decompression sickness, while cerebral decompression sickness is believed due to emboli. Microbubbles in the venous circulation would render gas uptake and elimination asymmetric, with uptake faster than elimination. Displacing blood, microbubbles would reduce the effective area and volume for tissue-blood gas exchange.

Altitude Extrapolations And Ratios

Decompression at reduced ambient pressure, $P < 33 \text{ fsw}$, has been a study in itself, as reported by many researchers over the years. Recall that ambient pressure, P_h , at elevation, h , in multiples of 1,000 ft , is written

$$P_h = 33 \exp(-0.038h)$$

Studies developed separately above and below sea level, referenced as aerial and underwater decompression, also by the adjectives, hypobaric and hyperbaric. Aerial decompression differs from routine underwater decompression because the blood and tissues are equilibrated (saturated) with nitrogen ambient pressure before ascent. Breathing pure oxygen before ascent helps to protect against decompression sickness by washing out nitrogen. Up to about 18,000 ft , such procedure offers a considerable degree of protection. Beyond that, silent bubbles may retard nitrogen elimination. Simple bubble mechanics suggest that bubble excitation and growth are enhanced as ambient pressure decreases, and so decompression problems are theoretically exacerbated by altitude. Nucleation theory also suggests that critical radii increase with decreasing pressure, offering larger, less stable gas seeds for possible excitation and growth into bubbles. Larger bubbles possess smaller constricting surface tensions, and will thus grow faster in conducive situations. Such facts have been verified in the laboratory, and follow from simple bubble theory. Certainly the same considerations confront the diver at altitude, and are compounded with increasing nitrogen tension upon surfacing at reduced atmospheric pressure.

Lower ambient pressures at elevation, as depicted in Figure 13, and the lesser density of fresh water in smaller degree, affect gas uptake and elimination rates in tissues and blood. If critical critical tensions are employed to limit exposures, an immediate question centers upon their extrapolation and testing at altitude. Looking at Figure 1, a linear extrapolation of the critical tensions seems obvious, indeed just such an extrapolation of the US Navy critical tensions was proposed and tested by Bell and Borgwardt. Buhlmann, employing a different set of halftimes and critical tensions, also extended the Haldane algorithm to altitudes near 10,000 ft . Along with reduced critical tensions at altitude, reduced nonstop time limits, compared to sea level, are a natural consequence.

Another approach developed by Wienke reduces critical tensions exponentially with decreasing ambient pressure. Such an extrapolation turns the curves in Figure 1 down through the origin at zero ambient pressure. Intuitively, an exponential extrapolation of critical tensions through the origin is more conservative than the linear extrapolation, since corresponding critical tensions for given ambient pressure are smaller, also noted by others. If the extrapolation of critical tensions is allowed to follow the same exponential decrease of ambient pressure with altitude, then the ratio of the critical tension over ambient pressure, R , remains constant. Nonstop time limits in the exponential

scheme are also smaller than corresponding time limits in the linear scheme. As seen in Table 9, atmospheric pressure falls off approximately 1 *fsw* for every 1,000 *ft* of elevation. Exponential extrapolations of critical tensions have been tested, and serve as the operational basis of altitude procedures suggested by many others. Correlations of altitude chokes data for goats with constant ratio, *R*, trigger points have also been established, along with similar suggestions for the nitrogen washout data in aviators.

Tables and meters designed for sea level need be conservatively modified at altitude if possible, otherwise, not employed. Decomputer and table use are best left to manufacturer and designer discretions, but in any case, modification of critical tensions is central to any Haldane altitude algorithm. We detail the similarity method, using, for example, the US Navy Tables.

Many diving schedules are based on the Haldane model discussed in the previously, constraining activities so that *M* or *R* are not compromised. An approach to altitude diving, roughly as conservative as the tested schemes of early researchers, holds the ratios, *R*, constant at altitude, forcing altitude exposures to be *similar* to sea level exposures. Such similarity will force *M* to decrease exponentially with increasing altitude, keeping *R* constant with commensurate exponential reduction in the ambient pressure, *P*. Constant *R* extrapolations of this sort should be confined to nominal diving activities, certainly not heavy repetitive, decompression, nor saturation exposures.

The sought ratio constancy, *R*, at altitude induces a necessary scaling of actual depth to *equivalent sea level depth* (ESLD) for table entry, while all times remain unchanged. Actual depths at altitude are multiplied by factors, α , called altitude correction factors, which are just the ratios of sea level atmospheric pressure to altitude atmospheric pressure, multiplied by the specific density of fresh water (0.975). Neglect of the specific density scaling is a conservative convenience, and one of minimal impact on these factors. Today, wrist altimeters facilitate rapid, precise estimation of α on site. They can also be estimated from the *barometer* equation and are always greater than one. Table 9 lists correction factors at various altitudes, *z*, ranging to 10,000 *ft*. Up to about 7,000 *ft* elevation, $\alpha \approx 1 + .038 h$, with *h* measured in multiples of 1,000 *ft*, that is, $z = 1000 h$. The higher one ascends to dive, the deeper is his relative exposure in terms of equivalent sea level depth. Figure 9 contrasts correction factors scaled by the specific density of fresh water for elevations up to 18,000 *ft*. Relative increases in correction factors hasten rapidly above 10,000 *ft*. As described and seen in Table 9, *P* and α are reciprocally related, inverses actually. Again, time is measured directly, that is, correction factors are only applied to underwater depths, ascent rates, and stops.

Table 9. Altitude Correction Factors And US Navy Altitude Groups.

altitude, or change <i>z</i> (<i>ft</i>)	atmospheric pressure <i>P_h</i> (<i>fsw</i>)	correction factor α	penalty group on arrival at altitude	permissible group for ascension to altitude
0	33.00	1.00		
1,000	31.9	1.04	A	L
2,000	30.8	1.07	B	K
3,000	29.7	1.11	B	J
4,000	28.5	1.16	C	I
5,000	27.5	1.20	D	H
6,000	26.5	1.24	E	G
7,000	25.4	1.29	E	F
8,000	24.5	1.34	F	E
9,000	23.6	1.39	G	D
10,000	22.7	1.45	H	C

The similarity rule for altitude table modification and applying correction factors to calculations is straightforward. Convert depths at altitude to sea level equivalent depths through multiplication by α . Convert all table sea level stops and ascent rates back to actual altitude through division

by α . Ascent rates are always less than 60 *fsw/min*, while stops are always less than at sea level. Thus, a diver at 60 *fsw* at an elevation of 5,000 *ft* uses a depth correction of 72 *fsw*, taking $\alpha = 1.2$. Corresponding ascent rate is 50 *fsw/min*, and a stop at 10 *fsw* at sea level translates to 8 *fsw*. A capillary gauge at altitude performs these depth calculations automatically, and on the fly, as described below. Here the 3% density difference between salt and fresh water is neglected. Neglecting the 3% density correction is conservative, because the correction decreases equivalent depth by 3%. The effect on ascent rate or stop level is not on the conservative side, but is so small that it can be neglected in calculations anyway.

If a diver has equilibrated with ambient pressure at any elevation, than any reduction in ambient pressure will put the diver in a repetitive group, merely because tissue tensions exceed ambient pressure. If the original and new pressures are specified, it is possible to estimate tissue saturation and, hence, repetitive group for the excursion. Similar comments apply to pressure reductions following any diving activity, with sea level diving the usual bill of fare. These considerations are treated as follows.

At sea level, each repetitive group represents an increment of tissue pressure over ambient ($P_0 = 33$ *fsw*). For the US Navy tables, this increment is 2 *fsw* (absolute). If we compute the difference between sea level pressure and altitude pressure, and then scale the difference by the ratio of sea level atmospheric pressure to that altitude atmospheric pressure (correction factor α), we can estimate the repetitive group in which a sea level diver finds himself following immediate ascent to altitude. These group specifications are listed in column 4 of Table 9, and represent penalty time for the excursion to altitude, Entries were computed using sea level as the baseline, but are also appropriate (conservative) for any excursion between differing elevations.

In similar fashion, excursions to higher altitude following diving are limited by tissue critical tensions, and minimal repetitive group designators can be attached to any planned excursion. For the 120 minute compartment, the surfacing critical tension (sea level) is 51 *fsw*. On the safer side, we take 44 *fsw* as the limiting tension, convert it to an absolute tension of 56 *fsw* ($44/0.79$), and then inversely scale it to altitude by the ratio of sea level pressure to altitude pressure, that is, α . The resulting limiting tensions at altitude can then be converted to standard US Navy groups which are tabulated in column 5 of Table 9. Entries represent maximum permissible groups for immediate altitude excursions, and do not account for any travel time. Thus a diver would have to wait some length of time after a dive, until he dropped into the permissible group category, before ascending. The *D - group* rule for flying after diving is seen as a subcase for an altitude excursion to 9,000 *ft* (maximum cabin pressure). The question of altitude delay is timely, subject of recent discussions.

Time delays before altitude ascension, implicit to the permissible groups listed in the last column of Table 9, ultimately depend on the tissue compartment controlling the surface interval. In the US Navy tables, the 120 minute compartment controls surface intervals, and indeed Table 9 can be routinely applied to the US Navy Surface Interval Table to ascertain delay. With a 120 minute controlling compartment, corresponding time delays are compatible with a 12 hour rule for flying after diving. If a faster compartment is used to control surface intervals, a less conservative flying after diving rule would result, and similarly, if a slower compartment were employed, a more conservative rule would ensue.

Today, the 24 hour rule for flying after nominal diving is popular. Such a rule is more compatible with the 635 minute controlling compartment in Swiss tables (Buhlmann) than the 120 minute compartment in the US Navy tables (Workman). However, using a 635 minute compartment, we can still compute time delays for altitude excursions with the help of Table 9.

The calculation of permissible time for an altitude excursion following a dive, or flying after diving, amounts to determining the permissible altitude group from Table 9, the repetitive group following the dive, the standard (US Navy) surface interval to drop into the permissible altitude group, and multiplication of that surface interval by roughly 5.4. The factor of 5.4 results from replacement of the US Navy 120 minute compartment by the 635 minute compartment in the Surface Interval

Table, so that intervals times are increased by roughly 635/120 plus rounding calculations at group boundaries. For given repetitive group and altitude excursion (change in elevation), Table 10 list minimum delay times for altitude excursions as a function of altitude and repetitive dive group. Entries are consistent with a 635 minute compartment controlling offgassing, and 44 *fsw* limiting dissolved gas buildup in that compartment.

The approach outlined above has been used by both NASA and the US Navy.

Table 10. Altitude Delay Chart For The 24 Hour Rule.

altitude change <i>z</i> (<i>ft</i>)	group								
	D	E	F	G	H	I	J	K	L
2,000	0:00	0:00	0:00	0:00	0:00	0:00	0:00	0:00	2:26
3,000	0:00	0:00	0:00	0:00	0:00	0:00	0:00	2:37	4:08
4,000	0:00	0:00	0:00	0:00	0:00	0:00	2:53	4:30	5:51
5,000	0:00	0:00	0:00	0:00	0:00	3:04	4:57	6:29	7:44
6,000	0:00	0:00	0:00	0:00	3:20	5:24	7:12	8:38	9:54
7,000	0:00	0:00	0:00	3:41	6:02	8:06	9:43	11:10	12:36
8,000	0:00	0:00	4:08	6:50	9:11	11:04	12:41	14:19	15:40
9,000	0:00	4:50	8:06	10:48	12:58	14:51	16:39	18:11	23:09
10,000	6:18	10:37	13:25	15:56	18:05	20:10	21:18	23:24	24:50

Note, in Table 10, that some 24 *hours* must elapse before the L-group diver can ascend to an altitude of 10,000 *ft*, reflecting the current 24 hour delay recommended before flying after diving.

At altitude, the formal equivalence withh diving at sea level can be established through the similarity method, noting that ambient pressure, P , at depth, d , is less than at sea level,

$$P = P_h + \eta d$$

with atmospheric pressure, P_h , at altitude, h , depicted in Figure 13 and given by (*fsw*),

$$P_h = 33 \exp(-0.0381h) = \frac{33}{\alpha} ,$$

$$\alpha = \exp(0.0381 h) ,$$

for h in multiples of 1,000 *ft*, and then requiring that dives at altitude be equivalent to dives at sea level as far as decompression ratios, R , are concerned. Extrapolations of critical tensions, below $P = 33$ *fsw*, must then fall off more rapidly than in the linear case, since surfacing ambient pressures decreases exponentially.

The similarity (exponential) extrapolation holds the ratio, $R = M/P$, constant at altitude. Denoting a *sea level equivalent depth*, δ , at altitude, h , one has for an excursion to actual depth, d ,

$$\frac{M(d)}{d + 33\beta^{-1}} = \frac{M(\delta)}{\delta + 33} ,$$

$$\beta = \eta\alpha$$

so that the equality is satisfied when,

$$\delta = \beta d$$

$$M(\delta) = \beta M(d) .$$

As limit point, similarity extrapolation need be confined to elevations below 10,000 *ft*, and neither for decompression nor heavy repetitive diving. Again, the exponential factor, α , is the altitude

correction factor and is plotted in Figure 2. Consequently at altitude, h , the previously defined fitted critical tensions, $M(d)$, are then written,

$$M_h(d) = \beta^{-1}M(\delta) = \beta^{-1}M_0 + \beta^{-1}\Delta M\delta = \beta^{-1}M_0 + \Delta Md$$

preserving the altitude similarity ratios as required above. The relationship is fundamental to altitude diving within the critical tension framework.

Operational consistency of Haldane table and meter algorithms is also of interest here, and part of the reason is reflected in Table 11, which contrasts surfacing critical tensions, M_0 , for a number of meter algorithms. Entries were estimated (computed) from quoted meter nonstop time limits, t_n , using the 5, 10, 20, 40, 80, and 120 *min* compartments for convenience of illustration, that is to say that arbitrary τ and M_0 can be fitted to any set of nonstop time limits. Ascent and descent rates of 60 *fsw/min* were also employed in calculations. The Workman, Buhlmann, and Spencer critical surfacing tensions are fixed, while the equivalent Wienke-Yount surfacing critical tensions vary, depending on repetitive exposure. Entries are representative of nominal critical tensions.

Table 11. Comparative Surfacing Critical Tensions (M_0).

halftime τ (<i>min</i>)	Workman M_0 (<i>fsw</i>)	Spencer M_0 (<i>fsw</i>)	Buhlmann M_0 (<i>fsw</i>)	Wienke-Yount M_0 (<i>fsw</i>)
5	104	100	102	100-70
10	88	84	82	81-60
20	72	68	65	67-57
40	58	53	56	57-49
80	52	51	50	51-46
120	51	49	48	48-45

A glance at Table 11 underscores the operational consistency of classes of Haldane meter algorithms, with the Wienke-Yount approach effectively reducing critical tensions in multiding applications as the simplest meter implementation of a dual phase model. The variation in M_0 within the same compartments is relatively small. Table 12 collates the corresponding nonstop time limits, t_n , for completeness.

Table 12. Comparative Nonstop Time Limits (t_n).

depth d (<i>fsw</i>)	Workman t_n (<i>min</i>)	Spencer t_n (<i>min</i>)	Buhlmann t_n (<i>min</i>)	Wienke-Yount t_n (<i>min</i>)
30		225	290	250
40	200	135	125	130
50	100	75	75	73
60	60	50	54	52
70	50	40	38	39
80	40	30	26	27
90	30	25	22	22
100	25	20	20	18
110	20	15	17	15
120	15	10	15	12
130	10	5	11	9

Variation in the nonstop limits is greater than in the critical tensions, with the US Navy set the most liberal. Using the equivalent depth approach within the similarity method, the nonstop limits

in Table 12 can be extrapolated to altitude with correction factors. Figure 15 plots the Wienke-Yount nonstop time limits at various altitudes directly, using a bubble model constraint on the separated phase volume. Correction factors, depicted in Figure 14, are routinely employed to scale (multiply) actual depths at altitude for direct table entry. Scaled depths for table entry at altitude are always greater than actual dive depths, as discussed earlier. If correction factors are applied to the Wienke-Yount critical tensions in Table 11, virtually the same set of nonstop limits at altitude result. This is no real surprise, since phase volume models recover Haldane predictions for short and shallow exposures.

Hypobaric And Hyperbaric Asymptotics

Models for controlling and limiting hypobaric and hyperbaric exposures have long differed over ranges of applicability. Recent testing and comparison of altitude washout data question the hypobaric extension of the linear (hyperbaric) saturation curve, pointing instead to the correlation of altitude data (Conkin) with constant decompression ratios, R , in humans. Similar altitude correlations in sheep were noted by Lanphier and Lehner. Extensions of the saturation curve to altitude have been discussed by many, including Ingle, Bell and Borgwardt, Wienke, Cross, Smith, and Bassett in the not too distant past, with correlations and fits over small altitude excursions nicely established. However, in the limit of zero ambient pressure, P , these linear extrapolations are neither consistent with data nor with simple underlying physics (absolute law of entropy). Thermodynamics requires that supersaturation cannot be supported at zero ambient pressure, and that as ambient pressure goes to zero, the permissible supersaturation goes to zero faster. This means that diving M-values must pass through the origin at zero ambient pressure. Closure, then, of hypobaric and hyperbaric diving data is necessary, and must be effected with a more inclusive form of the saturation curve, one exhibiting proper behavior in both limits (pressure asymptotes).

Using the phase models just such a saturation curve was obtained by Wienke in a coupled framework treating both free and dissolved gas buildup and elimination in tissues. Within the phase volume constraint in correlated bubble dynamics, a general saturation curve of the form,

$$M = [\zeta + 1 - \exp(-\xi/P)]P$$

ensues for critical tensions, M , at ambient pressure, P , for ζ , ξ bubble number constants, and has the proper (zero entropy) limiting form. Related critical gradients, G , and critical ratios, R , take the standard form,

$$G = M - P$$

$$R = \frac{M}{P}$$

In the hypobaric limit, as $P \rightarrow 0$, then $M \rightarrow 0$, while in the hyperbaric limit, as $P \rightarrow \infty$, then $M \rightarrow \zeta P + \xi$. Corresponding tissue ratios, $R = M/P$, are bounded for all pressures. In the hypobaric regime, as $P \rightarrow 0$, then $R \rightarrow \zeta + 1$, while in the hyperbaric limit, $P \rightarrow \infty$, then $R \rightarrow \zeta$.

The above follow by noting, for m positive,

$$\lim_{P \rightarrow 0} \exp(-\xi/P^m) \rightarrow 0$$

$$\lim_{P \rightarrow \infty} \exp(-\xi/P^m) \rightarrow 1 - \xi/P^m$$

so that, we can write in general, hypobaric regime first,

$$M \rightarrow (\zeta + 1)P \rightarrow 0$$

$$G \rightarrow \zeta P \rightarrow 0$$

$$R \rightarrow \zeta + 1$$

and, in the hyperbaric regime,

$$M \rightarrow \xi + \zeta P$$

$$G \rightarrow \xi + (\zeta - 1)P$$

$$R \rightarrow \zeta$$

Typical ranges for the bubble constants, ζ and ξ , when nested within other model requirements for extrapolations, are

$$10.4 fsw \leq \xi \leq 18.5 fsw$$

$$1.25 \leq \zeta \leq 1.48$$

A more general representation can also be obtained in extending assumptions about permissible bubble excess, M-values, and excitation radii of bubble seeds as a function of powers of ambient pressure, P . A permissible bubble excess, Λ , takes general form, as before,

$$\Lambda = N\beta \int_0^r \exp(-\beta r) dr \propto 1 - \exp(-\beta r)$$

assuming all nuclei beyond r are excited by the compression-decompression exposure. In dual phase and bubble models, we have simple inverse relationships between pressure, P , and excitation radius, r ,

$$\frac{1}{r} \propto P^m \quad m \geq 1$$

Recall that in the RGBM, $m = 4/3$, while in the VPM, $m = 1$, roughly. On the dissolved gas side, we know that critical tensions scale with absolute pressure, P ,

$$M \propto P^n \quad n \geq 1$$

with $n = 1$ the usual value in classical Haldane approaches. And on the free side, critical tensions scale with the bubble excess,

$$M \propto \Lambda$$

Putting these qualitative expressions in mathematical terms, we can equate directly, for ζ and ξ proportionality constants, to the bilinear form,

$$M = \zeta P^n + \Lambda P^m$$

with ζ with ξ subsuming all other previously defined parameters. The limiting forms drop from the above expressions. Consider results for $n = m$ and $n \neq m$, with both n and m greater than 1.

1. Equal Power Law ($n = m$)

Analysis closely parallels the original case ($m = 1$), as follows. In the hypobaric regime,

$$M \rightarrow (\zeta + 1)P^m \rightarrow 0$$

$$G \rightarrow (\zeta + 1)P^m - P \rightarrow 0$$

$$R \rightarrow (\zeta + 1)P^{m-1} \rightarrow 0$$

In the hyperbaric regime,

$$M \rightarrow \xi + \zeta P^m$$

$$G \rightarrow \xi + \zeta P^m - P$$

$$R \rightarrow \zeta P^{m-1}$$

The previous hyperbaric *straightline* tension and hypobaric *constant* ratio are thus recovered in a generalized phase representation when $m = 1$. In that same regime, $\xi = 14.4 \text{ fsw}$ and $\zeta = 1.35$ in fitting data.

When $m = 4/3$, M increases more rapidly, G increases more slowly, and R varies as a function of ambient pressure. At zero pressure, M , G , and R all approach zero. And that is the correct behavior according to thermodynamics. The latter representation is not classical and follows from a low order EOS expansion of the excitation radius as a function of pressure at nominal temperatures and pressures. In this case, $\xi = 64.5 \text{ fsw}$ and $\zeta = 0.18$.

2. Unequal Power Law ($n \neq m$)

Here the analysis changes from the above cases, because of different asymptotic behavior of powers of P . The critical tensions assume the form,

$$M = \zeta P^n + [1 - \exp(-\xi/P^m)]P^m$$

with the asymptotic behavior, for the hypobaric region,

$$M \rightarrow \zeta P^n + \xi P^m \rightarrow 0$$

$$G \rightarrow \zeta P^n + \xi P^m - P \rightarrow 0$$

$$R \rightarrow \zeta P^{n-1} + P^{m-1} \rightarrow 0$$

and in the hyperbaric region,

$$M \rightarrow \xi + \zeta P^n$$

$$G \rightarrow \xi + \zeta P^n - P$$

$$R \rightarrow \zeta P^{n-1}$$

This recovers the same hypobaric limits as the preceding case when $n, m > 1$, that is, M , G , and R all approach zero. But, for purposes of illustration, we take $n = 1$ (dissolved gas) and $m = 4/3$ (RGBM). Fits to the same data yield, $\xi = 0.37 \text{ fsw}$ and $\zeta = 11.8$.

There are moderate differences in the various saturation data fits above, suggesting nominal model differences for asymptotic forms. However, the case, $n = m = 4/3$, yields the usual linear critical tension curve, M , in the hyperbaric regime, and a slowly varying, but approaching zero, critical ratio, R , in the hypobaric limit.

PHASE MECHANICS AND DECOMPRESSION THEORY IN DEPTH
CHAPTER 5: MIXED GASES AND DECOMPRESSION

Mixtures And Biological Reactivities

Mixed breathing gases, in a spectrum of underwater activities, have been utilized successfully, mostly mixtures of nitrogen, helium, and oxygen, differing from pure air, and lately those with higher oxygen content than air (*enriched*), which can be employed efficiently in shallow diving. Normoxic mixtures of nitrogen/oxygen (nitrox), helium/oxygen (heliox), and helium/nitrogen/oxygen (trimix) have long been employed commercially in deep and saturation diving. Recently, mixtures of hydrogen/oxygen (hydrox) have also been tested. A closer look at these inert gases in a range of diving applications is illuminating, particularly gas properties, advantages and disadvantages, and interplay.

Low pressure oxygen toxicity can occur if a gas mixture with 60% oxygen is breathed at 1 *atm* for 12 *hours* or more. Pulmonary damage, irritation, and coughing are manifestations (pulmonary toxicity). High pressure oxygen toxicity can occur when breathing pure oxygen at pressures greater than 1 *atm* for periods of minutes to hours, the lower the oxygen pressure the longer the time for symptoms to develop, and vice versa, as seen in Table 1 below. Twitching, convulsions, and dizziness are the symptoms (nervous system toxicity). On the other hand, if oxygen pressures fall below 0.16 *atm*, unconsciousness may result. Low levels of oxygen inhibit tissue cell metabolic function (hypoxia). Confusion and difficulty in maintaining coordination are milder symptoms. Severe hypoxia requires medical attention.

Table 1. Oxygen Depth-Time Limits (t_x).

oxygen depth d (<i>fsw</i>)	air depth d (<i>fsw</i>)	time limit t_x (<i>min</i>)
10	50	240
15	75	150
20	100	110
25	125	75
30	150	45
35	175	25
40	200	10

Clearly a constraint in mixed gas diving is the oxygen partial pressure. Inspired partial pressures of oxygen must remain below 1.6 *atm* (52.8 *fsw*) to prevent central nervous system (CNS) toxicity, and above 0.16 *atm* (5.3 *fsw*) to prevent hypoxia. This window, so to speak, is confining, some 1.44 *atm* (47.5 *fsw*). Denoting the mole fraction of oxygen, f_{O_2} , the upper and lower limits of this window, d_{max} and d_{min} , can be written (*fsw*),

$$\eta d_{max} = \frac{52.8}{f_{O_2}} - P_h \quad ,$$

$$\eta d_{min} = \frac{5.3}{f_{O_2}} - P_h \quad ,$$

$$\eta d_{max} - \eta d_{min} = \frac{47.5}{f_{O_2}} \quad ,$$

with η the specific density (with respect to sea water) and with working depths, d , limited by d_{max} and d_{min} ,

$$d_{min} \leq d \leq d_{max} \quad .$$

For fresh water, $\eta = 0.975$, and for sea water, $\eta = 1.000$. Certainly up to about 7,000 *ft* elevation, the lower limit, d_{min} , is no real constraint, with the surface accessible as the limit.

Another factor inhibiting performance underwater is inert gas narcosis, particularly at increasing ambient pressure. Although the common gases nitrogen and helium associated with diving are physiologically inert under normal atmospheric conditions, they both exhibit anesthetic properties as their partial pressures increase. The mechanism is not completely understood, but impaired carbon dioxide diffusion in the lungs, increased oxygen tension, fear, and related chemical reactions have all been implicated in the past. With 80/20 mixtures, symptom onset for nitrogen is near 100 *fsw*, and very much deeper for helium, in the 1,000 *fsw* range. Symptoms range from light headedness to unconsciousness at the extreme.

Nitrogen is limited as an inert gas for diving. Increased pressures of nitrogen beyond 130 *fsw* can lead to euphoria, and reduced mental and physical functional ability, while beyond 500 *fsw* loss of consciousness results. Individual tolerances vary widely, often depending on activity. Symptoms can be marked at the beginning of a deep dive, gradually decreasing with time. Flow resistance and the onset of turbulence in the airways of the body increase with higher breathing gas pressure, considerably reducing ventilation with nitrogen-rich breathing mixtures during deep diving. Oxygen is also limited at depth for the usual toxicity reasons. Dives beyond 150 *fsw* requiring bottom times of hours need employ lighter, more weakly reacting, and less narcotic gases than nitrogen, and all coupled to reduced oxygen partial pressures.

A number of inert gas replacements have been tested, such as hydrogen, neon, argon, and helium, with only helium and hydrogen performing satisfactorily on all counts. Because it is the lightest, hydrogen has elimination speed advantages over helium, but, because of the high explosive risk in mixing hydrogen, helium has emerged as the best all-around inert gas for deep and saturation diving. Helium can be breathed for months without tissue damage. Argon is highly soluble and heavier than nitrogen, and thus a very poor choice. Neon is not much lighter than nitrogen, but is only slightly more soluble than helium. Of the five, helium is the least and argon the most narcotic inert gas under pressure.

Saturation and desaturation speeds of inert gases are inversely proportional to the square root of their atomic masses. Hydrogen will saturate and desaturate approximately 3.7 times faster than nitrogen, and helium will saturate and desaturate some 2.7 times faster than nitrogen. Differences between neon, argon, and nitrogen are not significant for diving. Comparative properties for hydrogen, helium, neon, nitrogen, argon, and oxygen are listed in Table 2. Solubilities, S , are quoted in atm^{-1} , weights, A , in *atomic mass units (amu)*, and relative narcotic potencies, ν , are dimensionless (referenced to nitrogen in observed effect). The least potent gases have the highest index, ν .

Table 2. Inert Gas And Oxygen Molecular Weights, Solubilities, and Narcotic Potency.

	H_2	He	Ne	N_2	Ar	O_2
A (<i>amu</i>)	2.02	4.00	20.18	28.02	39.44	32.00
S (atm^{-1})						
blood	0.0149	0.0087	0.0093	0.0122	0.0260	0.0241
oil	0.0502	0.0150	0.0199	0.0670	0.1480	0.1220
ν	1.83	4.26	3.58	1.00	0.43	

The size of bubbles formed with various inert gases depends upon the amount of gas dissolved, and hence the solubilities. Higher gas solubilities promote bigger bubbles. Thus, helium is preferable to hydrogen as a light gas, while nitrogen is preferable to argon as a heavy gas. Neon solubility roughly equals nitrogen solubility. Narcotic potency correlates with lipid (fatty tissue) solubility,

with the least narcotic gases the least soluble. Different uptake and elimination speeds suggest optimal means for reducing decompression time using helium and nitrogen mixtures. Following deep dives breathing helium, switching to nitrogen is without risk, while helium elimination is accelerated because the helium tissue-blood gradient is increased when breathing an air mixture. By gradually increasing the oxygen content after substituting nitrogen for helium, the nitrogen uptake can also be kept low. Workable combinations of gas switching depend upon the exposure and the tissue compartment controlling the ascent.

While light-to-heavy gas switches (helium to nitrogen) are safe and commonplace in diving circles, the reverse is not generally true. In fact, heavy-to-light gas switches under pressure can be dangerous. In the former case, decreased tissue gas and bubble loading is a favorable circumstance following the switch. In the latter case, increased tissue gas and bubble loading could be hazardous. The two conditions are often termed *isobaric* desaturation and saturation. They are taken up shortly.

Mixed gas diving dates back to the mid 1940s, but proof of principle diving experiments were carried out in the late 50s. In 1945, Zetterstrom dove to 500 *fsw* using hydrox and nitrox as a travel mix, but died of hypoxia and DCS when a tender hoisted him to the surface too soon. In 1959, Keller and Buhlmann devised a heliox schedule to 730 *fsw* with only 45 *min* of decompression. Then, in 1962, Keller and Small bounced to 1,000 *fsw*, but lost consciousness on the way up due to platform support errors. Small and another support diver, Whittaker, died as a result. In 1965, Workman published decompression tables for nitrox and heliox, with the nitrox version evolving into USN Tables. At Duke University Medical Center, the 3 man team of Atlantis III made a record chamber dive to 2250 *fsw* on heliox, and Bennett found that 10% nitrogen added to the heliox eliminated high pressure nervous syndrome (HPNS). In deep saturation diving, *normoxic* breathing mixtures of gases are often advantageously employed to address oxygen concerns. A normoxic breathing mixture, helium or nitrogen, reduces the oxygen percentage so that the partial pressure of oxygen at the working depth is the same as at sea level, the obvious concerns, again, hypoxia and toxicity. Critical tensions can be employed in helium saturation diving in much the same fashion as nitrogen diving. A critical tension, recall, is the maximum permissible value of inert gas tension (*M*-value) for a hypothetical tissue compartment with specified halftime. An approach to helium exchange in tissue compartments employs the usual nitrogen set with halftimes reduced by 2.7, that is, the helium halftimes are extracted from the nitrogen halftimes following division by 2.7, and the same critical tension is assumed for both gas compartments. Researchers have tested schedules based on just such an approach. Tissue tensions scale as the relative proportion of inert gas in any mixture. More so than in air diving, computational methods for mixed gas diving and decompression are often proprietary information in the commercial sector.

Helium (normal 80/20 mixture) nonstop time limits are shorter than nitrogen, but follow a $t^{1/2}$ law similar to nitrogen, that is, depth times the square root of the nonstop time limit is approximately constant. Using standard techniques of extracting critical tensions from the nonstop time limits, fast compartment critical tensions can be assigned for applications. Modern bubble models, such as the reduced gradient bubble model, have also been used strategically in helium diving.

The three helium and nitrogen mixtures (nitrox, heliox, trimix) are employed for deep and saturation diving, with a tendency towards usage of enriched oxygen mixtures in shallow (recreational) diving. The use of enriched oxygen mixtures by recreational divers is growing, a concern for necessary training. Breathing mixture purity, accurate assessment of component gas ratios, oxygen toxicity, and appropriate decompression procedures are valid concerns for the mixed gas diver. Care, in the use of breathing mixtures, is to be underscored. Too little, or too much, oxygen can be disastrous. The fourth hydrogen mixture (hydrox) is much less commonplace.

Dividing Mixtures And Equivalent Depths

Today, mixtures of nitrogen, helium, and oxygen are common among commercial, scientific,

military, technical, and even recreational divers. And helium mixtures have been employed advantageously for decompression diving, replacing nitrogen mixtures once biblically prescribed.

Nitrox

Mixtures of oxygen and nitrogen with less oxygen than 21% (pure air) offer protection from oxygen toxicity in moderately deep and saturation diving. Moderately deep here means no more than a few hundred feet. Hypoxia is a concern with mixtures containing as much as 15% oxygen in this range. Saturation diving on oxygen-scarce nitrox mixtures is a carefully planned exposure. The narcotic effects of nitrogen in the 100 *fsw* to 200 *fsw* depth range mitigate against nitrox for deep diving.

Diving on enriched air mixtures need be carefully planned exposures, but for opposite reason, that is, oxygen toxicity. Mixtures of 30% more of oxygen significantly reduce partial pressures of nitrogen to the point of down loading tissue tensions compared to air diving. If standard air decompression procedures are employed, nitrox affords a diving safety margin. However, because of elevated oxygen partial pressures, a maximum permissible depth (floor) needs be assigned to any enriched oxygen mixture. Taking 1.6 *atm* (52.8 *fsw*) as the oxygen partial pressure limit, the floor for any mixture is easily computed. Enriched nitrox with 32% oxygen is floored at a depth of 130 *fsw* for diving, also called the oxygen limit point. Higher enrichments raise that floor proportionately.

Decompression requirements on nitrox are less stringent than air, simply because the nitrogen content is reduced below 79%. Many equivalent means to schedule nitrox diving exist, based on the standard Haldane critical tension approach. Air critical tensions can be employed with exponential buildup and elimination equations tracking the (reduced) nitrogen tissue gas exchange, or equivalent air depths (always less than the actual depths on nitrox) can be used with air tables. The latter procedure ultimately relates inspired nitrogen pressure on a nitrox mixture to that of air at shallower depth (equivalent air depth). For instance, a 74/26 nitrox mixture at a depth of 140 *fsw* has an equivalent air depth of 130 *fsw* for table entry. Closed breathing circuit divers have employed the equivalent air depth approach (discussed shortly) for many years.

Heliox

The narcotic effects of nitrogen in the several hundred feet range prompted researchers to find a less reactive breathing gas for deeper diving. Tests, correlating narcotic effects and lipid solubility, affirm helium as the least narcotic of breathing gases, some 4 times less narcotic than nitrogen according to Bennett, and as summarized in Table 2. Deep saturation and extended habitat diving, conducted at depths of 1,000 *ft* or more on helium/oxygen mixtures by the US Navy, ultimately ushered in the era of heliox diving. For very deep and saturation diving above 700 *fsw* or so, heliox remains a popular, though expensive, breathing mixture.

Helium uptake and elimination can also be tracked with the standard Haldane exponential expressions employed for nitrogen, but with a notable exception. Corresponding helium halftimes are some 2.7 times faster than nitrogen for the same hypothetical tissue compartment. Thus, at saturation, a 180 *minute* helium compartment behaves like a 480 *minute* nitrogen compartment. All the computational machinery in place for nitrogen diving can be ported over to helium nicely, with the 2.7 scaling of halftimes expedient in fitting most helium data.

When diving on heliox, particularly for deep and long exposures, it is advantageous to switch to nitrox on ascent to optimize decompression time, as discussed earlier. The higher the helium saturation in the slow tissue compartments, the later the change to a nitrogen breathing environment. Progressive increases of nitrogen partial pressure enhance helium washout, but also minimize nitrogen absorption in those same compartments. Similarly, progressive increases in oxygen partial pressures aid washout of all inert gases, while also addressing concerns of hypoxia.

An amusing problem in helium breathing environments is the high-pitched voice change, often requiring electronic voice encoding to facilitate diver communication. Helium is also very penetrating, often damaging vacuum tubes, gauges, and electronic components not usually affected by nitrogen.

Though helium remains a choice for deep diving, some nitrogen facilitates decompression, ameliorates the voice problem, and helps to keep the diver warm. Pure helium, however, can be an asphyxiant.

Trimix

Diving much below 1400 *fsw* on heliox is not only impractical, but also marginally hazardous. High pressure nervous syndrome (HPNS) is a major problem on descent in very deep diving, and is quite complex. The addition of nitrogen to helium breathing mixtures (trimix), is beneficial in ameliorating HPNS. Trimix is a useful breathing mixture at depths ranging from 500 *fsw* to 2,000 *fsw*, with nitrogen percentages usually below 10% in operational diving, because of narcotic effect.

Decompression concerns on trimix can be addressed with traditional techniques. Uptake and elimination of both helium and nitrogen can be limited by critical tensions. Using a basic set of nitrogen halftimes and critical tensions, and a corresponding set of helium halftimes approximately 3 times faster for the same nitrogen compartment, total inert gas uptake and elimination can be assumed to be the sum of fractional nitrogen and helium in the trimix breathing medium, using the usual exponential expressions for each inert gas component. Such approaches to trimix decompression were tested by researchers years ago, and many others after them.

Hydrox

Since hydrogen is the lightest of gases, it is reasonably expected to offer the lowest breathing resistance in a smooth flow system, promoting rapid transfer of oxygen and carbon dioxide within the lungs at depth. Considering solubility and diffusivity, nitrogen uptake and elimination rates in blood and tissue should be more rapid than nitrogen, and even helium. In actuality, the performance of hydrogen falls between nitrogen and helium as an inert breathing gas for diving.

Despite any potential advantages of hydrogen/oxygen breathing mixtures, users have been discouraged from experimenting with hydrox because of the explosive and flammable nature of most mixtures. Work in the early 1950s by the Bureau of Mines, however, established that oxygen percentages below the 3%-4% level provide a safety margin against explosive and flammability risks. A 97/3 mixture of hydrogen and oxygen could be utilized at depths as shallow as 200 *fsw*, where oxygen partial pressure equals sea level partial pressure. Experiments with mice also indicate that the narcotic potency of hydrogen is less than nitrogen, but greater than helium. Unlike helium, hydrogen is also relatively plentiful, and inexpensive.

In the case of mixtures of gases (nitrogen, helium, hydrogen), the Haldane decompression procedures (Chapters 1 and 2) can be generalized in a straightforward manner, using a set of nitrogen critical tensions, M , and halftimes, τ , as the bases. Denoting gas species, $j = N_2, He, H_2$, atomic masses, A_j , and partial pressures, p_j , each component satisfies a Haldane tissue equation, with rate modified coefficient, λ_j , given by,

$$p_j - p_{aj} = (p_{ij} - p_{aj}) \exp(-\lambda_j t) \quad ,$$

for p_{aj} and p_{ij} ambient and initial partial pressures of the j^{th} species, and with decay constant, λ_j , related by Graham's law to the nitrogen coefficient, $\lambda_{N_2} = \lambda$, by,

$$\lambda_j = \left[\frac{A_{N_2}}{A_j} \right]^{1/2} \lambda \quad .$$

Thus, for instance, one has,

$$\lambda_{He} = 2.7\lambda \quad ,$$

$$\lambda_{H_2} = 3.7\lambda \quad .$$

In a mixture, the total tension, Π , is the sum of all J partial tensions, p_j ,

$$\Pi = \sum_{j=1}^J [p_{aj} + (p_{ij} - p_{aj}) \exp(-\lambda_j t)]$$

and the decompression requirement is simply,

$$\Pi = \sum_{j=1}^J p_j \leq M \quad ,$$

for all exposures. Denoting ambient partial pressures, p_{aj} , as a fraction, f_j , of total pressure, P , that is,

$$p_{aj} = f_j P \quad ,$$

it follows that,

$$f_{O_2} + \sum_{j=1}^J f_j = 1$$

neglecting any carbon dioxide or water vapor in the mixture, of course. For 75/25 (enriched) nitrox, $f_{N_2} = 0.75$, for 90/10 heliox, $f_{He} = 0.90$, for 75/10/15 trimix, $f_{He} = 0.75$, $f_{N_2} = 0.10$, while for 95/5 hydrox, $f_{H_2} = .95$. For pure air obviously $f_{N_2} = 0.79$, as the common case. Clearly the treatment of breathing mixtures assumes a single critical tension, M , for each compartment, τ , in this case, extracted from the nitrogen data.

With nitrox ($f_{N_2} < 0.79$), it is clear that the nitrogen decompression requirements are reduced when using the same set of M , that is, the air set of M are assumed to apply equally to both air and other nitrogen mixtures. The procedure has been applied to heliox, trimix, and hydrox mixtures in similar vein. One important constraint in any mixture is the oxygen content. Partial pressures of oxygen must be kept below 52.8 *fsw* (1.6 *atm*) to prevent toxicity, and above 5.3 *fsw* (0.16 *atm*) to prevent hypoxia. Balancing diver mobility within this window at increasing depth is a delicate procedure at times.

Tables or staging algorithms based on on standard mixtures such as air, 80/20 heliox, 16/40 trimix, etc. can be employed for similar mixtures with different breathing gas fractions. The process merely amounts to computing *equivalent depths* by equating the partial pressures of gases in the new mixture to the partial pressures of those in the standard mixture. The computed equivalent depth for the mixture is then used to enter the standard table (usually), or algorithm. This method assumes that critical tensions, M , are the same for all mixtures.

Equivalent Air Depth

In extending air tables to other breathing mixtures, an extrapolation based on equal critical tensions anchors the *equivalent air depth* (EAD) method. The equivalent air depth method for table use derives from the imposed equality of mixture and inert gas partial pressures, and is very similar to the altitude equivalent depth method, but is not the same. For instance, with nitrox mixtures, the usual case, the equivalent air depth, δ , is related to the effective depth, d , by requiring equality of nitrogen partial pressures for air and nitrogen mixture with mole fraction f_{N_2} ,

$$\delta = \frac{f_{N_2}}{0.79}(P_h + d) - P_h.$$

At altitude, the effective depth, d , is the equivalent sea level depth described earlier. At sea level, the actual depth and effective depth are the same.

With enriched mixtures ($f_{N_2} < 0.79$), it is clear that the equivalent air depth, δ , is less than the effective depth, d , so that nitrogen decompression requirements are reduced when using δ to enter any set of air tables. Obviously. the same set of M are assumed to apply equally to both air and other mixture in the approach. At sea level, the above reduces to the form,

$$\delta = \frac{f_{N_2}}{0.79}(33 + d) - 33 \text{ fsw},$$

with d the actual depth, and has been utilized extensively in ocean diving. The EAD is also called the *equivalent nitrogen depth* (END) in some diving circles.

Equivalent Mixture Depth

The same procedure can be applied to arbitrary heliox, trimix, and hydrox mixtures in theory, basically an extrapolation from a reference (standard) table with the same gas components (helium, nitrogen, or hydrogen with oxygen). Denoting gas molar fractions in the standard (table) mixture, f_{sk} , with $k = N_2, He, H_2, O_2$, and molar fractions in the arbitrary mixture, f_k , we have for a K component mixture,

$$\delta = \frac{(1 - f_{O_2})}{(1 - f_{sO_2})}(P_h + d) - P_h$$

using mixture balance,

$$\sum_{k=1}^K f_k = 1 - f_{O_2}$$
$$\sum_{k=1}^K f_{sk} = 1 - f_{sO_2}$$

This approach yields the *equivalent mixture depth* (EMD). Both EAD and EMD are applied at altitude after the ESLD correction.

Having discussed equivalent depths, a next question focuses on the best diving mixtures to minimize decompression requirements, inert gas narcosis, and oxygen toxicity (discussed in the next section). The procedure is straightforward across commercial, military, and technical diving sectors, and goes like this.

1. determine oxygen fraction by specifying the maximum partial pressure, p_{O_2} , supported by the bottom depth and duration of the dive;
2. determine nitrogen fraction (if using nitrogen mixtures) by specifying maximum partial pressure, p_{N_2} , below narcosis threshold;
3. determine helium fraction (if using helium mixtures) by subtracting oxygen and nitrogen fraction from 1.

Isobaric Countertransport

Isobaric countertransport simply denotes isobaric diffusion of two gases in opposite directions. Perhaps a better descriptor is countercurrent diffusion. Historically, both terms have been used, with the former mostly employed in the decompression arena. Countertransport processes are a concern in mixed gas diving, when differing gas solubilities and diffusion coefficients provide a means for multiple inert gases to move in opposite directions under facilitating gradients. While ambient pressure remains constant, such counterdiffusion currents can temporarily induce high tissue gas supersaturation levels, and greater susceptibility to bubble formation and DCS. In general, problems can be avoided when diving by employing light to heavy (breathing) gas mixture switches, and by using more slowly diffusing gases than the breathing mixture inside enclosure suits (drysuits). Such procedure promotes *isobaric desaturation*, as termed in the lore. The opposite, switching from heavy to light gas mixtures and using more rapidly diffusing gases than the breathing mixture inside exposure suits, promotes *isobaric saturation* and enhanced susceptibility to bubble formation. More simply, the former procedure reduces gas loading, while the latter increases gas loading. The effects of gas switching can be dramatic, as is well known. For instance, a dive to 130 *fsw* for 120 *min* on 80/20 heliox with a switch to 80/20 nitrox at 60 *fws* requires 15 *min* of decompression time, while 210 *min* is required without the switch (Keller and Buhlmann in famous mixed gas tests in 1965). Yet, skin lesions and vestibular dysfunctionality have developed in divers breathing nitrogen

while immersed in helium (test chambers and exposure suits). And nitrogen-to-helium breathing mixture switches are seldom recommended for diving. A closer look at the isobaric countertransport phenomenon is interesting.

In the perfusion case, for a mixture of J gases, the total tissue tension, Π , at time, t , for ambient partial pressure, p_{aj} , and initial partial pressure, p_{ij} , with j denoting the gas species, can be written,

$$\Pi = \sum_{j=1}^J [p_{aj} + (p_{ij} - p_{aj}) \exp(-\lambda_j t)]$$

for, as usual,

$$\lambda_j = \frac{0.693}{\tau_j}$$

and τ_j the tissue halftime. In the diffusion case, we similarly find

$$\Pi = \sum_{j=1}^J \left[p_{aj} + (p_{ij} - p_{aj}) \frac{8}{\pi^2} \sum_{n=1}^{\infty} \frac{1}{(2n-1)^2} \exp(-\alpha_{2n-1}^2 D_j t) \right]$$

with,

$$\alpha_{2n-1} = \frac{(2n-1)\pi}{l}$$

for l a characteristic tissue scale parameter, and D_j the tissue diffusivity. These two expressions accommodate a multiplicity of initial conditions, gas switches, and provide a platform to discuss isobaric counterprocesses.

The form of the perfusion and diffusion total tensions, Π , is very similar. In fact, if we assume that the first term in the diffusion case dominates, we can write in general,

$$\Pi = \sum_{j=1}^J [p_{aj} + (p_{ij} - p_{aj}) \exp(-\kappa_j t)]$$

with, in the perfusion limit,

$$\kappa_j = \lambda_j$$

and, in the diffusion limit, taking just the first term ($n = 1$),

$$\kappa_j = \alpha_1^2 D_j = \frac{\pi^2 D_j}{l^2}$$

Simplifying matters by taking the case for two gases, $J = 2$, we have,

$$\Pi = (p_{a1} + p_{a2}) + (p_{i1} - p_{a1}) \exp(-\kappa_1 t) + (p_{i2} - p_{a2}) \exp(-\kappa_2 t)$$

for total tension, Π , as a function of individual gas initial tensions, time, and ambient partial pressures.

A local maxima or minima occurs in the total tension, Π , whenever,

$$\frac{\partial \Pi}{\partial t} = -\kappa_1 (p_{i1} - p_{a1}) \exp(-\kappa_1 t) - \kappa_2 (p_{i2} - p_{a2}) \exp(-\kappa_2 t) = 0$$

for constant ambient partial pressures, p_a . Or, equivalently written,

$$\frac{(p_{i1} - p_{a1})}{(p_{a2} - p_{i2})} = \frac{\kappa_2}{\kappa_1} \exp[(\kappa_1 - \kappa_2)t]$$

The equation is satisfied at a time, t_m , such that,

$$t_m = \frac{1}{(\kappa_1 - \kappa_2)} \ln \left[\frac{\kappa_2(p_{i2} - p_{a2})}{\kappa_1(p_{i1} - p_{a1})} \right]$$

and represents a local maxima in total tension, Π , if (after some algebra),

$$\left[\frac{\partial^2 \Pi}{\partial t^2} \right]_{t=t_m} < 0$$

or, a local minima, if,

$$\left[\frac{\partial^2 \Pi}{\partial t^2} \right]_{t=t_m} > 0$$

Some interesting features of isobaric counterdiffusion are imbedded in the above relationships, such as flow directionality, time scales, effects of switching, light versus heavy gases, and isobaric supersaturation or desaturation.

With positive time, $t_m > 0$, only two conditions are permissible:

$$\frac{\kappa_1(p_{i1} - p_{a1})}{\kappa_2(p_{a2} - p_{i2})} > 1 \quad , \quad \kappa_1 > \kappa_2$$

or,

$$\frac{\kappa_1(p_{i1} - p_{a1})}{\kappa_2(p_{a2} - p_{i2})} < 1 \quad , \quad \kappa_1 < \kappa_2$$

and the argument of the log function must be greater than zero always. The above relationships are complex functions of diffusivities, initial tensions, and ambient tensions before and after gas switching. The former case, $\kappa_1 > \kappa_2$, represents light-to-heavy gas switching (helium-to-nitrogen, for instance, where $\kappa_{He} = 2.7\kappa_{N_2}$), facilitating rapid desaturation of the lighter gas before heavier gas buildup. The latter case, $\kappa_1 < \kappa_2$, enhances supersaturation, as the lighter gas builds up rapidly before the heavier gas is eliminated.

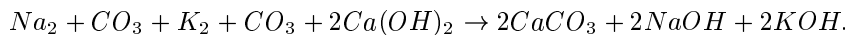
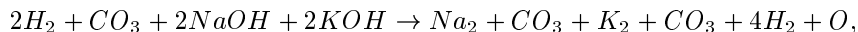
Figure 1 tracks gas supersaturation following nitrogen-to-helium switching due to the isobaric counterdiffusion of both gases. For helium-to-nitrogen switching (usual case for technical and commercial divers), a state of gas desaturation would ensue due to isobaric counterdiffusion.

Oxygen Rebreathing And Dose

As early as 1880, Fleuss developed and tested the first closed circuit, oxygen rebreathing system. At that time, of course, oxygen toxicity was not completely understood, though the effects of breathing pure oxygen were coupled to excitability and fever. In ensuing years, the apparatus was refined considerably, and was used by underwater combatants in World War II. During the 1950s, recreational divers used oxygen rebreathers. However, by the late 1950s, recreational divers switched to the popular open circuit device developed by Cousteau and Gagnan, thereby trading oxygen toxicity and caustic carbon dioxide concerns for decompression sickness and nitrogen narcosis. Today, rebreathers are witnessing a rebirth among technical divers. And, US Navy Underwater Demolition (UDT) and Sea Air Land (SEAL) Teams have continuously employed rebreathers for tactical operations.

In closed circuit systems, exhaled gas is kept in the apparatus, scrubbed of carbon dioxide by chemical absorbents, and then returned to the diver. No gas is released into the water (no bubbles). Gas consumption is related only to the physiological consumption of oxygen. Only a small amount of oxygen is required for extended exposures. Oxygen is taken directly from a breathing bag, and

exhaled gas passes separately through an alkaline, absorbent material, where it is scrubbed of carbon dioxide. A typical reduction process involves water vapor, sodium and potassium hydroxide, and carbon dioxide in the reaction chain,



Rebreathers today last about 3 *hr*, using approximately 6 m^3 of oxygen and 4 *lbs* of absorbent. Because of oxygen toxicity, depth is a limitation for oxygen rebreathing. Depth limitation for pure oxygen rebreathing is near 20 *fsw*. Today, closed circuit mixed gas rebreathers blend inert gases with oxygen (lowering oxygen partial pressure) to extend depth limitations. Two cylinders, one oxygen and the other inert gas (or a premixed cylinder), are employed, and the mixture is scrubbed of carbon dioxide before return to the breathing bag.

Closed circuit oxygen scuba takes advantage of gas conservation, but is limited in dive depth and duration by oxygen toxicity effects. Open circuit scuba offers greater depth flexibility, but is limited in depth and duration by the inefficiency of gas utilization. To bridge this gap, semi-closed circuit mixed gas rebreathers were developed. The semi-closed circuit rebreather operates much like the closed circuit rebreather, but requires a continuous, or frequent, purge to prevent toxic inert gas buildup. Two cylinders of oxygen and inert gas (or one premixed), are charged with safe levels of both, usually corresponding to safe oxygen partial pressure at the maximum operating depth. Gas flow from the high pressure cylinders the breathing circuit is controlled by a regulator and nozzle, admitting a continuous and constant mass flow of gas determined by oxygen consumption requirements. The diver inhales the mixture from the breathing bag and exhales it into the exhalation bag. Pressure in the exhalation bag forces the gas mixture through the carbon dioxide scrubber, and from the scrubber back into the breathing bag for diver consumption. When gas pressure in the breathing circuit reaches a preset limit, a relief valve opens in the exhalation bag, purging excess gas into the water.

Oxygen rebreathing at high partial pressures can lead to central nervous system (or pulmonary) oxygen poisoning. It is thought that high pressure oxygen increases the production of oxygen free radicals disrupting cell function. The US Navy conducted research into safe depths and durations for oxygen diving, and concluded that there is very little risk of central nervous system oxygen toxicity when partial pressures of oxygen are maintained below 1.6 *atm*. Additionally, risk only increases slightly when oxygen partial pressures are maintained below 1.8 *atm*. Operationally though, tech and mixed gas divers on rebreathers usually dive in the 1.4 to 1.2 *atm* range for extended exposures, and frequently detox on other less enriched breathing mixtures in the shallow zone (switching every 20 minutes or so).

High pressure oxygen is not just a magic gas for diving and decompression staging, it also has many important medical applications. Hyperbaric chambers are used to treat a number of maladies with different high pressure gases, maladies such as wounds, gangrene, DCI, cerebral palsy (CP), and multiple sclerosis (MS). Often the treatment mixture is oxygen (or mostly oxygen), and the treatment process is called hyperbaric oxygen therapy (HBOT). This is particularly true for wounds, gangrene, and MS. With DCI, treatment includes mixtures of nitrogen, helium, and oxygen blended in proportions to avoid oxygen toxicity and inert gas narcosis. The combination of increased ambient pressure and elevated levels of oxygen help to dissolve bubbles and also wash out inert gases.

Oxygen, when breathed under increased atmospheric pressure, is a potent drug. Hyperbaric oxygen, if administered indiscriminantly, can produce noticeable toxic effects. Safe time-dose limits have been established for hyperbaric oxygen, and these profiles form the basis of treatment protocols. The past 10 to 15 years have seen the introduction of disease specific hyperoxic dosing. Emergency cases, such as carbon monoxide poisoning or cerebral arterial gas embolism (AGE) may only require

one or two treatment schedules. In cases where angiogenesis is the primary goal, as many as 20 to 40 visits to the hyperbaric chamber may be requisite. The precise number of treatments often depends upon the clinical response of the patient. Transcutaneous oximetry can often provide more exacting dose schedules, improving treatment and cost effectiveness. With the exception of DCI and AGE, periods of exposure last approximately 2 hours. Treatments may be given once, twice, or occasionally three times daily, and provided in both inpatient and outpatient settings.

Several beneficial mechanisms are associated with intermittent exposure to hyperbaric doses of oxygen. Either alone, or more commonly in combination with other medical and surgical procedures, these mechanisms serve to enhance the healing process in treatable circumstances.

1. *Hyperoxygenation* provides immediate support to poorly perfused tissues in sections of compromised blood flow. The elevated pressure within the hyperbaric chamber results in a 10 to 15 fold increase in plasma oxygen concentrations. Translated to arterial oxygen tensions, values near 1,500 to 2,000 *mmHg* are observed, thereby producing a 4 fold increase in the diffusion length of oxygen from functioning capillaries. While this form of hyperoxygenation is only temporary, it does buy time and maintain tissue viability until corrective measures or new blood supply are established.
2. *Neovascularization* represents an indirect and delayed response to hyperbaric oxygen therapy. Therapeutic effects include enhanced fibroblast division, neof ormation of collagen, and capillary angiogenesis in areas of sluggish vascularization, such as radiation damaged tissue, refractory osteomyelitis, and chronic ulceration in soft tissue.
3. *Antimicrobial inhibition* has been demonstrated at a number of levels. Hyperbaric oxygen induces toxin inhibition and toxin inactivation in clostridial perfringens (gas gangrene). Hyperoxia enhances phagocytosis and white cell oxidative killing, and has been shown to support aminoglycoside activity. Recent studies suggest that prolonged antibiotic screening follows application of high pressure oxygen.
4. *Phase reduction*, application of Laplace's and Boyle's law to separated gases in tissue and blood, forms the basis of hyperbaric treatment of decompression sickness and arterial gas embolism, as known for more than a century. Commonly associated with divers and diving, AGE is a frequent iatrogenic event in modern medicine, resulting in significant morbidity and mortality, and remains grossly underdiagnosed. The process is enhanced gas diffusion from free phases to the venous blood flow for elimination through the lungs. Increasing pressure increases the outgassing gradient, and shrinks gas phases by Boyle contraction.
5. *Vasoconstriction* is an important spinoff of hyperbaric oxygen, manging intermediate compartment syndrome and other acute ischemias, as well as reducing interstitial edema in grafted tissues. Studies in burn wound applications indicate a significant decrease in fluid resuscitation requirements when HBOT is added to wound therapy.
6. *Reperfusion injury attenuation* is a recently discovered mechanism associated with hyperbaric oxygen. Leukocyte deactivation has been traced to high concentrations of oxygen in the blood, with the net effect the preservation of tissues that might otherwise be lost to ischemia-reperfusion injury. Reperfusion injury occurs with direct hypoxia and inappropriate activation of leukocytes.

Decompression sickness could be avoided by breathing just pure oxygen. And the usage of higher concentrations of oxygen in breathing mixtures not only facilitates metabolic function, but also aids in the washout of inert gases such as nitrogen and helium. Despite the beneficial effects of breathing oxygen at higher concentrations, oxygen proves to be toxic in excessive amounts, and over cumulative time intervals. Too little oxygen is equally detrimental to the diver. As discussed, limits

to oxygen partial pressures in breathing mixtures range, 0.16 *atm* to 1.6 *atm*, roughly, but symptoms of hypoxia and hyperoxia are dose dependent. Or, in other words, symptom occurrences depend on oxygen partial pressures and exposure times, just like inert gas decompression sickness. The mixed gas diver needs to pay attention not only to helium and nitrogen in staged decompression, but also cumulative oxygen exposure over the dive, and possible underexposure on oxygen depleted breathing mixtures.

The neurotoxic actions of high pressure oxygen are thought to relate directly to biochemical oxidation of enzymes, either those linked to membrane permeability or metabolic pathways. The list below is not exhaustive, but includes the following mechanisms:

1. the inability of blood to remove carbon dioxide from tissue when hemoglobin is oxygen saturated;
2. inhibition of enzymes and coenzymes by lipid peroxides;
3. increased concentration of chemical free radicals which attack cells;
4. oxidation of membranes and structural deterioration reducing electrical permeability for neuron activation;
5. direct oxygen attack on smooth muscle fibres;
6. oxygen induced vasoconstriction in arterioles;
7. elevation of brain temperature due to lack of replacement of oxygen by carbon dioxide in hemoglobin;
8. and, simple chemical kinetic redistribution of cellular carbon dioxide and oxygen with high surrounding oxygen tensions.

Fortunately for the diver, there are ways to avoid complications of hyperoxia. Careful attention to dose (depth-time) limitations for oxygen exposures is needed.

Despite the multiplicity and complexity of the above, limits for safe oxygen exposure are reasonably defined. Table 3 below lists NOAA CNS oxygen exposure time limits, t_x , for corresponding oxygen partial pressures, p_{O_2} . Below 0.5 *atm*, oxygen toxicity (CNS or pulmonary) is not really a problem. Figure 2 depicts these oxygen partial pressure limits for pulmonary and neurological toxicity manifestations, suggested by the US Navy and Lambertsen. Recent working NOAA limits, suggested by Table 3, track closely.

Table 3. Oxygen Dose-Time Limits

oxygen partial pressure p_{O_2} (<i>atm</i>)	oxygen time limit t_x (<i>min</i>)	oxygen tolerance (OTU) Υ (<i>min</i>)
1.6	45	87
1.5	120	213
1.4	150	244
1.3	180	266
1.2	210	278
1.1	240	279
1.0	300	300
0.9	360	299
0.8	450	295
0.7	570	266
0.6	720	189

The CNS data in Table 3 is easily fitted to a dose time curve, using least squares, yielding,

$$t_x = \exp \left[\frac{3.0 - p_{O_2}}{0.36} \right] = 4160 \exp (-2.77p_{O_2})$$

or, equivalently,

$$p_{O_2} = 3.0 - 0.36 \ln (t_x)$$

in the same units, that is p_{O_2} and t_x in *atm* and *min* respectively. The last column tabulates a pulmonary exposure dose, Υ , for divers, called the oxygen tolerance unit (OTU), developed by Lambertsen and coworkers at the University of Pennsylvania. Formally, the oxygen tolerance, Υ , is given by,

$$\Upsilon = \left[\frac{p_{O_2} - 0.5}{0.5} \right]^{0.83} t$$

and can be cumulatively applied to diving exposures according to the following prescriptions:

1. maintain single dive OTUs below 1440 *min* on the liberal side, or allow for 690 *min* of that as possible full DCS recompression treatment on the conservative side, that is, 750 *min*;
2. maintain repetitive total dive OTUs below 300 *min*.

The expression is applied to each and all segments of a dive, and summed accordingly for total OTUs, and then benchmarked against the 750 *min* or 300 *min* rough rule. The 750 *min* and 300 *min* OTU rules are not cast in stone in the diving community, and 10% to 25% variations are common, in both conservative and liberal directions. Formally, if Υ_n is the oxygen tolerance for the n^{th} segment of a dive, with segment time, t_n , and oxygen partial pressure, p_{nO_2} , the total OTU accumulated, Υ , is,

$$\Upsilon = \sum_{n=1}^N \Upsilon_n = \sum_{n=1}^N \left[\frac{p_{nO_2} - 0.5}{0.5} \right]^{0.83} t_n$$

with N the total number of dive segments (multilevel, deco, repetitive). Originally, Lambertsen defined a unit pulmonary toxicity dose (UPTD), Φ , given by,

$$\Phi = \left[\frac{p_{O_2} - 0.5}{0.5} \right]^{1.2} t$$

weighing oxygen partial pressure more than the OTU, but the definitions share the same basis, though slightly different fits to oxygen dose data. In the diving community, both representations have their proponents, favoring the oxygen partial pressure or time in oxygen dose estimations.

For exceptional and multiple exposures, the USN and University of Pennsylvania suggest the limits summarized in Table 4, where for multiple exposures, N , and segment times, t_{x_n} ,

$$T_x = \sum_{n=1}^N t_{x_n}$$

Table 4. Oxygen Exceptional Exposure Time Limits

oxygen partial pressure p_{O_2} (atm)	single exposure t_x (min)	multiple exposures T_x (min)
2.0	30	
1.9	45	
1.8	60	
1.7	75	
1.6	120	150
1.5	150	180
1.4	180	180
1.3	240	210
1.2	270	240
1.1	300	270
0.9	360	360
0.8	450	450
0.7	570	570
0.6	720	720

Note the severe reduction in multiple oxygen exposure time at 1.6 atm in Table 4. For this reason, technical divers generally restrict mixed gas diving exposures to $p_{O_2} \leq 1.6$ atm throughout any sequence of dives.

There are many ways to measure oxygen, with devices called oxygen analyzers. They are employed in chemical plants and refineries, hyperbaric chambers, intensive care units, and nurseries. The paramagnetic analyzer is very accurate, and relies on oxygen molecular response to a magnetic field in displacing inert gases from collection chambers. Thermal conductivity analyzers differentiate oxygen and nitrogen conduction properties in tracking temperatures in thermistors, with difference in temperatures proportional to the oxygen concentration. Magnetic wind analyzers combine properties of paramagnetic and thermal analyzers. Polarographic analyzers measure oxygen concentration by resistance changes across permeable oxygen membranes. Galvanic cell analyzers are microfuel cells, consuming oxygen on touch and generating a small current proportional to the amount of oxygen consumed. In all cases, analyzer response is linear in oxygen concentration.

Although it is tempting to avoid problems of oxygen toxicity by maintaining oxygen partial pressures, p_{O_2} , far below toxic limits, this is not beneficial to inert gas elimination (free or dissolved state). Higher levels of inspired oxygen, thus correspondingly lower levels of inert gases, are advantageous in minimizing inert gas buildup and maximizing inert gas washout. Coupled to narcotic potency of helium and nitrogen, and molecular diffusion rates, balancing and optimizing breathing mixtures with decompression requirements is truly a complex and careful technical diving exercise.

For the diver, all the foregoing translates into straightforward oxygen management protocols for both CNS and pulmonary toxicity. They are similar to inert gas management, but individual susceptibilities to oxygen seem to vary more widely, though reported statistics are more scattered. Consider CNS oxygen management first, using the CNS clock as it is popularly termed, and then pulmonary oxygen management, using the OTU as described.

CNS Toxicity Management

The various oxygen time limits, t_x , tabulated in the Tables above, obviously bound exposures, t , at oxygen partial pressure, p_{O_2} . Converting the exposure time to a fraction of the limit, Ξ_n , we can define a CNS oxygen clock, Ξ , that is over N exposure levels,

$$\Xi = \sum_{n=1}^N \Xi_n$$

where,

$$\Xi_n = \frac{t_n}{t_{xn}}$$

for exposure time, t_n , at level, n , with oxygen time limit, t_{xn} . Tabulating Ξ is most easily done by a computer. The prescription might be, depending on degree of conservatism,

$$0.7 \leq \Xi \leq 1.3$$

and where $\Xi = 1$ is the nominal choice. The fit equation for p_{O_2} and t_x suffices to range estimates of Ξ across all depths.

For repetitive dives, a surface interval penalty, similar to the nitrogen penalty in the USN Tables, can be levied for oxygen. A 90 *min* half-time is employed today, that is, the decay constant for residual oxygen CNS management, λ_{O_2} , is,

$$\lambda_{O_2} = \frac{0.693}{90} \text{ min}^{-1} = 0.0077 \text{ min}^{-1}$$

For surface interval, t , initial CNS clock, Ξ_i , and for 90 *min* folding time, the penalty (or residual) CNS clock, Ξ , is simply,

$$\Xi = \Xi_i \exp(-0.0077t)$$

The residual value is added to the planned repetitive dive additively, just like nitrogen penalty bottom time.

Pulmonary Toxicity Management

Pulmonary oxygen toxicity, Υ , follows a similar management scheme. As described, the total exposure, Υ , is the sum of interval exposures, Υ_n ,

$$\Upsilon = \sum_{n=1}^N \Upsilon_n = \sum_{n=1}^N \left[\frac{p_{nO_2} - 0.5}{0.5} \right]^{0.83} t_n$$

and is limited,

$$300 \text{ min} \leq \Upsilon \leq 750 \text{ min}$$

depending on desired degree of conservatism, and multiplicity of repetitive dives. Variations of 15% to 25% in the exposure limits are common.

PHASE MECHANICS AND DECOMPRESSION THEORY IN DEPTH CHAPTER 6: COMPARATIVE PROFILES AND OPERATIONAL DIVING

Haldane Profiles

In applying models and equations, we are faced with either fitting data to situations using plausible bases, or synthesizing mathematical models based strategically on first principles. Present practice relies upon the former, and calculational methods target a limited range of conditions. With that understanding, we can launch into specific application of the Haldane model. In presenting gas buildup and elimination curves, square wave profiles, assuming maximum gas tension over any time interval of interest, will be employed for graphical simplicity, and without loss of generality.

In compressed air diving, nitrogen tensions are measured in weight fractions of ambient (absolute) pressure, with nitrogen fraction the usual 0.79. By conventions, both pressures and depths are measured in feet-of-sea-water (*fsw*). Degrees to which compartments tolerate supersaturation are limited by critical values, M , fitted to the historical data by straight lines, depicted in Figure 1 (Chapter 4), with τ , M_0 , and ΔM tabulated in Table 6 (Chapter 4). They are representative of multitissue sets employed in tables and meters. Ranges of variation are neither large, nor diverse in application. How they are employed, that is, their implementation across a spectrum of exposures, also does not vary theoretically from table to meter. Self consistency is somewhat a keynote, though claims about advantages of particular sets of tissue parameters can be made on bases of test ranges, statistics, and correlations.

Parameter sets and critical values derive from data fits, iterative repetitions, hindsight, possibly venous gas emboli correlations, and bootstrapping of earlier models. Ranges are bounded, as are permissible activities. If extended to altitude, the surfacing limits, M_0 , decrease either exponentially (very rapidly) or linearly (more gradually). With notable parameter leeway in Table 1, additional leeway in permissible ascent and descent rates, and a set of non-stop time limits, a multiplicity of (safe) schedules are possible within the model framework. After testing, such schedules would then be fit for general diving consumption. Similar comments apply to the software driving any digital meter, effectively employing some equivalent version of Table 6 (Chapter 4), or Table 2 (Chapter 4).

Repetitive and decompression diving must contend with a greater fraction of separated gas. And this makes extrapolations of bounce diving fits more difficult. In the early days, slower tissue compartments were added to accommodate deeper, prolonged, and decompression exposures. Ostensibly, slower compartments might track a greater proportion of separated gas, possibly dumped from tissues into gas micronuclei. Laboratory studies in decompressed gels bear witness to typical growth and elimination patterns in gas nuclei and bubbles spanning hours. Of course, bubbles and nuclei in the body are both perfused and metabolic, adding to complexity. While not always optimal, tissue response functions with very slow compartments can be coupled to critical tensions for repetitive diving. The approach is more limited for repetitive diving than bounce diving, as possibly witnessed by higher bends incidence in divers embarking on multiday and repetitive activity, according to Vann and Dovenbarger. In such repetitive application, tables and meters which do not accommodate slower compartments, like $\tau > 60$ minutes, appear further limited. For that very reason, the US Navy expanded the original set some fifty years ago, replacing the 70 minute compartment with an 80 minute compartment and adding the 120 minute compartment. Yet, the tendency today to add compartments in the several hundred minutes range, while well-intentioned, is probably not the best means for tracking separated phases. Very slow compartments, in the several hundred minute range, cannot really control multiday and heavy repetitive diving by tracking just dissolved phases. Present consensus thus cautions against 3 or more repetitive dives in any 24 hour period, especially in the deeper categories (beyond 100 *fsw*), and relaxation periods of at least a day following 3-4 days of repetitive activity.

Bounce Diving

In bounce diving, exposures at depth for any time are followed by immediate return to the surface. Accordingly, consider a bounce dive to 60 *fsw* for 40 minutes, an exposure in the nonstop category for tables and meters. Figure 1 depicts both gas uptake (solid line) in the 20 minute compartment as a function of time and corresponding M (dotted line) throughout the exposure, neglecting the time to surface from 60 *fsw*, and thus any outgassing during the interval. Note that at no time underwater nor at the surface, is M exceeded by the tissue tension, the case in all compartments for this exposure. Bounce diving within dissolved gas models is well parameterized.

But, suppose we lengthen the exposure to 70 minutes, certainly a decompression dive. Figure 2 contrasts nitrogen uptake against M for the 40 minute compartment, should the diver surface immediately after 70 minutes. While M is not exceeded at 60 *fsw*, the surfacing limit M_0 , is exceeded. Clearly this diver would need to first decompress before surfacing. Here, only the 40 minute compartment is impacted. In general more than one compartment can be affected by exposures exceeding the nonstop time limits. If the diver, after 70 minutes at 60 *fsw*, makes a stop at 10 *fsw* for 2 minutes, he could safely ascend to the surface. The profile for the 40 minute compartment is depicted in Figure 3 in that case. Again, critical tensions are not exceeded.

Repetitive Diving

The Haldane approach to repetitive diving parallels that for bounce diving. Critical tensions again limit permissible degrees of compartment saturation. As an example of both repetitive application and diving idiom, *deepest dive first*, consider the profiles in Figures 4 and 5 for the 40 minute compartment. In the first case (Figure 4), an exposure to 70 *fsw* for 45 minutes is followed by a surface interval of 35 minutes, and then another dive to 50 *fsw* for 35 minutes. In the second case (Figure 5), the order is reversed, that is 50 *fsw* for 35 minutes, 35 minutes of surface interval, followed by 70 *fsw* for 45 minutes. Clearly, the first repetitive case is a nonstop exposure, while the second is not. In Figure 4, critical tensions are not exceeded, while in Figure 5, the critical tension, M_0 , is compromised at the end of the dive.

Repetitive application of dissolved gas models does not enjoy the same success as bounce diving application. Free phases in the tissues have had some time to grow between dives, and the next dive then pumps in a fresh supply of dissolved gas, possibly feeding phase growth if elimination has not been effective.

Multilevel Diving

Multilevel diving presents additional challenges to the classical scheme, though most problems occur with table usage, and less so with digital devices. The reason is not too complicated. Tables generally rely on the slowest tissue compartment to dictate staging and repetitive formats. Repetitive intervals are chosen so that the faster compartments cannot control the exposure upon surfacing, with 10 minutes the usual limit. Tables cannot account for gas uptake or elimination in faster compartments for shorter time intervals, and thus request that shorter time intervals be added directly to exposure times. In multilevel table application, the 10 minute interval is neglected, and gas exchange in the faster compartments is not considered. At times, neglect of the faster compartments causes trouble, especially when their critical tensions are exceeded with the tables blind for some 10 minutes. Because meters continuously monitor activities in all compartments, these table concerns are minimized in multilevel excursions. While such a problem is more an implementation issue than fundamental issue, foregoing concerns in bounce, repetitive, and decompression exposures still carry over here.

As a comparison of multilevel table and meter diving, consider Figure 6. Tissue and critical tensions in the 10 minute compartment for a multilevel exposure are depicted. The exposure consists of three segments, 120 *fsw* for 12 minutes, 90 *fsw* for 10 minutes, and 80 *fsw* for 2 minutes. According to the USN tables, the profile is marginally safe. But, according to Figure 6, the surfacing critical tension, M_0 , is violated. A meter could arrest this problem before it occurred, while a table might exhibit marginal indifference (depending on user discretion).

Systematically deeper-to-shallow diving practices are optimal in all cases. Deeper-than-previous excursions have the potential to excite smaller, more stable, gas nuclei into growth. Deeper-spike and sawtooth diving profiles become more hazardous as repetitive frequency increases, likely due to the presence of growing bubbles and excitable gas nuclei in slower tissues and slingshot effect of higher tensions surrounding them.

Saturation Diving

Like bounce diving, saturation diving, especially with mixed gases, has received considerable attention. Following exposures near 12 *hr*, all compartments are essentially equilibrated with ambient pressure. Ascent is then controlled by the slowest compartment, the one with the smallest critical tension, M . Compartments with halftimes in the range, $160 \leq \tau \leq 720$ *minutes*, are usually employed. In spite of compartment structure chosen, an interesting feature, consistent with Figure 2 (Chapter 4), arises in terms of critical tension in the slowest compartments.

From experiments, the saturation curve, relating permissible tissue tension to ambient pressure, has been well established for almost any gas mixture. In the case of air, Figure 4 depicts that relationship in absolute units, that is, $Q = M/0.79$ versus P . In terms of a linear, M the saturation air curve requires $M_0 = 44$ *fsw*, while $\Delta M = 1.06$. While time scales for ascent vary according to the half-time of the slowest compartment, critical tensions for saturation staging vary slightly. Similar structure is seen in diffusion algorithms, employing a critical gradient, G . For example, in the Royal Navy tables, Rashbass first employed a fixed gradient, $G = 30$ *fsw*, compared to $(M_0/0.79 - 33) = 23$ *fsw* in Figure 2 (Chapter 4). Later, Hempleman reduced the surfacing gradient, $G = 20$ *fsw*. As seen, the equivalent tissue half-time for the diffusion algorithm is 87 *minutes*. In short, no matter what the table or model, saturation staging formats are usually consistent with the saturation curve, more particularly, the slope and intercept. In that sense, all models collapse to a slow, single tissue equivalent, as discussed by Hennessy and Hempleman. For bounce diving, of course, models vary in their tissue number, critical parameters, or trigger points.

Empirical Practices

Utilitarian procedures, entirely consistent with phase mechanics and bubble dissolution time scales, have been developed under duress, and with trauma, by Australian pearl divers and Hawaiian diving fishermen, for both deep and repetitive diving with possible in-water recompression for hits. While the science behind such procedures was not initially clear, the operational effectiveness was always noteworthy and could not be discounted easily. Later, the rationale, essentially recounted in the foregoing, became clearer.

Pearling fleets, operating in the deep tidal waters off northern Australia, employed Okinawan divers who regularly journeyed to depths of 300 *fsw* for as long as one hour, two times a day, six days per week, and ten months out of the year. Driven by economics, and not science, these divers developed optimized decompression schedules empirically. As reported by Le Messurier and Hills, deeper decompression stops, but shorter decompression times than required by Haldane theory, were characteristics of their profiles. Such protocols are entirely consistent with minimizing bubble growth and the excitation of nuclei through the application of increased pressure, as are shallow safety stops and slow ascent rates. With higher incidence of surface decompression sickness, as might be expected, the Australians devised a simple, but very effective, in-water recompression procedure. The stricken diver is taken back down to 30 *fsw* on oxygen for roughly 30 minutes in mild cases, or 60 minutes in severe cases. Increased pressures help to constrict bubbles, while breathing pure oxygen maximizes inert gas washout (elimination). Recompression time scales are consistent with bubble dissolution experiments.

Similar schedules and procedures have evolved in Hawaii, among diving fishermen, according to Farm and Hayashi. Harvesting the oceans for food and profit, Hawaiian divers make between 8 and

12 dives a day to depths beyond 350 *fsw*. Profit incentives induce divers to take risks relative to bottom time in conventional tables. Three repetitive dives are usually necessary to net a school of fish. Consistent with bubble and nucleation theory, these divers make their deep dive first, followed by shallower excursions. A typical series might start with a dive to 220 *fsw*, followed by 2 dives to 120 *fsw*, and culminate in 3 or 4 more excursions to less than 60 *fsw*. Often, little or no surface intervals are clocked between dives. Such types of profiles literally clobber conventional tables, but, with proper reckoning of bubble and phase mechanics, acquire some credibility. With ascending profiles and suitable application of pressure, gas seed excitation and any bubble growth are constrained within the body's capacity to eliminate free and dissolved gas phases. In a broad sense, the final shallow dives have been tagged as prolonged safety stops, and the effectiveness of these procedures has been substantiated *in vivo* (dogs) by Kunkle and Beckman. In-water recompression procedures, similar to the Australian regimens, complement Hawaiian diving practices for all the same reasons.

The past ten years, or so, have witnessed a number of changes and additions to diving protocols and table procedures, such as shorter nonstop time limits, slower ascent rates, discretionary safety stops, ascending repetitive profiles, deep decompression stops, helium based breathing mixtures, permissible, reverse profiles, multilevel techniques, both faster and slower controlling repetitive tissue halftimes, lower critical tensions (*M*-values), longer flying-after-diving surface intervals, and others. Stimulated by Doppler technology, decompression meter development, theory, statistics, or safer diving consensus, these modifications affect a gamut of activity, spanning bounce to decompression, single to multiday, and air to mixed gas diving. As it turns out, there is good support for these protocols on operational, experimental, and theoretical grounds, and bubble models addressing these concerns on firmer basis than earlier models exist now, having been proposed and tested by numbers of investigators.

Spencer pioneered the use of Doppler bubble counting to suggest reductions in the nonstop time limits of the standard US Navy Tables, on the order of a repetitive group or two at each depth in the Tables (1-4 *fsw* in critical tensions), basing recommendations on lowering bubble counts at shorter nonstop time limits. Others have also made similar recommendations over the past 15 years.

Smith and Stayton noted marked reductions in recordial bubbles when ascent rates were cut from 60 *fsw/min* to 30 *fsw/min*. In similar studies, Pilmanis witnessed an order of magnitude drop in venous gas emboli (VGE) counts in divers making short, shallow, safety stops following nominal bounce exposures at the 100 *fsw* level, while Neumann, Hall, and Linaweaver recorded comparable reductions in divers making short, but deeper, stops after excursions to 200 *fsw* for longer periods of time.

An American Academy Of Underwater Sciences (AAUS) workshop on repetitive diving, recorded by Lang and Vann, and Divers Alert Network (DAN) statistics suggest that present diving practices appear riskier under increasing exposure time and pressure loading, spawning development of ancillary safety measures for multiday diving. Dunford, Wachholz, and Bennett noted persistent Doppler scores in divers performing repetitive, multiday diving, suggesting the presence of VGE in divers, all the time, under such loadings.

Ascent rates, safety stops, decompression computers, altitude diving reverse profiles, nitrox, deep, mixed gas, and technical diving have been the subject of extensive discussion at workshops and technical forums sponsored by the American Academy of Underwater Sciences, Smithsonian Institute, and the Undersea And Hyperbaric Medical Society (UHMS), as summarized by Lang and Hamilton, Lang and Egstrom, Lang and Vann, Sheffield, Wienke and O'Leary, Schreiner and Hamilton, and Smith. Some results of discussions culminated in sets of recommendations, folded within standard Haldane table and meter procedures, even for exposures exceeding neither time limits nor critical tissue tensions. Other sets, framed against modern decompression theory, underscored the significance of deep decompression stops, the coupled use of helium rich breathing mixtures, decompression software, technical diving training, and modern dive testing and validation.

In the past 5 years or so, the introduction of deep stops into diving and decompression regimens has also gained prominence and widespread acceptance, particularly in the mixed gas and technical sectors.

Bennett suggested that decompression injuries are likely due to ascending too quickly. He found that the introduction of deep stops, without changing the ascent rate, reduced bubble grades to near zero, from 30.5% without deep stops.

Marroni suggested the same, but found ascent speed itself did not reduce bubble formation. He suggested that a slowing down in the deeper phases of the dive (deep stops) should reduce bubble formation.

Brubakk and Wienke saw more bubbling in chamber tests when pigs were exposed to longer but shallower decompression profiles, where staged shallow decompression stops produced more bubbles than slower (deeper) linear ascents.

The upshot of these studies, workshops, discussions, and tests are a set of discretionary protocols, not necessarily endorsed in all diving sectors, but which might be summarized as follows:

1. reduce nonstop time limits a repetitive group, or two, below the standard US Navy limits;
2. maintain ascent rates below $33\text{ fsw}/\text{min}$, preferably slower, and requisitely slower at altitude;
3. limit repetitive dives to a maximum of three per day, not exceeding the 100 fsw level;
4. avoid multiday, multilevel, or repetitive dives to increasing depths;
5. wait 12 hr before flying after nominal diving, 18 hr after heavy diving (taxing, decompression, or prolonged repetitive) activity, and 24 hr after repetitive decompression diving;
6. avoid multiple surface ascents and short repetitive dives (spikes) within surface intervals of 1 hr ;
7. surface intervals of more than an hour are recommended for repetitive diving;
8. a deep stop for a minute or two in the range of $1/2$ the bottom depth is a prudent exercise for recreational divers, while systematic deep stops at $1/2$ the distance to the first required stops (ala Haldane staging) are similarly expedient for decompression and mixed gas divers;
9. safety stops for $2\text{-}4\text{ min}$ in the $10\text{-}20\text{ fsw}$ zone are advisable for all diving, but particularly for deep (near 100 fsw), repetitive, and multiday exposures;
10. do not dive at altitudes above $10,000\text{ ft}$ using modified conventional tables, or linear extrapolations of sea level critical tensions;
11. ride helium rich diving mixtures as close to the surface as possible (decompression diving) before switching to oxygen rich nitrox, and switch to pure oxygen in the shallow zone (20 fsw);
12. dual phase staging algorithms for mixed gas, decompression, extended range, and deep diving have been largely validated by the worldwide technical diving community (especially the dual phase RGBM protocols);
13. use dual phase diving tables, software, and decompression meters on the market today;
14. in short, dive conservatively, remembering that tables and meters are not bends proof, and also remembering that Haldane protocols (if they must be used) are only half correct (address dissolved gas only).

Procedures such as those above are prudent, theoretically sound, and safe diving protocols. Ultimately, they link to free phase and bubble mechanisms.

Validation is central to diving, and significant testing of nonstop and saturation diving schedules has transpired. In between, repetitive (more than one dive in a 12 hour period), multilevel (arbitrary depths throughout the course of a single dive), reverse profile (second repetitive dive deeper than first), and multiday (repetitive dives over days) diving cannot claim the same benefits, though some ongoing programs are breaking new ground. Application of (just) dissolved gas models in latter cases possibly has witnessed slightly higher decompression sickness (bends) incidence than in the former ones, as discussed in newsletters, workshops, and technical forums. Some hyperbaric specialists also suggest higher incidence of rash (skin bends) under repetitive loading. While statistics are not yet conclusive, they raise some concerns theoretically addressed by considering both dissolved and free phase gas buildup and elimination in broader based bubble models. Such models often focus on the amount of free phase precipitated by compression-decompression, and contain dissolved gas models as subset. In limiting the volume of free phase in time, they must also limit the growth rate.

RGBM Profiles And Validation

Suunto, Mares, Dacor, HydroSpace, Plexus, and Abyssal Diving have released products incorporating a modern phase algorithm, the reduced gradient bubble model (RGBM), for technical and recreational diving. An iterative approach to staging diver ascents, the RGBM employs separated phase volumes as limit points, instead of the Haldane (maximum) critical tensions across tissue compartments. The model is inclusive (altitude, repetitive, mixed gas, decompression, saturation, nonstop exposures), treating both dissolved and free gas phase buildup and elimination. NAUI Technical Diving employs the RGBM to schedule nonstop and decompression training protocols on trimix, heliox, and nitrox while also advocating gas switching alternatives for deep exposures. The RGBM draws on some of the earlier work of the Tiny Bubble Group at the University of Hawaii, but supplies missing physics and revamps the varying permeability model (VPM) to multiday, altitude, and mixed gas applications. While certainly not radical, the RGBM is both different and new on the diving scene. And not unexpectedly, the RGBM recovers the Haldane approach to decompression modeling in the limit of relatively safe (tolerably little) separated phase, with *tolerably little* a qualitative statement here. And the RGBM been tested and validated over the past 3-5 years across technical and recreational diving, something not documented for other phase models. All are first-time-ever commercial products with realistic implementation of a diving phase algorithm across a wide spectrum of exposure extremes. And all accommodate user knobs for additional conservatism.

Here, we merely look at the coarse bases of both meter and diveware implementations of the RGBM algorithm, one with extended range of applicability based on simple dual phase principles. Haldane approaches have dominated decompression algorithms for a very long time, and the RGBM has been long in coming on the commercial scene. With recent technical diving interest in deep stop modeling, and concerns with repetitive diving in the recreational community, phase modeling is timely and pertinent.

So, a next question is how does the RGBM compare with classical Haldane models as far as staging ascents, limiting multiexposures, and treating mixed gases? Generally, for short nonstop air diving, the RGBM reproduces the Spencer limits. For multiday in spans shorter than 1-3 *hr*, the RGBM reduces nonstop limits by 10% to 20% depending on surface interval, depth, altitude, and duration of present and previous dive, Multiday diving is impacted to lesser degree. Some comparisons appear in Table 1 for 3 days of repetitive air diving (120 *fsw*/10 *min* twice a day with 45 *min* surface interval). Computer choices are illustrative, not inductive.

Table 1. Nonstop Limits For RGBM And Haldane Air Multidiving

Computer/Algorithm	Dive 1 (<i>min</i>)	Dive 2 (<i>min</i>)	Dive 3 (<i>min</i>)	Dive 4 (<i>min</i>)	Dive 5 (<i>min</i>)	Dive 6 (<i>min</i>)
VYPER, EXPLORER/RGBM	10	6	9	5	9	5
COBRA/Spencer	10	9	10	9	10	9
DATA PLUS/USN	12	6	12	6	12	6
DELPHI/USN	10	10	10	10	10	10
ABYSS/RGBM	6	6	6	6	6	6
DC12/ZHL	9	7	9	7	9	7
ALADIN/ZHL	8	8	8	8	8	8
ALADIN PRO/ZHL	10	7	10	7	10	7
SOURCE/USN	12	9	12	9	12	9

The RGBM (first dive) nonstop limits (depth/time) are roughly 150/6, 140/7, 130/9, 120/10, 110/13, 100/17, 90/22, 80/28, 70/36, 60/51, 50/69, and 40/120. In the mixed gas arena, Table 2 lists nonstop time limits for ranged trimix, that is, 13% to 17% helium, 61% to 53% nitrogen, and 26% to 30% oxygen, according to RGBM and ZHL (Buhlmann).

Table 2. Trimix Nonstop Limits For RGBM And ZHL (Haldane).

Depth (<i>fsw</i>)	RGBM (<i>min</i>)	ZHL (<i>min</i>)
80	28	26
90	23	22
100	19	18
110	16	15
120	14	13
130	12	11
140	11	10
150	10	9

These limits are used by NAUI Technical Diving for training purposes. While both sets of nonstop time limits are different in Tables 3 and 4, the more dramatic effects of the RGBM show up for deep staging, as seen in Table 3. Comparative deep schedules for a trimix dive to 250 *fsw* for 30 *min* are contrasted, following a switch to air at 100 *fsw* and a switch to pure oxygen at 20 *fsw* on the way up. RGBM and ZHL are again employed, but with and without conservative safety knobs. In the case of ZHL, the outgassing tissue halftimes are increased by 1.5 in the conservative case, while for RGBM the bubble excitation radius is increased by 1.2 for comparison. Deeper stops are noticeably requisite in RGBM, but total decompression times are less than ZHL. The trimix is 33% helium, 51% nitrogen, and 16% oxygen.

Table 3. Deep Schedules According To RGBM And ZHL (Haldane)

Stop	Depth (<i>fsw</i>)	ZHL (<i>min</i>) (<i>standard</i>)	RGBM (<i>min</i>) (<i>standard</i>)	ZHL (<i>min</i>) (<i>safer</i>)	RGBM (<i>min</i>) (<i>safer</i>)
1	180	0	0	0	1
2	170	0	1	0	1
3	160	0	1	0	1
4	150	0	1	0	1
5	140	0	1	0	2
6	130	0	2	0	2
7	120	0	2	0	2
8	110	0	2	1	2
9	100	0	2	2	2
10	90	2	2	3	3
11	80	2	2	4	3
12	70	2	3	5	4
13	60	5	5	8	6
14	50	7	6	12	7
15	40	12	9	18	19
16	30	18	12	28	13
17	20	16	10	28	11
18	10	28	16	48	18
		93	77	147	98

That in a nutshell is a comparison of major differences between phase and dissolved gas models. The phase models recover dissolved gas models for short and nominal exposures, but require deeper stops and shorter decompression times for longer and exceptional exposures. A rundown of the software configuration of the RGBM used in full blown simulations follows. The package is under constant refinement and updating.

1. Module: Integrated bubble excitation, dissolved gas and bubble gas transfer, and staging routines, with waypoints prior to ascent, for nitrox, heliox, and trimix.
2. Source Code: 1640 Lines
3. Language/Compiler: FORTRAN 77/90, BASIC.
4. CRAY YMP Running Time: 1 *sec* for deep trimix profile with 5 gas switches on way up.
5. Input: altitude, bottom mixture, ascent/descent rate, switch levels and gas mixtures, pre-dive breathing gas, safety knobs, previous dive history.
6. Output: controlling tissue compartments, stop depth and times, supersaturation gradient, permissible supersaturation, effective bubble and gas parameters, critical phase volume, dive profile.
7. Cost: \$7000

Testing is central to diving, and much testing of bounce (single), nonstop diving has transpired. Repetitive and multiday exposures can neither claim, nor reap, the same benefits, and application

of any algorithm in the latter cases has witnessed higher bends statistics than in the former one. Reasons, impacting modeling, can be conjectured. Most tables and meters use dissolved gas models, and so long as the bulk of tissue gas remains in the dissolved state, the more correct and useful will prove such approaches. But as increasing proportion of free phases grow, by direct excitation of critical micronuclei or more gradual bubble coalescing transitions, the algorithm can lose predictive capability. Invariably, such conditions attend diving activity *extrapolated* outside model and test ranges, sometimes as a surprise.

Certainly any algorithm can be piecewise safe over tested ranges, but not always globally. Some implementations, as pointed out by Weathersby and Homer, may not be statistically rigorous, relying on much too small a set of exposure data to confidently predict outcome. Models not strongly correlated with tests can promulgate wide variation in predictive capability. Similarly, models can often *interpolate* within data, while failing to *extrapolate* outside the data. And then we must modify procedures to accommodate the extrapolation. A good point in question is the repetitive use of the USN tables. It is now clear that single, nonstop (bounce) dives, followed possibly by one more repetitive dive, form the test basis of the nonstop parts of the schedules. Yet, we observe that multiple repetitive dives permitted by the tables incur higher bends statistics, particularly in the deeper categories. This results from both model shortcomings and less reliable statistics. Adequate testing of any algorithm is always requisite, that is, descent rate, exposure profile, ascent rate, surface interval, and repetitive loading, as reiterated by Schreiner. And, because differences in diver response have been noted in hyperbaric chambers and open water, for the same schedules, questions of wet versus dry testing are valid. As discussed in the next Chapter, statistically significant testing, at the few percent level of decompression incidence, usually requires some 20-40 trials,

Models need validation and testing. Often, strict chamber tests are not possible, economically nor otherwise, and models employ a number of benchmarks and regimens to underscore viability. The following are some supporting the RGBM phase model and (released) nitrox, heliox, and trimix diving tables and meters:

1. counterror and countermeasures (LANL) exercises have used the RGBM (full up iterative deep stop version) for a number of years, logging some 327 dives on mixed gases (trimix, heliox, nitrox) without incidence of DCS – 35% were deco dives, and 25% were repets (no deco) with at least 2 hr SIs, and in the forward direction (deepest dives first);
2. NAUI Technical Diving has been diving the deep stop version for the past 3 yrs, some estimated 600 dives, on mixed gases down to 250 *fsw*, without a single DCS hit. Some 15 divers, late 1999, in France used the RGBM to make 2 mixed gas dives a day, without mishap, in cold water and rough seas. Same thing in the warm waters of Roatan in 2000 and 2001;
3. NAUI Worldwide released a set of no-group, no-calc, no-fuss RGBM Tables for air, EAN32, and EAN36 recreational diving, from sea level to 10,000 ft, a few years ago. Minimum SIs of 1 hour are supported for repetitive diving in all Tables, and safety stops for 3 minutes in the 15 *fsw* zone are required always. Tables were tested by NAUI Instructor Trainers, Instructors, and Divemasters over a 2 year period without mishap;
4. modified RGBM recreational algorithms (Haldane imbedded with bubble reduction factors limiting reverse profile, repetitive, and multiday diving), as coded into Suunto, Mares, Dacor, ABYSS, HydroSpace, Plexus decometers, lower an already low DCS incidence rate of approximately 1/10,000 or less. More RGBM decompression meters, including mixed gases, are in the works (not named at this time);
5. a cadre of divers and instructors in mountainous New Mexico, Utah, and Colorado have been diving the modified (Haldane imbedded again) RGBM at altitude, an estimated 350 dives, without peril. Again, not surprising since the altitude RGBM is slightly more conservative than

the usual Cross correction used routinely up to about 8,000 ft elevation, and with estimated DCS incidence less than 1/10,000;

6. within decometer implementations of the RGBM, not a single DCS hit has been reported in nonstop and multiding categories, beyond 200,000 dives or more, up to now;
7. extreme chamber tests for mixed gas RGBM are in the works, and less stressful exposures will be addressed shortly – extreme here means 300 *fsw* and beyond;
8. probabilistic decompression analysis of some selected RGBM profiles, calibrated against similar calculations of the same profiles by Duke, help validate the RGBM on computational bases, suggesting the RGBM has no more theoretical risk than other bubble or dissolved gas models (Weathersby, Vann, Gerth methodology at USN and Duke);
9. all divers and instructors using RGBM decometers, tables, or NET software have been advised to report individual profiles to DAN Project Dive Exploration (Vann, Gerth, Denoble and others at Duke).
10. ABYSS is a NET software package that offers the modified RGBM (folded over the Buhlmann ZHL) and soon the full up, deep stop version for any gas mixture, has a fairly large contingent of tech divers already using the RGBM and has not received any reports of DCS;
11. outside of proprietary (commercial) and RGBM Tables, mixed gas tables are a smorgasboard of no longer applicable Haldane dynamics and discretionary stop insertions, as witnessed by the collective comments of a very vocal and extremely competent, experienced technical diving community;
12. extreme WKPP profiles in the 300 *fsw* range on trimix were used to calibrate the full RGBM. WKPP profiles are the most impressive application of RGBM staging, with as much as 12 hours less decompression time for WKPP helium based diving on RGBM schedules versus Haldane schedules;
13. a TDI instructor dived the Baden in the North Sea to 520 *fsw* on RGBM tables on two different occasions, and is planning a 620 *fsw* dive to an Andros Blue Hole with RGBM scheduling. In the North Sea dives, 3 hours were shaved off conventional hang time by RGBM application;
14. NAUI Worldwide released sets of deep stop RGBM nitrox, heliox, and trimix technical and recreational Tables that have been tested by NAUI Technical Diving Operations over the past 3 years, with success and no reported cases of DCS, for open circuit regulators and rebreathers.

Because DCS is binomially distributed in incidence probability, many trials are often needed (or other close profiles) to fully validate any model at the 1% level. Additionally, full validation requires DCS incidences, the higher the number, the better, contrary to desired dive outcomes.

Reverse Profiles

Though the manifestations of DCS are statistically distributed, tables and meters use deterministic models to stage divers, with models broadly categorized as Haldane (dissolved phase) or bubble (combinations of dissolved and free phases). And model differences depend on profiles, exposures, and model assumptions. For diversity, we will focus on reverse diving profiles (RPs), wherein the second dive is deeper than the previous in any repetitive sequence. A summary of models, their underpinnings, correlations with data, and predictions for 100/60 and 60/100 RPs with variable surface intervals are first presented, and then for deeper and greater reverse profile increments.

Diving models address the coupled issues of gas uptake and elimination, bubbles, and pressure changes in different computational frameworks. Application of a computational model to staging divers, recall, is called a diving algorithm. Consider the foregoing computational models and staging regimens for the popular algorithms, namely, the perfusion limited, diffusion limited, thermodynamic, varying permeability, reduced gradient bubble, and tissue bubble diffusion algorithms. The first two are Haldane models (workhorse algorithms in early tables and meters), while the remaining four are bubble models in the generic sense (coming online in tables and meters, often driven by tech diving). The first two track just dissolved gas transfer, using critical tissue tensions as limit points, while the latter four treat both dissolved and free phase transfer, using free phase volumes as limit points.

Comparative Model Reverse Profiles

Employing the above described algorithms, we consider model predictions for RPs, extract underlying features and tendencies, and draw comparisons. The code, *DECOMP*, containing a number of model kernels, is employed for calculations.

The RPs (100/60 and 60/100) are normalized to roughly the same NDLs so that the nonstop time limits at 100 *fsw* and 60 *fsw* are 15 *min* and 50 *min*, respectively. This normalization leans slightly toward the conservative side as far as NDLs are concerned. Table 4 encapsulates the results for the MTM, BDM, TM, VPM, RGBM, and TBDM. Typically, tracking bubble growth and dissolved gas buildup and elimination, phase models require slightly more decompression times for the RPs. The MTM and BDM are comparable, the TM, VPM, and TBDM also track closely, and the RGBM is most conservative. These profiles are relatively shallow, and the RP increment is small ($\Delta d = 40$ *fsw*). Generally, bubble models affect deep and prolonged exposures the most, requiring deeper stops, but usually shorter overall decompression times. The effect is not seen here trendwise, but will reappear as the RP increments increase. Bubble and Haldane models overlap for short and shallow exposures, such as these RPs, and entries in Table 4 are no exception. The observation has often been made that not much free gas phase has been excited during short and shallow exposures, and then, bubble models should collapse to dissolved gas phase models in the limit.

When exposures are deeper and RP increments are greater than 40 *fsw*, model differentiations between dissolved gas and dual phase models appear in the staging regimens, as seen in Table 5, contrasting the MTM and RGBM only for 160/40 and 40/160 RPs. Clearly phase models (RGBM) require deeper staging but shorter times, as seen in Table 5 for the same surface intervals in Table 4. The bottom times are 7 *min* and 100 *min* at 160 *fsw* and 40 *fsw* respectively in Table 5.

NEST Reverse Profile Data

The Nuclear Emergency Strategy Team (NEST) is involved in counterterrorism and countermeasures related to nuclear and biological threats. Exercises and tests have yielded scattered data about RPs across a spectrum of breathing gas mixtures (nitrox, heliox, trimix). Recent activities have settled on trimix as the bottom and ascent gas, with pure oxygen breathed at 20 *fsw*. Mixtures range 13-40% helium, 44-64% nitrogen, and 16-30% oxygen. RP increments, Δd , vary from 40 - 120 *fsw*, and surface intervals are nominally greater than 60 *min*. The RGBM is the staging algorithm.

Table 4. Comparative RPs And Algorithms

Algorithm	Dive 1	Deco 1	Surface Interval	Dive 2	Deco 2
MTM	100/15	none	30	60/30	10/2
BDM		none			10/2
TM		none			10/1
VPM		none			10/2
RGBM		none			10/4
TBDM		none			10/3
MTM	60/30	none		100/15	10/2
BDM		none			10/2
TM		none			10/2
VPM		none			10/3
RGBM		none			10/5
TBDM		none			10/3
MTM	100/15	none	60	60/30	10/1
BDM		none			10/1
TM		none			10/1
VPM		none			10/2
RGBM		none			10/4
TBDM		none			10/2
MTM	60/30	none		100/15	10/1
BDM		none			10/1
TM		none			10/1
VPM		none			10/3
RGBM		none			10/6
TBDM		none			10/2
MTM	100/15	none	120	60/30	none
BDM		none			none
TM		none			10/1
VPM		none			10/1
RGBM		none			10/3
TBDM		none			10/1
MTM	60/30	none		100/15	10/1
BDM		none			10/1
TM		none			10/1
VPM		none			10/2
RGBM		none			10/4
TBDM		none			10/2
MTM	100/15	none	240	60/30	none
BDM		none			none
TM		none			none
VPM		none			none
RGBM		none			10/1
TBDM		none			10/1
MTM	60/30	none		100/15	none
BDM		none			none
TM		none			none
VPM		none			10/1
RGBM		none			10/2
TBDM		none			10/1

Table 6 tabulates results of NEST field activities, with nominal surface intervals of an hour or more. Maximum bottom depth is 250 *fsw*, and exposures are near trimix NDLs. Dives are grouped in RP categories of 40 *fsw*. The NDLs computed from the RGBM for trimix in the range down to 250 *fsw* are roughly:

100 *fsw* 8 - 10 *min*
 150 *fsw* 5 - 7 *min*
 200 *fsw* 4 - 6 *min*
 250 *fsw* 2 - 3 *min*

similar in duration to Haldane trimix NDLs. The ascent profile is different under the RGBM, as compared to standard Haldane staging. And this is well known, especially in technical diving circles where mixed gas diving pushes the exposure envelope.

Table 5. Comparative MTM And RGBM (Deep) RPs

Algorithm	Dive 1	Deco 1	Surface Interval	Dive 2	Deco 2
MTM	160/7	10/3	30	40/100	none
RGBM		10/1			10/4
MTM	40/100	none		160/7	10/11
RGBM		none			30/1,20/1,10/2
MTM	160/7	10/3	60	40/100	none
RGBM		10/1			10/3
MTM	40/100	none		160/7	10/3
RGBM		none			20/1,10/2
MTM	160/7	10/3	120	40/100	none
RGBM		10/1			10/2
MTM	40/100	none		160/7	10/3
RGBM		none			20/1,10/1
MTM	160/7	10/3	240	40/100	none
RGBM		10/1			10/1
MTM	40/100	none		160/7	10/3
RGBM		none			20/1,10/1

The incidence rate, *p*, in Table 6 is 6.7%, with highest count in the 40 - 120 *fsw* increment range. There are many variables here, such as staging depth, gas mixture, exposure time, and surface interval not tabulated separately.

Table 6. NEST RP Risk Table

Dives	RP Increment (<i>fsw</i>)	Probable Hits
36	0 - 40	0
18	40 - 80	2
6	80 - 120	2

Practices for the deeper increments may border the yo-yo category, though no prior history of repetitive diving existed. Exercises continue, and data will grow. Trends are apparent in the above Table 6, but further analysis is required.

Comparative NAUI Table Reverse Profiles

NAUI Training adopts a conservative view on RPs, contraindicated over many hour time intervals. Within the NAUI Tables (US Navy Tables with reduced NDLs), implications of this approach are discussed and quantified. NAUI Training has an admirable record of diving safety and surety, and

statistics underscore this fact. And so do other Training Agencies (PADI, SSI, YMCA, NASDS, TDI).

The US Navy Tables with reduced NDLs and the NAUI modifications based on consideration of multilevel activity (ascending or descending profiles) were discussed. For reference and comparison, a set of NAUI (modified) US Navy Tables is given in Figure 1 (Chapter 7), exhibiting reduced nonstop time limits, consistent with present safety margins associated with lower Doppler scores (Spencer reduction). But there is much more to the NAUI modification of the basic US Navy Tables, based on multilevel considerations. And that modification, coupled to recommended 1 *hr* surface intervals (SI) for repetitive diving, also impacts RPs favorably, as will be shown.

For the modified Tables (Figure 1), multilevel dives that stay to the left of the nonstop time limits never violate critical tensions, and are (hypothetically) sanctioned. Dive computers, of course, perform the same exercise underwater, comparing instantaneous values of computed tissue tensions in all compartments, throughout the duration of the dive, against stored M -values to estimate time remaining and time at a stop.

The set of NAUI NDLs corresponds to a reduced set of critical tensions, M_0 , ΔM , given by,

$$M_0 = 102, 86, 70, 57, 51, 50 \text{ fsw}$$

$$\Delta M = 2.27, 2.01, 1.67, 1.34, 1.26, 1.19$$

in round numbers for the same set of tissue halftimes, τ . With risk analysis performed by US Navy investigators (Chapter 30), the relative probability, p , of DCS in (always) diving to the NAUI NDLs limits is bounded by,

$$1\% < p < 5\%$$

yet remembering that divers never dive consistently to (any) Table limits. Interpolating between bounding NDLs, the estimated probability, p , is

$$p < 2.5\%$$

at the limit point of diving to NAUI NDLs. Simple difference weighting between bounding NDLs and NAUI NDLs was invoked for the estimate.

Consider the scripted RPs within the NAUI Table framework. In a rather simple sense, these RPs represent multilevel diving with nonzero surface intervals, at least when only dissolved gases are tracked. However, with bubble growth under decompression fueled by high tissue tensions, such extensions and analogies probably breakdown. Profiles are 100 *fsw* and 60 *fsw* for 15 *min* and 30 *min* as also contrasted in Table 4.

Table 7. NAUI Tables And RPs

Algorithm	Dive 1	Deco 1	Surface Interval	Dive 2	Deco 2
NAUI Tables/USN	100/15	none	30	60/30	15/5
	60/30	none		100/15	15/15
	100/15	none	60	60/30	none
	60/30	none		100/15	15/15
	100/15	none	120	60/30	none
	60/30	none		100/15	15/5
	100/15	none	240	60/30	none
	60/30	none		100/15	none

Clearly the step nature of Table decompression formats is evident in Table 7. The decompression stops at 15 *fsw* do not smoothly decrease in time as surface interval time increases. NAUI, of course, requires all training to be nonstop diving, so such profiles would not occur routinely.

NAUI Reverse Profile Statistics

In the 10 years since NAUI introduced these Tables, nearly 1,000,000 divers were certified at an entry level. This represents some 5,000,000 actual dives, mainly performed above 60 *fsw*, with surface intervals beyond 60 *min*, and no more than 2 dives per day. Reverse profiles are not suggested, and training regimens also mandate minimum 60 *min* surface intervals, depth floors at 60 *fsw*, and less than 3 dives per day. To build diver confidence, much activity occurs at depths in the 20 - 30 *fsw* range. All recreational NAUI diving is limited to 130 *fsw*, as are the NAUI Tables. These limits and mandates restrict all diving, and certainly impact RPs favorably.

Accident reports gathered by NAUI in this time average 50 per year (required for insurance and liability coverage). Of these 50 reports, only 5 relate (average) to DCS afflictions. This suggests an incidence rate, p , on the order of 1×10^{-5} , certainly a very low annual rate. Other Training Agencies (PADI, SSI, YMCA, NASDS, TDI) should echo the same ballpark figure, since training regimens across recreational diving are roughly the same.

Thus, any RPs probably range 30 - 40 *fsw* as far as depth increment, Δd , in training maneuvers. This is small, as are actual training depths. Based on low DCS incidence rate, NAUI Table conservatism, small RP increment, and shallow staging depths, RPs appear to have not been a major problem for NAUI Training Operations. But as RP depths and increments increase, the situation becomes less clear and riskier, as Table 6 suggests.

Deep Stops

Deep stops are what the name suggests, just decompression stops made at deeper depths than those traditionally dictated by classical (Haldane) dive tables or algorithms. They are fairly recent (last 15 years) protocols, suggested by modern decompression theory, but backed up by extensive diver practicum with success in mixed gas and decompression arenas, that is, technical diving. Tech diving encompasses scientific, military, commercial, and exploration underwater activities. The impact of deep stops has been a revolution in diving circles. So have slower ascent rates across recreational and technical diving. In quantifiable terms, slower ascent rates are very much akin to deep stops, though not as pronounced as decompression stops. Deep stops plus slow ascent rates work together. And they work together safely and efficiently, and particularly when coupled to helium decompression strategies.

Deep stops usually reduce overall decompression time (hang time) too. And when coupled to the use of helium in the breathing mixture (trimix) to reduce narcotic effects of nitrogen, technical divers report feeling much better physically today when they leave the water. The reduction in hang time ranges from 10% to as high as 50%, depending on diver, mix, depth, and exposure time. Feeling better while decompressing for shorter periods of time is certainly a win-win situation that would have been thought an impossibility not too long ago. The basic tenets of Haldane decompression theory (neoclassical dissolved gas theory) postulate that deeper exposures (deep stop plus bottom time) incur greater offgassing penalties in the shallow zone. To see, check decompression tables based on Haldane methodology, and understand that such tables take no account of bubble growth in staging divers. But this is not seen in dual phase staging, where bubbles are prevented in the deep zone instead of being treated in the shallow zone ala Haldane methodology. The depth at which the first deep stops are made can be dramatically deeper than those required by conventional tables. For instance, a dive to 300 *fsw* on trimix for 30 minutes, with switches to progressively higher enrichments of nitrox at 120, 70, and 20 *fsw*, calls for the first deep stops in the 250 *fsw* range. Conventional tables require the first stops in the 100 *fsw* range. If trimix is substituted for nitrox on the way up, total decompression time further can be reduced, and divers today leave the water feeling better than they would on nitrox.

For most early technical divers, obtaining deep and mixed gas decompression tables constituted one of many roadblocks to safe deep and exploration diving. Existing tables ranged from ultra

conservative as an insulation against harm to a hodgepodge of protocols based on total misunderstanding. From this background, and driven by a need to optimize decompression schedules, deep stops steadily advanced as a safe and efficient change to diver staging. And this even though formal tests were usually not conducted in controlled environments, like hyperbaric chambers.

Haldane originally found that deep stops were sometimes necessary in decompression formats and tests, but abandoned them, and could not incorporate them easily or naturally into a dissolved gas, critical tension (M -value) model on first principles. Nor can anybody these modern days. All he had to do was couple his dissolved gas dynamics to bubble dynamics. Deep stops do not emerge naturally in dissolved gas models. And Haldane didn't test deep enough either. Deep stops are patently a *deep* phenomena, whose utility and worth increase steadily with depth and exposure time.

Though deep stops are regarded as a major development in diving, the first experiments were more trial and error than scientific in nature. Just like so many other important developments in the real world. Underlying science with mechanistics would follow in the late 80s and 90s, and so with helium breathing mixtures.

Maybe experiments is too strict a description. Individuals, particularly in the cave diving community, toyed with decompression regimens in hopes of minimizing their decompression time. The cave exploration Woodville Karst Plain Project (WKPP), mapping subsurface topographies in Florida, pioneered deep stop technology, establishing many rule of thumb protocols to be imposed on conventional tables. Irvine, Jablonski, and Mees stand at the forefront here, successfully conducting 6 hour dives at 280 *fsw* in the Wakulla cave complex with deep stop decompression times of 8.5 hours versus traditional Haldane hang times of 20 hours. Also, the horizontal penetrations of 19,000 *fsw* are world records (Guinness). Figure 1 sketches comparison profiles, along with mixtures, times, switches, and depths. Spectacular is a gross understatement. Certainly such contributions to diving science and spinoff model validation parallel Haldane a hundred years ago.

WKPP initially found that common decompression assumptions subjected divers to extremely long decompression obligations, and ones that, regardless of their length, were inefficient. Divers also felt badly upon surfacing from extended decompression dives. Operationally (many dives over many years), WKPP divers found that the insertion of deep stops permitted shortening of shallower stops with an overall reduction in total decompression time. The decompression schedule was more effective, with effectiveness represented by subjective diver health and sense of well being. In so doing, WKPP also dispelled the voodoo helium myth as switches away from nitrox to trimix decompression schedules finalized after WKPP-testing-years. In lockstep mode, like (unpublicized) strategies developed in military, security, scientific, and even commercial sectors.

As discussed in previous Chapters, there is science behind deep stops. The science is fairly simply. It's just a matter of how dissolved gases and bubbles behave under pressure changes. We use to think that controlling dissolved gas buildup and elimination in tissue and blood was the basis for staging divers and astronauts. And that bubbles didn't form unless dissolved gas trigger points were exceeded. At least that was the presumption that went into conventional (Haldane) tables. Chemists, physicists, and engineers never bought off on that. When silent bubbles were tracked in divers not experiencing any decompression problems, of course, this changed. And since bubbles need be controlled in divers, focus changed and switched from just dissolved gases to both bubbles and dissolved gases. Within such framework, deep stops emerge as a natural consequence. So do dual phase (bubbles plus dissolved gas) models.

To eliminate dissolved gases, the driving outgassing gradient is maximized by reducing ambient pressure as much as possible. That means bringing the diver as close to the surface as possible. But, to eliminate bubbles (gases inside them), the outgassing gradient is maximized by increasing ambient pressure as much as possible. That means holding the diver at depth when bubbles form. Deep stops accomplish the latter.

Clearly, from all the above, dominant modes for staging diver ascents depend upon the preponderance of free (bubbles) or dissolved phases in the tissues and blood, their coupling, and their relative

time scales for elimination. This is now (will always be) a central consideration in staging hyperbaric or hypobaric excursions to lower ambient pressure environments. The dynamics of elimination are directly opposite, as depicted in Chapter 2 (Figure 2). To eliminate dissolved gases (central tenet of Haldane decompression theory), the diver is brought as close as possible to the surface. To eliminate free phases (coupled tenet of bubble decompression theory), the diver is maintained at depth to both crush bubbles and squeeze gas out by diffusion across the bubble film surface. Since both phases must be eliminated, the problem is a playoff in staging. In mathematical terms, staging is a *minimax* problem, and one that requires full blown dual phase models, exposure data, and some consensus of what is an acceptable level of DCS incidence.

Extreme WKPP divers make their first decompression stops at roughly 80% of actual dive depth for any dive. They dive helium exclusively, and the deep stop schedules they generate are not even remotely possible with air. WKPP schedules agree with reduced gradient bubble model (below and previous Chapters) calculations of the staging regimen, in both decompression profile shape and duration.

Other prescriptions for deep stops were imbedded in conventional tables. Something like this is employed, trial and error, and this one has been around for years in tech diving circles, often attributed to Pyle, an underwater fish collector in Hawaii:

1. calculate your decompression schedule from tables, meters, or software;
2. half the distance to the first decompression stop and stay there a minute or two;
3. recompute your decompression schedule with time at the deep stop included as way time (software), or bottom time (tables);
4. repeat procedure until within some 10 -30 ft of the first decompression stop;
5. and then go for it.

Within conventional tables, such procedure was somewhat arbitrary, and usually always ended up with a lot of hang time in the shallow zone. Such is to be expected within dissolved gas decompression frameworks. So, deep stop pioneers started shaving shallow decompression time off their schedules. And jumped back into the water, picking up the trial and error testing where it left off. Seasoned tech divers all had their own recipes for this process. And sure, what works works in the diving world. What doesn't is usually trashed.

Concurrently, full up dual phase models, spawned by the inadequacies and shortcomings of conventional tables, emerged on the diving scene. Not only did deep stops evolve self consistently in these models, but dive and personal computers put decompression scheduling with these new models in the hands of real divers. And real on the scene analysis and feedback tuned arbitrary, trial and error, and theoretical schedules to each other.

One thing about these bubble models, as they are collectively referenced, common to all of them is deeper stops, shorter decompression times in the shallow zone, and shorter overall decompression times. And they all couple dissolved gases to bubbles, not focusing just on bubbles or dissolved gas.

Details elsewhere, a few of the important ones can be summarized. The thermodynamic model of Hills really got the ball rolling so to speak:

1. thermodynamic model (Hills, 1976) – assumes free phase (bubbles) separates in tissue under supersaturation gas loadings. Advocates dropout from decompression schedule somewhere in the 20 ft zone.
2. varying permeability model (Yount, 1986) – assumes preformed nuclei permeate blood and tissue, and are excited into growth by compression-decompression. Model patterned after gel bubbles studied in the laboratory.

3. reduced gradient bubble model (Wienke, 1990) – abandons gel parametrization of varying permeability model, and extends bubble model to repetitive, altitude, and reverse profile diving. Employed in recreational and technical diving meters, and basis for new tested NAUI tables;
4. tissue bubble diffusion model (Gernhardt and Vann, 1990) – assumes gas transfer across bubble interface, and correlates growth with DCS statistics. Probably employed in the commercial diving sector.

Not all these models have seen extensive field testing, but since they are all similar, earlier exposition, addressing testing and validation of the reduced gradient bubble model (RGBM), holds in broad terms. The 1,000s of tech dives on deep stops, of course, already validate deep stop technology and models to most, but the testing and validation described earlier spans deep stops to recreational diving in single model framework. And that is a very desired feature of any decompression theory and/or model. It almost goes without saying that models such as these have reshaped our decompression horizons, and will continue doing so.

One last item concerning deep stops remains, that is, laboratory experiments. Doppler and ultrasound imaging are techniques for detecting moving bubbles in humans and animals following compression-decompression. While bubble scores from these devices do not always correlate with the incidence of DCS, the presence or non-presence of bubbles is an important metric in evaluating dive profiles.

Analysis of more than 16,000 actual dives by Diver's Alert Network (DAN), prompted Bennett to suggest that decompression injuries are likely due to ascending too quickly. He found that the introduction of deep stops, without changing the ascent rate, reduced high bubble grades to near zero, from 30.5% without deep stops. He concluded that a deep stop at half the dive depth should reduce the critical fast gas tensions and lower the DCS incidence rate.

Marroni concluded studies with DAN's European sample with much the same thought. Although he found that ascent speed itself did not reduce bubble formation, he suggested that a slowing down in the deeper phases of the dive (deep stops) should reduce bubble formation. He will be conducting further tests along those lines.

Brubakk and Wienke found that longer decompression times are not always better when it comes to bubble formation in pigs. They found more bubbling in chamber tests when pigs were exposed to longer but shallower decompression profiles, where staged shallow decompression stops produced more bubbles than slower (deeper) linear ascents. Model correlations and calculations using the reduced gradient bubble model suggest the same.

Deep stop technology has developed successfully over the past 15 years or so. Tried and tested in the field, now some in the laboratory, deep stops are backed up by diver success, confidence, theoretical and experimental model underpinnings, and general acceptance by seasoned professionals.

Helium Strategies

Helium is a noble gas for deep diving, but was not always thought so. In the early days of technical and recreational diving, the use of helium for deep diving was discouraged, indeed, really feared. Based on misinformation and a few early problems in the deep diving arena, helium acquired a voodoo gas reputation, with a hands off label.

Some misapprehension stemmed from the Hans Keller tragedy on helium mixes in 1962, some from misconceptions about isobaric switches ala light-to-heavy gases, some from tales of greater CNS risk, and some from a paucity of published and reliable decompression tables. Some concerns arose because 80/20 heliox no-decompression time limits (NDLs) for short and shallow dives were longer than air limits. So people assumed helium decompression was longer, and more hazardous, than nitrogen. In short, helium was getting a bad rap for a lot of wrong reasons.

It was also religion that switches from helium bottom mixtures to nitrogen should be made as early as possible, and that so doing, would reduce overall decompression time the most. Not exactly so, at least according to modern decompression theory, and even classical Haldane theory if deep stops are juxtaposed on the profile. If helium and nitrogen are decreased in roughly same proportions as oxygen is increased until a big isobaric switch is made in the shallow zone to an enriched nitrox mix, decompression differences between early switches to nitrogen versus riding lighter helium mixes longer are small. Small according to modern decompression theory and practice, but more important, such helium protocols leave the decompression diver feeling better. As witnessed under field conditions, collective experiences of technical and scientific diving operations support that assertion today. And so do modern decompression theories that have seen field testing, like the RGBM, and ad hoc deep stop protocols used by saavy divers.

Indeed there may be no need to switch to nitrogen mixtures at all. Riding helium mixtures to the surface, with a switch to pure oxygen in the shallow zone can be decompression efficient, and safe too. So much so, that NAUI Technical Diving Operations has built a training regimen for divers and instructors based on helium for technical diving, and even offers a helitrox (enriched heliair) course. And a full set of RGBM Tables supports helium based training and tech diving.

In the same vein, the operational experiences of WKPP and LANL dive teams underscore many years of safe and efficient helium based decompression diving. And that couples to a modern revolution in decompression theory and practice. In fact, WKPP exploits on helium could fill a book. LANL too. NAUI Technical Diving has been utilizing helium based training for the past three years, or so, without problems. All this means many, many 1000s of tech dives with helium based mixes.

Today, helium is proving its worth as a safe and reliable technical mix. Its use is changing technical and exploration diving. Exit deep air, and enter deep helium and deep stops. It seems about time, plus time for modern decompression theory to flush the dissolved gas theory entrenching diving for close to a century.

The size of bubbles formed with various inert gases depends upon the amount of gas dissolved, and hence the solubilities. Higher gas solubilities promote bigger bubbles. Thus, helium is preferable to hydrogen as a light gas, while nitrogen is preferable to argon as a heavy gas. Neon solubility roughly equals nitrogen solubility. Narcotic potency correlates with lipid (fatty tissue) solubility, with the least narcotic gases the least soluble. Different uptake and elimination speeds suggest optimal means for reducing decompression time using helium and nitrogen mixtures. Following deep dives breathing helium, switching to nitrogen is without risk, while helium elimination is accelerated because the helium tissue-blood gradient is increased when breathing nitrogen. By gradually increasing the oxygen content after substituting nitrogen for helium, the nitrogen uptake can also be kept low. Workable gas switches depend on exposure and tissue compartment controlling ascent.

While light-to-heavy gas switches (such as helium to nitrogen) are safe and common practices, the reverse is not generally true. In fact, all heavy-to-light switches can be dangerous. In the former case, decreased tissue gas loading is a favorable circumstance following the switch. In the latter case, increased tissue gas loading can be disastrous. This is popularly termed the *isobaric* playoff.

Consensus among helium divers is that they feel better, less enervated, and subjectively healthier than when diving nitrogen mixtures. WKPP, LANL, and NAUI Technical Operations strongly attest to this fact. Though a personal and subjective evaluation, this remains very, very important. Physiological factors cannot be addressed on first principles always, and for some, just feeling better is good justification. Works for many. Postdive decompression stress on helium appears to be less than postdive nitrogen stress.

Another positive feature of helium diving underscores the minimum-bends depth (MBD), that is, the saturation depth on a mix from which immediate ascension to the surface precipitates decompression sickness (DCS). For helium mixes, the MBD is always greater than that for proportionate nitrogen mix. For instance, the MBD for air (80/20 nitrox) is 33 *fsw*, while the MBD for 80/20 heliox is 38 *fsw*. This results from helium's lesser solubility compared to nitrogen as it impacts

deeper and longer diving.

On most counts, helium appears superior to nitrogen as a diving gas. Helium bubbles are smaller, helium diffuses in and out of tissue and blood faster, helium is less narcotic, divers feel better when they leave the water after diving on helium, and helium MBDs are greater than nitrogen MBDs.

Helium NDLs are actually shorter than nitrogen for shallow exposures, as seen comparatively in Table 8 for 80/20 heliox and 80/20 nitrox (air). Reasons for this stem from kinetic versus solubility properties of helium and nitrogen, and go away as exposures extend beyond 150 *fsw*, and times extend beyond 40 *min* or so.

Table 8. Comparative Helium And Nitrogen No Decompression Limits

depth (<i>fsw</i>)	heliox (80/20) NDL (<i>min</i>)	nitrox (80/20) NDL (<i>min</i>)
30		
40	260	200
50	180	100
60	130	60
70	85	50
80	60	40
90	45	30
100	35	25
110	30	20
120	25	15
130	20	10
140	15	8
150	12	5
160	10	4
170	8	3

Helium ingasses and outgasses 2.7 times faster than nitrogen, but nitrogen is 1.5 to 3.3 times more soluble in body aqueous and lipid tissue than helium. For short exposures (bounce and shallow), the faster diffusion rate of helium is more important in gas buildup than solubility, and shorter NDLs than nitrogen result. For long bottom times (decompression and extended range), the lesser solubility of helium is a dominant factor in gas buildup, and helium outperforms nitrogen for staging. Thus, deep implies helium bottom and stage gas. Said another way, transient diving favors nitrogen while steady state diving favors helium as a breathing gas.

Top of all this, modern decompression theory (like RGBM) requires deep stops which do not fuel helium buildup as much as nitrogen in addressing both dissolved gas buildup and bubble growth. And helium deep stops, like nitrogen deep stops, couple to shorter and safe overall decompression. Some helium versus nitrogen decompression profiles follow, and they are not academic, having been actually dived (WKPP, LANL, NAUI). Profiles were generated with the RGBM (ABYSS software package marketed by Abyssal Diving, Boulder, Colorado). RGBM staging is always deeper, but shorter overall, than Haldane staging with Buhlmann ZHL or Workman USN parameters.

The first, in Table 9, is a comparison of enriched air and enriched heli-air decompression diving, with a switch to 80% oxygen at 20 *fsw*. Dive is 100 *fsw* for 90 *min*, on EAN35 and EAH35/18 (nitrox 35/65 and trimix 35/18/47), so oxygen enrichment is the same. The decompression profile (fairly light by tech standards, but manageable and easy for training purposes) is listed in Table 9. Descent and ascent rates are 75 *fsw/min* and 25 *fsw/min*.

Table 9. Enriched Air And Heliar Deco Profile Comparison

depth (<i>fsw</i>)	enriched heliair	enriched air
	EAH35/18	EAN35
	stop time (<i>min</i>)	stop time (<i>min</i>)
100	90	90
30	2	4
20	5	7
10	12	11
	119	122

Overall the enriched heliair decompression schedule for the dive is shorter than for the enriched air. As the helium content goes up, the decompression advantage for enriched heliair increases.

This may surprise you. But either way, now check out corresponding USN or ZHL decompression requirements for these dives. In the enriched heliair case, ZHL decompression time is 39 *min* versus 19 *min* above, and in the enriched air case, ZHL decompression time is 33 *min* versus 22 *min* above. This not only underscores helium versus nitrogen misfact in staging, but also points out significant differences in modern algorithms versus Haldane.

Lastly consider a deep trimix dive with multiple switches on the way up. Table 10 below contrasts stop times for two gas choices at the 10 below 0 *fsw* switch. The dive is a short 10 *min* at 400 *fsw* on 10/65/25 trimix, with switches at 235 *fsw*, 100 *fsw*, and 30 *fsw*. Descent and ascent rates are 75 *fsw/min* and 25 *fsw/min*. Obviously, there are many other choices for switch depths, mixtures, and strategies. In the below comparison, the oxygen fractions were the same in all mixes, at all switches. Differences between a nitrogen or a helium based decompression strategy, even for this short exposure, are nominal. Such usually is the case when oxygen fraction is held constant in helium or nitrogen mixes at the switch.

Comparative calculations and experience seem to suggest that riding helium to the 70 *fsw* level with a switch to EAN50 is good strategy, one that couples the benefits of well being on helium with minimal decompression time and stress following isobaric switch to nitrogen. Shallower switches to enriched air also work, with only a nominal increase in overall decompression time.

Helium has been a mainstay, of course, in commercial diving. But its emergence and use in the technical diving community has been more recent, like the past 10 years or so. Some of this is due to cost certainly. It's not cheap to dive helium. But a lot of it is due to misconception. The activities of a very knowledgeable and vocal technical diving community are changing both.

Table 10. Comparative Helium And Nitrogen Gas Switches

depth (<i>fsw</i>)	stop time (<i>min</i>)	
	10/65/25 trimix	10/65/25 trimix
400	10.0	10.0
260	1.5	1.5
250	1.0	1.0
240	1.0	1.0
	18/50/32 trimix	18/50/32 trimix
230	0.5	0.5
220	0.5	0.5
210	0.5	0.5
200	0.5	0.5
190	1.0	1.0
180	1.5	1.5
170	1.5	1.0
160	1.5	1.5
150	1.5	2.0
140	2.0	1.5
130	2.0	2.5
120	4.0	4.0
110	4.5	4.0
	40/20/40 trimix	EAN40
100	2.5	2.0
90	2.5	2.0
80	2.5	2.0
70	5.0	4.0
60	6.5	5.5
50	8.0	6.5
40	9.5	7.5
	EAN80	EAN80
30	10.5	10.5
20	14.0	14.0
10	21.0	20.5
	123.0	116.0

Probabilistic Decompression

The systematics of gas exchange, nucleation, bubble growth and elimination, and decompression are so complicated that theories only reflect pieces of the puzzle. Computational algorithms, tables, and manned testing are requisite across a spectrum of activities. And the potential of electronic devices to process tables of information or detailed equations underwater is near maturity, with virtually any algorithm or model amenable to digital implementation. Pressures for even more sophisticated algorithms are expected to grow.

Still computational models enjoy varying degrees of success or failure. More complex models address a greater number of issues, but are harder to codify in decompression tables. Simpler models are easier to codify, but are less comprehensive. Some models are based on first principles, but many are not. Application of models can be subjective in the absence of definitive data, the acquisition of which is tedious, sometimes controversial, and often ambiguous. If deterministic models are abandoned, statistical analysis can address the variability of outcome inherent to random occurrences,

but only in manner indifferent to specification of controlling mechanisms. The so called dose-reponse characteristics of statistical analysis are very attractive in the formulation of risk tables. Applied to decompression sickness incidence, tables of comparative risk offer a means of weighing contributing factors and exposure alternatives. At the basis of statistical and probabilistic analyses of decompression sickness is the binomial distribution. The binomial distribution is the fundamental frequency distribution governing random events.

Decompression sickness is a hit, or no hit, situation. Statistics are binary, as in coin tossing. Probabilities of occurrence are determined from the binomial distribution, which measures the numbers of possibilities of occurrence and nonoccurrence in any number of events, given the incidence rate. Specifically, the probability, P , in a random sample of size, N , for n occurrences of decompression sickness and m nonoccurrences, takes the form,

$$P(n) = \frac{N!}{n! m!} p^n q^m ,$$

with,

$$n + m = N ,$$

p the underlying incidence rate (average number of cases of decompression sickness), and q ,

$$q = 1 - p ,$$

the underlying nonincidence.

Table 11 lists corresponding binomial decompression probabilities, $P(n)$, for 1% and 10% underlying incidence (99% and 90% nonincidence), yielding 0, 1, and 2 or more cases of decompression sickness. The underlying incidence, p , is the (fractional) average of hits.

As the number of trials increases, the probability of 0 or 1 occurrences drops, while the probability of 2 or more occurrences increases. In the case of 5 dives, the probability might be as low as 5%, while in the case of 50 dives, the probability could be 39%, both for $p = .01$. Clearly, odds even percentages would require testing beyond 50 cases for an underlying incidence near 1%. Only by increasing the number of trials for fixed incidences can the probabilities be increased. Turning that around, a rejection procedure for 1 or more cases of decompression sickness at the 10% probability level requires many more than 50 dives. If we are willing to lower the confidence of the acceptance, or rejection, procedure, of course, the number of requisite trials drops. Table 11 also shows that the test practice of accepting an exposure schedule following 10 trials without incidence of decompression sickness is suspect, merely because the relative probability of nonincidence is high, near 35%.

Questions as to how safe are decompression schedules have almost never been answered satisfactorily. As seen, large numbers of binary events are required to reliably estimate the underlying incidence. One case of decompression sickness in 30 trials could result from an underlying incidence, p , bounded by 0.02 and 0.16 roughly. Tens more of trials are necessary to shrink those bounds.

Table 11. Probabilities Of Decompression Sickness For Underlying Incidences.

N (dives)	n (hits)	$P(n)$	
		$p = 0.01$ $q = 0.99$	$p = 0.10$ $q = 0.90$
5	0	0.95	0.59
	1	0.04	0.33
	2 or more	0.01	0.08
10	0	0.90	0.35
	1	0.09	0.39
	2 or more	0.01	0.26
20	0	0.82	0.12
	1	0.16	0.27
	2 or more	0.02	0.61
50	0	0.61	0.01
	1	0.31	0.03
	2 or more	0.08	0.96

Biological processes are highly variable in outcome. Formal correlations with outcome statistics are then generally requisite to validate models against data. Often, this correlation is difficult to firmly establish (couple of percent) with fewer than 1,000 trial observations, while ten percent correlations can be obtained with 30 trials, assuming binomial distributed probabilities. For decompression analysis, this works as a disadvantage, because often the trial space of dives is small. Not discounting the possibly small trial space, a probabilistic approach to the occurrence of decompression sickness is useful and necessary. One very successful approach, developed and tuned by Weathersby, and others for decompression sickness in diving, called maximum likelihood, applies theory or models to diving data and adjusts the parameters until theoretical prediction and experimental data are in as close agreement as possible.

Validation procedures require decisions about uncertainty. When a given decompression procedure is repeated with different subjects, or the same subjects on different occasions, the outcome is not constant. The uncertainty about the occurrence of decompression sickness can be quantified with statistical statements, though, suggesting limits to the validation procedure. For instance, after analyzing decompression incidence statistics for a set of procedures, a table designer may report that the procedure will offer an incidence rate below 5%, with 90% confidence in the statement. Alternatively, the table designer can compute the probability of rejecting a procedure using any number of dive trials, with the rejection criteria any arbitrary number of incidences. As the number of trials increases, the probability of rejecting a procedure increases for fixed incidence criteria. In this way, relatively simple statistical procedures can provide vital information as to the number of trials necessary to validate a procedure with any level of acceptable risk, or the maximum risk associated with any number of incidences and trials.

One constraint usually facing the statistical table designer is a paucity of data, that is, number of trials of a procedure. Data on hundreds of repetitions of a dive profile are virtually nonexistent, excepting bounce diving perhaps. As seen, some 30-50 trials are requisite to ascertain procedure safety at the 10% level. But 30-50 trials is probably asking too much, is too expensive, or generally prohibitive. In that case, the designer may try to employ global statistical measures linked to models in a more complex trial space, rather than a single profile trial space. Integrals of risk parameters, such as bubble number, supersaturation, separated phase, etc., over exposures in time, can be defined as probability measures for incidence of decompression sickness, and the maximum likelihood method then used to extract appropriate constants.

Saturation Bends Probability

Many factors contribute to bends susceptibility. Age, obesity, temperature, physical condition, alcohol, and cigarettes are a few. Whatever the contributing factors, the distribution of bends depths for saturation exposures has been characterized in terms of the saturation tension, Q , and ambient pressure, P . by Hills. This characterization is not only of academic interest, but is also useful in assigning formal risk to decompression formats.

The distribution of saturation bends depths, χ , fits a Weibull function. This is true for all breathing mixtures, nitrox, heliox, trimix, etc. If cumulative fraction of air bends cases up to G is χ , the survivor fraction, $1 - \chi$, satisfies,

$$\ln (1 - \chi) = - \left[\frac{G - 14.3}{25.1} \right]^{4.73}$$

for cumulative bends probability, χ , the usual integral over bends risk, ζ , as a function of gradient, G ,

$$\chi = \int_0^G \zeta(G') dG'$$

with saturation bends gradient, G , measured in *fsw*,

$$G = Q - P$$

As the gradient grows, the survivor function approaches zero exponentially. The smallest bends gradient is 14.3 *fsw*, which can be contrasted with the average value of 26.5 *fsw*. The root mean square gradient is 27.5 *fsw*. At 27 *fsw*, the survivor fraction is 0.96, while 67% of survivors fall in the range, 26.5 ± 7.6 *fsw*, with 7.6 *fsw* the standard deviation. For gas mixtures other than air, the general form is given by,

$$\ln (1 - \chi) = -\epsilon \left[\frac{(P_f - 20.5)}{(P_i - 33.0)} - \frac{1}{f_i} \right]^\delta$$

where f_i is the total volume fraction of inert breathing gases, for $G = P_f - P_i$, and with ϵ , δ constants.

The efficiency of the Weibull distribution in providing a good fit to the saturation data is not surprising. The Weibull distribution enjoys success in reliability studies involving multiplicities of fault factors. It obviously extends to any set of hyperbaric or hypobaric exposure data, using any of the many parameter risk variables described above.

Table And Profile Risks

A global statistical approach to table fabrication consists of following a risk measure, or factor p , throughout and after sets of exposures, tallying the incidence of DCS, and then applying maximum likelihood to the risk integral in time, extracting any set of risk constants optimally over all dives in the maximization procedure. In analyzing air and helium data, Weathersby assigned risk as the difference between tissue tension and ambient pressure divided by ambient pressure. One tissue was assumed, with time constant ultimately fixed by the data in ensuing maximum likelihood analysis. The measure of nonincidence, q , was taken to be the exponential of risk integrated over all exposure time,

$$q(\kappa, \tau) = \exp \left[- \int_0^\infty \zeta(\kappa, \tau, t') dt' \right] ,$$

$$\zeta(\kappa, \tau, t') = \kappa \frac{p(t') - p_a}{p_a} ,$$

with κ a constant determined in the likelihood maximization, p_a ambient pressure, and $p(t')$ the instantaneous Haldane tension for tissue with halftime, τ , also determined in the maximization process, corresponding to arbitrary tissue compartments for the exposure data. Other more complex likelihood functions can also employed, for instance, the separated phase volume according to the varying permeability and reduced gradient bubble models,

$$\zeta(\kappa, \xi, \tau, t') = \kappa \Lambda(t') G(t') \quad ,$$

$$\Lambda(t') = \left[1 - \frac{r(t')}{\xi} \right] \quad ,$$

with Λ the permissible bubble excess, r the bubble radius, G the bubble diffusion gradient (dissolved-free gas), and κ and ξ constants determined in the fit maximization of the data. Another risk possibility is the tissue ratio,

$$\zeta(\kappa, \tau, t') = \kappa \frac{p(t')}{p_a} \quad ,$$

a measure of interest in altitude diving applications.

Hundreds of air dives were analyzed using this procedure, permitting construction of decompression schedules with 95% and 99% confidence (5% and 1% bends probability). These tables were published by US Navy investigators, and Table 12 tabulates the corresponding nonstop time limits ($p = 0.05, 0.01$), and also includes the standard US Navy (Workman) limits for comparison. Later re-evaluations of the standard set of nonstop time limits estimate a probability rate of 1.25% for the limits. In actual usage, the incidence rates are below 0.001%, because users do not dive to the limits generally.

Table 12. Nonstop Time Limits For 1% And 5% DCS Probability.

depth <i>d</i> (fsw)	nonstop limit <i>t_n</i> (min) <i>p</i> = .05	nonstop limit <i>t_n</i> (min) <i>p</i> = .01	nonstop limit <i>t_n</i> (min) US Navy
30	240	170	
40	170	100	200
50	120	70	100
60	80	40	60
70	80	25	50
80	60	15	40
90	50	10	30
100	50	8	25
110	40	5	20
120	40	5	15
130	30	5	10

For the past 10-15 years, this probabilistic approach to assessing risk in diving has been in vogue. Sometimes this can be confusing, or misleading, since definitions or terms, as presented, are often mixed. Also confusing are risk estimates varying by factors of 10 to 1,000, and distributions serving as basis for analysis, also varying in size by the same factors. So, before continuing with a risk analysis of recreational profiles, a few comments are germane.

Any set of statistical data can be analyzed directly, or sampled in smaller chunks. The smaller sets (samples) may or may not reflect the parent distribution, but if the analyst does his work correctly, samples reflecting the parent distribution can be extracted for study. In the case of dive profiles, risk probabilities extracted from sample profiles try to reflect the incidence rate, p , of the parent distribution (N profiles, and p underlying DCS rate). The incidence rate, p , is the most important

metric, followed by the shape of the distribution in total as measured by the variance, s . For smaller sample of profile size, $K < N$, we have mean incidences, Q , for sample incidence rate, r ,

$$Q = rK$$

and variance, v ,

$$v = r(1 - r)K$$

By the central limit theorem, the distribution of sample means, Q , is normally distributed about parent (actual) mean, M , with variance, $v = s/K$. Actually, the distribution of sample means, Q , is normally distributed no matter what the distribution of samples. This important fact is the basis for error estimation with establishment of confidence intervals, χ , for r , with estimates denoted, r_{\pm} ,

$$r_{\pm} = r \pm \chi \left[\frac{s}{K} \right]^{1/2}$$

$$0 < \chi < 1$$

The sample binomial probability, $B(k)$, is analogously,

$$B(k) = \frac{K!}{k! j!} r^k (1 - r)^j$$

constrained, $k + j = K$, for k number of DCS hits, and normalized,

$$\sum_{k=1}^K B(k) = 1$$

with important limiting property, if $K \rightarrow \infty$, then $B(k) \rightarrow 0$, when, $r \ll 1$.

For example, if 12 cases of DCS are reported in a parent set of 7,896 profiles, then,

$$N = 7896$$

$$p = \frac{12}{7896} = .0015$$

Smaller samples might be used to estimate risk, via sample incidence, r , with samples possibly chosen to reduce computer processing time, overestimate p for conservancy sake, focus on a smaller subregion of profiles, or any other reason. Thus, one might nest all 12 DCS incidence profiles in a smaller sample, $K = 1,000$, so that the sample risk, $r = 12/1,000 = 0.012$, is larger than p . Usually though the analyst wishes to mirror the parent distribution in the sample. If the parent is a set of benign, recreational, no decompression, no multiday dive profiles, and the sample mirrors the parent, then both risks, p and r , are reasonably true measures of actual risk associated with recreational diving. If sample distributions chosen are not representative of the class of diving performed, risk estimates are not trustworthy. For instance, if a high risk set of mixed gas decompression profiles were the background against which recreational dive profiles were compared, all estimates would be skewed and faulty (actually underestimated in relative risk, and overestimated in absolute risk). For this parent set, N is large, p is small, with mean, $M = pN = 0.0015 \times 7896 = 12$, and the applicable binomial statistics smoothly transition to Poisson representation, convenient for logarithmic and covariant numerical analysis (on a computer). Additionally, any parent set may be a large sample of a megaset, so that p is itself an estimate of risk in the megaset.

Turns out that our parent distribution above is just that, a subset of larger megaset, namely, the millions and millions of recreational dives performed and logged over the past 30 years, or so. The above set of profiles was collected in training and vacation diving scenarios. The set is recreational (no decompression, no multiday, light, benign) and representative, with all the distribution metrics as

listed. For reference and perspective, sets of recreational profiles collected by others (Gilliam, NAUI, PADI, YMCA, DAN) are similar in context, but larger in size, N , and smaller in incidence rate, p . Data and studies reported by many sources quote, $N > 1,000,000$, with, $p < 0.00001 = 0.001\%$. Obviously our set has higher rate, p , though still nominally small, but the same shape. So our estimates will be liberal (overestimate risk).

To perform risk analysis, a risk estimator need be employed. For diving, dissolved gas and phase estimators are useful. Two, detailed earlier, are used here. First is the dissolved gas supersaturation ratio, historically coupled to Haldane models, ϕ ,

$$\phi = \kappa \frac{p - \lambda p_a}{p_a}$$

and second, ψ , is the separated phase, invoked by phase models,

$$\psi = \gamma \left[1 - \frac{r}{\xi} \right] G$$

For simplicity, the asymptotic exposure limit is used in the likelihood integrals for both risk functions,

$$1 - r(\kappa, \lambda) = \exp \left[- \int_0^\infty \phi(\kappa, \lambda, t) dt \right]$$

$$1 - r(\gamma, \xi) = \exp \left[- \int_0^\infty \psi(\gamma, \xi, t) dt \right]$$

with *hit – no hit*, likelihood function, Ω , of form,

$$\Omega = \prod_{k=1}^K \Omega_k$$

$$\Omega_k = r_k^{\delta_k} (1 - r_k)^{1 - \delta_k}$$

where, $\delta_k = 0$ if DCS does not occur in profile, k , or, $\delta_k = 1$ if DCS does occur in profile, k . To estimate κ , λ , γ , and ξ in maximum likelihood, a modified Levenberg-Marquardt algorithm is employed (*SNLSE*, Common Los Alamos Applied Mathematical Software Library), just a nonlinear least squares data fit (NLLS) to an arbitrary function (minimization of variance over K data points here), with $L1$ error norm. Additionally, using a random number generator for profiles across 1,000 parallel SMP (Origin 2000) processors at LANL, we construct 1,000 subsets, with $K = 2,000$ and $r = 0.006$, for separate likelihood regression analysis, averaging κ , λ , γ , and ξ by weighting the inverse variance.

For recreational diving, both estimators are roughly equivalent, because little dissolved gas has separated into free phases (bubbles). Analysis shows this true for all cases examined, in that estimated risks for both overlap at the 95% confidence level. The only case where dissolved gas and phase estimators differ (slightly here) is within repetitive diving profiles. The dissolved gas estimator cues on gas buildup in the slow tissue compartments (staircasing for repets within an hour or two), while the phase estimator cues on bubble gas diffusion in the fast compartments (dropping rapidly over hour time spans). This holding true within all recreational diving distributions, we proceed to the risk analysis.

Nonstop limits (NDLs), denoted t_n as before, from the US Navy, PADI, and NAUI Tables, and those employed by the Oceanic decometer provide a set for comparison of relative DCS risk. Listed below in Table 13 are the NDLs and corresponding risks (in parentheses) for the profile, assuming ascent and descent rates of 60 *fsw/min* (no safety stops). Haldane and RGBM estimates vary little for these cases, and only the phase estimates are included.

Table 13. Risk Estimates For Various NDLS.

d (fsw)	USN	PADI	NAUI	Oceanic
	t_n (min)	t_n (min)	t_n (min)	t_n (min)
35	310 (4.3%)	205 (2.0%)		181 (1.3%)
40	200 (3.1%)	140 (1.5%)	130 (1.4%)	137 (1.5%)
50	100 (2.1%)	80 (1.1%)	80 (1.1%)	80 (1.1%)
60	60 (1.7%)	55 (1.4%)	55 (1.4%)	57 (1.5%)
70	50 (2.0%)	40 (1.2%)	45 (1.3%)	40 (1.2%)
80	40 (2.1%)	30 (1.3%)	35 (1.5%)	30 (1.3%)
90	30 (2.1%)	25 (1.5%)	25 (1.5%)	24 (1.4%)
100	25 (2.1%)	20 (1.3%)	22 (1.4%)	19 (1.2%)
110	20 (2.2%)	13 (1.1%)	15 (1.2%)	16 (1.3%)
120	15 (2.0%)	13 (1.3%)	12 (1.2%)	13 (1.3%)
130	10 (1.7%)	10 (1.7%)	8 (1.3%)	10 (1.7%)

Risks are internally consistent across NDLS at each depth, and agree with the US Navy assessments in Table 12. Greatest underlying and binomial risks occur in the USN shallow exposures. The PADI, NAUI, and Oceanic risks are all less than 2% for this set, thus binomial risks for single DCS incidence are less than 0.02%. PADI and NAUI have reported that field risks (p) across all exposures are less than 0.001%, so considering their enviable track record of diving safety, our estimates are liberal. Oceanic risk estimates track as the PADI and NAUI risks, again, very safely.

Next, the analysis is extended to profiles with varying ascent and descent rates, safety stops, and repetitive sequence. Table 14 lists nominal profiles (recreational) for various depths, exposure and travel times, and safety stops at 5 *msw*. Mean DCS estimates, r , are tabulated for both dissolved gas supersaturation ratio (ZHL) and bubble number excess (RGBM) risk functions, with, employing maximum variance, $r_{\pm} = r \pm 0.004$.

Table 14. Dissolved And Separated Phase Risk Estimates For Nominal Profiles.

profile (depth/time)	descent rate (msw/min)	ascent rate (msw/min)	safety stop (depth/time)	risk r_{RGBM}	risk r_{ZHL}
14 <i>msw</i> /38 <i>min</i>	18	9	5 <i>msw</i> /3 <i>min</i>	.0034	.0062
19 <i>msw</i> /38 <i>min</i>	18	9	5 <i>msw</i> /3 <i>min</i>	.0095	.0110
28 <i>msw</i> /32 <i>min</i>	18	9		.0200	.0213
37 <i>msw</i> /17 <i>min</i>	18	9	5 <i>msw</i> /3 <i>min</i>	.0165	.0151
18 <i>msw</i> /31 <i>min</i>	18	9	5 <i>msw</i> /3 <i>min</i>	.0063	.0072
	18	9		.0088	.0084
	18	18		.0101	.0135
	18	18	5 <i>msw</i> /3 <i>min</i>	.0069	.0084
17 <i>msw</i> /32 <i>min</i> SI 176 <i>min</i>	18	9	5 <i>msw</i> /3 <i>min</i>		
13 <i>msw</i> /37 <i>min</i> SI 174 <i>min</i>	18	9	5 <i>msw</i> /3 <i>min</i>		
23 <i>msw</i> /17 <i>min</i>	18	18	5 <i>msw</i> /3 <i>min</i>	.0127	.0232

The ZHL (Buhlmann) NDLS and staging regimens are widespread across decompression meters presently, and are good representation for Haldane risk analysis. The RGBM is newer and more

modern (and more physically correct), and is coming online in decometers and associated software. For recreational exposures, the RGBM collapses to a Haldane dissolved gas algorithm. This is reflected in the risk estimates above, where estimates for both models differ little.

Simple comments hold for the analyzed profile risks. The maximum relative risk is 0.0232 for the 3 dive repetitive sequence according to the Haldane dissolved risk estimator. This translates to 0.2% binomial risk, which is comparable to the maximum NDL risk for the PADI, NAUI, and Oceanic NDLs. Again, this type of dive profile is common, practiced daily on liveboards, and benign. According to Gilliam, the absolute incidence rate for this type of diving is less than 0.02%. Again, our analyses overestimate risk.

Effects of slower ascent rates and safety stops are noticeable at the 0.25% to 0.5% level in relative surfacing risk. Safety stops at 5 *m* for 3 *min* lower relative risk an average of 0.3%, while reducing the ascent rate from 18 *msw/min* to 9 *msw/min* reduces relative risk an average of 0.35%.

Staging, NDLs, and constraints imposed by decometer algorithms are consistent with acceptable and safe recreational diving protocols. Estimated absolute risk associated across all ZHL NDLs and staging regimens analyzed herein is less than 0.232%, probably much less in actual practice. That is, we use $p = 0.006$, and much evidence suggests $p < 0.0001$, some ten times safer.

Implicit in such formulations of risk tables are assumptions that given decompression stress is more likely to produce symptoms if it is sustained in time, and that large numbers of separate events may culminate in the same probability after time integration. Though individual schedule segments may not be replicated enough to offer total statistical validation, categories of predicted safety can always be grouped within subsets of corroborating data. Since the method is general, any model parameter or meaningful index, properly normalized, can be applied to decompression data, and the full power of statistical methods employed to quantify overall risk. While powerful, such statistical methods are neither deterministic nor mechanistic, and cannot predict on first principles. But as a means to table fabrication with quoted risk, such approaches offer attractive pathways for analysis.

Validation procedures for schedules and tables can be quantified by a set of procedures based on statistical decompression analysis:

1. select or construct a measure of decompression risk, or a probabilistic model;
2. evaluate as many dives as possible, and especially those dives similar in exposure time, depth, and environmental factors;
3. conduct limited testing if no data is available;
4. apply the model to the data using maximum likelihood;
5. construct appropriate schedules or tables using whatever incidence of decompression sickness is acceptable;
6. release and then collect profile statistics for final validation and tuning.

Questions of what risk is acceptable to the diver vary. Sport and research divers would probably opt for very small risk (0.01% or less), while military and commercial divers might live with higher risk (1%), considering the nearness of medical attention in general. Many factors influence these two populations, but fitness and acclimatization levels would probably differ considerably across them. While such factors are difficult to fold into any table exercise or analysis, the simple fact that human subjects in dive experiments exhibit higher incidences during testing phases certainly helps to lower the actual incidence rate in the field, noted by Bennett and Lanphier.

PHASE MECHANICS AND DECOMPRESSION THEORY IN DEPTH CHAPTER 7: COMPUTING AND DECOMPRESSION ALGORITHMS

Computing Advances

Computing technology has made incredible progress in the past 50 years. In 1945, there were no stored program computers. Today, a few thousand dollars will purchase a desktop personal computer with more performance, more memory, and more disk storage than a million dollar computer in 1965. This rapid rate of improvement has come from advances in technology used to build the computer and from innovation in computer design. Performance increase is sketched in Figure 1, in terms of a nominal 1965 minicomputer. Performance growth rates for supercomputers, minicomputers, and mainframes are near 20% per year, while performance growth rate for microcomputers is closer to 35% per year. Supercomputers are the most expensive, ranging from one to tens of millions of dollars, and microprocessors are the least expensive, ranging from a few to tens of thousands of dollars. Supercomputers and mainframes are usually employed in high end, general purpose, compute intensive applications. Minicomputers and microprocessors address the same functionality, but often in more diverse roles and applications. The latter class of computers is usually more portable, because they are generally smaller in size. They are on your desktop.

The label *supercomputer* usually refers to the fastest, biggest, and most powerful computer in existence at any time. In the 1940s, supercomputers were employed in the design of nuclear weapons (as still today), In the 1950s, supercomputers were first used in weather forecasting, while in the 1960s, computational fluid dynamics problems in the aerospace industry were solved on supercomputers. In the 1970s, 1980s, and 1990s seismological data processing, oil reservoir simulation, structural analysis of buildings and vehicles, quantum field theory, circuit layout, econometric modeling, materials and drug design, brain tomography and imaging, molecular dynamics, global climate and ocean circulation modeling, and semiconductor fabrication joined the supercomputing revolution. Very few areas in science and engineering have not been impacted by supercomputers. Diving is still on the fringes of supercomputing, but applications are growing, particularly in the areas of dive profile analysis, statistics, data management, and biomodeling. Smaller and less powerful computers are now employed for monitoring, controlling, directing, and analyzing dives, divers, equipment, and environments. Wrist computers perform rudimentary decompression calculations and stage ascents with mostly Haldane models.

Operational supercomputers today process data and perform calculations at rates of 10^9 floating point operations per second (*gigaflops*), that is, 10^9 adds, subtracts, multiplies, or divides per second. At the edge today, and in the marketplace, are shared memory processors (SMPs) providing users with 10^{12} floating point operations per second (*teraflops*), impressively opening yet another age in computational science. These machines are massively parallel processors (MPPs), involving thousands of computing nodes processing trillions of data points. To support these raw computing speeds, networks transmitting data at gigabits/sec, and fast storage exchanging terabytes of information over simulation times are also requisite. Ultrafast, high resolution, graphics servers, able to process voluminous amounts of information, offer an expeditious means to assess output data. Differences in raw processing speeds between various components in a high performance computing environment can degrade overall throughput, conditions termed *latencies*, or simply, manifest time delays in processing data. Latencies are parasitic to sustained computing performance. Latencies develop at the nodes connecting various computer, storage, network, terminal, and graphics devices, simply because of impedance mismatch in data handling capabilities.

Obviously, computers work on processing information, doing calculations, and fetching and storing data in steps. A set of operations, performed in sequential fashion by one processor, is termed

serial. A set of operations performed in any fashion, by any number of processors, is roughly termed *parallel*. Serial computing architectures, once the standard, are now being replaced by parallel computing architectures, with anywhere from tens to thousands of central processing units (CPUs). Processors themselves can be *scalar*, or *vector*, that is, operating on a single entity, or group of entities (numbers).

The architectural feature associated with supercomputers in the 1970s was vector processing. Vector processing allowed large groups of numbers, or vectors, to be processed in parallel, resulting in performance speedups by factors of ten or more (compared to generational improvements on the order of 2 or 3). In the early 1980s, parallel supercomputing was introduced, allowing multiple processors to work concurrently on a single problem. By the end of the century, significantly greater computing parallelism (combining tens of thousands of processing units perhaps), and architectures that integrate modalities, such as numeric and symbolic processing, may be possible. As in the past, software developments on future state of the art supercomputers will probably trail hardware advances, perhaps with increasing distance due to increasingly more complex superparallel systems.

Networks are the backbone of modern computer systems. Supercomputers without high speed communications links and network interfaces are degraded in application processing speed, limited by the slowest component in the computing platform. Gigaflop computers need gigabit/sec network transmission speeds to expedite the flow of information.

Data, voice, image, and full motion video can be digitally encoded, and sent across a variety of physical media, including wire, fiber optics, microwaves, and satellites. The assumption is that all information transmitted will be digital. The greater the number of systems, people, and processes that need to transmit information to one another, the greater the speeds and bandwidths required. Like water in a pipe, to get more information through a network, one can increase the rate of flow (*speed*), and/or increase the amount that can flow through cross sectional area (*bandwidth*). Applications under development today presage the needs to transfer data very quickly tomorrow. To perform as a utility, that is, usefully communicate anything, anytime, anywhere, a network must possess four attributes:

1. connectivity – ability to move information regardless of the diversity of the media;
2. interoperability – ability of diverse intelligent devices to communicate with one another;
3. manageability – ability to be monitored, and to change with applications and devices;
4. distributed applications and connective services – ability to provide easy access to tools, data, and resources across different computing platforms, or organizations.

Commercial telecommunications links (modem connections to the Internet) are extremely slow, in the vicinity of 10 kilobits/sec to 56 kilobits/sec. Even dedicated communications lines are low speed, that is, T1 and T3 links (1.4 megabits/sec and 43 megabits/sec respectively), and cannot feed supercomputers with information fast enough to support economical processing. The 4 terabytes from a seismic map of an oil field in the Gulf (8 square miles) would take about 3 - 4 days to transmit from one site to another for processing. The 1 million dive profiles projected in DAN Project Dive Exploration stacks up to hundreds of gigabytes, depending on resolution.

Advances in massively parallel, large memory computers, and high speed networks have created computing platforms, depicted in Figure 2, which allow researchers to execute supercodes that generate enormous data files. The supercomputing environment depicted in Figure 2 can be found in large Universities, National and Regional Laboratories, dedicated Commercial Computing Centers, and various Governmental Agencies. The one in Figure 2 depicts the superplatform at the Los Alamos National Laboratory. These facilities are available to the commercial user, and computing costs range from \$100-\$300 per hour on vector supercomputers (YMP, T90, J90) to \$1 - \$4 per node per hour on massively parallel supercomputers (CM5, T3D, SP2 Cluster, Origin 2000 SMP).

Supercodes generate enormous amounts of data, and a typical large application will generate from tens of gigabytes up to several terabytes of data. Such requirements are one to two orders of magnitude greater than the comfortable capacities of present generation storage devices. New high performance data systems (HPDS) are online to meet the very large data storage and handling. Systems consist of fast, large capacity storage devices that are directly connected to a high speed network, and managed by software distributed across workstations. Disk devices are used to meet high speed and fast access requirements, while tape devices are employed to meet high speed and high capacity requirements. Storage devices usually have a dedicated workstation for storage and device management, and to oversee data transfer. Put simply, computer systems use a hierarchy to manage information storage:

1. primary storage – fast, solid state memory contained in the processor;
2. direct access storage – magnetic or optical disks, connected to the processor, providing fast access;
3. sequential access storage – magnetic tape cassettes or microfilm, providing large capacity.

Transfer rates in fast HPDS systems are presently near 800 megabits/sec. Moving down the hierarchy, access time goes up, storage capacity increases, and costs decrease. Today, of all computing components, the cost of storage is decreasing the most rapidly. A few hundred dollars will buy gigabyte hard drives for your PC. Renting storage commercially is also cheap (\$20 gigabyte/month).

In supercomputing today, there has been a paradigm shift towards shared memory processors (SMPs), many fast CPUs (64 or more) sharing common memory within an SMP, and communicating with other SMPs across very fast interconnects (switches) using message passing. Since 1999, the technology for their platform development has seen enormous advance, as depicted in Figure 3. Such advancement is ushering in the era of many tens of teraflops raw computing power.

Scientific advance rests on the interplay between theory and experiment. Computation closes the loop between theory and experiment in quantitative measure. Theory provides the framework for understanding. Experiment and data provide the means to verify and delineate that understanding. Although many disciplines rely on observational data (astronomy, geology, and paleontology, for instance), the hallmark of scientific endeavor is experiment. Clearly, the power of experimental science is its ability to design the environment in which data is gathered. And it is in the design process that modern computers play an important role.

While many believe that good experimentation depends on the skill and imagination of the designer, this is not entirely true. Insight and experience are certainly desirable to determine and optimize measurable response and procedures, but once this has been determined, it is the mathematics that dictates experimental structure, as detailed by Fisher some 70 years ago in noting that the real world is:

1. noisy – repeating an experiment under identical conditions yields different results;
2. multivariate – many factors potentially affect phenomena under investigation;
3. interactive – the effect of one factor may depend on the level of involvement of other factors.

Computers permit extension and analysis of experimental design methodology to problems for which only crude prescriptions have been hitherto available. Computer software is now widely and economically available to automate the basic and most useful procedures. This allows the user without extensive statistical background to routinely employ methods to optimize design.

Certainly, performing numerical experiments on computers, that is, leveraging model predictions to gain insight into phenomena under study, can often provide results that give the best possible estimate of overall experimental response and behavior. The approach here is to use the smallest

possible subsets of inputs to run the simulation model, thereby narrowing the focus. In designing experiments, Monte Carlo simulations are used in high energy and accelerator physics, semiconductor fabrication, material damage, neutron and photon shielding, and biomedical dose. Large deterministic modules, in excess of 100,000 lines of code, on the other hand, have been applied to the design of laser fusion target experiments. Similarly, atomistic simulations with millions and, in the future, billions of test atoms provide the opportunity for both fundamental and technological advances in material science. Nonequilibrium molecular dynamics calculations address basic scientific issues, such as interaction potentials and plastic flow. The interaction potentials developed in the last decade for metals, alloys, and ceramics can be used to model prototypical hardness experiments, such as crystal indentation. The underlying mechanisms for plastic flow are microscopic crystal defect motions, and molecular dynamics calculations yield quantitative estimates for hardness experiments. Linkages between experiment and supercomputer modeling are growing in scope and number. And diving is no exception. Consider the following three applications of supercomputing power to diving analysis.

Monte Carlo Bubble Simulations

Monte Carlo calculations explicitly employ random variates, coupled to statistical sampling, to simulate physical processes and perform numerical integrations. In computational science, Monte Carlo methods play a special role because of their combination of immediacy, power, and breadth of application. The computational speed and memory capacity of supercomputers have expedited solutions of difficult physical and mathematical problems with Monte Carlo statistical trials. Although Monte Carlo is typically used to simulate a random process, it is frequently applied to problems without immediate probabilistic interpretation, thus serving as a useful computation tool in all areas of scientific endeavor. Applied to bubble formation and tissue-blood interactions, Monte Carlo methods are truly powerful supercomputing techniques.

The Monte Carlo method is different than other techniques in numerical analysis, because of the use of random sampling to obtain solutions to mathematical and physical problems. A stochastic model, which may or may not be immediately obvious, is constructed. By sampling from appropriate probability distributions, numerical solution estimates are obtained. Monte Carlo calculations simulate the physical processes at each point in an event sequence. All that is required for the simulation of the cumulative history is a probabilistic description of what happens at each point in the history. This generally includes a description of the geometrical boundaries of regions, a description of material composition within each region, and the relative probability (functional) for an *event*. With high speed computers, millions of events can be generated rapidly to provide simulation of the processes defined by the probability function. Statistically, the accuracy of the simulation increases with number of events generated.

The generation of cavitation nuclei in tissue can be effected with Monte Carlo techniques, using the Gibbs potential (bubble formation energy) across liquid-vapor interfaces as a probability function for bubble radius as the random variable. Surrounded by dissolved gas at higher tension for any ambient pressure, bubbles generated can be tracked through growth and collapse cycles in time, allowed to move with surrounding material, coalesced with each other, and removed at external boundaries. Cavitation simulations are applied to multiphase flow in nuclear reactor vessels, cavitation around ship propellers, bubbles in gels, cloud and ice condensation processes in the atmosphere, cosmic ray tracking in chambers, and boiling processes in general.

Project Dive Exploration

Maximum likelihood is a statistical technique used to fit model equations to a sample with relative probabilities for occurrence and nonoccurrence given. We can never measure any physical variable

exactly, that is, without error. Progressively more elaborate experiments or theoretical representation only reduce the error in the determination. In extracting parameter estimates from data sets, it is also necessary to minimize the error (data scatter) in the extraction process. Maximum likelihood is one such technique applied to probabilistic decompression modeling.

DCS is a hit, or (hopefully) no-hit situation, and statistics are binary, as in coin tossing. As a random variable, DCS incidence is a complicated function of many physical variables, such as inert gas buildup, VGE counts, pressure reduction on decompression, volume of separated gas, number of bubble seeds, gas solubility in tissue and blood, ascent rate, nucleation rate, distribution of growing bubble sizes, and combinations thereof. Any, and all of these, can be assigned as risk functions in probabilistic decompression modeling, and associated constants deduced in the maximum likelihood fit process.

Project Dive Exploration is a DAN program to collect and analyze data on real dives in real time for profiles, behavioral, and health aspects associated with recreational diving. The study focuses on actual dives and profiles recorded by depth/time computers, and verifies the general condition of the diver up to 48 hours after exiting the water, regarding health problems. Upwards of a million dive profiles are anticipated for this study, mainly because DCS incidence is low probability and many trials are necessary for meaningful modeling, statistics, correlations, and estimates. Multivariate model equations are fitted to the dive profiles and observed DCS incidence rate using maximum likelihood, a technique which minimizes the variance in fitting equations to a recreational diving sample. The recreational data file sizes to hundreds of gigabytes, and requires gigaflop supercomputing resources for processing. A 10 parameter risk function fit to 1 million dive profiles would take about an hour on the 256 node CRI T3D, an MPP with 16 gigabytes of memory, 65 gigabytes of fast disk, and a peak speed near 38 gigaflops. Run times scale as the number of events times the number of risk function parameters squared.

Multilevel Dive Profile Analysis

Schemes for multilevel diving are employed in the commercial, scientific, and sport sectors. In addition to validation, questions arise as to method consistency with the formulation of the US Navy Tables on critical tension principles. One approach employs back to back repetitive sequencing, assigning groups at the start of each multilevel dive segment based on the total bottom time (actual plus residual nitrogen) of the previous segment. At times, the method allows critical tensions, other than the controlling (repetitive) 120 minute compartment tension, to be exceeded upon surfacing. In the context of the US Navy Tables, such circumstance is to be avoided. But, by tightening the exposure window and accounting for ascent and descent rates, such a multilevel technique can be made consistent with the permissible tension formulation of the US Navy Tables.

To adequately evaluate multilevel diving within any set of Tables, it is necessary to account for ascent and descent rates. While ascent and descent rates have small effect on ingassing and outgassing in slow tissue compartments, ascent and descent rates considerably impact fast tissue compartments. Model impact is measured in nitrogen buildup and elimination in hypothetical compartments, whose halftimes denote time to double, or half, existing levels of nitrogen. Buildup and elimination of nitrogen is computed with Haldane tissue equations (exponential rate expressions), and critical tensions, are assigned to each compartment to control diving activity and exposure time. In multilevel diving, computed tissue tensions in any and all compartments must be maintained below their critical values. This is a more stringent constraint than just flooring the 120 minute compartment tension, the approach used in the US Navy Tables for repetitive diving.

In the context of the US Navy Tables, from which many Tables with reduced nonstop time limits derive, six compartments with 5, 10, 20, 40, 80, and 120 minute halftimes limit diving through maximum tensions (M -values) of 104, 88, 72, 58, 52, and 51 fsw , respectively. The 5 and 10 minute compartments are fast, the 80 and 120 minute compartments are slow, and the others are often

between, depending on exposure profile. Dive exposure times, depths, ascent, and descent rates, affecting slow and fast compartments in a complicated manner, are virtually infinite in number, thus suggesting the need for both a supercomputer and meaningful representation of the results. A CRAY YMP supercomputer addressed the first concern, while the US Navy Tables provided a simple vehicle for representation of results.

Calculations were performed in roughly 1 minute time intervals, and 10 *fsw* depth increments for all possible multilevel dives up to, and including, the standard US Navy nonstop time limits, and down to a maximum depth of 130 *fsw*. Ascent and descent rates of 60 *fsw/min* were employed. Tissue tensions in all six compartments were computed and compared against their *M*-values. Dives for which the *M*-values were not violated were stored until the end of the multilevel calculations, for further processing. Dives violating any *M*-value, at any point in the simulation, were terminated, and the next dive sequence was initiated. The extremes in times for permissible multilevel dives form the envelope of calculations at each depth. The envelope turns out to be very close to the NAUI nonstop limits for the US Navy Tables, that is, the Tables shown in Table 5 (Chapter 4). Within a minute, on the conservative side, the envelope tracks the reduced nonstop limits. Approximately 16 million multilevel dives were analyzed on a CRAY YMP in about 8 minutes CPU time, including construction of the envelope, with 10 *fsw* and 1 minute resolution. The CRAY YMP has raw speed near 320 megaflops per CPU.

Adjunct to Table 5 (Chapter 4), one can summarize with regard to YMP calculations:

1. the deeper the initial depth, the shorter the total multilevel dive time;
2. maximum permissible multilevel dive times (total) vary between 100 and 60 minutes, depending on initial depths;
3. minimum permissible multilevel increments vary from 30 *fsw* to 10 *fsw* as the depth decreases from 130 *fsw* to 40 *fsw*;
4. multilevel US Navy Table dives falling within the envelope never exceed critical values, below or at the surface, in all compartments;
5. the multilevel envelope is the set of reduced nonstop limits.

In terms of modified USN Tables (Table 5, Chapter 4), multilevel dives that stay to the left of the nonstop time limits never violate critical tensions, and are (hypothetically) sanctioned. Dive computers, of course, perform the same exercise underwater, comparing instantaneous values of computed tissue tensions in all compartments, throughout the duration of the dive, against stored *M*-values to estimate time remaining and time at a stop.

Computational Algorithms

The models broached (Chapter 4) address the coupled issues of gas uptake and elimination, bubbles, and pressure changes in different computational approaches. Application of a computational model to staging divers and aviators is often called a diving algorithm. Consider the computational model and staging regimen for 7 popular algorithms, namely, the perfusion limited, diffusion limited, thermodynamic, varying permeability, reduced gradient bubble (2), and tissue bubble diffusion algorithms:

Dissolved Phase Algorithms

Dissolved gas diving algorithms historically trace back to the original Haldane experiments in the early 1900s. They are still around today, in tables, meters, and diving software. That is changing, however, as modern divers go deeper, stay longer, decompress, and used mixed gases.

1. Perfusion Limited

Exchange of inert gas, controlled by blood flow rates across regions of varying concentration, is driven by the gas gradient, that is, the difference between the arterial blood tension, p_a , and the instantaneous tissue tension, p . This behavior is modeled in time, t , by classes of exponential response functions, bounded by p_a and the initial value of p , denoted p_i . These multitissue functions satisfy a differential perfusion rate equation,

$$\frac{\partial p}{\partial t} = -\lambda(p - p_a)$$

and take the form, tracking both dissolved gas buildup and elimination symmetrically,

$$p - p_a = (p_i - p_a) \exp(-\lambda t)$$

$$\lambda = \frac{0.693}{\tau}$$

with perfusion constant, λ , linked to tissue half-time, τ . Compartments with 1, 2.5, 5, 10, 20, 40, 80, 120, 180, 240, 360, 480, and 720 minute half-times, τ , are employed, and half-times are independent of pressure.

In a series of dives or multiple stages, p_i and p_a represent extremes for each stage, or more precisely, the initial tension and the arterial tension at the beginning of the next stage. Stages are treated sequentially, with finishing tensions at one step representing initial tensions for the next step, and so on. To maximize the rate of uptake or elimination of dissolved gases the *gradient*, simply the difference between p_i and p_a , is maximized by pulling the diver as close to the surface as possible. Exposures are limited by requiring that the tissue tensions never exceed M , written,

$$M = M_0 + \Delta M d$$

as a function of depth, d , for ΔM the change per unit depth. A set of M_0 and ΔM are listed in Table 6 (Chapter 4). In absolute units, the corresponding critical gradient, G , is given by,

$$G = \frac{M}{0.79} - P$$

with P ambient pressure, and M critical nitrogen pressure. Similarly, the critical ratio, R , takes the form,

$$R = \frac{M}{P}$$

At altitude, some critical tensions have been correlated with actual testing, in which case, the depth, d , is defined in terms of the absolute pressure,

$$d = P - 33$$

with absolute pressure, P , at altitude, z , given by (*fsw*),

$$P = 33 \exp(-0.0381z) = 33\alpha^{-1}$$

$$\alpha = \exp(0.0381z)$$

and z in multiples of 1,000 feet. However, in those cases where the critical tensions have not been tested nor extended to altitude, an exponentially decreasing extrapolation scheme, called *similarity*, has been employed. Extrapolations of critical tensions, below $P = 33$ *fsw*, then fall off more rapidly than in the linear case. The similarity extrapolation holds the ratio,

$R = M/P$, constant at altitude. Denoting an equivalent sea level depth, δ , at altitude, z , one has for an excursion to depth d ,

$$\frac{M(d)}{d + 33\alpha^{-1}} = \frac{M(\delta)}{\delta + 33}$$

so that the equality is satisfied when,

$$\delta = \alpha d$$

$$M(\delta) = \alpha M(d).$$

Considering the minimum surface tension pressure of bubbles, G^{min} (near $10fsw$), as a limit point, the similarity extrapolation should be limited to 10,000 feet in elevation, and neither for decompression, nor heavy repetitive diving.

As described previously, depth-time exposures are often limited by a law of the form,

$$dt_n^{1/2} = H$$

with t_n the nonstop time limit, and $400 \leq H \leq 500 fsw \text{ min}^{1/2}$. One can obtain the corresponding tissue constant, λ , controlling the exposure at depth d , for nonstop time t_n , by differentiating the tissue equation with respect to depth, d , and setting the result to zero. With $p_a = 0.79(d + 33)$ at sea level, there results,

$$1 - \exp(-\lambda t_n)(1 + 2\lambda t_n) = 0.$$

Corresponding critical tensions, M , are then easily obtained using d , λ , and t_n . In the above case, the transcendental equation is satisfied when,

$$\lambda t_n = 1.25$$

Time remaining before a stop, time at a stop, or surface interval before flying can all be obtained by inverting the tissue equation. Denoting the appropriate critical tension at some desired stage, M , and the instantaneous tension at that time, p , at stage, p_a , the time remaining, t_r , follows from,

$$t_r = \frac{1}{\lambda} \ln \left[\frac{p - p_a}{M - p_a} \right]$$

for each compartment, λ . Obviously, the smallest t_r controls the ascent.

2. Diffusion Limited

Exchange of inert gas, controlled by diffusion across regions of varying concentration, is also driven by the local gradient. As before, denoting the arterial blood tension, p_a , and instantaneous tissue tension, p , the gas diffusion equation takes the form in one dimensional planar geometry,

$$D \frac{\partial^2 p}{\partial x^2} = \frac{\partial p}{\partial t}$$

with D a single diffusion coefficient appropriate to the media. Using standard techniques of separation of variables, with ω^2 the separation constant (eigenvalue), the solution is written,

$$p - p_a = (p_i - p_a) \sum_{n=1}^{\infty} W_n \sin(\omega_n x) \exp(-\omega_n^2 D t)$$

assuming at the left tissue boundary, $x = 0$, we have $p = p_a$, and with W_n a set of constants obtained from the initial condition. First, requiring $p = p_a$ at the right tissue boundary, $x = l$, yields,

$$\omega_n = \frac{n\pi}{l}$$

for all n . Then, taking $p = p_i$ at $t = 0$, multiplying both sides of the diffusion solution by $\sin(\omega_n x)$, integrating over the tissue zone, l , and collecting terms gives,

$$W_{2n} = 0$$

$$W_{2n-1} = \frac{4}{(2n-1)\pi}$$

Averaging the solution over the tissue domain eliminates spatial dependence, that is $\sin(\omega_n x)$, from the solution, giving a bulk response,

$$p - p_a = (p_i - p_a) \sum_{n=1}^{\infty} \frac{8}{(2n-1)^2 \pi^2} \exp(-\omega_{2n-1}^2 Dt).$$

The expansion resembles a weighted sum over *effective* tissue compartments with time constants, $\omega_{2n-1}^2 D$, determined by diffusivity and boundary conditions.

Diffusion models fit the time constant, K ,

$$\kappa = \pi^2 D l^2$$

to exposure data, with a typical value employed by the Royal Navy given by,

$$\kappa = 0.007928 \text{ min}^{-1}.$$

The approach is aptly single tissue, with equivalent tissue half-time, τ_D ,

$$\tau_D = \frac{0.693}{\kappa} = 87.5 \text{ min}$$

close to the US Navy 120 minute compartment used to control saturation, decompression, and repetitive diving. Corresponding critical tensions in the bulk model, take the form,

$$M = \frac{709 P}{P + 404}$$

falling somewhere between fixed gradient and multitissue values. At the surface, $M = 53 \text{ fsw}$, while at 200 fsw , $M = 259 \text{ fsw}$. A critical gradient, G , satisfies,

$$G = \frac{M}{0.79} - P = \frac{P(493 - P)}{(P + 404)}.$$

The limiting features of bulk diffusion can be gleaned from an extension of the above slab model in the limit of thick tissue region, that is, $l \rightarrow \infty$. Replacing the summation over n with an integral as $l \rightarrow \infty$, we find

$$p - p_a = (p_i - p_a) \bar{erf} [l/(4Dt)^{1/2}]$$

with \bar{erf} the average value of the *error-function* over l , having the limiting form (Abramowitz and Stegun),

$$\bar{erf} [l/(4Dt)^{1/2}] = 1 - (4Dt)^{1/2} l \pi^{1/2}$$

for short times, and

$$\bar{erf} [l/(4Dt)^{1/2}] = \frac{l}{(4\pi Dt)^{1/2}}$$

for long times.

Unlike the perfusion case, the diffusion solution, consisting of a sum of exponentials in time, cannot be formally inverted to yield time remaining, time at a stop, nor time before flying. Such information can only be obtained by solving the equation numerically, that is, with computer or hand calculator for given M , p , and p_a .

If we wrap the above planar geometry around into a hollow cylinder of inner radius, a , and outer radius, b , we generate Krogh geometry. The hollow cylindrical model retains all the features of the planar model, and additionally includes curvature for small a and b , with $l = b - a$ from before. Assigning the same boundary conditions at a and b , namely, the tissue tension, p , equals the arterial tension, p_a , writing the diffusion equation in radial cylindrical coordinates,

$$D \frac{\partial^2 p}{\partial r^2} + \frac{D}{r} \frac{\partial p}{\partial r} = \frac{\partial p}{\partial t}$$

and solving yields,

$$p - p_a = (p_i - p_a) \sum_{n=1}^{\infty} X_n U_0(\epsilon_n r) \exp(-\epsilon_n^2 D t)$$

with X_n a constant satisfying initial conditions, U_0 the cylinder functions (Abramowitz and Stegun), and ϵ_n the eigenvalues satisfying,

$$U_0(\epsilon_n a) = \frac{\partial U_0(\epsilon_n b/2)}{\partial r} = 0$$

Averaging over the tissue region, $a \leq r \leq b$, finally gives,

$$p - p_a = (p_i - p_a) \frac{4}{(b/2)^2 - a^2} \sum_{n=1}^{\infty} \frac{1}{\epsilon_n^2} \frac{J_1^2(\epsilon_n b/2)}{J_0^2(\epsilon_n a) - J_1^2(\epsilon_n b/2)} \exp(-\epsilon_n^2 D t)$$

with J_1 and J_0 Bessel functions, order 1 and 0. Typical vascular parameters are bounded roughly by,

$$\begin{aligned} 0 < a &\leq 4 \mu m \\ 10 &\leq b \leq 32 \mu m. \end{aligned}$$

Dual Phase Algorithms

Dual phase diving algorithms are rather recent innovations, coming online in the past 20 years or so. They are more correct than dissolved gas algorithms, because they couple dissolved gases to bubbles, and lead to deeper staging as a result. Meters, tables, and software employing these algorithms do exist, and are supplanting traditional versions.

1. Thermodynamic

The thermodynamic model couples both the tissue diffusion and blood perfusion equations. Cylindrical symmetry is assumed in the model. From a boundary vascular zone of thickness, a , gas diffuses into the extended extravascular region, bounded by b . The radial diffusion equation is given by,

$$D \frac{\partial^2 p}{\partial r^2} + \frac{D}{r} \frac{\partial p}{\partial r} = \frac{\partial p}{\partial t}$$

with the tissue tensions, p , equal to the venous tensions, p_v , at the vascular interfaces, a and b . The solution to the tissue diffusion equation is given previously,

$$p - p_v = (p_i - p_v) \frac{4}{(b/2)^2 - a^2} \sum_{n=1}^{\infty} \frac{1}{\epsilon_n^2} \frac{J_1^2(\epsilon_n b/2)}{J_0^2(\epsilon_n a) - J_1^2(\epsilon_n b/2)} \exp(-\epsilon_n^2 D t)$$

with ϵ_n eigenvalue roots of the boundary conditions,

$$J_0(\epsilon_n a) Y_1(\epsilon_n b/2) - Y_0(\epsilon_n a) J_1(\epsilon_n b/2) = 0$$

for J and Y Bessel and Neumann functions, order 1 and 0. Perfusion limiting is applied as a boundary condition through the venous tension, p_v , by enforcing a mass balance across both the vascular and cellular regions at a ,

$$\frac{\partial p_v}{\partial t} = -\kappa(p_v - p_a) - \frac{3}{a} S_p D \left[\frac{\partial p}{\partial r} \right]_{r=a}$$

with S_p the ratio of cellular to blood gas solubilities, κ the perfusion constant, and p_a the arterial tension. The coupled set relate tension, gas flow, diffusion and perfusion, and solubility in a complex feedback loop.

The thermodynamic trigger point for decompression sickness is the volume fraction, χ , of separated gas, coupled to mass balance. Denoting the separated gas partial pressure, P_{N_2} , under worse case conditions of zero gas elimination upon decompression, the separated gas fraction is estimated,

$$\chi P_{N_2} = S_c (p - P_{N_2})$$

with S_c the cellular gas solubility. The separated nitrogen partial pressure, P_{N_2} is taken up by the inherent unsaturation, and given by (*fsw*),

$$P_{N_2} = P + 3.21$$

in the original Hills formulation, but other estimates have been employed. Mechanical fluid injection pain, depending on the injection pressure, δ , can be related to the separated gas fraction, χ , through the tissue modulus, K ,

$$K \chi = \delta$$

so that a decompression criteria requires,

$$K \chi \leq \delta$$

with δ in the range, for $K = 3.7 \times 10^4 \text{ dyne cm}^{-2}$,

$$0.34 \leq \delta \leq 1.13 \text{ fsw.}$$

Identification of the separated phase volume as a critical indicator is a significant development in decompression theory.

2. Varying Permeability

The critical radius, r_i , at fixed pressure, P_i , represents the cutoff for growth upon decompression to lesser pressure. Nuclei larger than r_i will all grow upon decompression. Additionally, following an initial compression, a smaller class of micronuclei of critical radius, r , can be excited into growth with decompression. If r_i is the critical radius at P_i , then, the smaller family, r , excited by decompression from P , obeys,

$$\frac{2\gamma}{r} - P = \frac{2\gamma}{r_i} - P_i$$

with roughly,

$$50.0 \leq \gamma 250.0 \text{ fsw } \mu m$$

for P measured in fsw , and r in μm . Table 1 (Chapter 1) lists critical radii, r , excited by sea level compressions ($P_i = 33 fsw$), assuming $r_i = 0.8 \mu m$. Entries also represent the equilibrium critical radius at pressure, P .

The permissible gradient, G , is written for each compartment, τ , using the standard formalism,

$$G = G_0 + \Delta G d$$

at depth $d = P - 33 fsw$. A nonstop bounce exposure, followed by direct return to the surface, thus allows G_0 for that compartment. Both G_0 and ΔG are tabulated in Table 2 (Chapter 4), with ΔG suggested by Buhlmann. The minimum excitation, G^{min} , initially probing r , and taking into account generation of nuclei over time scales τ_r , is (fsw),

$$G^{min} = \frac{2\gamma (\gamma_c - \gamma)}{\gamma_c r(t)} = \frac{11.01}{r(t)}$$

with,

$$r(t) = r + (r_i - r) [1 - \exp(-\lambda_r t)]$$

γ , γ_c film, surfactant surface tensions, that is, $\gamma = 17.9 \text{ dyne/cm}$, $\gamma_c = 257 \text{ dyne/cm}$, and λ_r the inverse of the generation time for stabilized gas micronuclei (many days in the VPM). Prolonged exposure leads to saturation, and the largest permissible gradient, G^{sat} , takes the form (fsw), in all compartments,

$$G^{sat} = \frac{58.6}{r} - 49.9 = 0.372 P + 11.01.$$

On the other hand, G^{min} is the excitation threshold, the amount by which the surrounding tension must exceed internal bubble pressure to just support growth.

Although the actual size distribution of gas nuclei in humans is unknown, experiments *in vitro* suggest that a decaying exponential is reasonable,

$$n = N \exp(-\beta r)$$

with β a constant, and N a convenient normalization factor across the distribution. For small values of the argument, βr ,

$$\exp(-\beta r) = 1 - \beta r$$

as a nice simplification. For a stabilized distribution, n_0 , accommodated by the body at fixed pressure, P_0 , the excess number of nuclei, Λ , excited by compression-decompression from new pressure, P , is,

$$\Lambda = n_0 - n = N\beta r_i \left[1 - \frac{r}{r_i} \right].$$

For large compressions-decompressions, Λ is large, while for small compressions-decompressions, Λ is small. When Λ is folded over the gradient, G , in time, the product serves as a critical volume indicator and can be used as a limit point in the following way.

The rate at which gas grows in tissue depends upon both the excess bubble number, Λ , and the gradient, G . The critical volume hypothesis requires that the integral of the product of the two must always remain less than some limit point, αV , with α a proportionality constant,

$$\int_0^\infty \Lambda G dt = \alpha V$$

for V the limiting gas volume. Assuming that gradients are constant during decompression, t_d , while decaying exponentially to zero afterwards, and taking the limiting condition of the equal sign, yields simply for a bounce dive, with λ the tissue constant,

$$\Delta G (t_d + \lambda^{-1}) = \alpha V.$$

In terms of earlier parameters, one more constant, δ , closes the set, defined by,

$$\delta = \frac{\gamma_c \alpha V}{\gamma \beta r_i N} = 7180 \text{ fsw min}$$

so that,

$$\left[1 - \frac{r}{r_i}\right] G (t_d + \lambda^{-1}) = \delta \frac{\gamma}{\gamma_c} = 500.8 \text{ fsw min}.$$

The five parameters, γ , γ_c , δ , λ_r , r_i , are five of the six fundamental constants in the varying permeability model. The remaining parameter, λ_m , interpolating bounce and saturation exposures, represents the inverse time constant modulating multiding. Doppler experiments suggest that λ_m^{-1} is in the neighborhood of an hour. Discussion of λ_m follows in the next section (RGBM).

The depth at which a compartment controls an exposure, and the excitation radius as a function of halftime, τ , in the range, $12 \leq d \leq 220 \text{ fsw}$, satisfy,

$$\frac{r}{r_i} = 0.90 - 0.43 \exp(-\zeta\tau)$$

with $\zeta = 0.0559 \text{ min}^{-1}$. The generation constant, λ_r , is on the order of inverse days, that is, $\lambda_r = .0495 \text{ days}^{-1}$. Characteristic halftimes, τ_r and τ_h , take the values $\tau_r = 14 \text{ days}$ and $\tau_h = 12.4 \text{ min}$. For large τ , r is close to r_i , while for small τ , r is on the order of $0.5 r_i$. At sea level, $r_i = 0.8 \text{ }\mu\text{m}$ as discussed.

3. Reduced Gradient Bubble

Two versions exist. One is a Haldane folded (single phase) algorithm using phase factors from the full iterative model to limit Haldane repetitive, reverse profile, multiday activities, and flying after diving. The folded version is found in many decometers on the market today. The full (dual phase) version is the basis of released mixed gas technical tables and simplified no-group, no-calc recreational air and nitrox tables up to 10,000 ft elevation. Meter implementations of the full RGBM are underway. Both modified and iterative RGBM are offered to users of ABYSS diveaware.

Dual Phase

As mentioned the full RGBM employs a phase volume constraint across the total dive profile. The gel parameterization is replaced by flexible seed skins with appropriate EOS, permeable to gas diffusion at all pressures and temperatures. Gas diffuses across the bubble interface, and the bubble is subjected to Boyle expansion-contraction.

The phase volume constraint equation is rewritten in terms of a phase function, $\dot{\phi}$, varying in time,

$$\int_0^\tau \frac{\partial \phi}{\partial t} dt \leq \Phi$$

with, as before,

$$\dot{\phi} = \frac{\partial \phi}{\partial t}$$

for Φ the separated phase, and τ some (long) cutoff time. More particularly, for Π the total gas tension,

$$\dot{\phi} = \left[\frac{\partial V}{\partial t} \right]_{diffusion} + \left[\frac{\partial V}{\partial t} \right]_{Boyle} + \left[\frac{\partial V}{\partial t} \right]_{excitation}$$

for,

$$\begin{aligned} \left[\frac{\partial V}{\partial t} \right]_{diffusion} &= 4\pi DS \int_r^\infty nr \left(\Pi - P - \frac{2\gamma}{r} \right) dr \\ \left[\frac{\partial V}{\partial t} \right]_{Boyle} &= \int_r^\infty n \left(\frac{T}{P} \frac{\partial PV}{\partial t} \frac{1}{T} \right) dr \\ \left[\frac{\partial V}{\partial t} \right]_{excitation} &= \frac{\partial}{\partial t} \left(4\pi \int_0^\infty nr^2 dr \right) \end{aligned}$$

with all quantities as denoted previously, and the bubble number integrand normalized,

$$\int_0^\infty ndr = 1$$

Thus the phase function, $\dot{\phi}$, depends on the number of bubbles, n , stimulated into growth by compression-decompression, the supersaturation gradient, G , seed expansion-contraction by radial diffusion, $\partial r/\partial t$, Boyle expansion-contraction, PV , under pressure changes, and temperature, T , in general. The excitation radius, r , depends on the material properties, and is given for nitrogen (μm),

$$r_{N_2} = 0.007655 + 0.001654 \left[\frac{T}{P} \right]^{1/3} + 0.041602 \left[\frac{T}{P} \right]^{2/3}$$

and for helium,

$$r_{He} = 0.001946 + 0.009832 \left[\frac{T}{P} \right]^{1/3} + 0.016183 \left[\frac{P}{T} \right]^{2/3}$$

for T measured in absolute K° , and P given in fsw , as before. with ranges for virial coefficients, aqueous to lipid materials, varying by factors of 0.75 to 4.86 times the values listed above. Both expression above represent fits to RGBM mixed gas data across lipid and aqueous bubble films, and are different from other phase models. Values of excitation radii, r , above range from 0.01 to 0.05 μm for sea level down to 500 fsw . This is compared to excitation radii in other models (VPM and TBDM) which vary in the 1 μm range. In the very large pressure limit, excitation radii (like beebees) are in the 1/1,000 μm range. Table 1 lists excitation radii (air) according to the RGBM.

Table 1. Reduced Gradient Bubble Model Excitation Radii

pressure P (fsw)	excitation radius r (μm)	pressure P (fsw)	excitation radius r (μm)
13	0.174	153	0.033
33	0.097	183	0.029
53	0.073	283	0.024
73	0.059	383	0.016
93	0.051	483	0.011
113	0.046	583	0.009

Single Phase

The following is specific to the ZHL implementation of the RGBM across critical parameters and nonstop time limits of the RGBM/ZHL algorithm. Extensive computer fitting of profiles and recalibration of parameters to maintain the RGBM within the ZHL limits is requisite here. ABYSS has implemented this synthesis into Internet diveware. Deep stops, not not intrinsic in this limited, still basically Haldane approach, can be inserted empirically as described earlier.

Haldane approaches use a dissolved gas (tissue) transfer equation, and a set of critical parameters to dictate diver staging through the gas transfer equation. In the Workman approach, the critical parameters are called M -values, while in the Buhlmann formulation they are called a and b . They are equivalent sets, slightly different in representation but not content. Consider air, nitrox, heliox, and trimix in the ZHL formalism.

Air tissue tensions (nitrogen partial pressures), p , for ambient nitrogen partial pressure, p_a , and initial tissue tension, p_i , evolve in time, t , in usual fashion in compartment, τ , according to,

$$p - p_a = (p - p_a) \exp(-\lambda t)$$

for,

$$\lambda = \frac{0.693}{\tau}$$

with τ tissue halftime, and, for air,

$$p_a = 0.79 P$$

and with ambient pressure, P , given as a function of depth, d , in units of fsw ,

$$P = \eta d + P_0$$

Staging is controlled in the Buhlmann ZHL algorithm through sets of tissue parameters, a and b , listed below in Table 2 for 14 tissues, τ , through the minimum permissible (tolerable) ambient pressure, P_{min} , by,

$$P_{min} = (p - a)b$$

across all tissue compartments, τ , with the largest P_{min} limiting the allowable ambient pressure, P_{min} . Recall that,

$$1 \text{ bar} = 1.013 \text{ atm} \quad , \quad 1 \text{ atm} = 33 \text{ fsw}$$

as conversion metric between bar and fsw in pressure calculations. Linear extrapolations across tissue compartments are often used for different sets of halftimes and critical parameters, a and b .

Table 2. Nitrogen ZHL Critical Parameters (a , b)

halftime τ (min)	critical intercept a (bar)	critical slope b
5.0	1.198	0.542
10.0	0.939	0.687
20.0	0.731	0.793
40.0	0.496	0.868
65.0	0.425	0.882
90.0	0.395	0.900
120.0	0.372	0.912
150.0	0.350	0.922
180.0	0.334	0.929
220.0	0.318	0.939
280.0	0.295	0.944
350.0	0.272	0.953
450.0	0.255	0.958
635.0	0.236	0.966

In terms of critical tensions, M , according to the USN, the relationship linking the two sets is simply,

$$M = \frac{P}{b} + a = \Delta M P + M_0$$

so that,

$$\Delta M = \frac{1}{b}$$

$$M_0 = a$$

in units of bar , though the usual representation for M is fsw . The above set, a and b , hold generally for nitrox, and, to low order, for heliox (and trimix too). Tuned modifications for heliox and trimix are also tabulated below.

Corresponding nonstop time limits, t_n , are listed in Table 3, and the nonstop limits follow the Hempleman square root law, roughly,

$$dt_n^{1/2} = 475 fsw min^{1/2}$$

in a least squares fit. The square root law also follows directly from the form of the bulk diffusion transfer equation, but not from any Haldane assumptions nor limiting forms of the tissue equation.

Table 3. Air ZHL Nonstop Time Limits

depth	time
d	t_n (min)
30	290
40	130
50	75
60	54
70	38
80	26
90	22
100	20
110	17
120	15
130	11
140	9
150	8
160	7
170	6
180	5
190	4
200	3

Over ranges of depths, tissue halftimes, and critical parameters of the ZHL algorithm, approximately 2,300 dive profiles were simulated using both the RGBM and Haldane ZHL algorithms. To correlate the two as closely as possible to the predictions of the RGBM across these profiles, maximum likelihood analysis is used, that is, extracting the temporal features of three bubble parameters mating the RGBM and ZHL algorithms extending critical parameters of the ZHL Haldane model to more complete bubble dynamical framework and physical basis. These factors, f , are described next, with their linkages to a and b , and are the well known *reduction factors* of the RGBM.

According to the RGBM fits across the ZHL profiles (2,300), a correlation can be established through multiding reduction factors, f , such that for any set of nonstop gradients, G ,

$$G = M - P$$

a reduced set, G_f , obtains from the nonstop set, G , for multiding through the reduction factors, $f \leq 1$,

$$G_f = fG$$

so that,

$$M_f = \frac{P}{b_f} + a_f = G_f + P = fG + P$$

but, since,

$$fG = f(M - P) = f \left[\frac{P}{b} + a - P \right]$$

we have,

$$a_f = fa$$

$$b_f = \frac{b}{f(1-b) + b}$$

The new (reduced) staging regimen is then simply,

$$P_{min} = (p - a_f)b_f$$

using *reduced* critical parameters, a_f and b_f . Certainly, as $f \rightarrow 1$, then $a_f \rightarrow a$, and $b_f \rightarrow b$, as requisite. Now all that remains is specification of f , particularly in terms of repetitive, reverse profile, and multiday diving, as limited by the bubble dynamical RGBM. The full factor, f , depends on tissue half-time, τ , generally through the relationship (for nitrox),

$$f = (1 - f_0) \frac{\tau}{180} + f_0 \quad (f = 1, \quad \tau \geq 180 \text{ min})$$

as the tissue scaling up through the 180 *min* nitrogen compartment, with multiday weighting,

$$f_0 = .45 f_{rp} + .30 f_{dp} + .25 f_{dy}$$

where f_{rp} , f_{dp} , and f_{dy} are reduction factors for repetitive, reverse profile (deeper than previous), and multiday (time spans of 30 *hrs* or more) diving. These forms for multiday f are dependent on time between dives, t_{sur} , ambient pressure difference between reverse profile dives, ΔP , ambient pressure, P , and multiday diving frequency, n , over 24 *hr* time spans. Specifically, they are written,

$$f_{rp} = 1 - .45 \exp \left[-\frac{(t_{sur} - \eta_{rp})^2}{4\eta_{rp}^2} \right]$$

$$10 \text{ min} \leq \eta_{rp} \leq 90 \text{ min}$$

$$f_{dp} = 1 - .45 \left[1 - \exp \left(-\frac{\Delta P}{P} \right) \right] \exp \left[-\frac{(t_{sur} - \eta_{dp})^2}{4\eta_{dp}^2} \right]$$

$$30 \text{ min} \leq \eta_{dp} \leq 120 \text{ min}$$

$$f_{dy} = .70 + .30 \exp \left(-\frac{n}{\eta_{dy}} \right)$$

$$12 \text{ hrs} \leq \eta_{dy} \leq 18 \text{ hrs}$$

with t_{sur} measured in *min*, and n the number of consecutive days of diving within 30 *hr* time spans. These factors are applied after 1 *min* of surface interval (otherwise, previous dive continuation). The difference, ΔP , is the time averaged difference between depths on the present and previous dives (computed on the fly). Reduction factors are consistent (folded in maximum likelihood in the RGBM) with the following:

- (a) Doppler bubble scores peak in an hour or so after a dive;
- (b) reverse profiles with depth increments beyond 50 *fsw* incur increasing DCS risk, somewhere between 5% and 8% in the depth increment range of 40 *fsw* - 120 *fsw*;
- (c) Doppler bubble counts drop tenfold when ascent rates drop from 60 *fsw/min* to 30 *fsw/min*;
- (d) multiday diving risks increase by factors of 2 -3 (though still small) over risk associated with a single dive.

The standard set, a , b , and τ , given in Table 7 hold across nitrox exposures, and the tissue equation remains the same. The obvious change for a nitrox mixture with nitrogen fraction, f_{N_2} , occurs in the nitrogen ambient pressure, p_{aN_2} , at depth, d , in analogy with the air case,

$$p_{aN_2} = f_{N_2} P = f_{N_2} (d + P_0)$$

with P ambient pressure (*fsw*). All else is unchanged. The case, $f_{N_2} = 0.79$, obviously represents an air mixture.

The standard set, a , b , and τ is modified for helium mixtures, with basic change in the set of halftimes, τ , used for the set, a and b . To lowest orderset, a and b for helium are the same as those for nitrogen, though we will list the modifications in Table 4 below. Halftimes for helium are approximately 2.65 times faster than those for nitrogen, by Graham's law (molecular diffusion rates scale inversely with square root of atomic masses). That is,

$$\tau_{He} = \frac{\tau_{N_2}}{2.65}$$

because helium is approximately 7 times lighter than nitrogen, and diffusion rates scale with square root of the ratio of atomic masses. The tissue equation is the same as the nitrox tissue equation, but with helium constants, λ , defined by the helium tissue halftimes. Denoting the helium fraction, f_{He} , the helium ambient pressure, p_{aHe} , is given by,

$$p_{aHe} = f_{He} P = f_{He} (d + P_0)$$

as with nitrox. Multidiving fractions are the same, but the tissue scaling is different across the helium set,

$$f = (1 - f_0) \frac{\tau}{67.8} + f_0 \quad (f = 1, \quad \tau \geq 67.8 \text{ min})$$

and all else is the same.

Table 4. Helium ZHL Critical Parameters (a , b)

halftime τ (<i>min</i>)	critical intercept a (<i>bar</i>)	critical slope b
1.8	1.653	0.461
3.8	1.295	0.604
7.6	1.008	0.729
15.0	0.759	0.816
24.5	0.672	0.837
33.9	0.636	0.864
45.2	0.598	0.876
56.6	0.562	0.885
67.8	0.541	0.892
83.0	0.526	0.901
105.5	0.519	0.906
132.0	0.516	0.914
169.7	0.510	0.919
239.6	0.495	0.927

For trimix, both helium and nitrogen must be tracked with tissue equations, and appropriate average of helium and nitrogen critical parameters used for staging. Thus, denoting nitrogen and helium fractions, f_{N_2} , and f_{He} , ambient nitrogen and helium pressures, p_{aN_2} and p_{aHe} , take the form,

$$p_{aN_2} = f_{N_2} P = f_{N_2} (d + P_0)$$

$$p_{aHe} = f_{He} P = f_{He} (d + P_0)$$

Tissue halftimes are mapped exactly as listed in Tables 3 and 4, and used appropriately for nitrogen and helium tissue equations. Additionally,

$$f_{O_2} + f_{N_2} + f_{He} = 1$$

and certainly in Tables 3 and 4, one has the mapping,

$$\tau_{He} = \frac{\tau_{N_2}}{2.65}$$

Then, total tension, Π , is the sum of nitrogen and helium components,

$$\Pi = (p_{aN_2} + p_{aHe}) + (p_{iN_2} - p_{aN_2}) \exp(-\lambda_{N_2} t) + (p_{iHe} - p_{aHe}) \exp(-\lambda_{He} t)$$

with λ_{N_2} and λ_{He} decay constant for the nitrogen and helium halftimes in Tables 3 and 4. Critical parameters for trimix, α_f and β_f , are just weighted averages of critical parameters, a_{N_2} , b_{N_2} , a_{He} b_{He} , from Tables 3 and 4, that is, generalizing to the reduced set, a_f and b_f ,

$$\alpha_f = \frac{f_{N_2} a_{fN_2} + f_{He} a_{fHe}}{f_{N_2} + f_{He}}$$

$$\beta_f = \frac{f_{N_2} b_{fN_2} + f_{He} b_{fHe}}{f_{N_2} + f_{He}}$$

The staging regimen for trimix is,

$$P_{min} = (\Pi - \alpha_f) \beta_f$$

as before. The corresponding critical tension, M_f , generalizes to,

$$M_f = \frac{P}{\beta_f} + \alpha_f$$

Overall, the RGBM algorithm is conservative with safety imparted to the Haldane ZHL model through multidinging f factors. Estimated DCS incidence rate from likelihood analysis is 0.01% at the 95% confidence level for the overall RGBM. Table and meter implementations with consistent coding should reflect this estimated risk. Similar estimates and comments apply to the ZHL mixed gas synthesis.

4. Tissue Bubble Diffusion

Bubbles shrink or grow according to a simple radial diffusion equation linking total gas tension, Π , ambient pressure, P , and surface tension, γ , to bubble radius, r ,

$$\frac{\partial r}{\partial t} = \frac{DS}{r} \left[\Pi - P - \frac{2\gamma}{r} \right]$$

with D the gas diffusion coefficient, and S the gas solubility. Bubbles grow when the surrounding gas tension exceeds the sum of ambient plus surface tension pressure, and vice versa. Higher gas solubilities and diffusivities enhance the rate. Related bubble area, A , and volume, V , changes satisfy,

$$\frac{\partial A}{\partial t} = 8\pi r \frac{\partial r}{\partial t}$$

$$\frac{\partial V}{\partial t} = 4\pi r^2 \frac{\partial r}{\partial t}$$

Using Fick's law, a corresponding molar current, J , of gas into, or out of, the bubble is easily computed assuming an ideal gas,

$$J = -\frac{DS}{RT h} \left[\Pi - P - \frac{2\gamma}{r} \right]$$

for R the ideal gas constant, T the temperature, and h an effective diffusion barrier thickness. And the molal flow rate is just the molal current times the interface area, that is,

$$\frac{\partial n}{\partial t} = JA$$

for n the number of moles of gas. The change in pressure and volume of the bubble, due to gas diffusion, follows simply from the ideal gas law,

$$\frac{\partial(PV + 2\gamma r^{-1}V)}{\partial t} = R \frac{\partial(nT)}{\partial t}$$

for V the bubble volume.

Obviously, the above constitute a coupled set of differential equations, solvable for a wide range of boundary and thermodynamic conditions connecting the state variables, namely, P , V , Π , r , n , and T .

A bubble dose, based on the hypothetical volume of an expanding test bubble, is linked to decompression data for the exposure. Maximum likelihood regression is used to correlate bubble dose with DCS risk.

RGBM Computational Issues

Diving models address the coupled issues of gas uptake and elimination, bubbles, and pressure changes in different computational frameworks. Application of a computational model to staging divers is called a diving algorithm. The Reduced Gradient Bubble Model (RGBM) is a modern one, treating the many facets of gas dynamics in tissue and blood consistently. Though the systematics of gas exchange, nucleation, bubble growth or collapse, and decompression are so complicated that theories only reflect pieces of the decompression sickness (DCS) puzzle, the risk and DCS statistics of staging algorithms can be easily collected and analyzed. And the record of the RGBM, just over the past 5 years or so, has been spectacular, especially so far as safe staging coupled to deep stops with overall shorter decompression times. This is important. Models are one thing, even with all the correct biophysics, and actual diving and testing are something else.

RGBM Motivation And Implementations

The RGBM grew from needs of technical divers to more efficiently stage ascents consistent with coarse grain dissolved gas and bubble dynamics, and not just dissolved gas (Haldane) constraints. And the depth, diversity, mix variation, and self consistency of RGBM diving applicability has satisfied that need. And safely.

The RGBM has gained tremendous popularity in the recreational and technical diving worlds in just the past 2 - 3 years, due to meter implementations, Internet software packages, specialized Table releases, technical word of mouth, NAUI training testing and adoption, Internet traffic, chamber tests, and, most of all, actual technical and recreational RGBM diving and validation. And the reasons are fairly clear.

Present notions of nucleations and bubbles suggest that decompression phase separation is random, yet highly probable, in body tissue. Once established, a gaseous phase will further grow by acquiring gas from adjacent saturated tissue, according to the strength of the free-dissolved gradient. Although exchange mechanisms are better understood, nucleation and stabilization mechanisms remain less so, and computationally elusive. But even with a paucity of knowledge, many feel that existing practices and recent studies on bubbles and nuclei shed considerable light on growth and elimination processes, and time scales. Their consistency with underlying physical principles suggest directions for table and meter modeling, beyond parameter fitting and extrapolation techniques. Recovering dissolved gas algorithms for short exposure times, phase models link to bubble mechanics and critical volume trigger points. The RGBM incorporates all of the above in all implementations, and additionally supports the efficacy of recently suggested safe diving practices, by simple virtue of its dual phase mechanics:

- reduced nonstop time limits;
- safety stops (or shallow swimming ascents) in the 10-20 *fsw* zone;
- ascent rates not exceeding 30 *fsw/min*;
- restricted repetitive exposures, particularly beyond 100 *fsw*,
- restricted reverse profile and deep spike diving;
- restricted multiday activity;
- smooth coalescence of bounce and saturation limit points;
- consistent diving protocols for altitude;
- deep stops for decompression, extended range, and mixed gas diving with overall shorter decompression times, particularly for the shallow zone;
- use of helium rich mixtures for technical diving, with shallower isobaric switches to nitrox than suggested by Haldane strategies;
- use of pure oxygen in the shallow zone to eliminate both dissolved and bubble inert gases.

Bubble models tend to be consistent with the utilitarian measures detailed earlier, and have the right signatures for diving applications across the full spectrum of activities. Or, said another way, bubble models are more powerful, more correct, and more inclusive. In terms of RGBM implementations, the mechanistic of dissolved gas buildup and elimination, inert gas diffusion across bubble interfaces, bubble excitation and elimination persistence time scales of minutes to hours from tissue friction, lipid and aqueous surfactant material properties, and Boyle expansion and contraction under ambient pressure change, are sufficient to address all of the above considerations.

So Mares, Dacor, Plexus, Suunto, HydroSpace, and Abyssal Diving developed and released products incorporating one such validated phase algorithm, the Reduced Gradient Bubble Model (RGBM), for diving. An iterative approach to staging diver ascents, the RGBM employs separated phase volumes as limit points, instead of the usual Haldane (maximum) critical tensions across tissue compartments. The model is tested and inclusive (altitude, repetitive, mixed gas, decompression, saturation, nonstop exposures), treating both dissolved and free gas phase buildup and elimination. NAUI Technical Diving employs the RGBM to schedule nonstop and decompression training protocols on trimix, helitrox, air, and nitrox, and will be releasing an exhaustive set of RGBM tables for those mixes shortly (some 500 pages of Tables). Included are constant ppO₂ Tables for rebreathers. Mares, Dacor, and Plexus are also developing RGBM meters.

Suunto VYPER/COBRA/STINGER are RGBM meters for recreational diving (plus nitrox), while ABYSS/RGBM is a licensed Abyssal Diving software product. The HydroSpace EXPLORER is a mixed gas decompression meter for technical and recreational diving, as is the ABYSS/RGBM software vehicle. All are first-time-ever commercial products with realistic implementation of a diving phase algorithm across a wide spectrum of exposure extremes. And all accommodate user knobs for aggressive to conservative diving. Expect RGBM algorithms to surface in other meters and software packages on the Internet. NAUI Worldwide just released a set of RGBM no-group, no-calc, no-fuss recreational Tables for air and nitrox, sea level to 10,000 feet elevation.

The Countermeasures Dive Team at LANL employs the RGBM (last 8 years). Military, commercial, and scientific sectors are using and further testing the RGBM. And scores of technical divers are reporting their RGBM profiles over the Internet and in technical diving publications. There are presently other major RGBM implementation projects in the works for meters and software packages.

The RGBM extends earlier work of the Tiny Bubble Group at the University of Hawaii, updating missing physics and extending their Varying Permeability Model (VPM) to multiding, altitude, and mixed gas applications. While certainly fundamental, the RGBM is also different and new on the diving scene. And not unexpectedly, the RGBM recovers the Haldane approach to decompression modeling in the limit of relatively safe (tolerably little) separated phase, with tolerably little a qualitative statement here. There is quite a bit more and different about the RGBM than other and related phase models. Differences focalize, in a word or two, on source generation mechanisms and persistence time scales for bubbles and seeds, bubble structural mechanics and materials, consistent treatment of all bubble expansion and contraction venues, and real world testing.

RGBM Underpinnings

Here, our intent is to (just) look at the underpinnings of table, meter, and diveware implementations of the RGBM algorithm, one with extended range of applicability based on simple dual phase principles. Haldane approaches have dominated decompression algorithms for a very long time, and the RGBM has been long in coming on the commercial scene. With technical diving interest in deep stop modeling, helium, and concerns with repetitive diving in the recreational and technical community, phase modeling is timely and pertinent.

The establishment and evolution of gas phases, and possible bubble trouble, involves a number of distinct, yet overlapping, steps:

- nucleation and stabilization (free phase inception);
- supersaturation (dissolved gas buildup);
- excitation and growth (free-dissolved phase interaction);
- coalescence (bubble aggregation);
- deformation and occlusion (tissue damage and ischemia).

The computational issues of bubble dynamics (formation, growth, and elimination) are mostly outside Haldane framework, but get folded into halftime specifications in a nontractable mode. The very slow tissue compartments (halftimes large, or diffusivities small) might be tracking both free and dissolved gas exchange in poorly perfused regions. Free and dissolved phases, however, do not behave the same way under decompression. Care must be exercised in applying model equations to each component. In the presence of increasing proportions of free phases, dissolved gas equations cannot track either species accurately. Computational algorithms tracking both dissolved and free phases offer broader perspectives and expeditious alternatives, but with some changes from classical schemes. Free and dissolved gas dynamics differ. The driving force (gradient) for free phase elimination increases with depth, directly opposite to the dissolved phase elimination gradient which decreases with depth. Then, changes in operational procedures become necessary for optimality.

Considerations of excitation and growth invariably require deeper staging procedures than supersaturation methods. Though not as dramatic, similar constraints remain operative in multiexposures, that is, multilevel, repetitive, and multiday diving.

Other issues concerning time sequencing of symptoms impact computational algorithms. That bubble formation is a predisposing condition for decompression sickness is universally accepted. However, formation mechanisms and their ultimate physiological effect are two related, yet distinct, issues. On this point, most hypotheses makes little distinction between bubble formation and the onset of bends symptoms. Yet we know that silent bubbles have been detected in subjects not suffering from decompression sickness. So it would thus appear that bubble formation, per se, and bends symptoms do not map onto each other in a one-to-one manner. Other factors are truly operative, such as the amount of gas dumped from solution, the size of nucleation sites receiving the gas, permissible bubble growth rates, deformation of surrounding tissue medium, and coalescence mechanisms for small bubbles into large aggregates, to name a few. These issues are the pervue of bubble theories, but the complexity of mechanisms addressed does not lend itself easily to table, nor even meter, implementation. But implement and improve we must, so consider the RGBM issues and tacks taken in the Suunto, Mares, Dacor, Hydrospace, and ABYSS implementations:

1. Perfusion And Diffusion

Perfusion and diffusion are two mechanisms by which inert and metabolic gases exchange between tissue and blood. Perfusion denotes the blood flow rate in simplest terms, while diffusion refers to the gas penetration rate in tissue, or across tissue-blood boundaries. Each mechanism has a characteristic rate constant for the process. The smallest rate constant limits the gas exchange process. When diffusion rate constants are smaller than perfusion rate constants, diffusion dominates the tissue-blood gas exchange process, and vice-versa. In the body, both processes play a role in real exchange process, especially considering the diversity of tissues and their geometries. The usual Haldane tissue halftimes are the inverses of perfusion rates, while the diffusivity of water, thought to make up the bulk of tissue, is a measure of the diffusion rate.

Clearly in the past, model distinctions were made on the basis of perfusion or diffusion limited gas exchange. The distinction is somewhat artificial, especially in light of recent analyses of coupled perfusion-diffusion gas transport, recovering limiting features of the exchange process in appropriate limits. The distinction is still of interest today, however, since perfusion and diffusion limited algorithms are used in mutually exclusive fashion in diving. The obvious mathematical rigors of a full blown perfusion-diffusion treatment of gas exchange mitigate against table and meter implementation, where model simplicity is a necessity. So one or another limiting models is adopted, with inertia and track record sustaining use. Certainly Haldane models fall into that categorization.

Inert gas transfer and coupled bubble growth are subtly influenced by metabolic oxygen consumption. Consumption of oxygen and production of carbon dioxide drops the tissue oxygen tension below its level in the lungs (alveoli), while carbon dioxide tension rises only slightly because carbon dioxide is 25 times more soluble than oxygen. Figure 3 (Chapter 1) compares the partial pressures of oxygen, nitrogen, water vapor, and carbon dioxide in dry air, alveolar air, arterial blood, venous blood, and tissue (cells).

Arterial and venous blood, and tissue, are clearly unsaturated with respect to dry air at 1 *atm*. Water vapor content is constant, and carbon dioxide variations are slight, though sufficient to establish an outgradient between tissue and blood. Oxygen tensions in tissue and blood are considerably below lung oxygen partial pressure, establishing the necessary ingradient for oxygenation and metabolism. Experiments also suggest that the degree of unsaturation increases linearly with pressure for constant composition breathing mixture, and decreases linearly with mole fraction of inert gas in the inspired mix.

Since the tissues are unsaturated with respect to ambient pressure at equilibrium, one might exploit this window in bringing divers to the surface. By scheduling the ascent strategically, so that nitrogen (or any other inert breathing gas) supersaturation just takes up this unsaturation, the total tissue tension can be kept equal to ambient pressure. This approach to staging is called the zero supersaturation ascent.

The full blown RGBM treats coupled perfusion-diffusion transport as a two step flow process, with blood flow (perfusion) serving as a boundary condition for tissue gas penetration (diffusion). Depending on time scales and rate coefficients, one or another (or both) processes dominate the exchange. However, for the Suunto, Mares, Dacor, Hydrospace, Plexus, and ABYSS implementations, perfusion is assumed to dominate, simplifying matters and permitting on-line calculations. Additionally, tissues and blood are naturally undersaturated with respect to ambient pressure at equilibration through the mechanism of biological inherent unsaturation (oxygen window), and the RGBM includes this debt in calculations. Independent of perfusion or diffusion dominated gas transport, the RGBM tracks bubble excitation and number, inert gas transfer across the surfactant skin, and Boyle-like expansion and contraction of bubbles with ambient pressure changes.

2. Bubbles

We do not really know where bubbles form nor lodge, their migration patterns, their birth and dissolution mechanisms, nor the exact chain of physico-chemical insults resulting in decompression sickness. Many possibilities exist, differing in the nature of the insult, the location, and the manifestation of symptoms. Bubbles might form directly (de novo) in supersaturated sites upon decompression, or possibly grow from preformed, existing seed nuclei excited by compression-decompression. Leaving their birth sites, bubbles may move to critical sites elsewhere. Or stuck at their birth sites, bubbles may grow locally to pain-provoking size. They might dissolve locally by gaseous diffusion to surrounding tissue or blood, or passing through screening filters, such as the lung complex, they might be broken down into smaller aggregates, or eliminated completely. Whatever the bubble history, it presently escapes complete elucidation. But whatever the process, the end result is very simple, both separated and dissolved gas must be treated in the transfer process.

Bubbles may hypothetically form in the blood (intravascular) or outside the blood (extravascular). Once formed, intravascularly or extravascularly, a number of critical insults are possible. Intravascular bubbles may stop in closed circulatory vessels and induce ischemia, blood sludging, chemistry degradations, or mechanical nerve deformation. Circulating gas emboli may occlude the arterial flow, clog the pulmonary filters, or leave the circulation to lodge in tissue sites as extravascular bubbles. Extravascular bubbles may remain locally in tissue sites, assimilating gas by diffusion from adjacent supersaturated tissue and growing until a nerve ending is deformed beyond its pain threshold. Or, extravascular bubbles might enter the arterial or venous flows, at which point they become intravascular bubbles.

Spontaneous bubble formation in fluids usually requires large decompressions, like hundreds of atmospheres, somewhere near fluid tensile limits. Many feel that such circumstance precludes direct bubble formation in blood following decompression. Explosive, or very rapid decompression, of course is a different case. But, while many doubt that bubbles form in the blood directly, intravascular bubbles have been seen in both the arterial and venous circulation, with vastly greater numbers detected in venous flows (venous gas emboli). Ischemia resulting from bubbles caught in the arterial network has long been implied as a cause of decompression sickness. Since the lungs are effective filters of venous bubbles, arterial bubbles would then most likely originate in the arteries or adjacent tissue beds. The more numerous venous bubbles, however, are suspected to first form in lipid tissues draining the veins. Lipid tissue sites also

possess very few nerve endings, possibly masking critical insults. Veins, thinner than arteries, appear more susceptible to extravascular gas penetration.

Extravascular bubbles may form in aqueous (watery) or lipid (fatty) tissues in principle. For all but extreme or explosive decompression, bubbles are seldom observed in heart, liver, and skeletal muscle. Most gas is seen in fatty tissue, not unusual considering the five-fold higher solubility of nitrogen in lipid tissue versus aqueous tissue. Since fatty tissue has few nerve endings, tissue deformation by bubbles is unlikely to cause pain locally. On the other hand, formations or large volumes of extravascular gas could induce vascular hemorrhage, depositing both fat and bubbles into the circulation as noted in animal experiments. If mechanical pressure on nerves is a prime candidate for critical insult, then tissues with high concentrations of nerve endings are candidate structures, whether tendon or spinal cord. While such tissues are usually aqueous, they are invested with lipid cells whose propensity reflects total body fat. High nerve density and some lipid content supporting bubble formation and growth would appear a conducive environment for a mechanical insult.

To satisfy thermodynamic laws, bubbles assume spherical shapes in the absence of external or mechanical (distortion) pressures. Bubbles entrain free gases because of a thin film, exerting surface tension pressure on the gas. Hydrostatic pressure balance requires that the pressure inside the bubble exceed ambient pressure by the amount of surface tension, γ . Figure 2 (Chapter 3) depicts the pressure balance in a spherical (air) bubble. At small radii, surface tension pressure is greatest, and at large radii, surface tension pressure is least.

Gases will also diffuse into or out of a bubble according to differences in gas partial pressures inside and outside the bubble, whether in free or dissolved phases outside the bubble. In the former case, the gradient is termed free-free, while in the latter case, the gradient is termed free-dissolved. Unless the surface tension is identically zero, there is always a gradient tending to force gas out of the bubble, thus making the bubble collapse on itself because of surface tension pressure. If surrounding external pressures on bubbles change in time, however, bubbles may grow or contract. Figure 3 (Chapter 3) sketches bubble gas diffusion under instantaneous hydrostatic equilibrium for an air bubble.

Bubbles grow or contract according to the strength of the free-free or free-dissolved gradient, and it is the latter case which concerns divers under decompression. The radial rate at which bubbles grow or contract depends directly on the diffusivity and solubility, and inversely on the bubble radius. A critical radius, r_c , separates growing from contracting bubbles. Bubbles with radius $r > r_c$ will grow, while bubbles with radius $r < r_c$ will contract. Limiting bubble growth and adverse impact upon nerves and circulation are issues when decompressing divers and aviators.

Bubbles grow or contract by gaseous diffusion across the thin film interface, due to dissolved gas gradients. Bubbles also expand or contract upon pressure changes according to Boyle-like equations of state (EOS), with the expansion or contraction rate a function of the material composition of the surfactants coating the inside of the bubble. Material behavior can vary from thin elastic films to almost solid shell beebees,

depending on the coefficients and pressure regimes of the EOS.

The RGBM assumes that a size distribution of seeds (potential bubbles) is always present, and that a certain number is excited into growth by compression-decompression. An iterative process for ascent staging is employed to control the inflation rate of these growing bubbles so that their collective volume never exceeds a phase volume limit point. Gas mixtures of helium, nitrogen, and oxygen contain bubble distributions of different sizes, but possess the same phase volume limit point. Distributions have lifetimes of minutes to many hours, impacting repetitive, reverse

profile, multiday, altitude, and gas mixes on varying time scales. Colloidal particles are not the stabilizing material inside seeds and bubbles.

3. Temperature

Bubbles are affected by temperature much like gases, but only coupled through skin EOS of the material surrounding the gases inside the bubbles. Broadly speaking, bubbles will expand with temperature increases, and contract with temperature decreases, all subject to skin behavior, and material properties of same.

The effects of temperature over nominal water temperatures and diving activities are small, especially since body core temperatures and those of surrounding tissues and blood vary little under changes in outside temperature. Some data support higher DCS incidence rates for divers undergoing both warm-to-cold and cold-to-warm temperature switches following diving. But more reliable data support higher DCI incidence in warm environment versus colder ones. Naval Special Warfare suggests that underwater operations in temperature zones above 90 F° pose higher risks to SEALs. Divers salvaging TWA 200 in hot suits exhibited a higher proportion of DCS than those in wetsuits. Back in the early 50s, USN studies suggested that divers in colder waters (45 C°) had lower DCS incidence rates than divers in warmer waters (73 C°).

Still, cold divers are expected to eliminate inert gases slower than warm divers, and so risk of DCS might increase in divers who are cold following exposure. Doppler studies by Dunford and Hayward in the early 80s confirm the presence of more VGE in warm divers versus cold divers. Of course, if DCS correlates with Doppler score, these warm divers should be at higher risk. And they were not.

The RGBM treats temperature explicitly in skin EOS and staging regimens. Warmer temperatures promote larger bubbles and bubble seeds. Colder temperatures, however, in warm-to-cold temperature switches also provide a fracture mechanism for skins through the EOS. The fracture mechanics suggest a means to bubble depletion in the model.

4. Bubble Seeds

Bubbles, which are unstable, are thought to grow from micron size, gas nuclei which resist collapse due to elastic skins of surface activated molecules (surfactants), or possibly reduction in surface tension at tissue interfaces or crevices. If families of these micronuclei persist, they vary in size and surfactant content. Large pressures (not really known) are necessary to crush them. Micronuclei are small enough to pass through the pulmonary filters, yet dense enough not to float to the surfaces of their environments, with which they are in both hydrostatic (pressure) and diffusion (gas flow) equilibrium. When nuclei are stabilized, and not activated to growth or contraction by external pressure changes, the skin (surfactant) tension offsets both the Laplacian (film) tension and any mechanical help from surrounding tissue. Then all pressures and gas tensions are equal. However, on decompression, the seed pockets are surrounded by dissolved gases at high tension and can subsequently grow (bubbles) as surrounding gas diffuses into them. The rate at which bubbles grow, or contract, depends directly on the difference between tissue tension and local ambient pressure, effectively the bubble pressure gradient. At some point in time, a critical volume of bubbles, or separated gas, is established and bends symptoms become statistically more probable. On compression, the micronuclei are crunched down to smaller sizes across families, apparently stabilizing at new reduced size. Bubbles are also crunched by increasing pressure because of Boyle's law, and then additionally shrink if gas diffuses out of them. As bubbles get smaller and smaller, they probably restabilize as micronuclei.

The RGBM postulates bubble seeds with lipid or aqueous surfactants. Bubble skins are assumed permeable under all ambient pressure, unlike the VPM. The size of seeds excited into growth

is inversely proportional to the supersaturation gradient. RGBM excitation radii, r , start in the 0.01 μm range, far smaller than other dual phase models, because the RGBM tracks Boyle expansion and bubble gas diffusion across the tissue seed interface (across the surfactant). At increasing pressure, bubble seeds permit gas diffusion at a slower rate. The RGBM assumes bubble skins are stabilized by surfactants over calculable time scales, producing seeds that are variably persistent in the body. Bubble skins are probably molecularly activated, complex, bio-substances found throughout the body. Whatever the formation process, the RGBM assumes the size distribution is exponentially decreasing in size, that is, more smaller seeds than larger seeds in exponential proportions. Skin response of the bubbles to pressure change is dictated by a material equation-of-state (EOS), again unlike the VPM. As stated, the RGBM diffuses gas from tissues to bubbles (and vice-versa) using a transfer equations across the film interface. This requires a mass transfer coefficient dependent on the gas solubility and diffusivity. The source of bubbles and seeds is probably tribonucleation due to muscle and tissue interfriktion, and persistence time scales range from minutes to tens of hours.

5. Slow Tissue Compartments

Based on concerns in multiday and heavy repetitive diving, with the hope of controlling stair-casing gas buildup in exposures through critical tensions, slow tissue compartments (halftimes greater than 80 minutes) have been incorporated into some algorithms. Calculations, however, show that virtually impossible exposures are required of the diver before critical tensions are even approached, literally tens of hours of near continuous activity. As noted in many calculations, slow compartment cannot really control multiding through critical tensions, unless critical tensions are reduced to absurd levels, inconsistent with nonstop time limits for shallow exposures. That is a model limitation, not necessarily a physical reality. The physical reality is that bubbles in slow tissues are eliminated over time scales of days, and the model limitation is that the arbitrary parameter space does not accommodate such phenomena.

And that is no surprise either, when one considers that dissolved gas models are not suppose to track bubbles and free phases. Repetitive exposures do provide fresh dissolved gas for excited nuclei and growing free phases, but it is not the dissolved gas which is the problem just by itself. When bubble growth is considered, the slow compartments appear very important, because, therein, growing free phases are mostly left undisturbed insofar as surrounding tissue tensions are concerned. Bubbles grow more gradually in slow compartments because the gradient there is typically small, yet grow over longer time scales. When coupled to free phase dynamics, slow compartments are necessary in multiding calculations.

The RGBM incorporates a spectrum of tissue compartments, ranging from 1 min to 720 min, depending on gas mixture (helium, nitrogen, oxygen). Phase separation and bubble growth in slower compartments is a central focus in calculations over long time scales, and the same for fast tissue tissue compartments over short time scales, that is, scales over 2 or 3 times the compartment halftime.

6. Venous Gas Emboli

While the numbers of venous gas emboli detected with ultrasound Doppler techniques can be correlated with nonstop limits, and the limits then used to fine tune the critical tension matrix for select exposure ranges, fundamental issues are not necessarily resolved by venous gas emboli measurements. First of all, venous gas emboli are probably not the direct cause of bends per se, unless they block the pulmonary circulation, or pass through the pulmonary traps and enter the arterial system to lodge in critical sites. Intravascular bubbles might first form at extravascular sites. According to studies, electron micrographs have highlighted bubbles breaking into capillary walls from adjacent lipid tissue beds in mice. Fatty tissue, draining the veins and possessing few nerve endings, is thought to be an extravascular site

of venous gas emboli. Similarly, since blood constitutes no more than 8% of the total body capacity for dissolved gas, the bulk of circulating blood does not account for the amount of gas detected as venous gas emboli. Secondly, what has not been established is the link between venous gas emboli, possible micronuclei, and bubbles in critical tissues. Any such correlations of venous gas emboli with tissue micronuclei would unquestionably require considerable first-hand knowledge of nuclei size distributions, sites, and tissue thermodynamic properties. While some believe that venous gas emboli correlate with bubbles in extravascular sites, such as tendons and ligaments, and that venous gas emboli measurements can be reliably applied to bounce diving, the correlations with repetitive and saturation diving have not been made to work, nor important correlations with more severe forms of decompression sickness, such as chokes and central nervous system (CNS) hits.

Still, whatever the origin of venous gas emboli, procedures and protocols which reduce gas phases in the venous circulation deserve attention, for that matter, anywhere else in the body. The moving Doppler bubble may not be the bends bubble, but perhaps the difference may only be the present site. The propensity of venous gas emboli may reflect the state of critical tissues where decompression sickness does occur. Studies and tests based on Doppler detection of venous gas emboli are still the only viable means of monitoring free phases in the body.

The RGBM uses nonstop time limits tuned to recent Doppler measurements, conservatively reducing them along the lines originally suggested by Spencer (and others), but within the phase volume constraint. The Mares, Dacor, and Suunto implementations penalize ascent violations by requiring additional safety stop time dictated by risk analysis of the violation. All RGBM implementations supply user knobs for aggressive to conservative diving modifications, thru EOS in the full versions and M-values in the Haldane folded algorithms. Doppler scores over surface intervals are employed to calibrate RGBM bubble factors, both short and long intervals.

7. Multidiving

Concerns with multidiving can be addressed through variable critical gradients, then tissue tensions in Haldane models. While variable gradients or tensions are difficult to codify in table frameworks, they are easy to implement in digital meters. Reductions in critical parameters also result from the phase volume constraint, a constraint employing the separated volume of gas in tissue as trigger point for the bends, not dissolved gas buildup alone in tissue compartments. In the VPM the phase volume is proportional to the product of the dissolved-free gas gradient times a bubble number representing the number of gas nuclei excited into growth by the compression-decompression, replacing just slow tissue compartments in controlling multidiving. In the RGBM, the phase volume depends on the number of seeds excited and the Boyle and gas diffusion expansion-contraction of the seeds excited into growth.

In considering bubbles and free-dissolved gradients within critical phase hypotheses, repetitive criteria develop which require reductions in Haldane critical tensions or dissolved-free gas gradients. This reduction simply arises from lessened degree of bubble elimination over repetitive intervals, compared to long bounce intervals, and need to reduce bubble inflation rate through smaller driving gradients. Deep repetitive and spike exposures feel the greatest effects of gradient reduction, but shallower multiday activities are impacted. Bounce diving enjoys long surface intervals to eliminate bubbles while repetitive diving must contend with shorter intervals, and hypothetically reduced time for bubble elimination. Theoretically, a reduction in the bubble inflation driving term, namely, the tissue gradient or tension, holds the inflation rate down. Overall, concern is bubble excess driven by dissolved gas. And then both bubbles and dissolved gas are important. In such an approach, multidiving exposures experience reduced permissible tensions through lessened free phase elimination over time spans of two days. Parameters are consistent with bubble experiments, and both slow and fast tissue compartments must be considered.

The RGBM reduces the phase volume limit in multiding by considering free phase elimination and buildup during surface intervals, depending on altitude, time, and depth of previous profiles. Repetitive, multiday, and reverse profile exposures are tracked and impacted by critical phase volume reductions over appropriate time scales.

8. Adaptation

Divers and caisson workers have long contended that tolerance to decompression sickness increases with daily diving, and decreases after a few weeks layoff, that in large groups of compressed air workers, new workers were at higher risk than those who were exposed to high pressure regularly. This acclimatization might result from either increased body tolerance to bubbles (physiological adaptation), or decreased number and volume of bubbles (physical adaptation). Test results are totally consistent with physical adaptation.

Yet, there is slight inconsistency here. Statistics point to slightly higher bends incidence in repetitive and multiday diving. Some hyperbaric specialists confirm the same, based on experience. The situation is not clear, but the resolution plausibly links to the kinds of first dives made and repetitive frequency in the sequence. If the first in a series of repetitive dives are kept short, deep, and conservative with respect to nonstop time limits, initial excitation and growth are minimized. Subsequent dives would witness minimal levels of initial phases. If surface intervals are also long enough to optimize both free and dissolved gas elimination, any nuclei excited into growth could be efficiently eliminated outside repetitive exposures, with adaptation occurring over day intervals as noted in experiments. But higher frequency, repetitive and multiday loading may not afford sufficient surface intervals to eliminate free phases excited by earlier exposures, with additional nuclei then possibly excited on top of existing phases. Physical adaptation seems less likely, and decompression sickness more likely, in the latter case. Daily regimens of a single bounce dive with slightly increasing exposure times are consistent with physical adaptation, and conservative practices. The regimens also require deepest dives first. In short, acclimatization is as much a question of eliminating any free phases formed as it is a question of crushing or reducing nuclei as potential bubbles in repetitive exposures. And then time scales on the order of a day might limit the adaptation process.

The RGBM generates bubble seed distributions on time scales of minutes for fast tissues and hours for slow tissues, adding new bubbles to existing bubbles in calculations. Phase volume limit points are also reduced by the added effects of new bubbles. Repetitive and reverse profile diving are impacted by bubble growth in the fast compartments, while flying after diving and multiday diving are affected by bubble growth in the slow compartments.

EPILOGUE

Gas exchange, bubble formation and elimination, and compression-decompression in blood and tissues are governed by many factors, such as diffusion, perfusion, phase separation and equilibration, nucleation and cavitation, local fluid shifts, and combinations thereof. Owing to the complexity of biological systems, multiplicity of tissues and media, diversity of interfaces and boundary conditions, and plethora of bubble impacting physical and chemical mechanisms, it is difficult to solve the decompression problem *in vivo*. Early decompression studies adopted the supersaturation viewpoint. Closer looks at the physics of phase separation and bubbles in the mid-1970s, and insights into gas transfer mechanisms, culminated in extended kinetics and dissolved-free phase theories. Integration of both approaches can proceed on the numerical side because calculational techniques can be made equivalent. Phase and bubble models are more general than supersaturation models, incorporating their predictive capabilities as subsets. Statistical models, developed mostly in the mid-1980s, are gray from mechanistic viewpoint, but offer the strongest correlations with actual experiments and exposures, possibly the best approach to table fabrication.

Computational models gain efficacy by their ability to track data, often independently of physical interpretation. In that sense, the bottom line for computational models is utility, operational reliability, and reproducibility. Correct models can achieve such ends, but almost any model with sufficient parameter latitude could achieve those same ends. It is fair to say that deterministic models admit varying degrees of computational license, that model parameters may not correlate as complete set with the real world, and that not all mechanisms are addressed optimally. That is, perhaps, one reason why we see representative diving sectors, such as sport, military, commercial, and research, employing different tables, meters, models, and algorithms. Yet, given this situation, phase models attempting to treat both free and dissolved gas exchange, bubbles and gas nuclei, and free phase trigger points appear preferable to other flags. Phase models have the right physical signatures, and thus the potential to extrapolate reasonably when confronting new applications and data. Expect to see their further refinement and development in the future.

Technical diving encompasses a wide spectrum of related disciplines, from geosciences to biosciences, atmospheric sciences to hydrodynamics, medical sciences to engineering sciences, and mathematical physics to statistical analysis. The scope is immense, and so any monograph need be selective, and probably not in depth as possible. And diving physics can be a tedious exercise for readers. Obviously, physiology is an even more complicated mix of physics, chemistry, and biology. Like comments apply to decompression theory, a combination of biophysics, physiology, and biochemistry in a much cloudier picture within perfused and metabolic tissue and blood. Biological systems are so complex, beyond even the fastest and biggest supercomputers for modeling analysis.

So, selectivity with mathematical application was a direction taken here in narrative. Mathematical equations were kept at definitional level to facilitate description. The hope was to better encapsulate a large body of underlying physical principle in very readable form. Bibliographies offer full blown treatments of all principles detailed for diving. For highlight, Figures included some mathematical definitions for completeness, with intended purpose of extending discourse.

Many thanks go to my colleagues here at Los Alamos National Laboratory, to collaborators in the industrial, military, and academic sectors, and to investigators and teachers over the years who ask interesting diving questions. Affiliations with the American Physical Society, American Nuclear Society, American Academy Of Underwater Sciences, Undersea And Hyperbaric Medical Society, South Pacific Underwater Medicine Society, and Society Of Industrial And Applied Mathematics are also gratefully acknowledged. Thanks to the diver training agencies for their constant support, but especially the technical training agencies, NAUI, TDI, IANTD, and ANDI, and Divers Alert Network (DAN).

Safe and fun diving always.

RGBM RECREATIONAL AIR AND NITROX TABLES

RGBM TECHNICAL MIXED GAS AND DECOMPRESSION TABLES

REFERENCES

References span a wide spectra of technical diving material and details, broaching historical to modern developments. Entries are alphabetically and chronologically listed, completing or extending related reading at the end of each Chapter.

1. Abramowitz M. and Stegun I.A., 1972, *Handbook Of Mathematical Functions*, New York: Dover Publications.
2. Adamson A.W., 1976, *The Physical Chemistry Of Surfaces*, New York: John Wiley And Sons.
3. Albano G., Griscuoli P.M., and Ciulla C., 1962, *La Sindrome Neuropsichica Di Profundita*, *Lav. Um.* 14, 351-358.
4. Atkins C.E., Lehner C.E., Beck K.A., Dubielzig R.R., Nordheim E.V. and Lanphier E.H., 1988, *Experimental Respiratory Decompression Sickness In Sheep*, *J. Appl. Physiol.* 65, 1163-1171.
5. Bassett B.E., 1979, *And Yet Another Approach To The Problems Of Altitude Diving And Flying After Diving, Decompression In Depth Proceedings*, Professional Association Of Diving Instructors, Santa Ana.
6. Batchelor G.K., 1953, *Theory Of Homogeneous Turbulence*, New York: Cambridge University Press.
7. Bateman J.B. and Lang J., 1945, *Formation And Growth Of Bubbles In Aqueous Solutions*, *Canad. J. Res.* E23, 22-31.
8. Beckwith B., 1969, *Mechanical Measurement*, Reading: Addison Wesley.
9. Bell R.L. and Borgwardt R.E., 1976, *The Theory Of High Altitude Corrections To The US Navy Standard Decompression Tables*, *Undersea Biomed. Res.* 3, 1-23.
10. Behnke A.R., 1971, *Decompression Sickness: Advances And Interpretations*, *Aerospace Med.* 42, 255-267.
11. Behnke A.R., 1967, *The Isobaric (Oxygen Window) Principle Of Decompression*, *Trans. Third Annual Conf. Marine Tech, Soc.* 1, 213-228.
12. Behnke A.R., 1945, *Decompression Sickness Incident To Deep Sea Diving And High Altitude*, *Medicine* 24, 381-402.
13. Bennett P.B. and Elliot D.H., 1996, *The Physiology And Medicine Of Diving And Compressed Air Work*, London: Bailliere Tindall And Cassell.
14. Bennett P.B. and Hayward A.J., 1968, *Relative Decompression Sickness In Rats Of Neon And Other Inert Gases*, *Aerospace Med.* 39, 301-302.
15. Berghage T.E. and Durman D., 1980, *US Navy Air Recompression Schedule Risk Analysis*, *Nav. Med. Res. Bull.* 1, 1-22.
16. Bert P., 1878, *La Pression Barometrique*, Paris: Masson.
17. Boni M., Schibli R., Nussberger P. and Buhlmann A. A., 1976, *Diving At Diminished Atmospheric Pressure: Air Decompression Tables For Different Altitudes*, *Undersea Biomed. Res.* 3, 189-204.

18. Bookspan J., 1997, *Diving Physiology In Plain English*, Bethesda: Undersea And Hyperbaric Medical Society.
19. Bove A.A. and Davis J.C., 1990, *Diving Medicine*, Philadelphia: W.B. Saunders.
20. Bowker A.H. and Lieberman G.J., 1964, *Engineering Statistics*, Engelwood Cliffs: Prentice-Hall.
21. Boycott A.E., Damant G.C.C., and Haldane J.S., 1908, *The Prevention Of Compressed Air Illness*, *J. Hyg.* 8, 342-443.
22. Brereton R.G., 1974, *US Navy SEAL Combat Manual*, Memphis: Naval Technical Training.
23. Buckles R.G., 1968, *The Physics Of Bubble Formation And Growth*, *Aerospace Med.* 39, 1062-1069.
24. Buhlmann A.A., 1984, *Decompression/Decompression Sickness*, Berlin: Springer Verlag.
25. Buhlmann A.A., 1966, *Saturation And Desaturation With N₂ And He At 4 Atmospheres*, *J. Appl. Physiol.* 23, 458-462.
26. Carslaw H.S. and Jaeger J.C., 1950, *Conduction Of Heat In Solids*, Oxford: Clarendon Press.
27. Carter L.L. and Cashwell E.D., 1975, *Particle Transport Simulations With The Monte Carlo Method*, Oak Ridge: United States Energy And Research Development Administration.
28. Case K.M. and Zweifel P.F., 1977, *Linear Transport Theory*, Reading: Addison Wesley.
29. Conkin J. and Van Liew H.D., 1991, *Failure Of The Straight Line Boundary Between Safe And Unsafe Decompressions When Extrapolated To The Hypobaric Regime*, *Undersea Biomed. Res.* 18, 16.
30. Crocker W.E. and Taylor H.J., 1952, *A Method Of Calculating Decompression Stages And The Formulation Of New Diving Tables*, *Investigation Into The Decompression Tables*, Medical Research Council Report, UPS 131, London.
31. Cross E.R., 1970, *High Altitude Decompression*, *Skin Diver Magazine* 19, 17-18.
32. Davidson W.M., Sutton B.M., and Taylor H.J., 1950, *Decompression Ratio For Goats Following Long Exposure And Return To Atmospheric Pressure Without Stoppage*, Medical Research Council Report, UPS 110, London.
33. Des Granges M., 1957, *Repetitive Diving Decompression Tables*, USN Experimental Diving Unit Report, NEDU 6-57, Washington DC.
34. Duffner G.J., Synder J.F., and Smith L.L., 1959, *Adaptation Of Helium-Oxygen To Mixed Gas Scuba*, USN Experimental Diving Unit Report, NEDU 3-59, Washington, DC
35. Dwyer J.V., 1956, *Calculation Of Repetitive Diving Decompression Tables*, USN Experimental Diving Unit Report, NEDU 1-57, Washington DC.
36. Eckenhoff R.G., Olstad C.E. and Carrod G.E., 1990, *Human Dose Response Relationship For Decompression And Endogenous Bubble Formation*, *J. Appl. Physiol.* 69, 914-918.
37. Eckenhoff R.G., Olstad C.E., Parker S.F. and Bondi K.R., 1986, *Direct Ascent From Shallow Air Saturation Exposures*, *Undersea Biomed. Res.* 13, 305-316.

38. Eckenhoff R.G., 1985, *Doppler Bubble Detection*, *Undersea Biomed. Res.* 12, 485-489.
39. Edmonds C., Lowry C., and Pennefather J., 1994, *Diving And Subaquatic Medicine*, Portland: Book News.
40. Edmonds C, McKenzie B., and Thomas R., 1997, *Diving Medicine For Scuba Divers*, Sydney: Aquaquest Publications.
41. Eisenberg P., 1953, *Progress On The Mechanics Of Cavitation*, David Taylor Model Basin Rept. 842.
42. Epstein P.S. and Plesset M.S., 1950, *On The Stability Of Gas Bubbles In Liquid-Gas Solutions*, *J. Chm. Phys.* 18, 1505-1509.
43. Evans A. and Walder D.N., 1969, *Significance Of Gas Macronuclei In The Aetiology Of Decompression Sickness*, *Nature London* 222, 251-252.
44. Farm F.P., Hayashi E.M., and Beckman E.L., 1986, *Diving And Decompression Sickness Treatment Practices Among Hawaii's Diving Fisherman*, University of Hawaii Sea Grant Report, UNIHI-SEAGRANT-TP-86-01, Honolulu.
45. Feynman R.P., Leighton R.B., and Sands M., 1975, *The Feynman Lectures On Physics I, II, III*, Reading: Addison Wesley.
46. Fisher J.C., 1948, *The Fracture Of Liquids*, *J. Appl. Phys.* 19, 1062-1067.
47. Fleagle R.G. and Businger J.A., 1963, *Introduction To Atmospheric Physics*, New York: Academic Press.
48. Frenkel J., 1946, *Kinetic Theory Of Liquids*, New York: Oxford University Press.
49. Gernhardt M.L., Lambertsen C.J., Miller R.G., and Hopkins E., 1990, *Evaluation Of A Theoretical Model Of Tissue Gas Phase Growth And Resolution During Decompression From Air Diving*, *Undersea Biomed. Res.* 17, 95.
50. Gernhardt M.L., 1985, *Tissue Gas Bubble Dynamics During Hypobaric Exposures*, Society Of Automotive Engineers Report, SAE-851337, Warrendale.
51. Gilliam B., Webb D. and von Maier R., 1995, *Deep Diving*, San Diego: Watersports.
52. Golding F.C., Griffiths P.D., Paton W.D.M., Walder D.N., and Hempleman H.V., 1960, *Decompression Sickness During Construction Of The Dartford Tunnel*, *Brit. J. Ind. Med.* 17, 167-180.
53. Goldstein H., 1969, *Mechanics*, Reading: Addison Wesley.
54. Gradshteyn I.S. and Ryzhik I.M., 1965, *Table Of Integrals, Series, And Products*, New York: Academic Press.
55. Gray J.S., Masland R.L., and Mahady S.C., 1945, *The Effects Of Breathing Carbon Dioxide On Altitude Decompression Sickness*, US Air Force School Of Aviation Medicine Report, Project 409, Randolph Field.
56. Groen P., 1967, *The Waters Of The Sea*, University Park: Pennsylvania State University Press.
57. Guillen M., 1995, *Five Equations That Changed The World*, New York: Hyperion.

58. Hamilton R.W., 1975, *Development Of Decompression Procedures For Depths In Excess Of 400 Feet, Undersea And Hyperbaric Medical Society Report, WS: 2-28-76, Bethesda.*
59. Harvey E.N., 1945, *Decompression Sickness And Bubble Formation In Blood And Tissue, Bull. N.Y. Acad. Med. 21, 505-536.*
60. Harvey E.N., Barnes D.K., McElroy W.D., Whiteley A.H., Pease D.C., and Cooper K.W., 1944, *Bubble Formation In Animals. I. Physical Factors, J. Cell. Comp. Physiol. 24, 1-22.*
61. Harvey E.N., Whiteley A.H., McElroy W.D., Pease D.C., and Barnes D.K., 1944, *Bubble Formation In Animals. II. Gas Nuclei And Their Distribution In Blood And Tissues, J. Cell Comp. Physiol. 24, 23-24.*
62. Harvey E.N., McElroy W.D., Whiteley A.H., Warren G.H., and Pease D.C., 1944, *Bubble Formation In Animals. III. An Analysis Of Gas Tension And Hydrostatic Pressure In Cats, J. Cell. Comp. Physiol. 24, 117-132.*
63. Hawkins J.A., Shilling C.W., and Hansen R.A., 1935, *A Suggested Change In Calculating Decompression Tables For Diving, USN Med. Bull. 33, 327-338.*
64. Hempleman H.V., 1957, *Further Basic Facts On Decompression Sickness, Investigation Into The Decompression Tables, Medical Research Council Report, UPS 168, London.*
65. Hempleman H.V., 1952, *A New Theoretical Basis For The Calculation Of Decompression Tables, Medical research Council Report, UPS 131, London.*
66. Heine J., 1991, *Cold Water Diving, Flagstaff: Best.*
67. Hennessy T.R. and Hempleman H.V., 1977, *An Examination Of The Critical Released Gas Concept In Decompression Sickness, Proc. Royal Soc. London B197, 299-313.*
68. Hennessy T.R., 1974, *The Interaction Of Diffusion And Perfusion In Homogeneous Tissue, Bull. Math. Biol. 36, 505-527.*
69. Hills B.A., 1977, *Decompression Sickness, New York: John Wiley And Sons.*
70. Hills B.A., 1976, *Supersaturation By Counterdiffusion And Diffusion Of Gases, J. Appl. Physiol. 43, 56-69.*
71. Hills B.A., 1969, *Radial Bulk Diffusion Into Heterogeneous Tissue, Bull. Math. Biophys. 31, 25-34.*
72. Hills B.A., 1968, *Linear Bulk Diffusion Into Heterogeneous Tissue, Bull. Math. Biophys. 30, 47-59.*
73. Hills B.A., 1968, *Variation In Susceptibility To Decompression Sickness, Int. J. Biometeor. 12, 343-349.*
74. Hills B.A., 1968, *Relevant Phase Conditions For Predicting The Occurrence Of Decompression Sickness, J. Appl. Physiol. 25, 310-315.*
75. Hirschfelder J.O., Curtiss C.F., and Bird R.B., 1964, *Molecular Theory Of Gases And Liquids, New York: John Wiley And Sons.*
76. Huang K., 1973, *Statistical Mechanics, New York: John Wiley And Sons.*

77. Huggins K.E., 1987, *Multiprocessor Applications To Multilevel Air Decompression Problems*, Michigan Sea Grant Publication, MICHU-SG-87-201, Ann Arbor.
78. Irving J. and Mullineux N., 1972, *Mathematics In Physics And Engineering*, London: Academic Press.
79. Johnson L.W. and Riess R.D., 1962, *Numerical Analysis*, Reading: Addison Wesley.
80. Kahaner D., Moler C., and Nash S., 1989, *Numerical Methods And Software*, Englewood Cliffs: Prentice Hall.
81. Keller H. and Buhlmann A.A., 1965, *Deep Diving And Short Decompression By Breathing Mixed Gases*, *J. Appl. Physiol.* 20, 1267.
82. Kunkle T.D. and Beckman E.L., 1983, *Bubble Dissolution Physics And The Treatment Of Decompression Sickness*, *Med. Phys.* 10, 184-190.
83. Lamb J.S., 1999, *The Practice Of Oxygen Management For Divers*, Flagstaff: Best.
84. Lambertsen J.L. and Bornmann R.C., 1979, *Isobaric Inert Gas Counterdiffusion*, Undersea And Hyperbaric Medical Society Publication 54WS(IC)1-11-82, Bethesda.
85. Lambertsen C.J. and Bardin H., 1973, *Decompression From Acute And Chronic Exposure To High Pressure Nitrogen*, *Aerospace Med.* 44, 834-836.
86. Landau L.D. and Lifshitz E.M., 1985, *Fluid Mechanics*, Reading: Addison Wesley.
87. Landau L.D. and Lifshitz E.M., 1980, *Mechanics*, Reading: Addison Wesley.
88. Lang M.A. and Vann R.D., 1992, *Proceedings Of The American Academy Of Underwater Sciences Repetitive Diving Workshop*, AAUS Safety Publication AAUSDSP-RDW-02-92, Costa Mesa.
89. Lang M.A. and Egstrom G.H., 1990, *Proceedings Of The American Academy Of Underwater Sciences Biomechanics Of Safe Ascents Workshop*, American Academy Of Underwater Sciences Diving Safety Publication, AAUSDSP-BSA-01-90, Costa Mesa.
90. Lang M.A. and Hamilton R.W., 1989, *Proceedings Of The American Academy Of Underwater Sciences Dive Computer Workshop*, University Of Southern California Sea Grant Publication, USCSG-TR-01-89, Los Angeles.
91. Leebaert D., 1991, *Technology 2001: The Future Of Computing And Communications*, Cambridge: Massachusetts Institute Of Technology Press.
92. Lehner C.E., Hei D.J., Palta M., Lightfoot E.N., and Lanphier E.H., 1988, *Accelerated Onset Of Decompression Sickness In Sheep After Short Deep Dives*, University Of Wisconsin Sea Grant College Program Report, WIS-SG-88-843, Madison.
93. Leitch D.R. and Barnard E.E.P., 1982, *Observations On No Stop And Repetitive Air And Oxyntrogen Diving*, *Undersea Biomed. Res.* 9, 113-129.
94. Le Messurier D.H. and Hills B.A., 1965, *Decompression Sickness: A Study Of Diving Techniques In The Torres Strait*, *Hvaldradets Skrifter* 48, 54-84.
95. Loyst K., Huggins K.E. and Steidley M., 1991, *Dive Computers*, San Diego: Watersports.

96. Mathews J. and Walker R.L., 1975, *Mathematical Methods Of Physics*, New York: W.A. Benjamin.
97. Mount T. and Gilliam B., 1991, *Mixed Gas Diving*, San Diego: Watersport.
98. Neal J.G., O'Leary T.R. and Wienke B.R., 1999, *Trimix Diving*, Fort Lauderdale: Underwater Dynamics Incorporated.
99. Neuman T.S., Hall D.A. and Linaweaver P.G., 1976, *Gas Phase Separation During Decompression In Man*, *Undersea Biomed. Res.* 7, 107-112.
100. Nishi R.Y., Eatock B.C., Buckingham I.P. and Ridgewell B.A., 1982, *Assessment Of Decompression Profiles By Ultrasonic Monitoring: No Decompression Dives*, Defense And Civil Institute Of Environmental Medicine Report, D.C.IEM 82-R-38, Toronto.
101. Parzen E., 1970, *Modern Probability Theory And Its Applications*, New York: John Wiley And Sons.
102. Paton W.D.M. and Walder D.N., 1954, *Compressed Air Illness*, Medical Research Council Report, HMSO 281, London.
103. Pease D.C. and Blinks L.R., 1947, *Cavitation From Solid Surfaces In The Absence Of Gas Nuclei*, *J. Phys. Coll. Chem.* 51, 556-567.
104. Pilmanis A.A., 1976, *Intravenous Gas Emboli In Man After Compressed Air Ocean Diving*, Office Of Naval Research Contract Report, N00014-67-A-0269-0026, Washington, DC
105. Powell M.P. and Rogers R.E., 1989, *Doppler Ultrasound Monitoring Of Gas Phase Formation And Resolution In Repetitive Diving*, *Undersea Biomed. Res.* 16, 69.
106. Powell C.F., 1928, *Condensation Phenomena At Different Temperatures*, *Proc. Royal Soc. London A119*, 553-577.
107. Press W., Teukolsky S., Vetterling W., and Flannery B., 1992, *Numerical Recipes In FORTRAN*, New York: Cambridge University Press.
108. Rashbass C., 1955, *New Tables, Investigation Into The Decompression Tables*, 243 Medical Research Council Report, UPS 151, London.
109. Rogers R.E. and Powell M.R., 1989, *Controlled Hyperbaric Chamber Tests Of Multiday Repetitive Dives*, *Undersea Biomed. Res.* 16, 68.
110. Rossier R.N., 2000, *Recreational Nitrox Diving*, Flagstaff: Best.
111. Roughton F.J.W., 1952, *Diffusion And Chemical Reaction Velocity In Cylindrical And Spherical Systems Of Physiological Interest*, *Proc. Royal Soc. B140*, 203-221.
112. Rutkowski D., 1989, *Nitrox Manual*, San Diego: International Association of Nitrox Divers (IAND).
113. Sagan H., 1971, *Boundary And Eigenvalue Problems In Mathematical Physics*, New York: John Wiley And Sons.
114. Sawatzky K.D. and Nishi R.Y., 1990, *Intravascular Doppler Detected Bubbles And Decompression Sickness*, *Undersea Biomed. Res.* 17, 34-39.

115. Schreiner H.R. and Hamilton R.W., 1987, *Validation Of Decompression Tables, Undersea And Hyperbaric Medical Society Publication 74 (VAL)*, Bethesda.
116. Sears F.W., 1969, *Thermodynamics*, Reading: Addison Wesley.
117. Shapiro A.H., 1958, *Dynamics And Thermodynamics Of Compressible Fluid Flow*, New York: Ronald.
118. Sheffield P.J., 1990, *Flying After Diving, Undersea And Hyperbaric Medical Society Publication 77 (FLYDIV)*, Bethesda.
119. Shreider Y.A., 1966, *The Monte Carlo Method*, New York: Pergamon Press.
120. Smith K.H. and Stayton L., 1978, *Hyperbaric Decompression By Means Of Bubble Detection*, Office Of Naval Research Report, N0001-469-C-0402, Washington DC
121. Smith C.L., 1975, *Altitude Procedures For The Ocean Diver*, National Association Of Underwater Instructors Technical Publication 5, Colton.
122. Somers L.H., 1991, *The University Of Michigan Diving Manual*, Ann Arbor: University Of Michigan Press.
123. Spencer M.P., 1976, *Decompression Limits For Compressed Air Determined By Ultrasonically Detected Blood Bubbles*, *J. Appl. Physiol.* 40, 229-235
124. Spencer M.P. and Campbell S.D., 1968, *The Development Of Bubbles In The Venous And Arterial Blood During Hyperbaric Decompression*, *Bull. Mason Cli.* 22, 26-32.
125. Strauss R.H., 1974, *Bubble Formation In Gelatin: Implications For Prevention Of Decompression Sickness*, *Undersea Biomed. Res.* 1, 169-174.
126. Strauss R.H. and Kunkle T.D., 1974, *Isobaric Bubble Growth: Consequence Of Altering Atmospheric Gas*, *Science* 186, 443-444.
127. Thompson A.M., Cavert H.M., and Lifson N., 1958, *Kinetics Of D₂O And Antipyrine In Isolated Perfused Rat Liver*, *Amer. J. Physiol.* 192, 531-537.
128. Tikuisis P., 1986, *Modeling The Observations Of In Vivo Bubble Formation With Hydrophobic Crevices*, *Undersea Biomed. Res* 13, 165-180.
129. Tikuisis P., Ward C.A. and Venter R.D., 1983, *Bubble Evolution In A Stirred Volume Of Liquid Closed To Mass Transport*, *J. Appl. Phys.* 54, 1-9.
130. Van Liew H.D. and Hlastala M.P., 1969, *Influence Of Bubble Size And Blood Perfusion On Absorption Of Gas Bubbles In Tissues*, *Resp. Physiol.* 24, 111-121.
131. Van Liew H.D., Bishop B, Walder P.D., and Rahn H., 1975, *Bubble Growth And Mechanical Properties Of Tissue In Decompression*, *Undersea Biomed. Res.* 2, 185-194.
132. Vann R.D., Dovenbarger J., Wachholz C., and Bennett P.B., 1989, *Decompression Sickness In Dive Computer And Table Use*, *DAN Newsletter* 3-6.
133. Vann R.D., Grimstad J., and Nielsen C.H., 1980, *Evidence For Gas Nuclei In Decompressed Rats*, *Undersea Biomed. Res.* 7, 107-112.
134. Vann R.D. and Clark H.G., 1975, *Bubble Growth And Mechanical Properties Of Tissue In Decompression*, *Undersea Biomed. Res.* 2, 185-194.

135. Walder D.N., Evans A., and Hempleman H.V., 1968, *Ultrasonic Monitoring Of Decompression*, *Lancet*. 1, 897-898.
136. Walder D.N., 1968, *Adaptation To Decompression Sickness In Caisson Work*, *Biometeor.* 11, 350-359.
137. Wallace D., 1975, *NOAA Diving Manual*, Washington DC: US Government Printing Office.
138. Weathersby P.K., Survanshi S. and Homer L.D., 1985, *Statistically Based Decompression Tables: Analysis Of Standard Air Dives, 1950-1970*, Naval Medical Research Institute report, NMRI 85-16, Bethesda.
139. Weathersby P.K., Homer L.D., and Flynn E.T., 1984, *On The Likelihood Of Decompression Sickness*, *J. Appl. Physiol.* 57, 815-825.
140. Wienke B.R., 2001, *Technical Diving In Depth*, Flagstaff: Best.
141. Wienke B.R., 1998, *Physics, Physiology, And Decompression Theory For The Technical And Commercial Diver*, National Association Of Underwater Instructors Publication, Tampa.
142. Wienke B.R., 1993, *Diving Above Sea Level*, Flagstaff: Best.
143. Wienke B.R., 1994, *Basic Diving Physics And Application*, Flagstaff: Best.
144. Wienke B.R., 1992, *Numerical Phase Algorithm For Decompression Computers And Application*, *Comp. Biol. Med.* 22, 389-406.
145. Wienke B.R., 1991, *Basic Decompression Theory And Application*, Flagstaff: Best.
146. Wienke B.R., 1991, *Bubble Number Saturation Curve And Asymptotics Of Hypobaric And Hyperbaric Exposures*, *Int. J. Biomed. Comp.* 29, 215-225.
147. Wienke B.R., 1991, *High Altitude Diving*, National Association Of Underwater Instructors Technical Publication, Montclair.
148. Wienke B.R., 1990, *Reduced Gradient Bubble Model*, *Int. J. Biomed. Comp.* 26, 237-256.
149. Wienke B.R., 1990, *Modeling Dissolved And Free Phase Gas Dynamics Under Decompression*, *Int. J. BioMed. Comp.* 25, 193-205.
150. Wienke B.R., 1989, *Equivalent Multitissue And Thermodynamic Decompression Algorithms*, *Int. J. BioMed. Comp.* 24, 227-245.
151. Wienke B.R., 1989, *Tissue Gas Exchange Models And Decompression Computations: A Review*, *Undersea Biomed. Res.* 16, 53-89.
152. Wienke B.R., 1989, *N₂ Transfer And Critical Pressures In Tissue Compartments*, *Math. Comp. Model.* 12, 1-15.
153. Wienke B.R., 1987, *Computational Decompression Models*, *Int. J. BioMed. Comp.* 21, 205-221.
154. Wienke B.R., 1986, *DECOMP: Computational Package For Nitrogen Transport Modeling In Tissues*, *Comp. Phys. Comm.* 40, 327-336.
155. Wienke B.R., 1986, *Phenomenological Models For Nitrogen Transport In Tissues*, *Il Nuovo Cimento* 8D, 417-435.

156. Wilkes M.V., 1959, *Oscillations Of The Earth's Atmosphere*, London: Cambridge University Press.
157. Wittenborn A.F., 1963, *An Analytic Development Of A Decompression Computer*, Proc. Second Symp. Underwater Physiol., Washington, DC: National Academy Of Science 1, 82-90.
158. Workman R.D., 1965, *Calculation Of Decompression Schedules For Nitrogen-Oxygen And Helium-Oxygen Dives*, USN Experimental Diving Unit Report, NEDU 6-65, Washington DC
159. Yang W.J., 1971, *Dynamics Of Gas Bubbles In Whole Blood And Plasma*, J. Biomech. 4, 119-125.
160. Yarborough O.D., 1937, *Calculations Of Decompression Tables*, USN Experimental Diving Unit Report, EDU 12-37, Washington DC
161. Yount D.E. and Hoffman DC, 1986, *On The Use Of A Bubble Formation Model To Calculate Diving Tables*, Aviat. Space Environ. Med. 57, 149-156.
162. Yount D.E., Gillary E.W., and Hoffman DC, 1984, *A Microscopic Investigation Of Bubble Formation Nuclei*, J. Acoust. Soc. Am. 76, 1511-1521.
163. Yount D.E., 1982, *On The Evolution, Generation, And Regeneration Of Gas Cavitation Nuclei*, J. Acoust. Soc. Am. 71, 1473-1481.
164. Yount D.E., 1979, *Skins Of Varying Permeability: A Stabilization Mechanism For Gas Cavitation Nuclei*, J. Acoust. Soc. Am. 65, 1431-1439.
165. Yount D.E., Yeung C.M., and Ingle F.W., 1979, *Determination Of The Radii Of Gas Cavitation Nuclei By Filtering Gelatin*, J. Acoust. Soc. Am. 65, 1440-1450.
166. Yount D.E. and Strauss R.H., 1976, *Bubble Formation In Gelatin: A Model For Decompression Sickness*, J. Appl. Phys. 47, 5081-5089.
167. Zhang J., Fife C.E., Currie M.S., Moon R.E., Pintadosi C.A. and Vann R.D., 1991, *Venous Gas Emboli And Complement Activation After Deep Air Diving*, Undersea Biomed. Res. 18, 293-302.

INDEX